Development of Inhibitors of Hepatitis C Virus

Adam C. Rolt

Dr. Andrew V. Stachulski, Dr. T. Jake Liang, Prof. Paul O'Neill and Dr. Juan Marugan

Thesis submitted in accordance with the requirements of the University of Liverpool for the degree of Doctor in Philosophy by Adam Christopher Rolt

September 2016

UNIVERSITY OF LIVERPOOL

Declaration of Academic Integrity

Name: Adam Christopher Rolt
Student Number: 200594576

School of Physical Sciences / Department of Chemistry

Development of Inhibitors of Hepatitis C Virus

Student Declaration

I confirm that:

- I have read and understood the University's PGR Policy on Plagiarism and Dishonest Use of Data.
- I have acted honestly, ethically and professionally in conduct leading to assessment for the programme of study.
- I have not copied material from another source nor committed plagiarism nor fabricated, falsified or embellished data when completing the attached material.
- I have not copied material from another source, nor colluded with any other student in the preparation and production of this material.
- If an allegation of suspected academic malpractice is made, I give permission to the University to use source-matching software to ensure that the submitted material is all my own work.

Signature…….....

Date…….....

Table of Contents

Phenotype-based drug discovery: Pharmacological development of Chemotype 3 as an inhibitor of HCV assembly

Photoaffinity labelling in the elucidation of the mechanism of action of the HCV entry inhibitor Chlorcyclizine

List of figures

Chapter 1

Chapter 2

Chapter 3

Chapter 4

Acknowledgements

Firstly, I would like to extend my sincerest gratitude to my supervisors for the past 4 years – Dr Andrew Stachulski, Dr T. Jake Liang, Dr Juan Marugan and Prof Paul O'Neill for the patience, guidance, freedom, and for keeping me moving forwards.

Gratitude to all of the chemists on the 4th floor at the University of Liverpool, who gave me so much of their time and effort during such important periods in their lives: Shane M^{c}Kenna, Mark Huyton and esp. Paul M^{c}Gillan and Kathryn Price – **Dream Team 2014.**

I am grateful to the biology team at NIH for teaching me cellular/molecular biology from scratch and for helping me every step of the way – Zongyi, Melissa and Billy, and to thymine team at NCATS – esp. Juan and Andrés.

Other members of the NIH/WT program – Beeds, John, Geigs, Jo. For a group of friends that were put together arbitrarily I wouldn't have picked them better myself.

There will be a set of conditions that'll do that reaction
somewhere, you just haven't worked it out yet.
— M.H.

List of Abbreviations and acronyms

Abu	Aminobutyric acid
ADME	Absoption, Distribution, Metabolism, Excretion.
Ala	Alanine
apo-E	Apolipoprotein E
ASM	Acid sphingomyelinase
ATH	Asymmetric transfer hydrogenation
ATP	Adenosine triphosphate
BINAP	Binapthyl
BuLi	Butyllithium
Bz	Benzoyl
CC_{50}	Concentration leading to 50% cell death (cytotoxic concentration)
CCZ	Chlorcyclizine
CD81	Cluster of differentiation 81
CHV	Canine hepacivirus
CLDN1	Claudin
CN	Calcineurin
CsA	Cyclosporin A
CT3	Chemotype 3
CypA	Cyclophilin A
DAA	Directly acting anti-virals
de	Diastereomeric excess
dr	Diastereomeric ratio
DKR	Dynamic kinetic resolution
DMEM	Dulbecco's modification of Eagle's medium
DMSO	Dimethylsulfoxide
DMV	Double membrane vesicles
EC_{50}	Concentration leading to 50% of desired response (Effective Concentration)
EDTA	Ethylenediamine tetra-acetic acid
ee	Enantiomeric excess
er	Enantiomeric ratio
ER	Endoplasmic reticulum
FIASMA	Functional inhibitor of acid sphingomyelinase
FBS	Fetal bovine serum
GAG	Glycosaminoglycan
H-Bond	Hydrogen bond
HAART	Highly active anti-retroviral therapy
HATU	(1-[Bis(dimethylamino)methylene]-1H-1,2,3-triazolo[4,5-b] pyridinium 3-oxid hexafluorophosphate)
HCV	Hepatitis C virus
HCV-Luc	HCV-luciferase
HCVcc	HCV cell culture assay

HCVpp	HCV pseutotype assay
HCVsc	HCV single cycle assay
HDL	High density lipoproteins
HIV	Human immunodeficiency virus
HPLC	High performance liquid chromatography
HRP	Horseradish peroxidase
HSPG	Heparan sulfate proteoglycan
HTA	Host-targeted antivirals
IFN	Interferon
IP	Intraperitoneal
IRES	Internal ribosomal entry site
ISG	Interferon stimulating genes
IV	Intravenous
Jak1	Janus kinase 1
keq	Equilibrium constant
kg	Kilograms
LC/MS	Liquid chromatography mass spectrometry
LCMS/MS	Liquid chromatography tandem mass spectrometry
LD	Lipid droplets
LDLR	Low-density lipoprotein receptor
LVP	Lipoviral particle
M	Molar
$MeBm_2t$	Gamma-dimethyl MeBmt
MeBmt	(2S,3R,4R,6E)-3-Hydroxy-4-methyl-2-(methylamino)-6-octenoic acid.
MeLeu	N-methyl leucine
Met-ID	Metabolite identification
MeVal	N-methyl valine
mg	Milligrams
MHz	Megahertz
min	Minutes
miR-122	MicroRNA-122
MLSMR	Molecular libraries small molecule repository
mM	Millimoles
MMV	Multimebrane vesicles
MoA	Mechanism of action
mRNA	Messenger RNA
NADPH	Nicotinamide adenine dinucleotide phosphate
NCGC	National chemical genomics center
NFATc	Nuclear factor of activated T-cells
ng	Nanograms
NIH	National Institutes of Health
nM	Nanomolar
NMR	Nuclear magnetic resonance

NPC	NCGC pharmaceutical collection
NPC1L1	Niemann Pick-C like receptor 1L1
NPHV	Non primate hepacivirus
NS	Non-structural
°C	Degrees celcius
OCLN	Occludin
PAMPA	Parallel artificial membrane permeability assay
PBS	Phosphate buffered saline
Ph	Phenyl
PO	"Per os" Latin: By opening - oral administration of material
PVDF	Polyvinylidene difluoride
QSAR	Quantitative structure activity relationships
RBV	Ribavirin
RdRp	RNA dependent RNA polymerase
RNA	Ribonucleic acid
Ru	Ruthenium
S	"Sinister" Latin: On the left side - Chiral configuration label
Sar	Sarcosine
SAR	Structure activity relationships
SDS-PAGE	Sodium dodecyl sulfate - polyacrylamide gel electrophoresis
SIV	Simian immunodeficiency virus
SOCl2	Thionyl chloride
SOF	Sofosbuvir
SRB1	Scavenger receptor class B member 1
STAT	Signal transducers and activators of transcription
SVR	Sustained virologic response
TCID	Tissue culture infective dose
TLC	Thin-layer chromatography
Tyk2	Tyrosine kinase 2
µg	Micrograms
µM	Micromolar
uPA-SCID	Urokinase plasminogen activator-severe combined immunodeficiency
UTR	Untranslated region
UV	Ultraviolet
v/v	Volume for volume equivalency
VLDL	Very low-density lipoproteins
W	Watts
Z	Benzyloxycarbonyl
^{13}C NMR	^{13}C Nuclear magnetic resonance
^{19}F NMR	^{19}F Nuclear magnetic resonance
^{1}H NMR	^{1}H Nuclear magnetic resonance

Abstract

Hepatitis C virus (HCV) is the causative agent of hepatitis C, this virus infects approximately 170 million people worldwide, equivalent to more than half of the population of the USA, and approximately 600,000 deaths per year due to liver failure and hepatocellular carcinoma can be attributed to HCV. Directly acting antivirals, first introduced in 2011, have revolutionised treatment of the disease, the most contemporary multi-drug combination therapies are curative in >90% of treatment naïve patients in real-world scenarios. However, patient cohorts such as difficult to treat genotypes of HCV in combination with advanced liver cirrhosis and previous treatment failures, as well as HIV/HCV co-infected patients, respond relatively poorly.

To address the therapeutic need of these niche patient cohorts, candidates that target the entry and assembly stages, and host factors of the HCV life cycle were chosen specifically to develop, as combination of these therapeutics with the current replication stage inhibitors will reduce the probability of viral resistant mutations as an intrinsic pharmacodynamic property of the therapies, as well as reducing treatment duration, and importantly treatment cost.

To this end, three separate arms of research have been undertaken. Mechanistic parameters of asymmetric transfer hydrogenation of ketones were developed, allowing a short, modular and enantioselective synthesis of MeBmt, a component of the host-targeting HCV agent cyclosporin A, by dynamic kinetic resolution.

A novel assembly inhibitor of HCV, CT3, was optimised resulting in a lead compound **372** which boasts approximately fifteen fold increase in efficacy against HCV, more than ten fold increase in metabolic half life and an increase in other molecular efficiency metrics as compared to the original hit, which culminated in an *in-vivo* PK study in mice.

Lastly, a synthesis of a potent photoaffinity probe was designed and successfully implemented, designed around the framework of a novel inhibitor of HCV entry – chlorcyclizine. The probe is being utilized in biological experiments to understand molecular mechanism of action of chlorcyclizine against HCV, which may, perhaps, uncover biological mechanisms related to HCV entry.

1

Introduction to Hepatitis C

1.1 Hepatitis C

Hepatitis C virus (HCV) is the causative agent of hepatitis C. HCV is a small, single stranded, positive sense RNA virus that is transmitted by direct blood-to-blood or other percutaneous contact, with a significant proportion of the infected population unaware of their infection status due to the often asymptomatic onset. Persistent infection of HCV results in chronic hepatitis and liver disease, which may progress to a cirrhotic state, causally increasing the incidence of hepatocellular carcinoma and liver failure. Late stage progression of hepatitis ultimately may call for a liver transplant with universal graft re-infection. HCV infects approximately 170 million people worldwide and approximately 600,000 deaths per year due to liver failure and hepatocellular carcinoma can be attributed to HCV. Directly acting anti-virals have greatly improved the prognosis with the current state of the art delivering >90% sustained virologic response (SVR) across all genotypes in treatment naïve patients, however the global disease burden is not expected to peak until 2020.

1.2 Taxonomy, origin and epidemiological development of HCV

Hepatitis C virus (HCV) is the type species of the genus *Hepacivirus* other members include canine hepacivirus (CHV) and non-primate hepacivirus (NPHV), in turn classified as a part of the *Flaviviridae* family. Other members of this family include Zika virus, West Nile virus and Dengue virus.[10] HCV comprises a diverse set of virus subtypes, which can be categorized into seven

phylogenetic clades based on geographical location or origin. Of these subtypes, the most commonly encountered subtypes in western countries are 1a, 1b, 2a, 2b, 3a, 4a and 6a, of which 1a and 1b comprise 60% of all infections[11]. These HCV subtypes are genotypically and phenotypically distinct viruses and pertain to different and discrete subsets of the infected population epidemiologically[10].

The true origins of HCV in terms of virus evolution still remain unclear, leading hypotheses include a model of a non-human primate original host for HCV, with humans acquiring a stable infection variant zoonotically[12] in close analogy with Simian Immunodeficiency Virus (SIV) to Human Immunodeficiency Virus (HIV) [13]. This scenario is supported more in terms of epidemiology than by some genotypic classification – common and diverse HCV infections can be seen in areas of the world where human, ape and other monkey populations overlap, before the development of the ability of long range travels in these human populations, continued transmission and replication of HCV in geographically distinct locations accounts for the phylogenetic clade distribution of the HCV genotypes and subtypes.

Despite this, to date HCV or homologues have not been observed in any ape or monkey species other than humans. Recently however, an RNA virus (termed Canine Hepacivirus, CHV) was discovered in dogs that possesses similar sequence homology to HCV[14], though in this case the virus is largely localized in respiratory samples, with a presumed respiratory route of transmission, which has not been observed for HCV. Similarly, Non-Primate Hepacivirus (NPHV) has been observed in horses. Each of these hepaciviruses may be adapted completely to one particular species, with subtle species-dependent factors in replication being responsible for the lack of propensity for zoonotic transfer. It has been postulated therefore, in opposition to relatively recent virus transfer originating from another mammal, that HCV has simply always infected humans and their evolutionary ancestors, and that the virus has evolved to maintain infection along with us. It is possible the medical advances of the modern era - pushing the boundaries of the human lifespan, combined with systematic advances in understanding of the human body and an increase in opportunity for transmission have shone the light on this virus in terms of allowing the pathogenicity of HCV to reveal itself clinically, modern methods of detection notwithstanding.[12]

Recent phylogeographic analysis has shown that the current epidemic of HCV subtypes 1a and 1b in the developed world began as recently as 1940 as opposed to a more gradual increase across the 20th century as has been previously suggested[11]. The specificities of the time frames uncovered by this study suggest that the current HCV pandemic has causal roots in an increased number of parenteral iatrogenic procedures during and after World War II

(1939-1945) using contaminated blood for transfusions, the incorporation of plasma pooling and contamination during non-sterile procedures. Lyophilized, pooled plasma remains infectious for long periods of time. The increase in number of HCV genotype 1a infections also specifically coincides with peak intravenous drug use (late 1960's) before the public became aware of the dangers associated with non-A non-B hepatitis which would eventually come to be designated as hepatitis C.[11] In spite of this, intravenous drug use continues to be one of the highest risk factors for acquiring HCV, being responsible for approximately 90% of new cases worldwide[15].

Finally, HCV was officially discovered and classified in 1989[16] as a result of ongoing investigations into the causes of the aforementioned non-A, non-B hepatitis that had become associated with blood transfusions and intravenous drug use. Further development of diagnostic tests revealed the true extent of HCV pandemic, it is currently estimated that 170-200[17] million people are infected with HCV, approximately 2.7-3% of the worlds population.

1.3 Hepatitis C Virus life cycle, protein structure and function

HCV particles primarily infect and replicate in hepatocytes, but they may also infect peripheral blood mononuclear cells such as erythrocytes and monocytes, although they do not replicate in these cells. Evidenced by the low buoyant density of HCV compared to other viruses, it is proposed that circulating HCV is associated with human serum lipoviral particles (LVP), with HCV and the LVP sharing an external plasma membrane.[18]

Virions come into contact with hepatocytes in the space of Disse following diffusion across the fenestrated endothelium of the liver sinusoids, wherein they may bind with low affinity (initially) to cell surface receptors on hepatocytes[19]. In the liver biopsy samples of patients however, infected cells occur in clusters, pointing to a cell-to-cell spread as the predominant mode of HCV transmission[20,21]

These initial binding events with low-density lipoprotein receptor (LDLR), glycosaminoglycans (GAGs) facilitate stronger post binding interactions with HCV associated entry factors that trigger cellular entry, such as CD81, SRB1, claudin 1 (CLDN1) occludin (OCLN) and Niemann-Pick C1-like 1 receptor (NPC1L1). These factors interact with the HCV membrane and associated lipoproteins and facilitate migration to tight junctions ultimately resulting in clathrin-mediated vesiculation and endocytosis of the entire viral particle[22], as opposed to fusion with the cell membrane and injection of the viral machinery into the cytosol. The HCV particle enclosed in the endosomal vesicle matures

to an early endosome as part of the internalization process.[23] HCV evades lysosomal degradation and the viral genetic material is delivered to their cytoplasmic site of replication on the ER following HCV-endosomal fusion triggered by endosomal acidification (~pH5) - this consequently renders the HCV infection susceptible to lysosomotropic reagents such as bafliomycin and chloroquine that effect atypical pH changes in lysosomes[24].

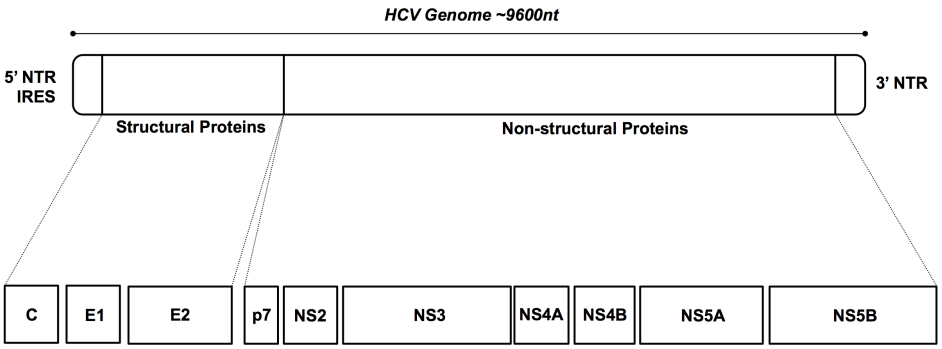

***Fig. 1.1**:* Representation of the coding region of the HCV genome partitioned to display polyprotein cleavage products.

The HCV **Core** protein forms the viral nucleocapsid and is involved in the localization of the HCV replication complex on the ER.[1] Multifunctional envelope glycoproteins **E1** and **E2** are essential for assembly and infectivity of the HC virion, E1 and E2 form heterodimers that are presented on the virus surface and interact with HSPG on the surface of hepatocytes. The **p7 viroporin** self-assembles into hexamers that may insert themselves into membranes and function as ion channels, it is observed to facilitate virus production and is found to be vital for infectivity in vivo[3] however the precise mechanisms remain unclear. p7 has been proposed to act as a low pH activated ion channel equilibrating pH of acidic compartments which is necessary in the later stages of HCV virion assembly[4], this function has been investigated by mutagenesis studies[5]. **NS2**, a cysteine protease liberates fully functional NS3/4A from the polyprotein promoting replication. The multifunctional serine protease/RNA helicase **NS3/4A** cleaves the HCV polyprotein at the NS3/4A, NS4A/4B, NS4B/ 5A, and NS5A/5B junctions once it has liberated itself from NS2,[6] it is also involved in evading the host innate immune response[7] The active site of NS3 is largely flat, with substrate recognition really being a result of molecular interactions over a large area of the protease more akin to protein-protein interactions, giving rise to high specificity[3]. **NS4B** lacks a discrete singular enzymatic function compared to, for example, a protease or an RNA polymerase and as such the structure and function of NS4B was relatively poorly characterized, however developing knowledge regarding interaction between the HCV proteins reveals that NS4B has been implicated in the modulation of the RNA-dependent RNA polymerase (RdRp) NS5B[8], and also as playing a crucial role in the induction and development of the membranous web that serves as a scaffold for the HCV replication compex.[3] The phosphoprotein **NS5A** is another multi-functional peptide that is involved in several different undertakings in proliferating HCV by its interaction with other proteins. NS5A is implicated in the modulation of the RdRp NS5B as well as alterations to the cellular environment increasing amenability for HCV replication[9 3]. Finally, **NS5B,** the RNA dependent RNA polymerase (RdRp) conducts the replication of HCV RNA via the synthesis of a complimentary negative strand of RNA and the subsequent synthesis of excess amounts of the positive stranded RNA from this template.[3]

The cellular machinery of the hepatocyte is directly recruited to begin initial translation of the HCV genome from the positive stranded RNA directly to the unprocessed polypeptide[25] (in analogy to mRNA). The HCV is constructed of one open reading frame of ~9600 nucleotides flanked on the 3' end by an untranslated region (UTR) and on the 5' end by an internal ribosomal entry site (IRES) responsible for the initiation of translation.

The polypeptide is cleaved into 10 functional proteins by the cellular peptidases and viral proteases: structural proteins Core, E1, E2, p7 and non-structural proteins, NS2, NS3, NS4A, NS5A and NS5B (*fig* **1.1***)* and the proteins are localized on endoplasmic reticulum (ER) derived membranes. In terms of functionality, the genome can be divided into an assembly module – C, E1, E2, p7 and NS2; and a replication module NS3-NS5B however many of the proteins have multiple functions facilitating both viral replication and assembly.[3] Membrane alterations in the ER of the hepatocyte driven by NS4B and others result in the formation of a "membranous web" as a site for continued replication. The membranous web and other ER substructures such as double or multi-membrane vesicles (DMV, MMV) serves to protect the viral RNA from potential host defences, as well as to compartmentalize and increase local concentrations of specific viral products, while providing physical support for the viral replication complex.[26] Viral replication continues with assistance from various host factors.

Assembly of the HCV virion is a complex effort involving the cellular localization of the HCV structural proteins in different compartments in the cell. The HCV core proteins form dimers and polymers that undergo trafficking to the surface of cytosolic lipid droplets. The Core proteins are then recruited along with E1 and E2 dimers to package HCV RNA, which undergoes budding into the ER, all in a concerted process. [27,28] During secretion and trafficking through the Golgi, the E1 and E2 are post-translationally modified, the virions interact with apoE-containing VLDL and HDL particles, acquiring their characteristic low buoyant density and the virions are released from the cells via a secretory pathway.[18]

Despite the intricate and extremely complicated nature of this process, an established HCV infection will result in the production of some 10^{12} virions per day in an infected individual.[29]

1.4 Treatment of Hepatitis C Virus

Great progress in terms of understanding HCV has been made since the discovery of the virus in 1989[16] - elucidation of the viral lifecycle and viral genome, with protein structure and function along with cell culture systems and animal models. Improved understanding of the virus inevitably translates

into improved therapeutic strategies as is evidenced by the classes of drugs that have been historically used to treat HCV, moving from broad spectrum anti-virals such as interferon and ribavirin where our knowledge and comprehension of HCV was minimal, to directly-acting and host-acting anti-virals, to target specific singular viral and host proteins, with distinct clinical end-points, as knowledge of HCV increases.

1.4.1 Interferon and Ribavirin

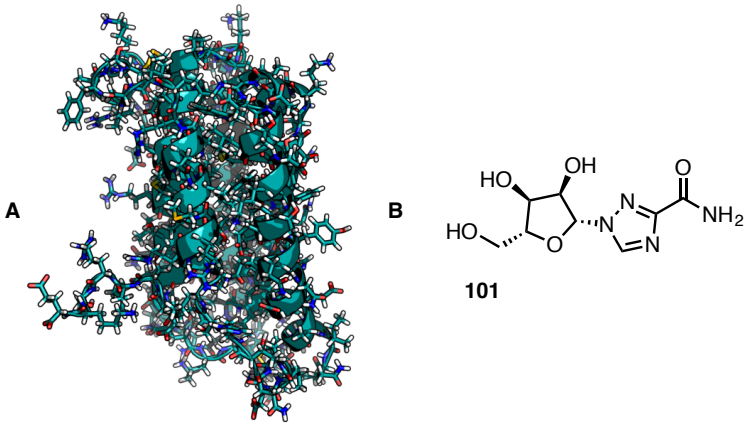

Figure 1.2 Graphical render of interferon-α and structure of Ribavirin

Interferons (IFN) (*fig.* **1.2A**) are cytokines that are critical mediators in the mounting of an immune response against viruses and are also the first class of therapeutic interventions that were used against HCV, along with the broad-spectrum anti-viral ribavirin, a ribonucleoside analogue[30-32]. IFN-α of the class IFN-type 1, suppresses HCV replication by the induction of eponymous IFN-stimulated genes (ISG's) through phosphorylation of the STAT1/2 complex mediated Jak1 and Tyk2 kinases. ISG expression acts to establish an anti-viral state within the cell, hundreds of genes are induced[33] which precipitates in changes to protein expression immune modulation and lipid metabolism in the cell population to name a few, that act to resist the proliferation of HCV.

Ribavirin (*fig.* **1.2B, 101**) is a broad spectrum anti-viral drug, that, when given in mono-therapy is not effective against HCV, but in combination therapy with IFN and other therapies, has been demonstrated to yield improvements in sustained virologic response (SVR48 IFN-16%, SVR48 IFN+ribavirin – 40%[34]). It is tempting to assume that ribavirin acts via chain termination of viral RNA replication via incorporation into viral RNA, analogous to other ribonucleoside analogues, however at clinically suitable concentrations, incorporation into RNA is too low.[35]

It is possible that incorporation into HCV RNA increases the error rate in HCV replication just enough to render the virus particle non-viable as an infectious agent. Only a very modest increase is required for this "error catastrophe" as HCV, akin to other RNA viruses, has no proofreading/error checking capabilities of it's own replication and as a result is very error prone regardless.[36] Ribavirin has also been observed to up-regulate specific IFN stimulated genes (ISG's), and when used in conjunction with IFN-α the effect was synergistic when compared with either drug applied separately due to the use of separate pathways to achieve these means.[37] Considering ribavirin given in monotherapy does not display any anti-HCV effect, it is likely that the IFN potentiating effect of ribavirin is the principal mechanism of action.

Pegylated IFN-α in combination with ribavirin is generally poorly tolerated with regards to numerous side effects, hence it is contraindicated for a large cohort of patients, and response rates to the treatment, at best, are 54-56% SVR[31]. Nonetheless without suitable alternatives, IFN/ribavirin remained the mainstay for HCV treatment until 2011.

1.4.2 Directly acting anti-virals (DAA)

To address this therapeutic need, a worldwide effort on behalf of academic institutions and pharmaceutical companies is currently underway to produce drugs that act directly on HCV proteins. Direct acting anti-virals (DAA's) have the potential to be efficacious while avoiding the side effects and other limitations that are associated with IFN-α and ribavirin through leveraging specificity.

Boceprevir and Telaprevir (*fig.* **1.3. 102, 103** respectively) were the first of the new cohort of DAA's to gain approval in mid-2011 on the back of successful phase 3 clinical trials (Boceprevir[38,39], Telaprevir[40,41]). They are first generation reversible covalent inhibitors of the HCV NS3/4A protease, possessing an α-keto amide functional group that allows reversible formation of a hemiacetal moiety, preventing dissociation (k_{off}) from the binding pocket. Boceprevir and Telaprevir bind to the active site of the protease, interrupting HCV polypeptide processing in a competitive manner (*fig.* **1.3**.)[42]

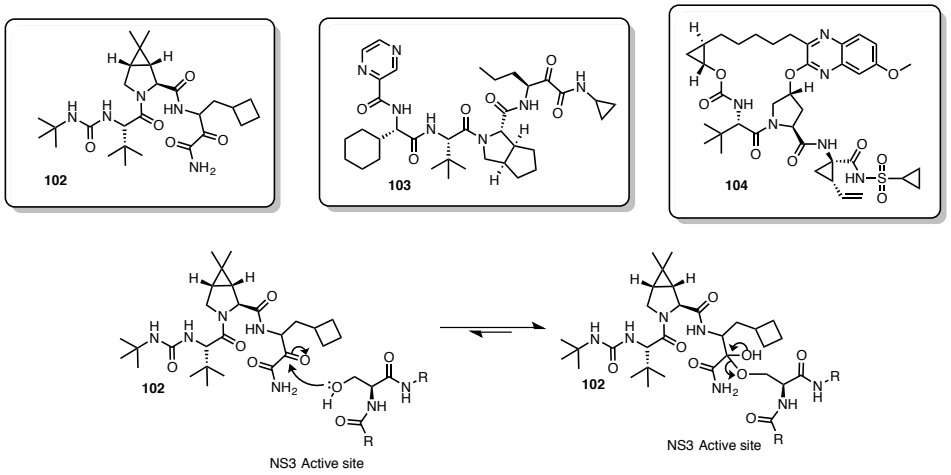

Figure 1.3 Structures of Boceprevir **102,** Telaprevir, **103** and Grazoprevir, **104.** Binding of Boceprevir to the NS3 active site – reversible covalent inhibition.

Second-generation NS3/4A inhibitors such as Grazoprevir (*fig* **1.3, 104**) a component of a contemporary two-drug combination Zepatier, are non-covalent inhibitors, possess pan-genotypic activity and improved resistance profiles.[43]

Following the successful introduction of Boceprevir and Telaprevir, Sofosbuvir (*fig* **1.3A, 105**) was the first NS5B inhibitor to be approved for use alone or in combination with other anti-HCV treatments in multi-drug regimens. Sofosbuvir is a nucleoside analogue whose incorporation into viral RNA by NS5B causes chain termination of RNA synthesis with a low nanomolar EC_{50} and pan-genotypic activity. Sofosbuvir in combination with Ribavirin in a 12 week treatment course resulted in sustained virologic response after 12 weeks (SVR12) in >90% of patients.[44] Sofosbuvir as a component triple therapy (SOF/RBV/IFN) affords excellent SVR rates in null-responders who are traditionally resistant to other forms of DAA triple therapy.[45]

The most recent class of DAA's to gain FDA approval, the NS5A inhibitors, also have found successful use in combination therapies. NS5A inhibitor Daclatasvir **100,** is a palindromic inhibitor of NS5A with a low picomolar EC_{50} Ledipasvir **107** is a component of the infamously expensive but efficacious Harvoni[46], a dual combination of Sofosbuvir and Ledipasvir[47] ($94,000/12 week course).

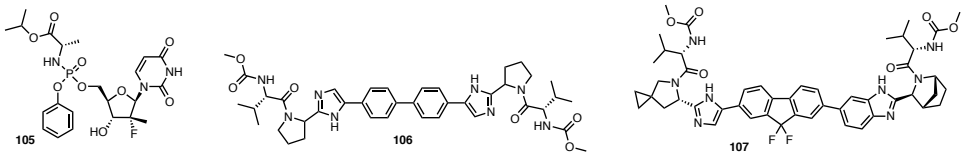

Figure 1.4 Structures of HCV inhibitors Sofosbuvir **105**, Daclatasvir **106** and Ledipasvir **107**.

Modern treatment regimens such as Harvoni, VIEKRA PAK, Technivie and Zepatier consist of all oral combinations, either double or triple therapy of NS3/4A, NS5A and NS5B inhibitors without ribavirin and interferon[48].

1.4.3 Host-targeting anti-virals

Host targeting anti-virals (HTA's), as opposed to targeting viral proteins directly, target host proteins that are implicated in the life cycle of HCV. The categorization of the drugs by target is appropriate as a result of the divergent pharmacodynamic implications of the drug class as a whole. The main advantages of using HTA's is that, in targeting a host factor in replication, the drugs are often intrinsically pan-genotypic. Furthermore, the virus cannot simply acquire resistance through a point mutation to prevent a ligand binding and often multiple changes are required to reduce or circumvent the dependence of the virus on the host factor in question. These changes often result in a loss of replicative fitness for the virus and present a high barrier for resistance. The immediate disadvantage of this therapeutic class is that in specifically targeting a host factor, consideration must be taken to avoid possible toxicity from compromising the endogenous role of the target.[49]

1.4.3.1 Entry inhibitors

There are several possible host-derived targets to block entry of HCV into the hepatocytes, with some potential treatments in the early stages of development. Discussion here is limited to treatments that have progressed into and beyond proof-of-principle experiments in mice.[50] Small molecule and antibody inhibitors of entry factors on the cell surface membranes have been shown to significantly reduce the kinetics of HCV infection in the uPA-SCID mouse model such as NPC1L1 small molecule inhibitor ezetimibe and EGFR inhibitor erlotinib[49] – these compounds act by preventing HCV association

with its entry factors. Monoclonal antibody inhibitors of CD81 and SRBI were found to completely protect mice from establishing HCV infection in a prophylactic manner. Several of the targets implicated in HCV entry also play a role in transmission from cell to cell.

1.4.3.2 Cyclophilin inhibitors

Cyclophilin A (CyPA) is an endogenous proline cis-trans isomerase that has been shown to be a critical component to HCV replication. Cyclophilin antagonists are potent inhibitors of HCV replication and are discussed at length in Chapter 2.

1.4.3.3 miR-122 antagonists

MicroRNA-122 (miR-122) is an endogenous microRNA found most frequently in the liver and is involved in regulation of liver metabolic processes; miR-122 is also implicated in HCV pathogenesis. MiR-122 binds to HCV in the 5'UTR region and has a positive effect on virus translation, replication, and the production of infectious virions.[51] Miravirsen is a single stranded RNA (15 nucleotides, MW 4897Da) that is the complimentary antisense sequence to miR-122, Miravirsen and binds miR-122 in a heteroduplex conformation, arresting HCV replication.[52] In a phase 2a clinical trial, Miravirsen dosed at up to 7mg/kg of bodyweight, with weekly injections for five weeks, resulted in a 3-log-drop in HCV viral load: the HCV viral load in four out of nine patients dosed at 7mg/kg became undetectable.

MiR-122 knockout mice have been shown to rapidly develop hepatocellular carcinoma and the sequestration of significant amounts of miR-122 by HCV is thought to contribute to this. [53] However sequestration in the short term using a therapeutic "miR-122 sponge" such as Miravirsen does not appear to contribute to this effect.[54]

1.5 Phase 4 analyses of DAAs

Post market surveillance, so called Phase 4 analysis, of modern anti-HCV treatments has shown that, in general, real-world scenarios of all-oral combination DAA regimens are, in terms of response rates, in-line with what has been reported in clinical trials.[55] Most treatment failures are as a result of a lack of patient compliance. The treatment effectiveness can be rescued by extending the length of therapy, or with the addition of Ribavirin or DAAs from other drug classes.[56]

HTA's by their nature, possess promising therapeutic potential for pharmacological development in the fight against HCV. Currently approved DAA's and compounds in late stage development will be sufficient to treat the vast majority of patient cohorts regardless of HCV genotype.

Continuing research in this area should be focused on further enhancing the response rate and shortening treatment duration for the most at-risk, niche patient cohorts such as difficult to treat genotypes of HCV in combination with advanced liver cirrhosis and previous treatment failures, as well as HIV/HCV co-infected patients[57], for which drug-drug interactions may be an issue.

In the light of this, the specific, intrinsic properties of HTAs indicates that these therapeutics would be ideal incorporations into DAA combinations to treat the most difficult cases of HCV in terms of efficacy, probability of escape mutant production, tolerability and importantly treatment cost[58]. Truly efficacious treatment of HCV began with DAA/HTA combinations for good reason, perhaps it will end with them too.[59]

1.6 Target- and phenotype-based drug discovery

There are two different conceptual models in drug discovery and optimisation, the target-based approach and the phenotype-based approach. The conceptual differences between these two classes can be thought of simply as the breadth of the disease phenotype that is considered.

Target-based drug discovery is a reductionist, mechanism based approach, focusing on the modulation of the activity of one particular validated target wherein the modification of this target is correlated causally with the treatment of a disease state. An example of this would be a high-throughput screen of small molecules in an in-vitro biochemical assay, targeted towards a specific viral protease[60].

Target-based approaches require prior understanding of the mechanistic underpinnings of a disease before an assay can be developed. When targeting specific proteins often crystal structures are available to help guide structure-based drug design. After a molecular target of therapeutic interest has been identified, target validation must be performed to guarantee that modulation of the target (receptor, enzyme, transporter, DNA etc.) in a physiological environment will result in a modification of the disease phenotype, here the specific molecular mechanism of action will play a role (types of

agonism/antagonism, receptor residence time, competitive/non-competitive, covalent/non-covalent, reversibility, allostery etc.) and in this manner the drug can be more finely tuned to the disease state it is intended to target[61].

Phenotypic drug discovery is different from target based approaches in that screens for target identification and development will take place in a phenotypic model for the disease state, and will focus on modulation of the whole disease state. Phenotypic approaches are holistic as opposed to reductionist, and as such do not require such extensive target validation. Phenotypic assays used in high-throughput screens have the potential to give rise to a large array of potential leads with varied mechanisms of action. Phenotypic drug discovery is the oldest form of drug discovery, and in its crudest sense has been practiced for several thousand years by way of chewing or stewing roots, herbs, berries and barks for their medicinal properties.[62] Modern examples move away from animal models and instead usually focus on a model of the disease in a physiologically relevant cell line. A prudent example of a phenotypic screen is a quantitative high-throughput cell based screen that was recently performed in our group against HCV[63] where the reduction of HCV virus load was the determinant of efficacy as opposed to some modulation of a specific receptor. Screens such as this are non-discriminatory in terms of the mechanisms of action that the leads may then possess, and as such many first-in-class approved drugs are now discovered using phenotypic screens[61]. Most 'follower' drugs however are discovered through target-based approaches once the target of the phenotype-based drug is identified.

In the specific case of HCV, target-based approaches should be leveraged towards better improvements of treatments with particularly strong biological mechanisms, that is, efficacious treatments with intrinsically high barriers to resistance. Alternatively it could be argued that phenotypic based approaches would find more utility in the discovery of novel HCV inhibitors with mechanisms of action that do not directly overlap with currently marketed drugs or even therapeutics that are in development.

1.7 This work

The following work is concerned with development of three inhibitors of HCV with mechanisms of action that do not coincide with currently approved drugs.

Chapter 2 describes the development of synthetic methodology with applications primarily directed towards the synthesis of MeBmt, a component of cyclosporin A (CsA) - a host-targeted replication stage inhibitor. The development of mechanistic parameters of dynamic kinetic resolution by asymmetric transfer hydrogenation of β-keto α-amido carbonyl derivatives is described,. And their subsequent use in the synthesis of MeBmt. The mechanism of action of cyclosporin A necessarily gives the compound a high barrier to resistance when being used as an anti-HCV compound. A target-based approach towards optimisation of CsA permits rational design through specific modifications guided by *in silico* docking experiments, as well as specific modifications to improve the pharmacokinetic profile of the molecule. It is anticipated that this chemistry will ultimately facilitate the production of analogues of CsA that have been optimised specifically towards HCV infection.

Chapter 3 describes the chemical optimisation of a late stage inhibitor of HCV derived from a phenotypic high-throughput screen. In lieu of a defined binding site and crystal structure, optimisation is iterative and is guided based on efficacy and toxicity feedback from cell-based biological assays as well as in-vitro measurements of ADME properties, working towards proof of principle experiments in a suitable rodent model.

Chapter 4 discusses the mechanism of action and attempted target deconvolution of chlorcyclizine – an HCV entry inhibitor, again derived from a phenotypic high throughput screen. Deciphering the mechanism of action and binding partner of chlorcyclizine can permit optimisation in a target based manner, in the same approach as is used for cyclosporin A.

2

Target-based drug discovery: Developing synthetic methodology towards derivatives of Cyclosporin A.

2.1 Introduction

Cyclosporin A (CsA, *fig.* **2.1**, **201**), a complex cyclic peptide, containing 11 amino acid residues, was originally isolated from the fungus *Tolypocladium inflatum* in 1969[64] and is a constituent of the Model List of Essential Medicines as determined by the World Health Organization. CsA is notable for being a potent immunosuppressive agent and is used to circumvent immunological graft rejection following transplantation, but is also known to be a potent, host-directed inhibitor of HCV replication.[57]

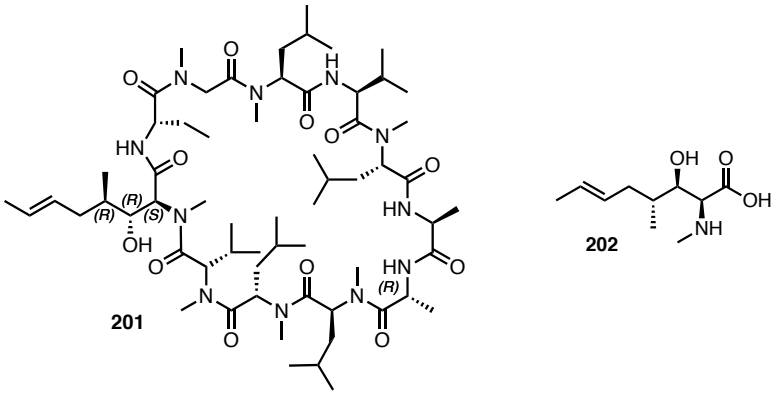

Figure 2.1 Structure of cyclosporin A and it's constituent amino acid MeBmt

CsA is composed of eleven amino acids, two of which are non proteinogenic (D-Ala and MeBmt) and seven are N-methylated[65]. Besides its biological profile, the compound possesses interesting physical properties. Especially the amino acid profile (mostly non-polar, lipophilic, branched) and their subsequent N-methylation make the compound quite unusually lipophilic for a peptide (clogP 3.6 at physiological pH). Owing to its lipophilicity, CsA is poorly soluble in water and is administered as an emulsion[66]: also the solubility of CsA in water decreases as the temperature of the aqueous solution increases[67]. Much of the biological profile of CsA, including the anti-HCV activity, is a result of interference with signalling cascades beginning with the interaction of CsA with the endogenous peptidyl-prolyl isomerase CypA[68] as mentioned in **Chapter 1**.

2.1.1 Cyclosporin A as an immunomodulatory agent

Foreign pathogens recognised by T-cells will have the eventual effect of activating the protein phosphatase calcineurin, via the calcium-sensitive messenger protein calmodulin. Calcineurin (CN) exerts its effect via dephosphorylation of the transcription factor – Nuclear Factor of Activated T-cells (NFATc). Once dephosphorylated, NFATc then increases the transcription and translation of interleukins in T-cells, thereby potentiating the immune response. Cyclosporin A also binds to CypA (*fig* **2.2-B**), then this binary complex may bind to and sequester CN via a protein-protein interaction, greatly reducing the T-cells' ability to elicit an immune response.[69-72] The presence of cyclosporin A imparts stability to the (CN-CyPA) protein-protein interaction; in the crystal structure it can be seen at the interface of the protein complex (*fig* **2.2-A**). Modifications to CsA have been shown to alter the immunosuppressive effect, whether by decreased binding affinity to CypA, or CN or both[73,74]

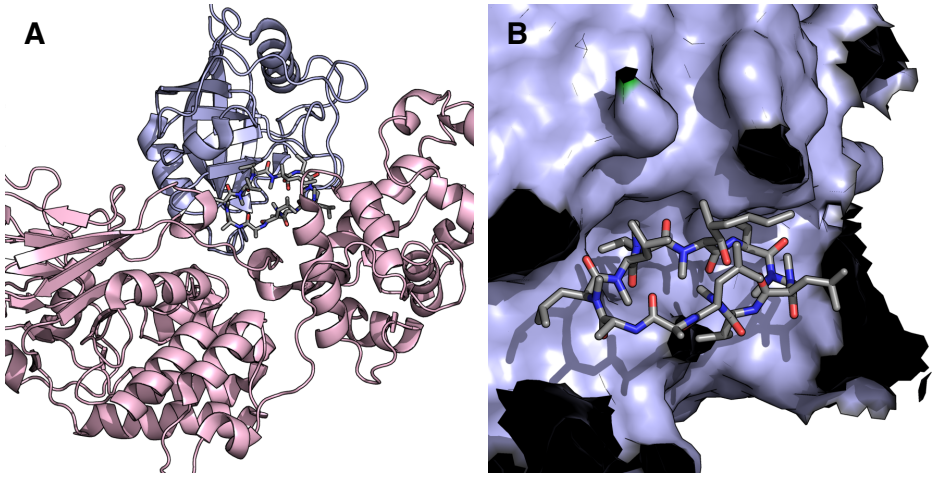

Figure 2.2. **A –** Ternary complex between CypA (lilac), CsA (stick model) and calcineurin (pink). **B** Crystal structure of cyclosporin A bound in the isomerase site of CsA

2.1.2 Cyclosporin as an anti-HCV agent

Cyclophilins, in particular CypA and CypB, have also been shown to be critical components to HCV replication. Investigations into the involvement of CsA and CypA, and as to their mechanistic involvement in HCV replication, began due to the observation that CsA inhibited proliferation of non-A non-B hepatitis following daily dosing. Huh7-Lunet cells transduced with a vector for silencing the expressions of CypA or CypB selectively showed that HCV replication is drastically inhibited under CypA knockdown but that knockdown of CypB had no effect. Inhibition of replication was rescued by overexpression of wild-type CypA, but importantly not by a CypA mutant lacking isomerase activity, demonstrating the necessity of the innate activity of the enzyme in HCV replication[75]. Further investigations into the involvement of CypA demonstrate the formation of stable complexes between CypA and proline rich regions of HCV non-structural protein NS5A – potentiating HCV replication[76,77]. CsA binds to the isomerase pocket of CypA, preventing the interaction with NS5A, inhibiting HCV proliferation[78] *via* a host-targeting mechanism.

2.1.3 Analogues of Cyclosporin A

Resistance to CsA and analogues is difficult to develop due to its host-acting mechanism. Since it acts on host CypA, the virus cannot simply develop a point mutation, and must circumvent the need for human CypA entirely, this is borne out in numerous in-vitro studies[79-81]. Due to its potency, attractive resistance profile, and the fact that it is already an approved drug, CsA is an attractive candidate for medicinal chemistry development and repurposing towards an anti-HCV drug. CsA binds to CyPA through 6 amino acids: Sar, Abu, MeBmt, MeVal MeLeu, MeLeu, shown in lilac, *fig.* **2.3, 201,** the CN binding domain is also shown in pink - compare to *fig* **2.2A/B.**

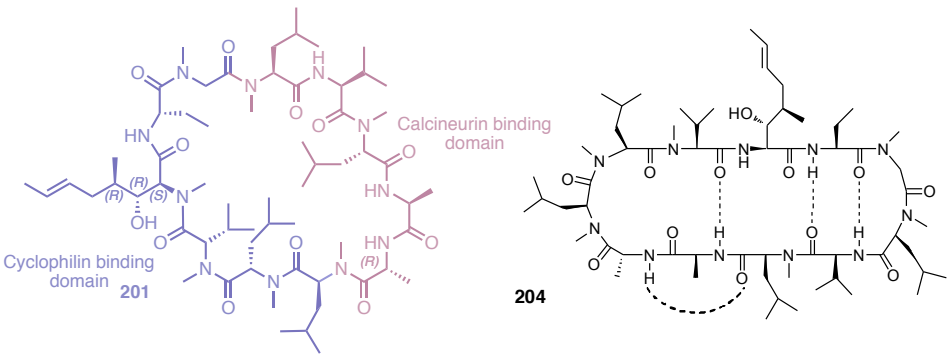

Figure 2.3 Representations of the binding domains of CsA with CyPA and CN, and a planar description of the intramolecular hydrogen bonding

The bioactive structure of CsA analogues bound to CypA has been calculated to be structurally very similar to the solution average conformer of CsA in water due to the intramolecular hydrogen bonding structure across the face of the cyclic peptide ring, *fig* **2.3, 204**.[82,83] MeBmt lies directly in the centre of the CypA binding domain: even small chemical alterations in MeBmt drastically affect the CyPA/CN binding and anti-HCV activity. The SAR is stringent: in general existing modifications have so far tended to reduce potency, but a few inspired modifications have been made, for example, as seen with Me_2Bmt-CsA[84]. Me_2Bmt-CsA (4-Dimethyl MeBmt) binds to CyPA with an affinity of 1% that of CsA: however, its immunosuppressive effect was reported to be 30% that of CsA. It has been proposed that the differences in efficacy are related to the equilibration between the CypA bound conformation and a non-binding conformation under physiological conditions[84]. The only modification that was found to improve the potency was the incorporation of an α methyl-thio substituent in place of the double bond. A summary is given below, *fig* **2.4.**

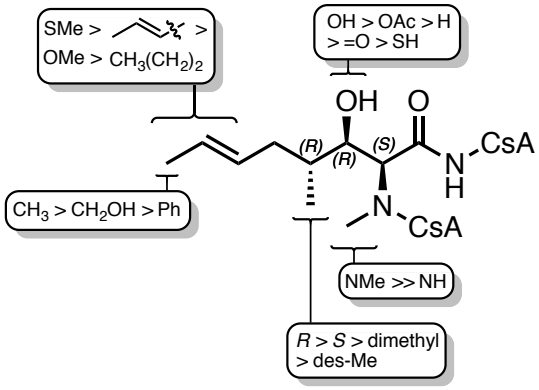

Figure 2.4 Summary of potency in CyP binding for MeBmt derivatives as part of CsA[2]

N-Methylation is favoured over N-H, however other N-alkyl derivatives have not been explored. The effect of stereochemistry at the α and β positions has not been addressed, but at the γ position the *R* configuration is favoured. Several analogues in the side chain have been tested against HCV: however, only the thioether derivative, *fig* **2.4,** has been shown to be more active than CsA itself.[74]

CsA analogues in the 1-position synthesised by Aebi *et al* universally decreased the immunosuppressive activity of CsA – replacement of the double bond with a triple bond or removing the methyl group at position 4 decreases activity by 90%, illustrating its occupation of the binding pocket. It was also noted, however, that the substitutions at MeBmt did not change the overall structure of the CsA molecule in any major way; the same hydrogen bonding patterns were retained. This is important when considering structural alterations – CsA has the potential to act as a rigid platform from which to build modifications in a rational manner.

2.1.3.1 Alisporivir, SCY635 and NIM811

Several analogues of CsA have entered clinical trials as antivirals, all more potent than the parent compound with reduced immunosuppressive effects (*fig* **2.5**) establishing clinical proof of concept**.** However none have emerged to become approved drugs for use as anti-HCV drugs (*fig* **2.5**).

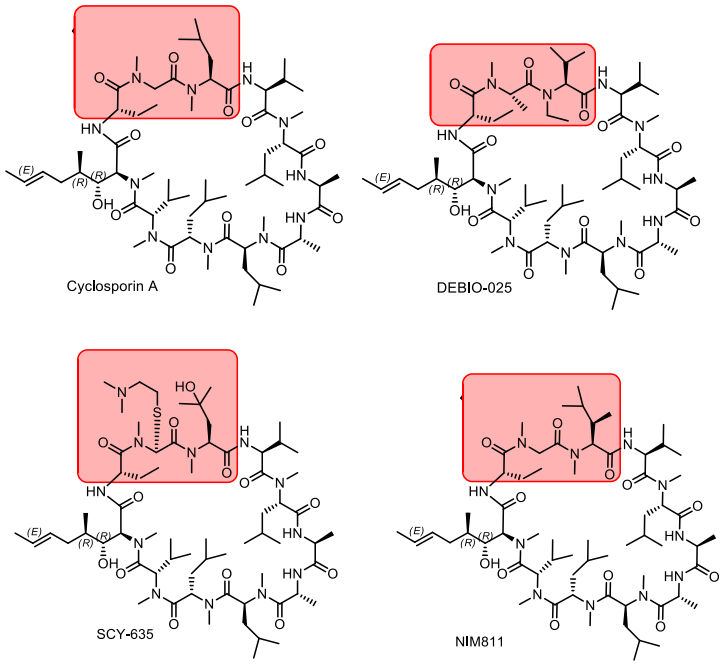

Figure 2.5 CsA derivatives that have entered clinical trials, structural differences highlighted.

DEBIO-025 (Alisporivir)

DEBIO-025 (Alisporivir) is a non-immunosuppressive cyclosporin analogue that has proved to be a much more potent inhibitor of HCV replication with approximately 10-fold potency increase in potency over CsA observed in the HCV subgenomic replicon assay, EC_{50} 9.8-28.9nM, depending on HCV genotype[57]. The structural modifications present in Alisporivir are located on the boundary of the CyP/CN binding domain resulting in low affinity for calcineurin; the MeLeu-Sar sequence is substituted with EtVal-MeAla. As a consequence Alisporivir lacks an immunosuppressive effect. DEBIO-025 was found to be 7000 fold less active than CsA at inhibiting IL-2 production.[57] Phase II clinical trials show that DEBIO-025 is generally well tolerated. ESSENTIAL[85] and VITAL-1[85] trials reported common side effects of reversible hyperbilirubinemia. SVR is achieved in 76% of patients receiving Alisporivir in combination with ribavirin and IFNα, with no null-responders, in comparison to ribavirin and interferon alone wherein 55% of patients achieved SVR. Alisporivir in monotherapy was shown to be nearly as effective as interferon and ribavirin with 53% SVR.

SCY-635

SCY-635 is an analogue of CsA possessing a dimethylamino-ethylthio substituent at the Sar^3 α carbon atom and a hydroxyl substituent at the gamma carbon of the $MeLeu^4$ residue. SCY-635 has an EC_{50} for HCV replication inhibition of 100nM and an EC_{50} for IL-2 inhibition of 4209nM whereas the respective EC_{50} values for CsA are 370/6.7nM.[86] The binary complex, CyP/SCY-635 exhibits a low binding affinity for CN [87].

NIM811

NIM811, originally isolated as a side-product of CsA biosynthesis is another potent inhibitor of CypA that does not possess any CN affinity and therefore has no immunosuppressive activity[88,89] A study to determine the antiviral efficacy of NIM811 in patients that had already experienced IFN/Rib based treatment failure, show a 2.85 (± 1.02) log_{10} fold drop in viral load. Clinical development of NIM811 has been discontinued due to a lack of efficacy when compared to Alisporivir.[89]

2.1.4 Derivatization of the MeBmt residue

Despite the on-going research into CsA structure-activity relationships, there are very few analogues of CsA incorporating different MeBmt derivatives and most have already been mentioned. MeBmt is a complex N-methylated amino acid possessing three contiguous stereocenters, as well as a trans double bond. There are many published routes towards MeBmt[83,90-115] having distinct strategies for tackling the aforementioned structural features. To thoroughly explore the SAR of cyclosporin A and derivatives for medicinal purposes, a totally flexible synthesis of MeBmt is fundamentally necessary.

2.2 Synthetic Chemistry of MeBmt

Immanently, the MeBmt side chain is constructed via the acetate pathway, analogous to other polyketides.[116] The natural biosynthetic pathways and the reported artificial synthetic routes share similarities in strategy, many reported routes are based on stereoselective aldol and Claisen chemistry, and these features and manners of bond forming processes are present in the biosynthetic pathway (*fig* **2.6**)

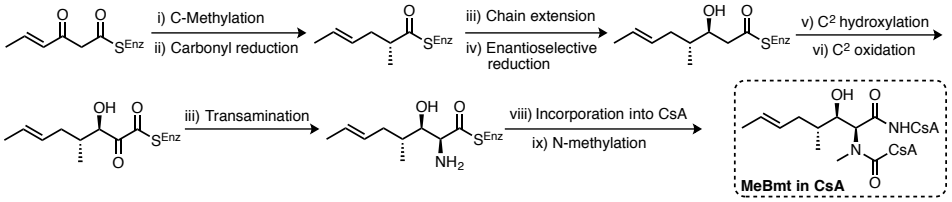

Figure 2.6 MeBmt biosynthetic pathway involves Claisen-like chain extensions, enantio- and chemoselective reductions, and has separate steps for N-methylation.

The olefinic side chain has previously been installed via regioselective alkyne reduction[108], *fig* **2.7A**, regiocontrolled Wittig chemistry[91] **2.7B,** or commonly through the synthesis of the aldehyde (2R,4E)-2-methyl-4-hexenal **205** which is a key synthetic intermediate in a number of synthetic routes to MeBmt. This in turn is derived from 3-buten-2-ol utilizing a Johnson-Claisen orthoester rearrangement as shown, **2.7C** with subsequent reduction/oxidation conversions.[95] Aldehyde **205** is volatile as well as being prone to racemization, limiting the effectiveness of routes utilising this material as an intermediate.

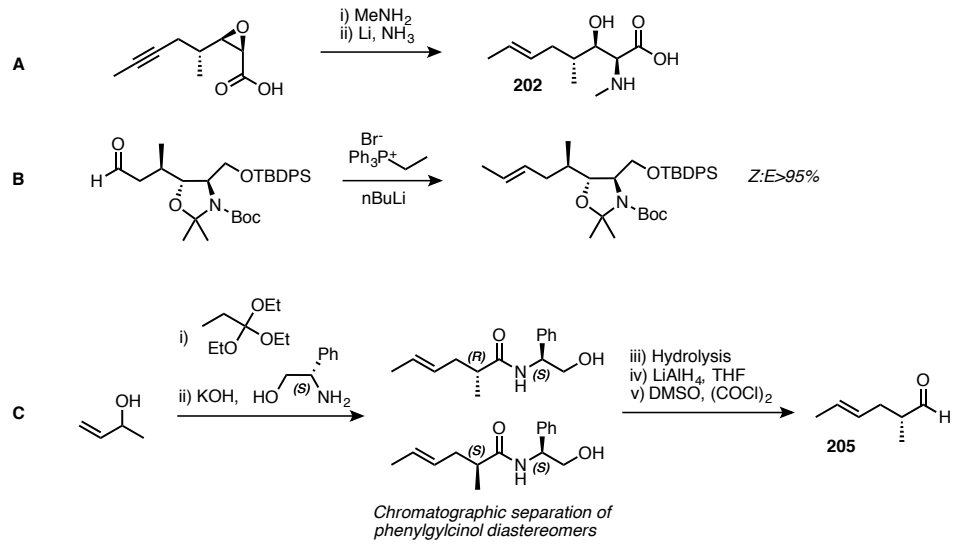

Figure 2.7 Some reported methods for installation of MeBmt trans double bond moiety involving regioselective reductions, or rearrangement reactions.

The stereochemistry at the 1 and 2 position of the amino acid has been established previously via chiral pool synthesis, Sharpless asymmetric epoxidation followed by ring opening, as well as asymmetric glycine aldol reactions[90] with either chiral auxiliaries or chelating metals, *fig* **2.8**.

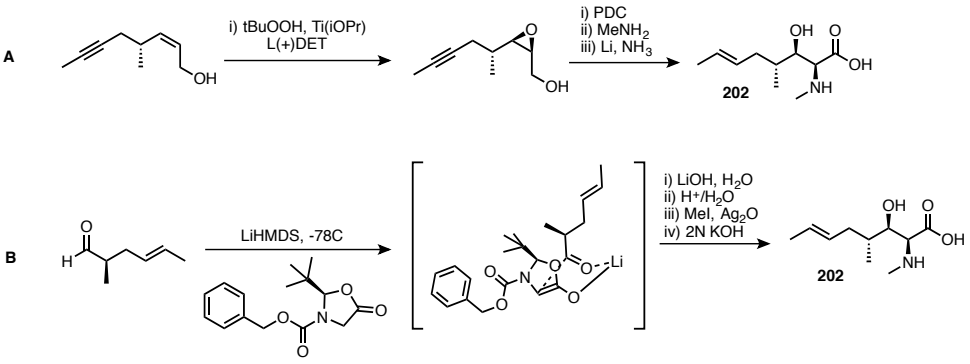

Figure 2.8 Sample of reported methods for installation of MeBmt 1,2-vicinal stereocenters

As described, published routes for MeBmt contain many steps, are often low yielding, linear, and the stereoselective transformations are often inflexible in terms of stereochemistry and side chain tolerance, and many require separate N-methylation steps. Allowance must be made in the synthetic routes for these features. In short, they are not suited for optimisation of the MeBmt residue in terms of CyP binding.

The synthetic route should ideally be short and modular with late incorporation of the side chain to facilitate analogue production, and stereodivergent in terms of position 1 and 2, with prior incorporation of N-methylation.

2.2.1 Proposed Strategy

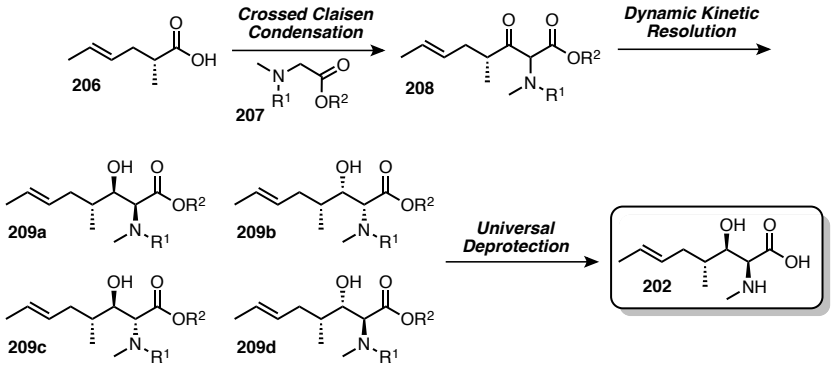

Figure 2.9 Proposed synthetic route towards MeBmt

The proposed synthetic route *fig* **2.9,** involves two key transformations: firstly a crossed Claisen condensation[117] of the previously reported[95] acid **206** to an appropriately protected sarcosine derivative **207** to yield the MeBmt scaffold **208** as a β-keto carbonyl analogue. Dynamic kinetic resolution (DKR) of **208** has the potential to selectively yield any one of four potential stereoisomers to investigate how the stereochemistry at these positions affects the biological profile of the molecule. The protecting groups that facilitate the crossed Claisen and direct the enantioselective reduction are ideally cleaved hydrolytically (esters, carbamates, amides) from **209** in a single step. The proposed route eliminates the need for stepwise chemoselective methylation of each target, benefits from late-stage incorporation of the side chain, is divergent in stereochemistry and avoids the problematic usage of aldehyde **205.**

2.2.2 Synthesis of β-hydroxy α-amino acids by dynamic kinetic resolution

Noyori[118] and Genet[119] describe the DKR by asymmetric hydrogenation (AH) of prochiral substrates, the stereochemical configurations of the product are dependent on both the structure of the catalyst, and that of the substrate. Hydrogenation of β-keto α-amido ester derivatives with the Ruthenium BINAP catalyst system under an atmosphere of hydrogen gives preferential *syn* stereochemistry, *fig* **2.10**.

The absolute stereochemistry of the products is derived from facial discrimination via the atropisomeric catalyst structure, and the stereocenter at the 2-position is set relative to this.

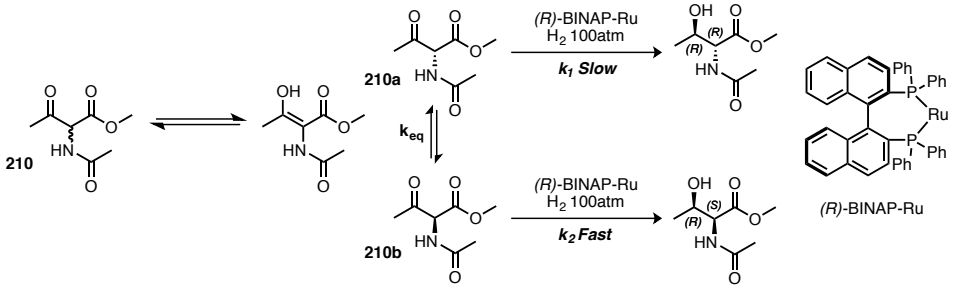

Figure 2.10 Asymmetric hydrogenation of α-amido β-keto esters

Very high enantiomeric excess (*ee*) and diastereomeric excess (*de*) can be achieved using these systems, provided that the rate of equilibration between the two isomers of the ketone substrate ($210_{a/b}$) is arbitrarily fast (k_{eq}) in comparison to the rate of reduction of the product (k_1, k_2) – the catalyst should be discriminating in an effective 1:1 distribution of substrate enantiomers as much as possible. Though syn-hydrogenation by this method would in theory give the desired (*2S,3R*) configuration of MeBmt, the high pressures of hydrogen required renders the method unsuitable, due to potential reduction of the olefinic side chain, experimental inconveniencies of using very high-pressure apparatus notwithstanding.

The technology has been expanded upon and has since been extended to asymmetric transfer hydrogenation (ATH) in which the reagent is not hydrogen gas, but another hydrogen source such as isopropanol[120], formic acid[121] and formate salts[122]. These conditions do not require specialist apparatus for high pressures, as such they are safer, have a broader substrate scope, and the catalysts are generally less sensitive. DKR via ATH has been shown to give both *anti* or *syn* products selectively depending on the structure of the substrate. [123]

α-amido ester substrates have been demonstrated to give anti products selectively under transfer hydrogenation conditions as demonstrated by Seashore-Ludlow et al[122]. It is postulated that this selectivity, shown in *fig* **2.11A,** is primarily due to intramolecular hydrogen bonding in the substrate as illustrated in *fig* **2.12.**

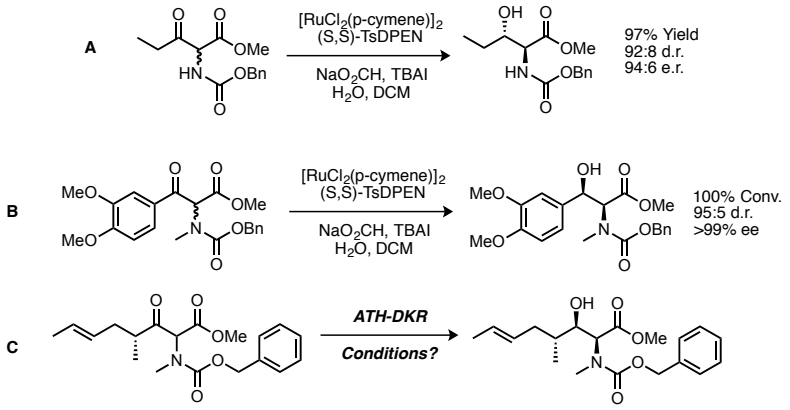

Figure 2.11 Literature examples of ATH DKR of selected substrates

The ketone is reduced stereoselectively with facial preference based on the structure of the catalyst, whereas the diastereoselectivity is a substrate-controlled factor, due to steric crowding (CO_2Me vs. H) in a transition state that is restrained by hydrogen bonding (*fig* **2.12**). If the approach of the catalyst to the ketone is sterically impaired then reduction may not occur.

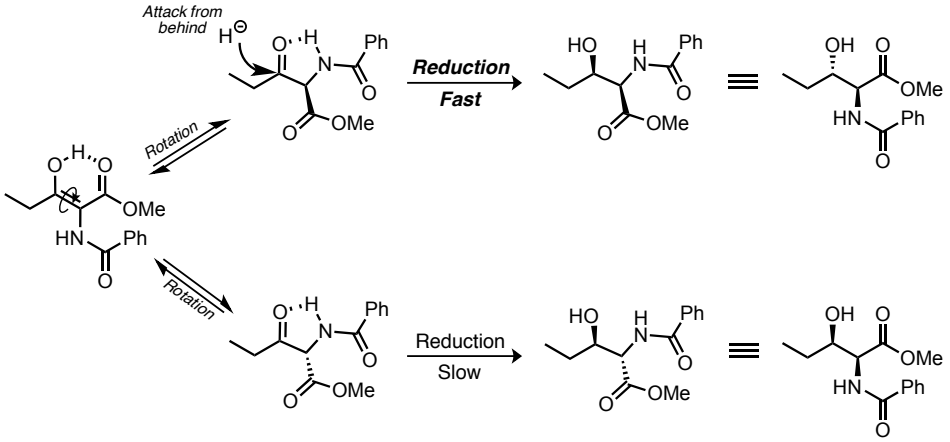

Figure 2.12 A working model of asymmetric induction in the ATH DKR of α-amido β-keto esters

If this intramolecular hydrogen bonding is interrupted, for example by substitution on the nitrogen, then syn configuration dominates, rationalized by a Felkin-Anh induction model: the configuration of the α carbon is constantly being racemised due to the facile tautomerism under the reaction conditions. Several substrates in the literature have been reduced that do not possess the capacity for intramolecular hydrogen bonding [120-122,124,125], all favouring syn reduction (ex *fig* **2.11B**).

Considering reduction of substrates containing fully substituted amides tends towards syn products, and that reduction of alkyl substituents has been previously demonstrated, we commenced a program to develop a short synthetic route towards MeBmt and derivatives by asymmetric transfer hydrogenation in order to modify the amino acid, allowing incorporation into CsA and study the modulation of biological activity.

2.3 Formal synthesis of MeBmt by ATH DKR via C^3 inversion

As a model system to develop the reaction conditions before using the synthetically valuable MeBmt side chain, we employed an isobutyric side chain as opposed to (R,E)-2-methylhex-4-enoic acid. Following the synthetic strategy to the end of the synthetic route would yield N-methyl (*2S, 3R)* 3-hydroxyleucine, **211** (*fig* **2.13**).

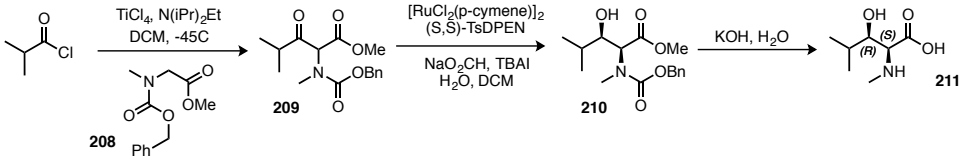

Figure 2.13 A pilot synthesis of N-Methyl (*2S, 3R)* 3-hydroxyleucine

Crossed-Claisen condensation of isobutyryl chloride with Z-Sar-OMe, **208** following the protocol of Misaki et al[117] gave the crossed product **209,** in disappointing 28% yield. The efficiency of this condensation reaction could not be improved by using longer reaction times, by altering the order of addition of reagents, or using 2 equivalents of **208.** Product **209** was unexpectedly isolated entirely as the enol tautomer **212** (>99% enol as judged by analysis using ^{1}H NMR in $CDCl_3$) as opposed to the keto form, and could not be reduced by ATH DKR to give **210** using the conditions employed by Ludlow *et al*[122].(as judged by TLC)

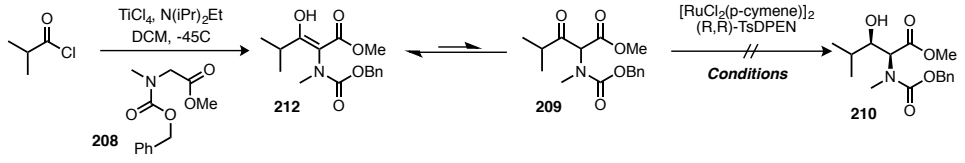

Figure 2.14 Unsuccessful reduction of 209 via ATH

We suspected that the cause of the failure to convert **209** into **210** resided in the position of the keto:enol equilibrium, and numerous different reaction conditions were employed in an attempt to circumvent this. There are several

published methods for the ATH of beta keto carbonyl derivatives[123] utilizing different hydrogen sources (HCO_2H, HCO_2H/NEt_3, HCO_2Na/H_2O, $^{i}PrOH$), catalysts (**213-215**, *fig* **2.15**), solvents (DCM, THF, $^{i}PrOH$, DMF, DCM/H_2O emulsion), temperatures (-5°C to 40°C). Hence a screen of reaction conditions was established to find an appropriate combination of conditions to reduce the challenging substrates **212:209**. A variety of solvents were examined, varying in degrees of polarity and capacity for hydrogen bonding in an attempt to preferentially stabilize the keto tautomer or by other means facilitate the reduction. By TLC no reduction was observed in H_2O (aggregation of starting materials), DMF[126], $DCM/HCO_2Na_{(aq)}$, iPrOH[120], DCM, a 5:2 HCO_2H/NEt_3 azeotrope or toluene. Catalyst loading could be increased up to 10% and the reaction run at 50°C with no trace of the desired product. Preforming the active 16 electron catalyst species is necessary for some reductions that are deemed particularly challenging[120] however reduction was again unsuccessful even with the more active tethered catalyst **213** (*fig* **2.15**). Finally, $ZnCl_2$ was introduced into the reaction wherein it was intended to function as a Lewis acid – stabilizing the di-keto arrangement, but conversion to the reduced product was not observed (*fig* **2.15B**).

Despite surveying a wide variety of reaction conditions, the starting material could not be reduced and was often recovered almost quantitatively.

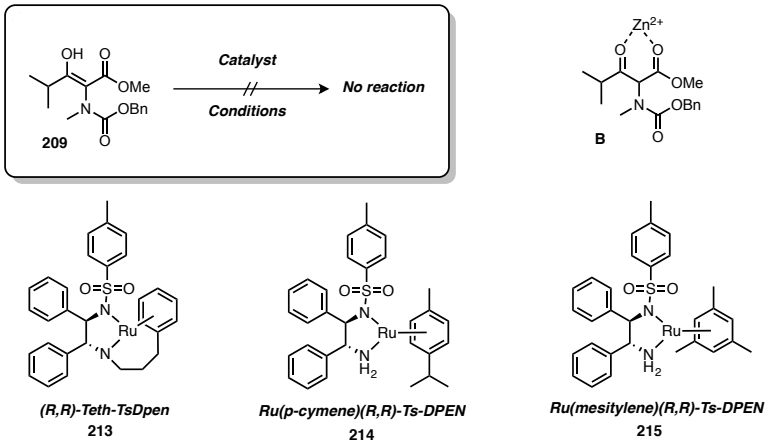

Figure 2.15 Catalysts employed in failed ATH DKR attempts

Following this investigation of reaction conditions, and varying the nitrogen protecting groups (CBz, Bz), it was concluded that the lack of reduction was directly due to a lack of keto tautomer at equilibrium, even though inter-conversion may take place to some extent.

The successful reduction of γ-alkyl β-keto α-amido esters has previously been reported[122], which were isolated primarily as ketones, as well as the separate reduction of γ-aryl N-methylated substrates[124]. The γ-alkyl substrates however, universally contained hydrogen on the amine in the alpha position for participation in intramolecular hydrogen bonding, or harboured an aryl group in the γ-position (*fig* **2.11A, B**). Both of these features stabilise the keto tautomer preferentially, compared to the enol tautomer.

To emphasize the vital importance of intramolecular H-bonding, a synthesis of N-methyl (*2S, 3R)* 3-hydroxyleucine was carried out, *fig* **2.16A** as well as a formal synthesis of MeBmt starting from 3-buten-2-ol, *fig* **2.16B**. Both syntheses required stepwise N-methylation and stereochemical inversion at the *3*-position of the resolved alcohols **217** and **220**.

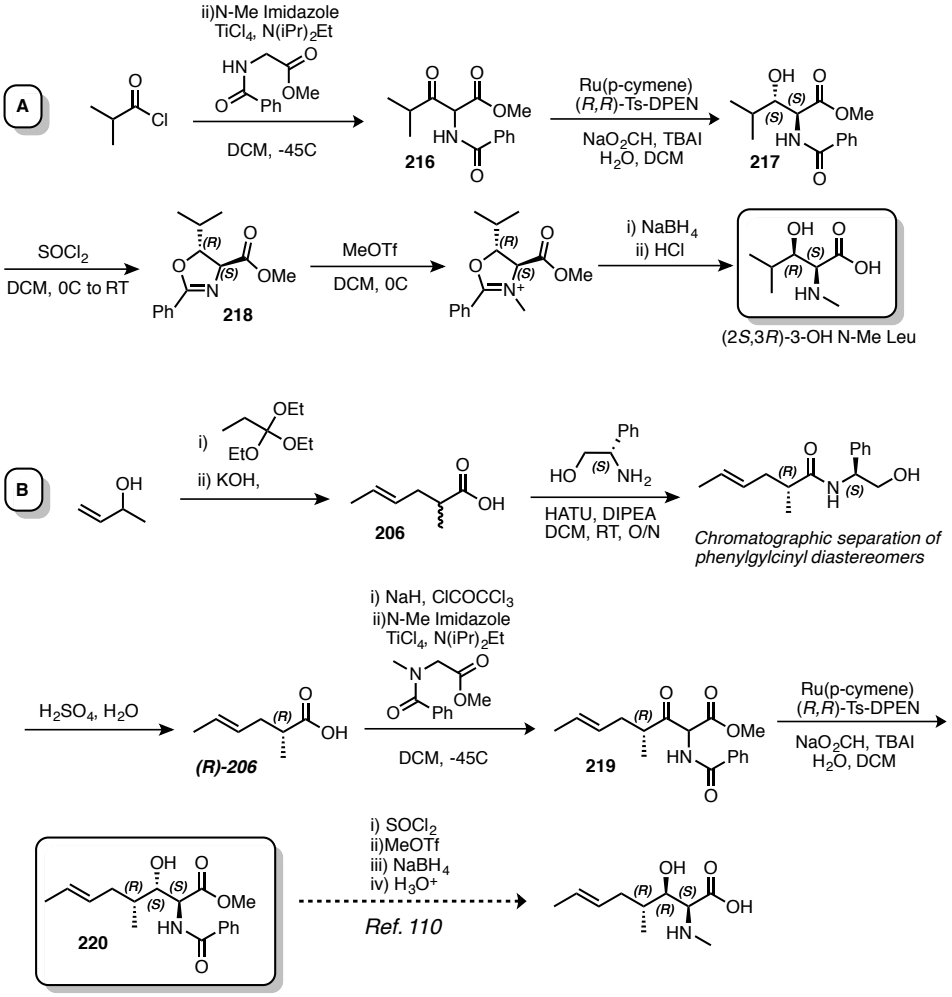

Figure 2.16 A synthesis of (2*S*,3*R*)-3-OH MeLeu and a formal synthesis of MeBmt starting from 3-buten-2-ol.

In the synthesis of N-Me leucine, *fig* **2.16A**, isobutyryl chloride undergoes a titanium chloride catalysed crossed Claisen condensation with a benzoyl protected glycine methyl ester, yielding ATH DKR substrate **216** in 54% yield. DKR as described by Somfai et al employing sodium formate and Ru(p-cymene) (R,R) Ts-DPEN gives β-hydroxy α-amino derivative **217** with good diastereo- and enantioselection**.** Cyclisation to the oxazolidinone **218** with inversion at C^2 proceeded smoothly, yielding **218** in 89% isolated yield, analysis of coupling constants at this stage reveals a *trans* relationship between the ring protons, corresponding to an 'anti' configuration in the starting material **217** as depicted in *fig* **2.16A**. Methylation with methyl triflate and subsequent hydrolysis affords (*2S,3R*)-3-OH N-Me Leu.

The formal synthesis of MeBmt outlined in *fig* **2.16B** commences with the synthesis of (*R*,*E*)-2-methylhex-4-enoic acid **206**, followed by elaboration to the amino acid derivative analogous to *fig* **2.16A**. Although the synthesis of chirally pure **206** is reported via the diastereomeric separation shown, we sought to improve upon this by means of a direct synthesis of **206** utilizing an Ireland-Claisen rearrangement, which was contingent on the synthesis of enantiopure (*S*)-3-buten-2-ol. It was proposed that the stereochemical information present in the kinetically resolved (*S*)-3- buten-2-ol would be retained when subjected to an Ireland Claisen rearrangement [127,128], this sequence is described in *fig* **2.17**.

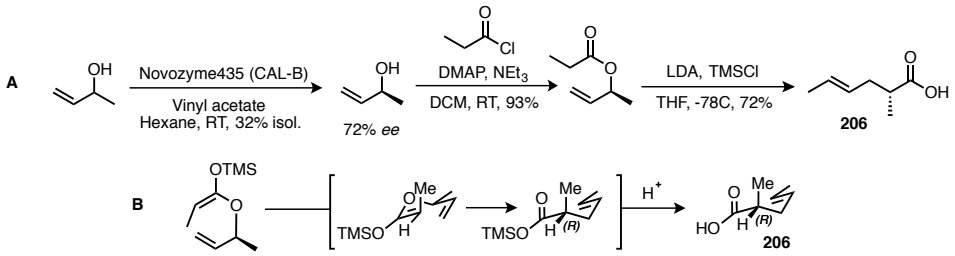

Figure 2.17 A synthesis of (*R*,*E*)-2-methylhex-4-enoic acid **206** from 3-buten-2-ol.

It can be seen how a 1-4 chirality transfer leads to retention of stereochemical information through the chair-like transition state, owing to the conformational bias of the equatorial methyl group (*fig* **2.17B**) after regioselective enolate formation. However, after a screen of ten commercially available lipases solvents and acyl donors, the maximum *ee* obtainable in the enzymatic kinetic resolution of (S)-3-buten-2-ol was 72%, with low yield resulting from difficult isolation of the volatile product. Further depletion of *ee* was observed in the Ireland-Claisen rearrangement step.

It was decided therefore, to move forward with the literature-established method for the synthesis and isolation of **206** previously discussed, *fig* **2.15**. Racemic (*E*)-2-methylhex-4-enoic acid was synthesized by a Claisen orthoester rearrangement of 3-buten-2-ol and triethyl orthopropionate. The acid was coupled to phenylglycinol utilizing HATU as a coupling reagent in DCM improving upon the literature yield. Complete chromatographic separation and acid catalyzed hydrolysis afforded the enantiopure acid **206**. Crossed Claisen condensation in a disappointing 22% yield furnished the β-keto derivative **219**, which was subsequently reduced to the *anti*- β-hydroxy α-amino precursor to MeBmt, **220**. The synthesis of MeBmt from intermediate **220** has been previously demonstrated[112] thus this constitutes a novel formal synthesis of MeBmt using ATH DKR as a key step.

2.4 Direct synthesis of MeBmt by *syn*-ATH DKR of β-keto amides

It has been noted that intramolecular hydrogen bonding is responsible for the anti-selectivity of reduction (*fig* **2.11***)*, however what has *not* been reported, as we have discovered, is that the hydrogen bonding appears to be responsible for the tautomer distribution and reactivity of this compound class *in general*.
On this basis it was postulated that a 6-membered ring intramolecular hydrogen bond could be introduced via replacement of the terminal ester moiety by an amide (*fig.* **2.18 B***)*. β-Keto amides have been previously utilized as ATH DKR substrates, though not for the synthesis of amino acids. It was hypothesized that intramolecular hydrogen bonding as described should provide the opportunity for stabilization via 6-membered ring hydrogen bonding leading to a substantial percentage of the keto tautomer and consequent *syn* reduction despite N-methylation.

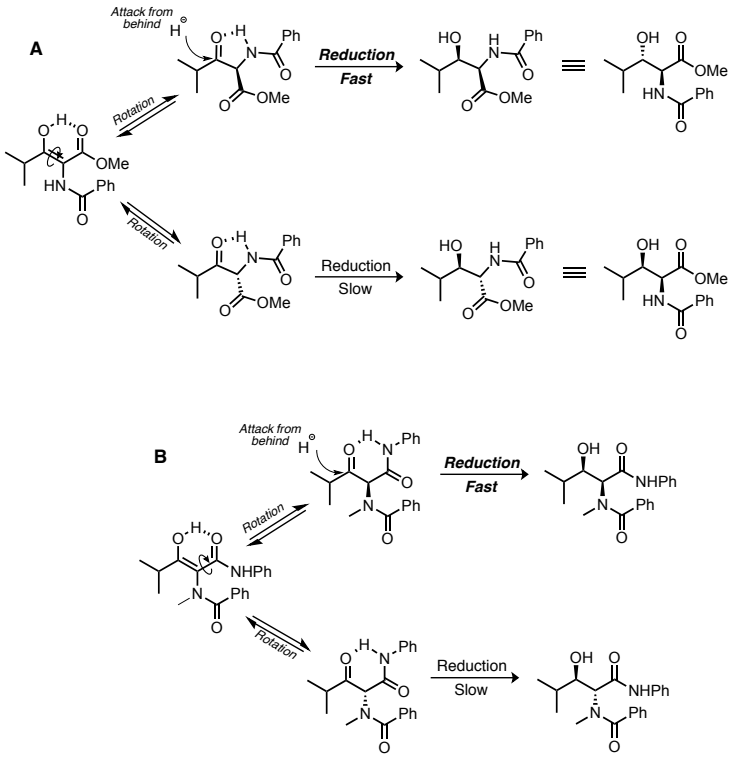

Figure 2.18 Comparative proposed intramolecular H-Bonding patterns in ATH DKR model

The Ti catalysed crossed-Claisen condensation proved unsuitable for the synthesis of N-methyl-β-keto precursors in the manner that we would desire. The alpha proton of was not acidic enough to be conveniently removed with the combination of $TiCl_4$ and Hunig's base; moreover the use of stronger bases such as LDA or LiHMDS is likely to lead to the racemisation of the α-position of the acid **206**, which would be untenable.

An excellent alternative proved to be a thioesters Claisen condensation. An optimized biomimetic crossed-Claisen condensation utilizing 'soft enolization' (Lewis acid assisted) of thioesters and N-acyl benzotriazoles gives reliable, high yielding gram-scale access to N-methyl-β-keto thioesters, which can be quantitatively transformed into the analogous β-keto amides in one step utilizing a thiophilic Lewis acid, silver trifluoroacetate, and an appropriate amine nucleophile[129] (*fig* **2.19**).

The efficiency of the Claisen condensation of thioesters is thought to be a consequence of the electronic structure of the sulphur atom. Due to the valence electrons of sulphur residing in the third shell the C-S bonds are longer in thioesters than the corresponding oxoester or amides. As a result there is less contribution to resonance stabilization caused by decreased O-S

orbital overlap. This raises the acidity of the protons on the neighbouring alpha carbon because the conjugate base can be appropriately stabilized as the enolate, thioesters therefore behave more like ketones than esters with regard to reactivity, which might not be expected considering S and O are both group 16 elements - and so the Claisen condensations are facile. The ubiquity of thioesters in biological systems for regioselective aldol reactions is testament to this.

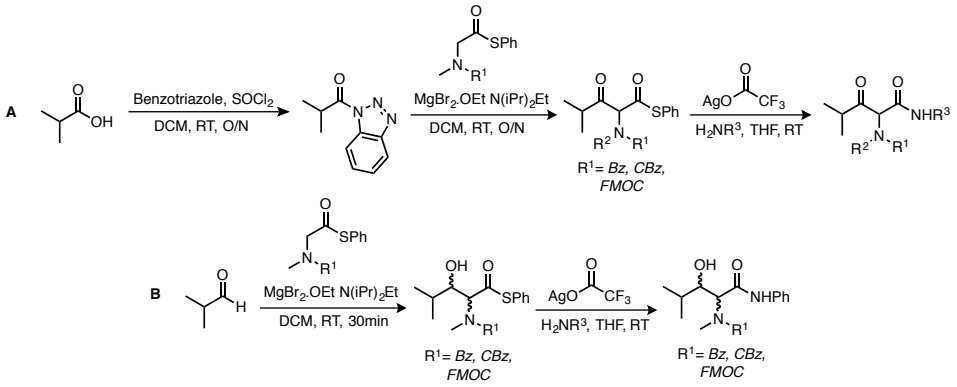

Figure 2.19 Synthesis of α-amido β-keto amides and α-amido β-hydroxy amides

2.4.1 Optimisation of *syn*-ATH DKR reaction

The reactivities and properties of these compounds are delineated in Table **2.1**. The ^{1}H NMR spectra of the N-methyl-β-keto amides ($CDCl_3$) are mixtures of keto and enol tautomers with substantial amounts of both, as opposed to the N-methyl esters, which exist entirely as the enol tautomers. The distinct proton environments (confirmed by analysis of HMBC spectra) can be discerned in the ^{1}H NMR of the beta keto amide substrates, which lends support to the hypothesis of *fig* **2.18B**, namely the intramolecular hydrogen bonding shifts the proton environments noticably downfield (H^b, H^c, *fig* **2.20**).

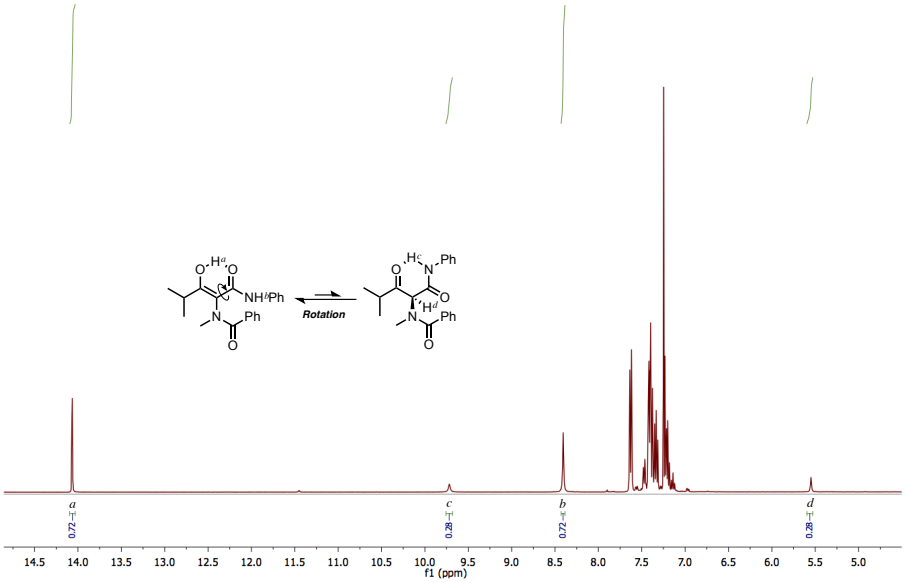

Figure 2.20 Analysis of intramolecular hydrogen bonding by NMR

FMOC, CBz and Bz were investigated as N-protecting groups for reduction - all three displayed susbtantial amounts of the keto tautomer at equilibrium as the N-Methyl-β-keto anilides.

To recapitulate, the N-Me methyl ester series exemplified by **209** is completely unreactive towards reduction, however under the same conditions successful reduction was observed for all three derivatives, entries **9**, **10** and **11** which proceed with very high enantio- and diastereoselectivity, albeit in poor overall yield. Although the Fmoc derivative gave the highest conversions, the CBz protecting group was chosen for optimization due to the substantially higher yields in the preceding reactions. Furthermore the Fmoc derivative decomposes under NEt_3/HCO_2H conditions, due to base-catalysed Fmoc deprotection (*Table* **2.1** [i]).

Table 2.1 DKR via ATH of α-amido β-keto amides

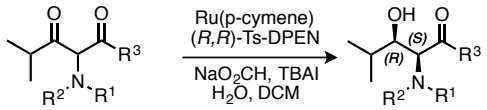

Entry	R_1	R_2	R_3	Keto:Enol[a]	Isolated Yield (%)	*dr*[c]	*er*[d]
1	H	Bz[e]	OMe	>99:1	26	15:85	50:50
2	H	CBz	OMe	>99:1	84	92:8	98:2
3	Me	Bz	OMe	>1:99	ND[l]	ND	ND
4	Me	CBz	OMe	>1:99	NR	ND	ND
5[g]	Me	CBz	NHPh	30:70	ND	ND	ND
6[h]	Me	CBz	NHPh	30:70	ND	ND	ND
7[i]	Me	CBz	NHPh	30:70	ND	ND	ND
8[j]	Me	CBz	NHPh	30:70	13	>95:5	>99:1
9[j]	Me	FMOC	NHPh	25:75	18	>95:5	>99:1
10[j]	Me	Bz	NHPh	28:72	4	>95:5	ND

[a] Keto:enol tautomers ^{1}H NMR, $CDCl_3$. [b] ^{1}H NMR of crude reaction material, [c] *syn:anti* ratio ^{1}H NMR of crude reaction mixture. [d] 3S:3R in major diastereomer. [e] Reduction with $NaBH_4$. [f] Product detected by LCMS but not in isolable amounts. [g] iPrOH, K_2CO_3. [h] HCO_2H:NEt_3 5:2, neat [i]DCM/HCO_2H/NEt_3. [j]DCM/HCO_2Na emulsion. [k]ND – Not Determined. [l]NR – No Reaction

A screen of five commercial catalysts (structures shown in Table **2.2**) reveals the tethered catalyst **D,** (*R,R*)-Ru Teth-TsDPEN (as pioneered by Wills[129] and coworkers) and to give the highest conversion, and isolated yield with almost complete stereocontrol, at 5% catalyst loading.

It was noted that the more contemporary tethered catalysts gave higher isolated yields than the non-tethered derivatives, (entries **1-6**) perhaps due to increased stability under the reaction conditions. Critically, an isolated yield above 50% demonstrates that the α-carbon is being racemised under the reaction conditions through tautomerism. In an attempt to increase the yield, the reaction time was increased to 120 hours, which resulted in no isolation of the product due to decomposition of the reaction materials.

Table 2.2 Optimisation of *syn* ATH DKR

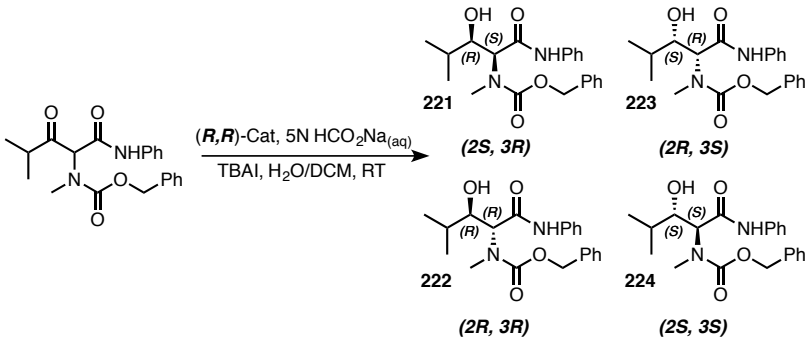

Entry	Catalyst	Cat. loading (%)	Solvent System	t (h)	Yield %[a]	*dr*[b]	*er*[c]
1	A	5	H_2O/DCM	40	36	>95:5	>99:1
2	B	5	H_2O/DCM	40	34	>95:5	96:4
3	C	5	H_2O/DCM	40	36	>95:5	97:3
4	**D**	**5**	**H_2O/DCM**	**40**	**64**	**>95:5**	**>99:1**
5	E	5	H_2O/DCM	40	40	>95:5	98:2
6	F	5	H_2O/DCM	40	42	>95:5	96:4
7	D	5	H_2O/DCM	120	ND	ND	ND
9	D	10	H_2O/DCM	40	(>99) 64	>95:5	>99:1

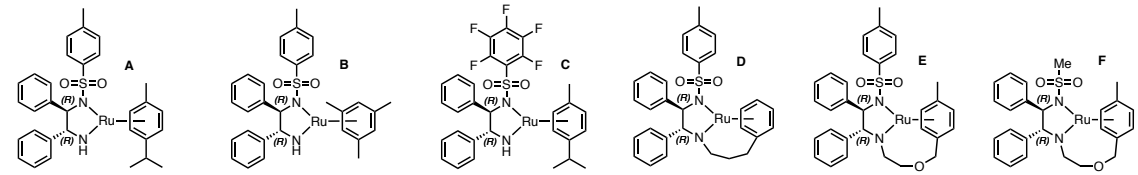

[a] Isolated yield following column chromatography (conversion in parentheses). [b] *syn:anti* ratio in H^1 NMR of crude reaction mixture. [c] 3S:3R ratio in major diastereomer – chiral HPLC.

2.4.2 Crystal Structure

The isolated virtually enantiopure product from entry **4**, *Table* **2.2** was recrystallized from a solvent system of hexane and Et_2O overnight to form fine, white needles, which were imaged using light-microscopy at various magnifications, shown in *fig* **2.21**

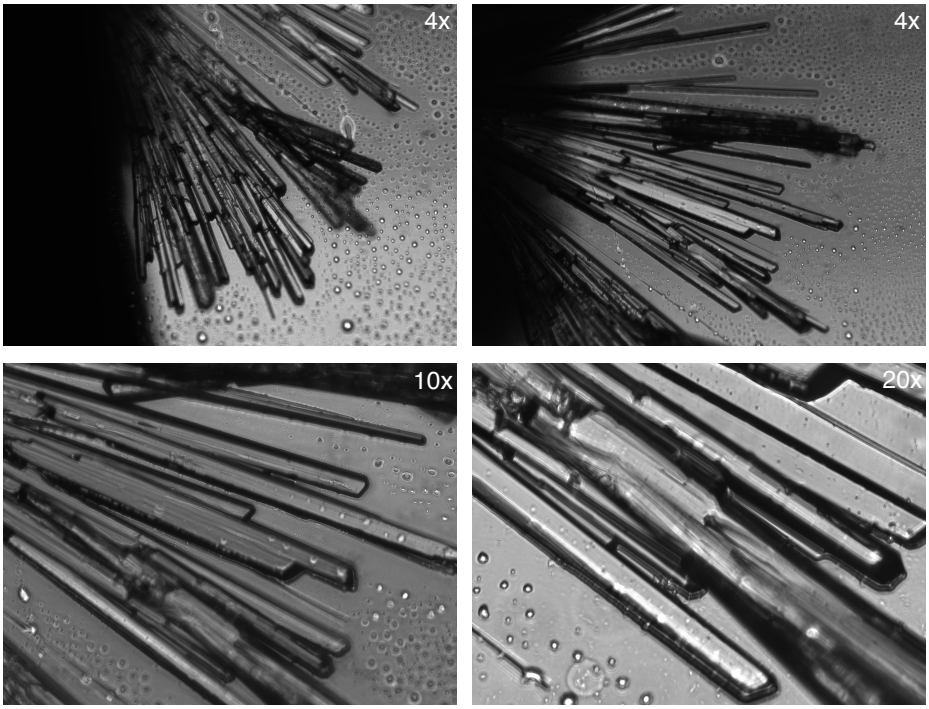

Figure 2.21 Microscopic images of re-crystallized ATH DKR product – entry **4**, *Table* **2.2**

The translucent crystals were analysed by Dr. Curtis Moore at the University of California – San Diego X-ray crystallography facility and the crystal structure thus obtained is shown below – *fig* ***2.20.***

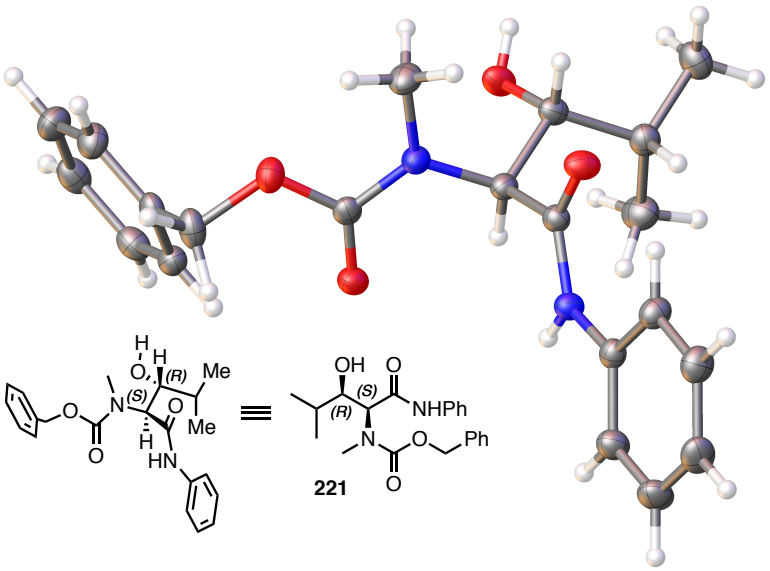

Figure 2.21 Crystal structure confirmation of bond connectivity and absolute stereochemistry - confirms *syn* (*2S, 3R)* - **221** as the major product of ATH DKR when using **(*R,R*)-Ru Teth-TsDPEN,** as predicted, *Fig* **2.15** *Tables* **2.1, 2.2.**

The structure is confirmed, unambiguously, to be (*2S,3R*) – **221**, as anticipated by rationalisation of catalyst approach. Stereocontrol is established through catalyst-selected *Re/Si* face attack, which occurs under the pre-requisite that this face is not blocked by the larger N-methyl-CBz substituent, this concept is illustrated in *fig* **2.21**[126]**.**

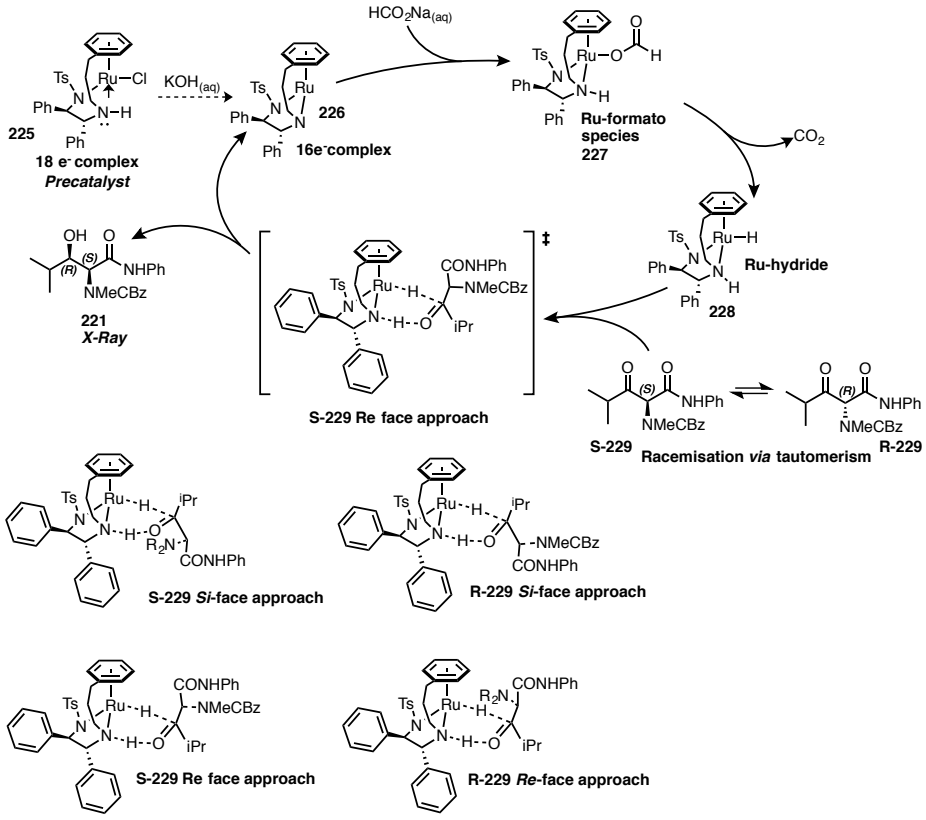

Figure 2.22 Proposed catalytic cycle of (*R,R*)-Ru Teth-TsDPEN in the synthesis of **221** by DKR/ATH.

2.4.3. Synthesis of MeBmt by *syn*-ATH DKR

The above, optimised, synthetic protocol was applied to **(R)-206.** Formation of the benzotriazolyl electrophile **230** by nucleophilic substitution, followed by crossed-Claisen condensation gives thioester **231** in 63% overall yield from **206**. Displacement of thioester with aniline and subsequent reduction of amide **232** by *syn*-ATH DKR affords N-methyl-β-keto amide **223**, which subsequently undergoes basic hydrolysis to MeBmt, **202**.

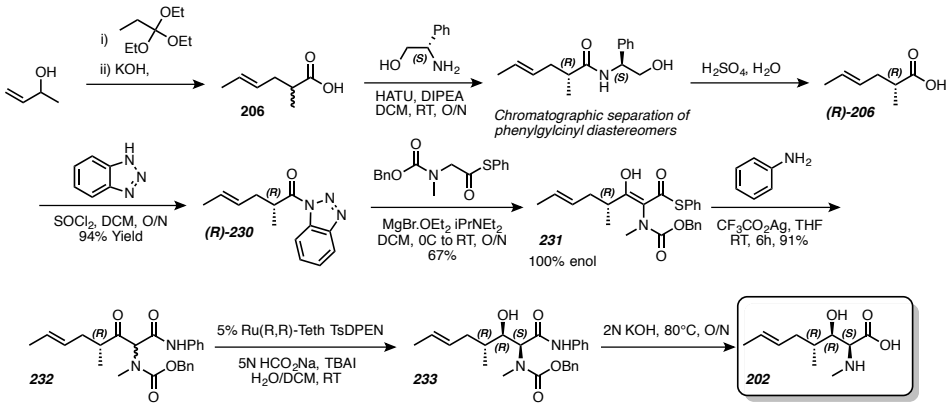

Figure 2.23 Synthesis of MeBmt via *syn*-ATH DKR

2.5 Summary, conclusions, and future work

We carried out a research programme to develop a synthetic route towards MeBmt, the unnatural constituent amino acid of CsA. The synthetic route thus developed is short, modular and stereodivergent, and will hopefully prove to be flexible in terms of alkyl side chain incorporation, which will enable the construction of CsA analogues that would not have been able to be synthesised by any other means. During the course of the programme, several key developments were made in understanding of the substrates for ATH DKR. Prediction and control of intramolecular hydrogen bonding has been proven to be pivotal in relation to predicting both the reactivity of the substrates, prediction of the 3 dimensional structures of reactive intermediates and stereoselection of the reaction. Rationalisation of the structure of stable reactive intermediates can be used to predict the *syn/anti* outcome of the reaction, the absolute configuration of which can be controlled by catalyst structure. In a medicinal aspect, future work in this area will concentrate foremost on synthesis of CsA analogues modified in the MeBmt position guided by molecular modelling. In terms of chemistry and methodology development, future work will focus on the use of protecting groups to direct the reaction, that are orthogonal in their deprotection procedure, to enable the synthesis of FMOC-protected derivatives directly. It is hoped that the methodology developed herein can be used to facilitate the synthesis of CsA analogues, specifically by solid phase peptide synthesis, with the goal of optimising the systematically optimising the properties of CsA for use in the treatment of HCV.

3

Phenotype based drug discovery: Pharmacological development of 'Chemotype 3' as an inhibitor of HCV assembly.

3.1 Introduction

As previously outlined, recent advances in HCV therapy since 2011 transformed frontline therapies with the introduction of DAA's and combination therapies of these treatments. End-game treatment of HCV will involve highly efficacious pan-genotypic multi-drug regimens. The individual drug components will likely exert their effect through different mechanisms of action to reduce the possibility of viral adaptive mutations and resistance. The regimens will be simple to administer to ensure patient compliance, as well as affordable by all patient populations.

While the current treatments are effective at clearing HCV, what cannot be accounted for is the build up of drug-resistant viral mutants in the exceptionally large treatment populations as seen with HCV (150-170 million infected individuals) particularly towards NS5A inhibitors. They are also notoriously expensive. The fact remains that the sheer scale of the HCV pandemic is such that if 100% of infected individuals, at a conservative estimate 150 million, could be instantly diagnosed, and following this, the current state of the art treatment with SVR~90%[15] is administered at a cost of 12 trillion USD, (Harvoni or VIEKRA PAK $86-88k/treatment course) then there would remain a cohort of 15 million people harbouring infectious,

presumably drug resistant HCV, with no treatment options - approximately equivalent to the entire population of Guatemala.

Therefore, in addition to the newer therapies that have emerged, it is still necessary to pursue the development of new therapeutics that can be used in combination with existing drugs, which possess novel mechanism of action against HCV. Cell based high throughput screens are an ideal platform for the discovery of such therapeutic agents because the suppression of viral proliferation (the phenotype) is not tied to the strength of interaction of a drug with one particular viral or host protein, but is tied simply to the decrease in viral load, for example by fluorescence output or viral protein staining quantification.[63]

3.2 Discovery of inhibitors of HCV through a phenotypic high-throughput screen

Previously in our group an assay platform with a cell-based HCV infection system was developed. The assay was successfully miniaturized to a 1536-well plate format that would be suitable for quantitative high-throughput screening of large chemical libraries to establish novel inhibitors of HCV[63]. A screen of the NIH molecular libraries small molecule repository (MLSMR, >340k small molecules[130]) was performed generating 4-point dose-response curves for every compound, resulting in approximately 3000 primary hits, that appeared to completely reduce HCV replication in the assay[131].

To ensure high quality hits further pruning of the data set was performed in terms of removing promiscuous binders and structural clustering analysis, resulting in a secondary set of 650 compounds. The 650 compound set were subject again to the initial efficacy test though this time developing an 11 point dose response curve, and also a cytotoxicity assay was carried out to remove any hits that were reducing HCV load by means of cytotoxicity. Following this an orthogonal HCV core staining efficacy assay was used to directly quantify the reduction in HCV proteins, confirming the specific action towards HCV. Using this system, more than 340k small molecules in the MLS library yielded 158 selective inhibitors of HCV for further investigation and development.

The 158 hits from the screen were further categorized by their structure, and the stage of the HCV life cycle they inhibited was deduced from a combination of cell-based infection assays.

3.2.1 Separation of hits by mechanism class

HCV pseudoparticles (HCVpp): These are defective retroviral particles which display HCV envelope glycoproteins, these virus particles may enter the cells but do not undergo replication. Culturing these viral particles with a drug candidate in hepatocytes, followed by isolation of intercellular HCV particles, and comparison with a control, allows us to ascertain whether there is an inhibitory effect on viral entry.[132,133]

HCV replicon assay: The HCV replicon assay is an older assay that utilizes integrated HCV RNA only, and is used to measure the effect that a particle may have specifically on the replication stages of HCV[133]

HCV single cycle assay (HCVsc): HCVsc infect cells in vitro and replicate but cannot assemble to form new virions, permitting study of inhibitory effects that would occur throughout the entire viral life cycle prior to assembly.

HCV cell culture (HCVcc): The isolation of the JF1 strain of HCV genotype 2a permitted the development of a cell culture assay in which HCV can infect, replicate and secrete from Huh-7 cells to form infectious HCV virions. This assay allows us to study the entire HCV replication cycle and was used as the primary assay in the high-throughput screen.

Using these assays, the 158 screen hits could be separated by class i.e. which stage of the HCV life cycle they act upon.

158 Candidates:

- 39 Entry inhibitors
- *14 Replication inhibitors*
- *18 Entry/replication*
- *37 Trafficking inhibitors*
- 47 Assembly/secretion inhibitors
- 3 Not determined

Based on these classes, and on the structural properties of the compounds, several hits were selected for lead optimization, chemical and pharmacological development.

With regards to ranking of assay hits in terms of favourable structures, the principle that the physicochemical properties of a molecule can be used to broadly predict aspects of its biological function, Lipinski's rule of 5[134] and its

more modern derivatives in QSAR analysis (polar surface area, rotatable bonds, various ligand efficiency metrics etc.) are useful tools for approximating the "drug-likeness" of a small molecule.

3.2 Drug interactions and resistance

Drugs that are used in combination have the capacity to modulate the potency of other drugs in a physiological setting. The effects can be antagonistic, sub-additive, additive or synergistic. Because the enzyme and receptor inhibition kinetics by a drug are hyperbolic in nature, *complete* suppression of viral replication can be more readily achieved in a physiological setting by inhibiting more than one enzyme that the virus is dependant on simultaneously. Using drugs in this manner is termed drug synergism. Strategies for drug synergy include: blocking multiple enzymes in the same pathway, blocking targets in different pathways that the target has in common, or the use of multiple drugs for the same target. As well as comprising extremely efficacious therapies, these strategies also make the development of resistant escape mutants much more unlikely. Highly active anti-retroviral therapy (HAART[135]) towards HIV is a relevant example of the benefits found from exploiting drug synergism, viral resistance can be avoided while still maintaining efficacy, and allows reducing the effective dose for each drug to minimise potential side effects. Direct acting anti-virals will always have the potential to create resistant strains through selection for viral mutants by point mutation among other possibilities.

Considering that most currently marketed drugs for HCV directly target the replication stages of the virus, the most attractive candidates in terms of looking towards a new synergistic therapy may reside in the less explored entry and assembly inhibitor classes of drugs.

3.3.1 Assembly inhibitors of HCV

There are several identified small molecule inhibitors of HCV that have their effects on the assembly stage of the virus[136-141]

Late stage trafficking of core proteins to the site of replication in lipid droplets requires the function of the diacylglycerol acyltransferase-1 (DGAT1)[142]. There are several known small molecule inhibitors of DGAT1[143] and inhibition of DGAT1 has been shown to severely impair infectious HCV virion production *in-vitro*, however a study attempting to determine the efficacy of DGAT1 inhibitors in treating HCV was terminated prematurely due to a lack of an antiviral effect.[144]

The grapefruit derived flavonoid Naringenin (*fig* **3.1**) has been demonstrated to inhibit HCV assembly[137,145]. Naringenin specifically blocks the assembly of viral particles - the proposed mechanisms are related to fatty acid synthesis, on which HCV is dependant for infectious particle production. Naringenin acts as a peroxisome proliferator-activated receptor α (PPARα) agonist leading to a decrease in VLDL production, which is required for effective HCV assembly and propagation of infectious particles. It has also been established that Naringenin inhibits the activity of microsomal triglyceride transfer protein (MTP), which in turn acts to inhibit ApoB mediated cellular egress of HCV.

Another inhibitor of the aforementioned transfer protein MTP is the antiarrhythmic compound Amiodarone, (*fig* **3.2**) which is found to inhibit both the assembly and secretion steps of the HCV life-cycle independent of genotype. Activity at the entry stage was attributed to down-regulation of CD81 receptors.[139]

Imino-sugar PBDNJ0804 was identified as an inhibitor of alpha glucosidases that are required for efficient folding and processing of HCV envelope glycoprotein E2, precluding HCV assembly and secretion.[138]

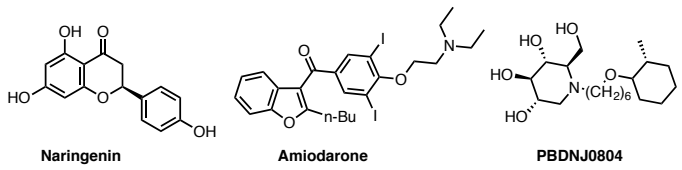

Figure 3.1 Previously identified small molecule inhibitors of HCV assembly

3.3 'Chemotype 3' as an inhibitor of Hepatitis C Virus assembly

From the assembly/inhibitor class, the candidate chosen for chemical optimization was N-benzyl-1-(2,4-dimethoxybenzyl)-N-phenethylpiperidin-4-amine, named Chemotype 3 (CT3), *fig* **3.2**.

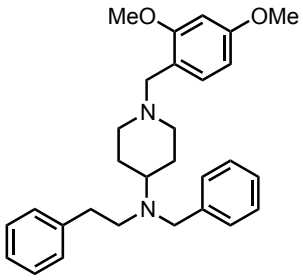

Assembly / Secretion Stage
Screening: IC_{50} = 4.67uM, CC_{50} 52.4uM
Commercial: IC_{50} = 1uM, CC_{50} = 11.5uM
Resynthesis: IC_{50} 2.03uM, CC_{50} 75.7uM
$T_{1/2}$: 2 min
cLogP: 5.41

Figure 3.2 Structure and pharmacological properties of CT3

CT3 is a potent inhibitor of HCV production acting on the assembly/secretion stage of the virus life cycle with an EC_{50} in the low single digit µM range, with an acceptable therapeutic index *in vitro*. CT3 displays no significant inhibition of replication in either the HCVpp, HCVsc or HCV replicon assays at a concentration of 10µM, however in the HCVcc assay CT3 displays >90% inhibition of viral replication at these concentrations. This demonstrates that CT3 must primarily act to inhibit HCV at a stage *after* viral RNA replication, for example viral capsid assembly in lipid droplets, trafficking to the cell surface, secretion into the extracellular environment or migration between cells.

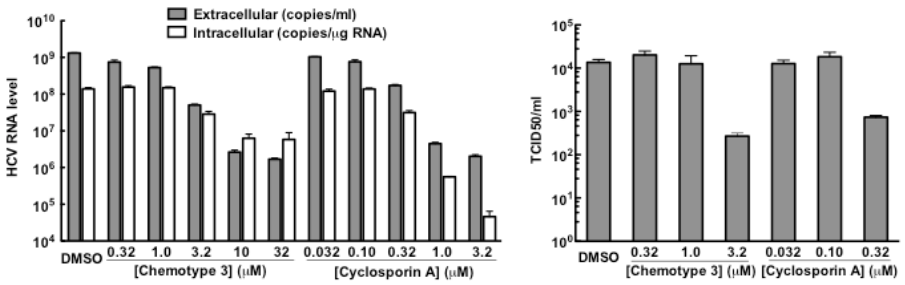

Figure 3.3 Analysis of differences between intra- and extracellular RNA upon treatment with CT3

Upon treatment of HCV *in vitro* with CT3, intra and extracellular viral RNA concentrations are measured. As the concentration of CT3 increases, both intracellular and extracellular RNA decreases. Cyclosporin A, affecting the replication stage of the HCV life cycle caused approximately 4-log fold reduction in intracellular RNA copies, while the extracellular level reduced less than 3-log fold. Conversely, CT3 leads to only about 1-log fold decrease in intracellular RNA copies when causing 3-log fold reduction in extracellular RNA level over the concentration ranges shown. When extracellular medium is used to re-infect naïve Huh 7.5.1 cells, CT3 is shown to cause a dose-dependent reduction in TCID50 values, an orthogonal confirmation of its effect on extracellular RNA copies, *fig* **3.3.**

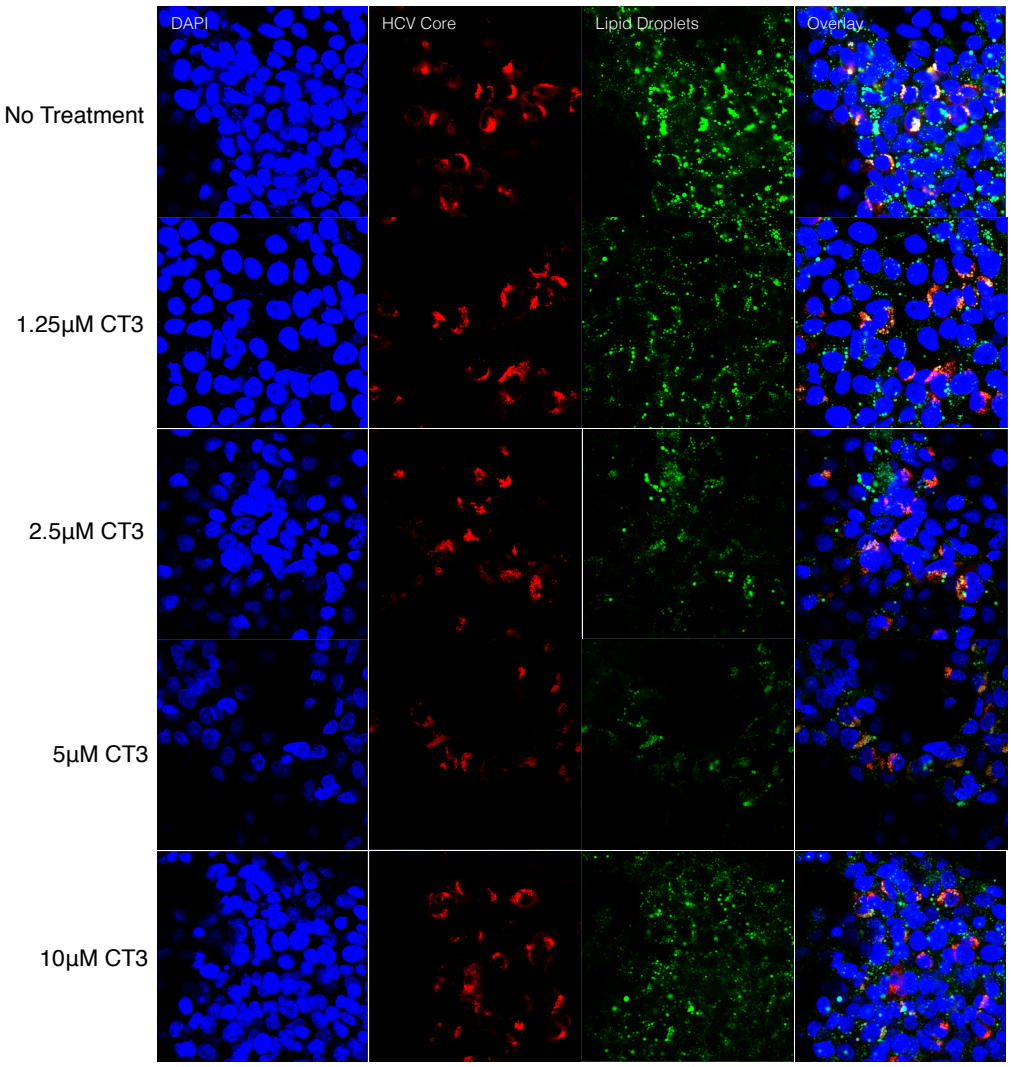

Figure 3.4 Immunostaining demonstrates CT3 specifically affects HCV assembly stages

Monitoring the co-localisation of HCV and cellular constructs allows us to discriminate between effects on viral assembly and viral secretion. HCV is known to assemble in lipid droplets, and as such HCV core proteins will co-localise with lipid droplets during viral assembly – *fig*. **3.4**. Upon treatment with CT3, co-localisation of HCV core proteins and lipid droplets (shown as yellow in overlay) decreases with increasing concentrations of CT3, indicating that assembly is inhibited, if CT3 did act on secretion we would still observe assembly in lipid droplets. In summary, CT3 inhibits HCV production but acts in such a way to stop the viral assembly in lipid droplets, as opposed to stopping its replication or secretion of virus particles. CT3 appears to have little affect on the stages of the HCV life cycle before virus assembly.

CT3 comfortably meets the Lipinski parameters for hydrogen bond donors and acceptors, having two hydrogen bond donors (at physiological pH) and four hydrogen bond acceptors; it is a reasonably low molecular weight compound at 444.6 Da. Though the cLogP is high as drawn above, CT3 would exist as a salt at physiological pH facilitating water solubility. A medicinal chemistry based optimization program on this compound class was undertaken that was guided by *in vitro* cell based assays for efficacy and toxicity, as well as *in vitro* ADME consisting of metabolic stability in cultured human microsomes, measurement of solubility in water, and membrane permeability. The overarching goals of the program were to increase the potency of the compound and widen the therapeutic window, while improving the compound's metabolic stability, with aims towards proof-of-concept efficacy studies in mice.

3.3.1 Iterative synthesis of derivatives of CT3 and analysis of SAR

Biological analysis of fragments of CT3 **301-305,** *fig.* **3.5,** reveals that the benzylic group at the top of the molecule designated R^1 did not have any bearing on the efficacy of the compound. As such it was classified as auxophoric and excluded from the scaffold moving forwards. Both phenyl rings were required for CT3 to exhibit the potency of the original hit compound. Since the molecular target for this compound is unknown, a broad systematic exploration of the requirements for potency was undertaken.

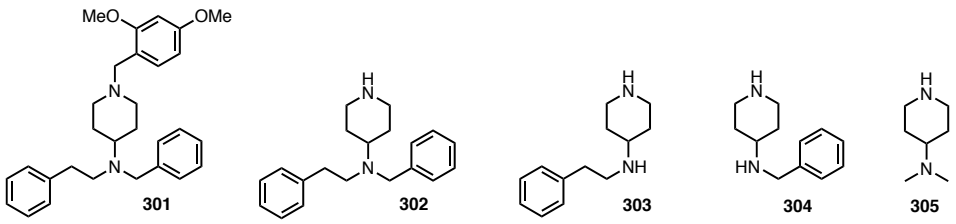

Figure 3.5 Analysis of fragments of CT3

The synthesis of analogues of CT3 at ring designated R^1 is outlined in *fig* **3.6**. Reductive amination of **306** utilizing sodium cyanoborohydride in DCE followed by acid catalysed Boc cleavage (*fig* **3.6 A**), or potassium carbonate catalysed S_N2 displacement of an α-bromo phenyl derivative (*fig* **3.6** ***B)*** facilitates the expedient synthesis of a wide variety of analogues in a systematic manner to probe the binding pocket. Amide analogues **331, 332, 336, 337, 342** and **343** are synthesized similarly - reductive amination followed by HATU catalysed amide coupling and Boc deprotection yields the primary and tertiary amide derivatives. The synthesis of benzoyl and sulfonamide derivatives **346** and **347** is also described below; they are synthesized by displacement of benzoyl chloride or sulfonyl chloride respectively under basic conditions. The first round SAR results are summarized in table **3.7** below. The activity and cytotoxicity are reported as the EC_{50} and CC_{50} respectively – the concentration of compound giving a 50% drop in viral load, and the concentration of compound exhibiting 50% cytotoxicity, in comparison with the DMSO negative controls. EC_{50} values are the average of at least 3 results.

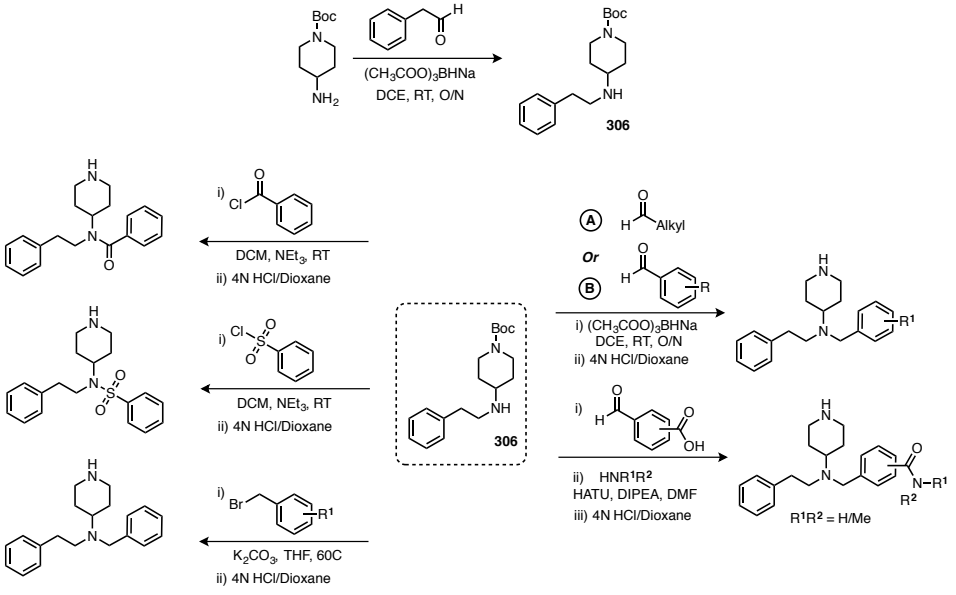

Figure 3.6 Different techniques employed in the synthesis of CT3 derivatives at R^1

3.4.1 Ring 1 Substitutions

In general, substitutions of hydrogen with moderately lipophilic, weakly electron withdrawing substituents such as halogens had a tendency to improve potency; Cl and Br substitutions **308, 309, 314 and 315 (Table 3.1)** exemplify this. Monosubstitution with Cl at either the *ortho, meta* or *para* positions improved potency to varying degrees across the board, with the *meta* position **314** exhibiting the biggest improvement decreasing the EC_{50} to 0.45μM. The same pattern is observed with Br substitutions **315, 309,** and **321** *meta* gives the biggest improvements in potency, followed by para and ortho. *Para* and *meta* F substitutions **310/316** gave modest increases in potency, as did *para* CF_3 **311**, but substitutions at other positions with these atoms did not improve potency. Notably, entry **333,** *meta*-Ph, improved the potency of the compound series slightly. The steric bulk of the phenyl ring with retention of potency indicates that steric clashes with the binding pocket (which remains unknown) likely do not affect decreases in potencies, and that the observed SAR in the *meta* and *para* positions can be well rationalized based on donation or withdrawal of electron density into or out of the benzene ring, as well as changes in the lipophilicity of the molecule overall - lipophilicity may be a crucial factor since the compounds are assessed in a cell-based assay.

p-CN derivative **328** was found to decrease activity, and so the potency may be quite reliant on lipophilicity. Electronically donating substituents methoxy and alkyl derivatives almost universally lowered the activity of the molecules. Amide derivatives **331, 332, 336, 337, 342** and **343** did not display any efficacy at the concentration limits of the assay (35μM), but they also did not display any toxicity (up to 100μM), potentially indicating that they were either not able to enter the cells, or that some sub-cellular localization of the materials was disrupted, again possibly alluding to the importance of lipophilicity in this series. Thiophene derivatives **324** and **325,** introduced as a bioisosteric replacement of a phenyl ring, did not maintain potency.

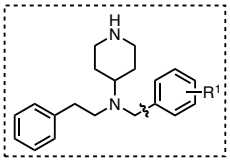

Structure	R^1	EC_{50} (μM)	CC_{50} (μM)	SI	Structure	R^1	EC_{50} (μM)	CC_{50} (μM)	SI
307		2.09 ± 0.41	26.29	12.55	326	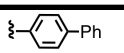	1.98 ± 1.28	15.85	4.86
308		1.36 ± 0.30	6.36 ± 1.74	4.68	327	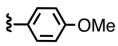	2.48 ± 0.33	25.24	10.18
309		1.78 ± 0.34	4.53 ± 0.14	2.54	328	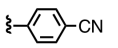	7.4 ± 2.14	27.3	3.69
310		0.92 ± 0.52	12.99	61.19	329	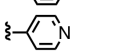	14.78	105 ± 0.00	7.1
311		1.07 ± 0.30	4.74 ± 0.02	4.45	330	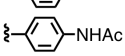	13.4	105 ± 0.00	
312		1.99	ND	ND	331	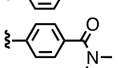	32.5	105	3.23
313		3.88 ± 0.79	4.86	1.25	332	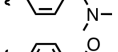	35 ± 0.00	105 ± 0.00	3.00
314		0.45 ± 0.13	4.55 ± 0.15	10.16	333	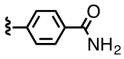	1.24 ± 0.20	10.06	8.11
315		0.98 ± 0.20	6.4 ± 1.60	6.55	334	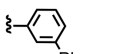	26.67	105 ± 0.00	3.94
316		1.21 ± 0.31	8.88 ± 4.01	7.35	335	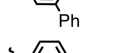	32.49	105 ± 0.00	3.23
317		1.76 ± 0.59	4.35	1.86	336	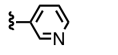	35 ± 0.00	105 ± 0.00	3.00
318		3.75	ND	ND	337	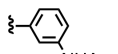	35 ± 0.00	105 ± 0.00	3.00
319		3.68 ± 0.55	5.40	1.47	338	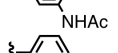	11.65	ND	
320		1.40 ± 0.18	4.45 ± 0.11	3.17	339	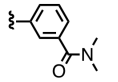	1.75 ± 0.37	20.81 ± 5.67	11.87
321		2.19 ± 0.77	4.56	2.08	340	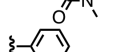	32.19	105 ± 0.00	3.26
322		5.22 ± 0.49	ND	20.11	341	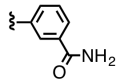	35 ± 0.00	82.98	2.37
323		2.61 ± 0.98	ND	1.79	342	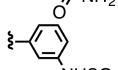	35 ± 0.00	105 ± 0.00	3.00
324		5.1	ND	ND	343	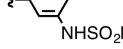	35 ± 0.00	105 ± 0.00	3.00
325		5.754	31.96	5.55					

Table 3.7 EC_{50} and CC_{50} of 1st round CT3 derivatives at R^1

Based on these results the binding site appears to favour electron withdrawing lipophilic substituents, though there is a possibility of halogen bonding arising from the antibonding orbital of the halogen substituents in the *meta* and *para* positions. Deactivating, electron-withdrawing substituents on the phenyl rings resulted in conservative increases in the metabolic half-life of the series, as described in table **3.8**. The emergent trend is one of steric bulk and deactivation of the phenyl ring resulting in a longer half-life, which may be expected. The most active analogue at this stage, **314**, increased the half-life from <1 min to 1.6 min. Though improvements were noted, it was clear that this was not the main substituent or area effecting the metabolic lability of the compound.

Structure	R^1	EC_{50}(μM)	CC_{50}(μM)	$T_{1/2}$ (min)	Structure	R^1	EC_{50}(μM)	CC_{50}(μM)	$T_{1/2}$ (min)
326	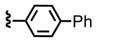	1.98 ± 1.28	15.85	23.4	308		1.36 ± 0.30	6.36 ± 1.74	3.7
311	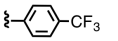	1.07 ± 0.30	4.74 ± 0.02	12.7	329		14.78	105 ± 0.00	3.6
333	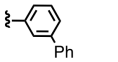	1.24 ± 0.20	10.06	8.9	330		7.4 ± 2.14	27.3	2.9
312	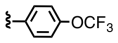	1.29 ± 0.70	ND	6.7	315		0.98 ± 0.20	6.4 ± 1.60	2.8
309	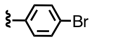	1.78 ± 0.34	4.53 ± 0.14	4.6	313		3.88 ± 0.79	4.86	2.3

Table 3.8 Top 10 slowest metabolized compounds from round 1 of synthesis arranged in order of decreasing half-life.

3.4.2 Linker 1 substitutions

Linker modifications from the primary amine in the 4-position of the piperidine scaffold to substituent R^1 were investigated in an attempt to improve the properties of the compound, described in table **3.9.** Lengthening the carbon chain to two, **344** and three carbons **345,** was found to slightly improve, and slightly decrease the EC_{50} respectively; amide and sulfonamide modifications **346** and **347** were deleterious - introduction of less lipophilic substituents again found to decrease the potency of the molecule, or alternatively the lone pair on the nitrogen atom now cannot form a salt at physiological pH, affecting the distribution of the molecule in the assay environment. Substitution of the R^1 side chain for n-alkyl **348 and 349** decreases potency, however the bioisosteric replacements cyclopentyl and cyclohexyl **350, 351** were still efficacious, giving the impression of building into a lipophilic pocket as before.

Again, it is noted that none of these compounds had any particularly positive effects on the half-life of the molecule.

Structure	R^1	EC_{50}	CC_{50}	SI	$T_{1/2}$ (min)	Structure	R^1	EC_{50}	CC_{50}	SI	$T_{1/2}$ (min)
344	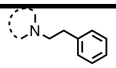	1.48 ± 0.05	19.54 ± 6.56	13.23	1.70	348		3.06 ± 0.26	97.15	31.75	<1
345	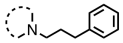	2.82 ± 0.46	9.00	3.19	<1	349		23.93	ND	ND	ND
346		> 35	ND	ND	1.60	350		1.16 ± 0.16	24.52 ± 1.62	21.2	1.7
347	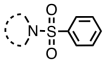	8.90	ND	ND	1.40	351		2.35	8.00	3.41	1.9

Table 3.9 Effects of R^1 linker modifications on the potency of the series

3.4.3 Ring 1 disubstituted analogues

Based on the efficacy results at this stage several *di*-substituted analogues were synthesized based on observed trends of the increases in potency in the Cl and Br series, as well as the increase in half-life. Results are described in table **3.10**.

Structure	R^1	EC_{50}	CC_{50}	SI	Structure	R^1	EC_{50}	CC_{50}	SI
352	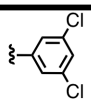	0.60 ± 0.12	4.40	7.33	358		2.31 ± 0.04	4.38	1.90
353		0.52 ± 0.3	14.10	27.38	359	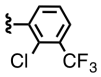	2.39 ± 0.28	7.15	3
354	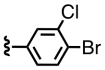	0.21 ± 0.04	5.64	27.29	360		3.42	7.40	2.16
355	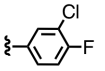	1.23	N/D	N/D	361	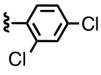	0.99 ± 0.35	25.50	25.8
356	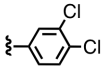	1.57	8.15	5.19	362	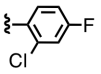	1.82 ± 0.06	4.57	2.52
357	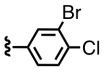	1.74 ± 0.7	8.28	4.75					

Table 3.10 Disubstituted R^1 analogues display high potency

As hypothesized, the molecules synthesized in table **3.10**, **353-363** were highly potent against HCV. Particularly noteworthy were compounds **353** and **354:** both compounds retained the *meta* chloro substituent from the first round of SAR, and boast sub-μM EC_{50}'s with a therapeutic index of above 25. Again for **354** the half-life was modestly increased from 1.6 min (**314**) to 2.4 min. The 3-chloro 4-bromo substituent of **354** shows increased potency and increased half-life while retaining the same therapeutic index as the original hit molecule.
While other compounds did out-perform this molecule at this stage in terms of half-life or other singular parameters, *on balance* it was decided that this was the most suitable molecule to take forwards for further modification.

3.4.4 Lipophilicity and met-ID analysis

Analysis of the lipophilicity of the compounds synthesised reveals a trend that does not correlate potency with a specific cLogP *per se*, but does appear to suggest a cut-off point after which compounds lose potency.

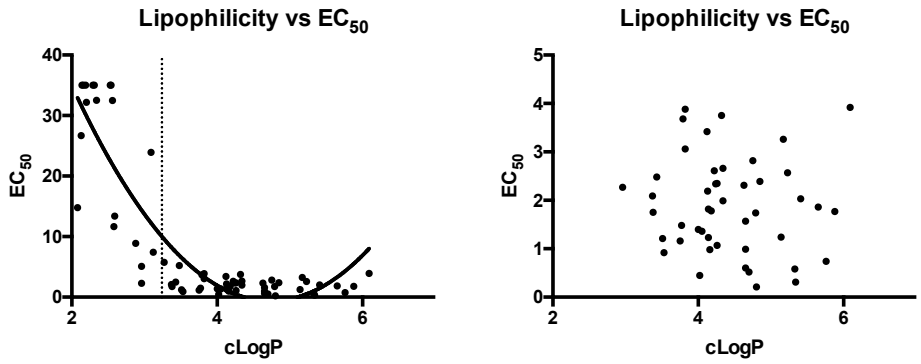

Figure 3.11. Analysis of how lipophilicity affects potency, calculated using ChemDraw 15 Professional (PerkinElmer Informatics)

Regardless of where the substitutions are in the molecule, potency drops off at cLogP values approximately equal to or below 3.2. However, if only potent compounds are analysed (EC_{50} less than 5μM), then there does not seem to be any correlation at all with lipophilicity and potency. To expedite the process of hit optimization from this point forwards target compounds were only considered if they possessed a cLogP ≥ 3.0.

A metabolite identification study (Met-ID) was performed to establish the particular points of metabolic susceptibility in the series.

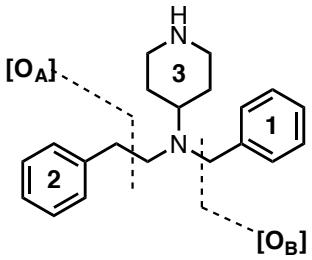

Figure 3.12 Locations of major metabolic cleavage for the CT3 series

Analysis of the microsome supernatant using mass spectrometry reveals major fragments corresponding to oxidative cleavage (**O**) in the benzylic position $\mathbf{O_A}$ as well as oxidative scission of the N-C bond towards ring **1**, $\mathbf{O_B}$, *fig* **3.9**. This leads us to the assumption that by modifying the linker between the central piperidine scaffold and ring **2** we may be able to effect metabolic changes in the molecule. Thus, several analogues were synthesised with modifications in the linker: N to Ring **2**, table **3.9**. Again, reductive amination of 1-Boc piperidine with 4-Cl, 3-Br benzaldehyde gives selectively monoalkylated **363,** which is used as a common intermediate in the synthesis of analogues.

3.4.5 Linker and ring 2 analogues

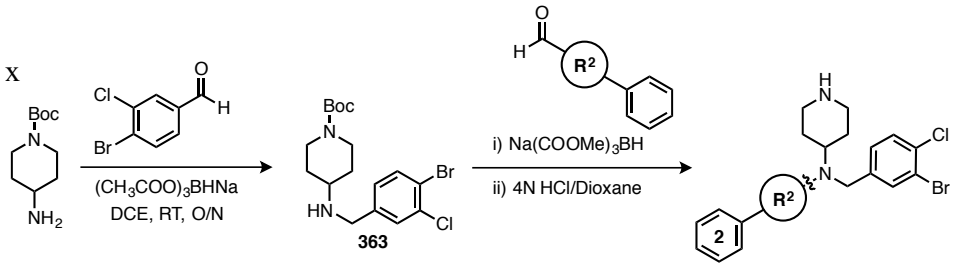

Structure	R[1]	EC50(µM)	CC50(µM)	SI	T1/2 (min)	Structure	R[1]	EC50(µM)	CC50(µM)	SI	T1/2 (min)
354		0.21 ± 0.04	5.64	27.29	2.6	368		0.48 ± 0.22	3.35 ±0.27	14.05	12.25
364		1.77	4.39	2.48	15.4	369		0.81 ± 0.26	1.24	1.52	ND
365		1.60 ±0.27	12.51	7.84	ND	370		2.57	ND	ND	1.89
366		2.55 ± 1.38	1.52	0.60	23.26	371	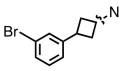	0.43	3.53	8.21	19.3
367		0.89 ± 0.31	6.47 ± 1.68	7.28	13.86	372	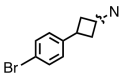	0.13	1.99	15.3	28.49

Table 3.13 Linker modifications and subsequent effect on metabolic stability

Besides the exception of the vicinal cyclobutane derivative **370**, modifications in this linker region were found to unilaterally increase the metabolic half life of the series, notably the introduction of the isopropyl moiety in compound **366** increased the half life by approximately 10-fold from 2.6 min to 23.2 min. The large difference in the half-lives for the cyclobutane derivatives **368** and **369** is especially noteworthy due to the similar structures. Compound **368** retains similar potency and toxicity profiles to the original **354** however the half-life has been increased from 2.6min to 11mins. **368** has fewer degrees of freedom and so may not be able to be accommodated into the CYP active site. The retention of potency speaks to the orientation of the phenyl ring in relation to the rest of the molecule, especially when comparing the potency of **368** and **369.** 1-3 or 1-2-substitution of the cyclobutane ring produces compounds with totally different geometries and this is reflected in the anti-HCV activity. It seems apparent that a phenyl group that protrudes away from the central scaffolding best serves this area of the molecule in terms of efficacy - this would mimic a presumed entropically favoured conformation in **354**. *Meta*- and *para*-Br derivatives **368, 371** and **372** respectively, again benefit from increases in metabolic stability, notably molecule **372** displays both the highest potency and metabolic half life seen in this series.

3.5 Comparative analysis of 372 and 301

A summary of the hit optimisation thus far is described in *fig* **3.14.** Compared to original assay hit **301**, compound **372** boasts a ~15 fold increase in potency in the cell-based HCV_{CC} assay and although the toxicity of the compound has increased, the therapeutic index change is offset by the increase in potency. The increased *in vitro* toxicity is definitely concerning but it is hoped that this can be addressed in further rounds of SAR. Compound **372** is slightly more lipophilic, though this alone does not significantly impact the molecular efficiency indices[146] - when studying the ligand efficiency (LE) and binding efficiency index (BEI), it can be seen that **372** is significantly more efficient in terms of potency per non-H atom (LE, *fig* **3.14**), and also potency per unit mass (kDa), even with the increased molecular weight (BEI *fig* **3.14**).[76] Ligand-lipophilicity efficiency (LLE) is a parameter that takes into account the lipophilicity of the compound founded on the observations of how lipophilicity tends to correlate with non-selective toxicity, and that this should factor into drug development when considering moving a compound forwards.[147]

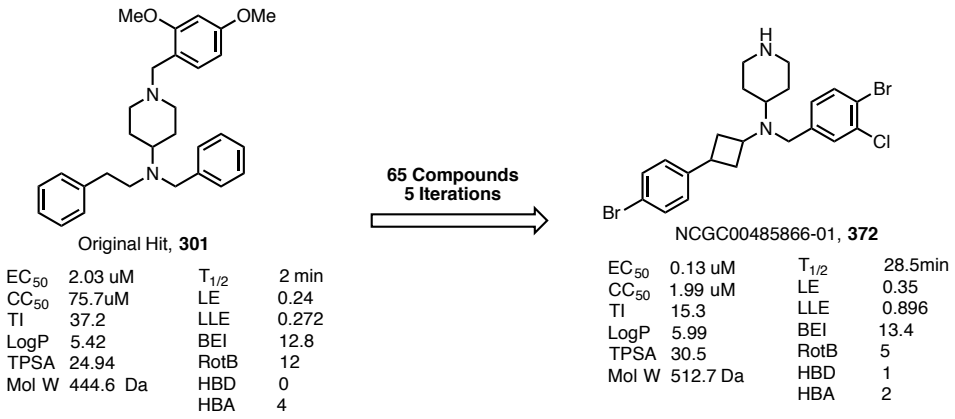

Figure 3.14 Comparison of some key chemical and biological descriptors between the CT3 original assay hit and the current lead **- 372**

The number of rotatable bonds has been decreased from 12 in **301** to 5 in **372** and as such **372** is more rigid and total hydrogen bond count (HBD+HBA) is lower. Rotatable bonds are an important molecular descriptor, correlated inversely with increased oral bioavailability independent of molecular weight. Increased MW tends to correlate with increased RotB, HBD and HBA by virtue of probability.[148]

Crucially the metabolic half-life ($T_{1/2}$) has been increased substantially from 2 min to 28.5 min in **372**, this was brought about initially by the finding that the cyclobutane linker was more metabolically stable, followed by further iterative derivatisation, and this value should be improvable in further rounds of modifications. Whether it is the alteration of the electronic/steric nature of the linker, or the increased rigidity of the molecule, or some other factor that is responsible for the change in metabolic lability is unknown. It may be that the less conformationally flexible derivative **372** is not able to accommodate into the metabolising enzyme's active site, as the flexibility of the molecule decreases and the equilibrium conformation moves away from what can be accommodated by an metabolic enzyme. We see an increase in the $T_{1/2}$, and this entropic cost is paid in synthesis of the molecule and its components. The drug is not the molecule as drawn, as a static entity, but a probabilistically distributed population of physiologically accessible conformational states. The goal here is to try to rigidify *into* the disease-relevant bioactive confirmations, and *out* of the metabolically labile (i.e. undesirable) conformations, assuming that these are not equivalent. It was primarily the increase in metabolic stability coupled with the retention of potency that led us to investigate the pharmacokinetics of **372** upon administration to mice.

3.6 In vivo, single dose, pharmacokinetics of 372 in CD-1 mice

Compound **372** is a lipophilic molecule and is completely insoluble in water so to increase its water solubility it was formulated as the oxalate salt (1:1). While the oxalate-**372** was also insoluble in water, it was found to be soluble in several organic/aqueous formulations, among others a 30% w/v solution of hydroxypropyl β-cyclodextrin (HPβCD) solubilized **372** at 2 mg/mL while remaining suitable for injection into mice. The material was only sparingly soluble in solutions below 30% HPβCD.

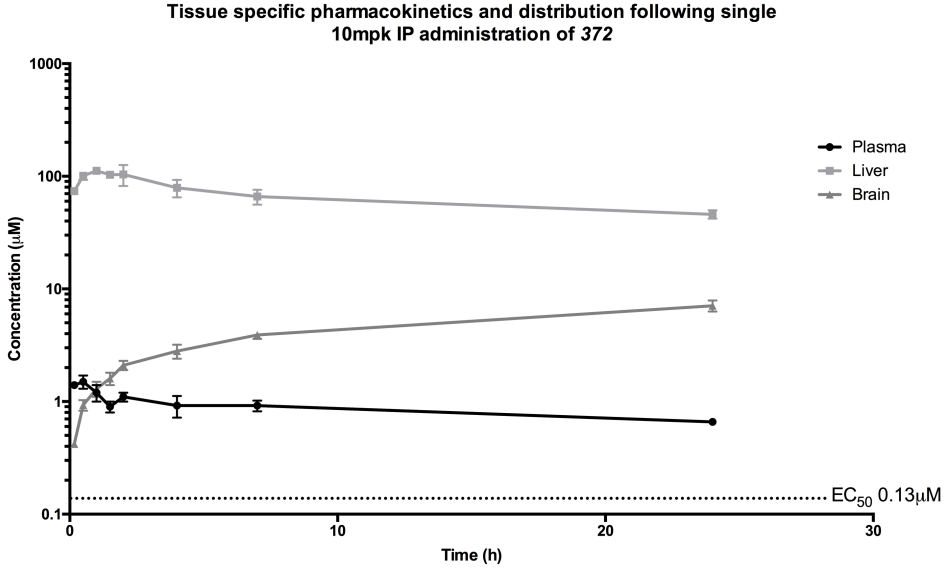

Figure 3.14 Plasma, liver and brain concentrations of **372** over a 24-hour time period after a single IP administration at 10mpk, average of 3 measurements.

The compound is solubilized in the vehicle and injected into the mouse peritoneum at a dose of 10 mg/kg - equivalent to a 62 mg dose in an average human. Following administration, maximum concentration is reached in 0.5 h in plasma, and 1 h in the liver. The levels of **372** continue to rise in the brain throughout the course of the experiment, whereas liver and plasma samples possess similar elimination profiles.

The maximum concentration reached in the liver is approximately 100-fold of the maximum concentration reached in the plasma and 1000-fold of the *in-vitro* EC_{50} of the drug (C_{max} liver and plasma: 112μM and 1.5μM respectively EC_{50} 0.13μM). In spite of *in vitro* CC_{50} of the molecule, no unusual behaviour or obvious toxicity of the mice was noted in the course of experiment.

The elimination phase of the experiment lasted too long, and the curve profile is too shallow, to accurately predict a $T_{1/2}$ from this experiment alone; the experiment should be repeated at a lower dose over a longer period of time in order to accurately determine the metabolic $T_{1/2.}$

Integrating the area under the curve AUC to determine the total exposure of material reveals that over 24 hours, compound **372** showed preferential liver localisation over plasma by a factor of 76. Considering that the compound is being developed as an anti-HCV treatment, extensive liver localisation is a favourable property, allowing appropriate therapeutic levels to be reached in the target organ with smaller doses of the compound.

3.7 Summary, conclusions, and future work.

A high throughout screen of small molecules yielded several candidates for hit optimisation and pre-clinical development. We specifically chose to develop candidates that target the entry and assembly stages of the HCV life cycle, since replication stage inhibitors are now both less suitable for incorporation into combination therapies, and more difficult to bring to market, making them less attractive to develop. The selected assembly inhibitor, designated CT3, has undergone 5 iterations of chemical modifications totalling 65 derivatives. This ultimately resulted in lead compound **372** which boasts approximately 15 fold increase in efficacy against HCV, more than 10 fold increase in metabolic half life and an increase in other molecule efficiency metrics as compared to the hit, though this is unfortunately offset by an increase in in-vitro cytotoxicity.

At this stage the molecule displays favourable liver distribution *in-vivo* with a long metabolic half-life. It must first be determined whether the half-life decreases at a lower dose in order to know how the molecule should be chemically modified to correctly tailor the molecule to suit daily dosing. SAR profiling should be continued to refine the potency, selectivity, toxicity and drug-like properties of the molecule, working towards a proof-of-principle study of efficacy in mice

4

Photoaffinity labelling in elucidation of the mechanism of action of the HCV entry inhibitor Chlorcyclizine

4.1 H_1-Antihistamines

H_1-antihistamines are histamine receptor inverse agonists that are specific for the H_1 receptor (of H_{1-4}) The four receptor subtypes have distinct and discrete biological functions with histamine as their endogenous ligand[149]. They are classified as inverse agonists as they stabilize the inactive state of the constitutively active histamine G-protein-coupled receptor (GPCR). There are over forty 1st and 2nd generation H_1 antihistamines available for clinical use. 2nd generation derivatives were introduced in an attempt to mitigate the CNS side effects associated with brain penetration.[150]

Antihistamine compounds as inhibitors of HCV

Recently, our group[151] and others[152] reported on the anti-HCV efficacy of the pre-approved drug chlorcyclizine (CCZ) *fig* **4.1B**. Using a previously established high-throughput format HCVcc assay, a screen of the NCGC pharmaceutical collection (NPC, 2400 small molecules[153]) was conducted for inhibitors of HCV. From this screen, eighteen anti-histamine compounds with diverse structural features were identified as primary hits. In a second confirmatory screen against HCV-Luc, fifteen exhibited more than 40% inhibition of HCV at 10μM concentration with acceptable toxicity profiles. Structures are shown below.

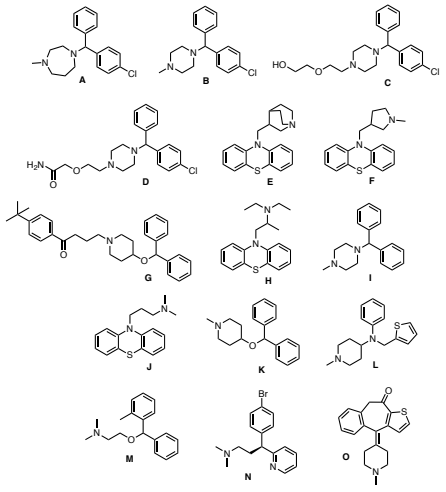

Structure	HCV-Luc % Inh ± SD	ATPlite % Tox ± SD
A	**93.8 ± 2.5**	**7.4 ± 6.9**
B	**91.4 ± 6.4**	**16.4 ± 7.4**
C	**89.5 ± 8.7**	**14.9 ± 7.9**
D	**89.3 ± 7.9**	**5.3 ± 2.1**
E	**73.7 ± 9.6**	**9.4 ± 6.8**
F	**70.8 ± 22.1**	**5.7 ± 5.4**
G	**70.3 ± 16.0**	**15.7 ± 11.0**
H	**68.6 ± 18.0**	**6.2 ± 6.4**
I	**68.0 ± 11.3**	**0.8 ± 12.4**
J	**64.4 ± 21.7**	**8.5 ± 7.3**
K	**55.2 ± 14.4**	**12.8 ± 3.9**
L	**53.9 ± 9.2**	**7.6 ± 4.5**
M	**49.7 ± 16.0**	**8.0 ± 7.2**
N	**46.5 ± 16.3**	**2.3 ± 6.3**
O	**45.5 ± 4.5**	**2.5 ± 1.9**
Cyclosporin A	**99.7 ± 0.1**	**14.2 ± 4.5**

Figure 4.1 Antihistamine derivatives that were found to inhibit HCV

The molecules are a mixture of both first and second-generation H_1 anti-histamines the anti-HCV potency of these drugs is not correlated with the potency of the compounds towards the histamine receptor, also the racemates of these compounds (ex. ***R*/*S*-CCZ)** are just as potent anti-HCV agents as their chirally pure counterparts, which is not the case in histamine receptor antagonism. Together this suggests that these compounds have a mechanism of HCV inhibition that is not related to their anti-histamine properties. In terms of structural features, these molecules in general possess 2 phenyl rings, or a lipophilic area of equivalent size that are attached via a linker (C, O, N) that is then joined by a 2-4 atoms linker unit to a basic amine. These amines would be largely protonated under physiological conditions and so these molecules would be amphiphilic – a lipophilic section composed of 2 phenyl rings (phenothiazine, benzhydryl or isosteres of such) linked to a quaternary amine.

Compound **4.1B**, the pre-approved first generation H_1 antihistamine chlorcyclizine (CCZ) displays high anti-HCV activity *in vitro* with an EC_{50} of 44 nM, a very acceptable *in vitro* cytotoxicity profile (CC_{50} 49.8 μM, selectivity index 1132) and importantly is synergistic with currently approved HCV therapies[154]. In the human liver uPA-SCID mouse model of HCV infection (immunosuppressed mice engrafted with human hepatocyte that are stably infected with HCV genotypes 1b and 2a,) CCZ was shown to reduce HCV load to 100 fold of its original concentration over the course of 4 weeks of treatment with no emergence of resistance over the administration window.

Following this proof-of-principle experiment, the CCZ scaffold was selected for a hit optimization program to further tailor its pharmacological profile towards HCV treatment with the aim of increasing both its anti-HCV potency, increase and its metabolic half-life. Also we aimed to reduce its H^1 ant-histamine potency to decrease potential CNS side-effects as noted with 1st generation anti-histamines – this could be accomplished by either reducing affinity for the H_1 receptor or decreasing brain penetration.

Interesting structure-activity relationships emerged from the hit optimisation program[155]. A broad range of substitutions to the molecule were permitted in both the phenyl rings and the piperazine ring that allowed activity to be retained, so long as the amphiphilic nature of the molecule was disrupted. A summary is described presented in figure **4.2**.

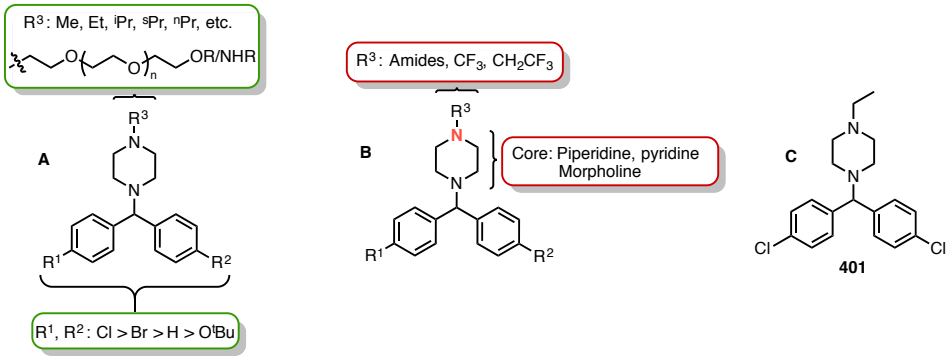

Figure 4.2 Highlighting key structural differences allowed. Substitutions permitted in **A** were broad in nature so long as the amphiphilic nature of the molecule was maintained. Removal of the acidity of the terminal **N** atom by induction with CF_3 or delocalization into a ring or amide bond abolished activity. **C** - Lead compound **401.**

At the R^3 position of the piperazine ring as drawn, H, alkyl substituents, and long polyethylene glycol derivatives were allowed and retained potency, *fig* **4.2A** However conversion of the basic amine to an amide or pyridine, substitution with CH_2CF_3 (Et is highly potent), or removal of the nitrogen resulted in a complete loss of activity, *fig* **4.2B**. Interestingly the isosteric replacement of the piperazine for a morpholine also completely abolished the activity suggesting that it is the ability of the terminal basic amine to become protonated at physiological pH that is important for its activity as opposed to other physicochemical properties (*fig* **4.2B, Red)**. Since the compounds are being assessed in a cell based assay, the increase in potency could be derived from specific intracellular localization caused by protonation in acidic cellular compartments such as mitochondria, lysosomes or other endosomal acidic compartments.

A hit optimisation program yielded a promising lead compound **401,** which, compared to CCZ**,** possesses 10-fold greater potency, a longer metabolic half-life, slightly less brain penetration than CCZ in mice, and an improved therapeutic window. Compound **401** was found to have 55% oral bioavailability at 10 mg/kg oral dosing in mice. Preferential liver distribution was observed over plasma with a 23:1 ratio over the course of 24 hours - *fig* **4.3**. The half life of the material was approximately 4 hours, with a major metabolite being identified as the des-ethyl analogue**,** which itself is a potent inhibitor of HCV. A dosing regimen was simulated based on the collected PK data arriving at the conclusion that dosing at 10mg/kg daily would be suitable to achieve a steady state concentration over one hundred fold the in-vitro EC_{50} even at trough concentrations.

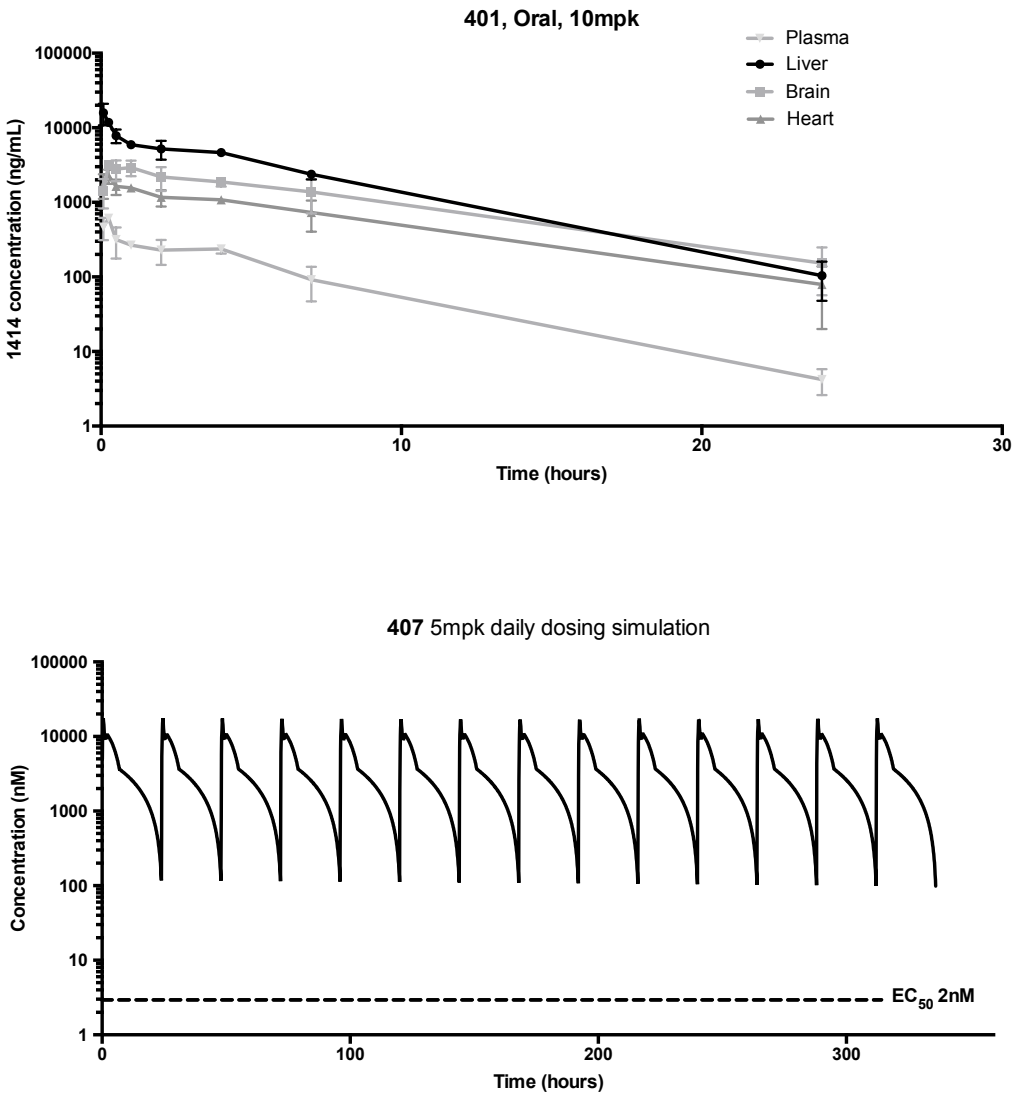

Figure 4.3 Single dose pharmacokinetic profile and simulated daily dosing regimen to achieve therapeutically relevant concentrations.

An IP efficacy study founded on the *in-vivo* PK data was conducted in the uPA-SCID mouse model that found daily IP dosing of 5mg/kg was sufficient to achieve a 1-log drop (90% decrease) in viral load over 28 days in 3 out of 4 mice (1 non-responder, data set **3,** *fig* **4.4**) with no emergence of resistance as is seen for DAA's in the same circumstances. Based on the data presented, and the fact that **401** is a minor and potentially benign modification of a pre-approved drug, it is an excellent candidate for further investigation with the aim of eventual incorporation into an anti-HCV combination drug regimen. Extensive pre-clinical evaluation is currently being pursued.

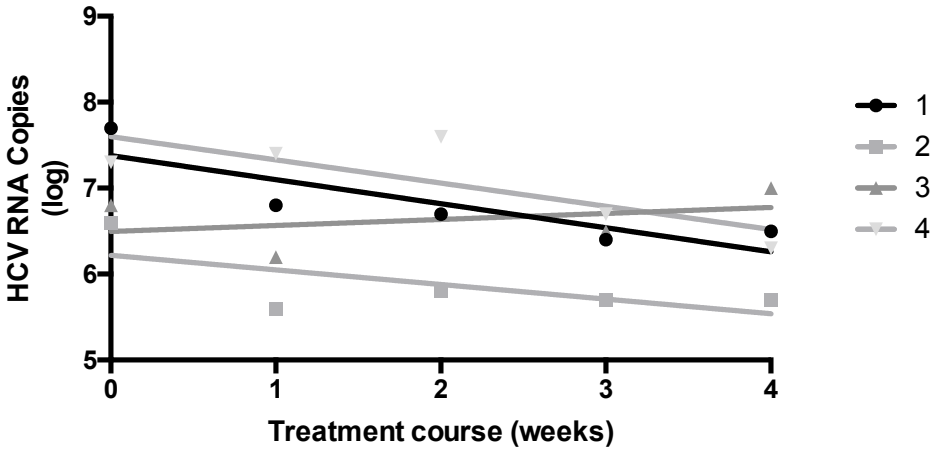

Figure 4.4 Decrease in HCV RNA copies during treatment with **401**

4.2 Investigating the mechanism of action of CCZ

As described in **Chapter 1** phenotypic screening does not discriminate based on biological or molecular mechanism of action, but solely on the ability of the small molecule candidate to affect a biological phenotype in question and in our system the read-out was reduced viral infection and replication. This has the potential to give rise to leads with broad and esoteric mechanisms of action that might not have been considered in a target-based approach scenario. We cannot know the mechanistic relationship of small molecule to HCV load decrease from the phenotypic assay alone and must either alter the small molecule to assess changes in outputs from the system (the phenotypic assay), or alter the system to assess the effect on the outcome of treatment. In this regard, referring to the latter, there are several cell-based HCV derived assays that can be used to probe different stages of the viral life cycle as described in detail in **Chapter 2**.

4.1.1 HCV life cycle assays

Based on its efficacy in the HCVsc and HCVcc assays, and the lack of potency observed in the HCVpp and HCV replicon assays, CCZ has been determined to act in the early stages of the HCV life cycle – before the assembly and replication stages, but without specifically targeting the early entry stages of the life cycle (extracellular binding events and particle endocytosis) as evidenced by a lack of potency in the HCVpp assays. Time of addition assays show that during synchronous entry, CCZ exhibits it's antiviral effect when administered before, during and up to 1 hour after viral entry into the cells - the inhibitory effect is lost when administered after 2 hours post-entry. This is in contrast to the fusion inhibitor Bafilomycin, which only showed significant inhibition when added up to 1.5-2 hours after synchronous entry.[151] Comparatively, this indicates that CCZ targets the late stages of entry into the cell - post viral entry but before replication. Convergence on a specific stage of the HCV life cycle gives us useful information: how best to optimize the material for optimal distribution, when might it be useful in a clinical setting, potential interactions with other drugs – positive or negative, but it does not give us a specific mechanism of action, and to elucidate *this* we need to ascertain precisely what CCZ binds to in order to exert its effect after it enters liver hepatocytes.

4.1.2 Target deconvolution approaches

There are several chemical techniques that can be used to deconvolute and resolve target protein identity that rely on the specific interaction of a probe molecule with a target of interest. Affinity chromatography is a well known technique of isolating purified proteins, and is a also an exploited technique in target deconvolution investigations, the modification of a small molecule with an affinity purification tag, such as biotin permits specific isolation of molecular targets, downstream processing and identification, often by mass spectrometry and sequencing. This process is known as affinity labelling.

A high binding affinity is necessary between the molecular probe and its target so that background proteins can be effectively removed during purification steps, but the reliance on this can be overcome by utilizing a specific cross-linking reaction between a modified version of the molecular probe and its putative target. For CCZ in particular, it may be expected that its potency relies to some extent on favourable localization within the cell, and this as well as its lack of numerous strongly coordinating groups (H-bond donors and

acceptors) implies that it may not have a very strong binding affinity for its target.

4.1.3 Photoaffinity labelling and purification in target deconvolution

*Photo*affinity labelling involves the use of a photo-cleavable reactive group; most widely used examples include diazirines, azides and benzophenones, each group with their respective advantages and disadvantages[156]. Once the small molecule of interest is reversibly, transiently associated with its protein target the photoreactive group is decomposed using UV light yielding a reactive intermediate that will covalently capture the target of interest enabling its identification. This approach to target identification requires careful planning and execution, but it removes the necessity for a high affinity to the target and can also increase specificity.

4.1.4 Proposed probe molecule for photoaffinity labelling

Trifluoromethyl diazirines[157] represent a small non-intrusive modification to the molecule of interest that can be reliably decomposed under UV light. Incident UV light promotes the decomposition of the CF_3-diazirine to a carbene with concomitant loss of N_2, the reactive singlet carbene species will then insert itself into a nearby molecule. In this manner, attachment of a diazirine species to a small molecule drug (SM), *fig* **4.5** allows the irreversible labelling of its target. The combined approach of photoaffinity labelling in combination with biotin mediated affinity chromatography has been central to the discovery of primary and secondary binding partners for several drugs in clinical development.[158,159] This methodology was applied to attempt to elucidate the mechanism of action of CCZ.

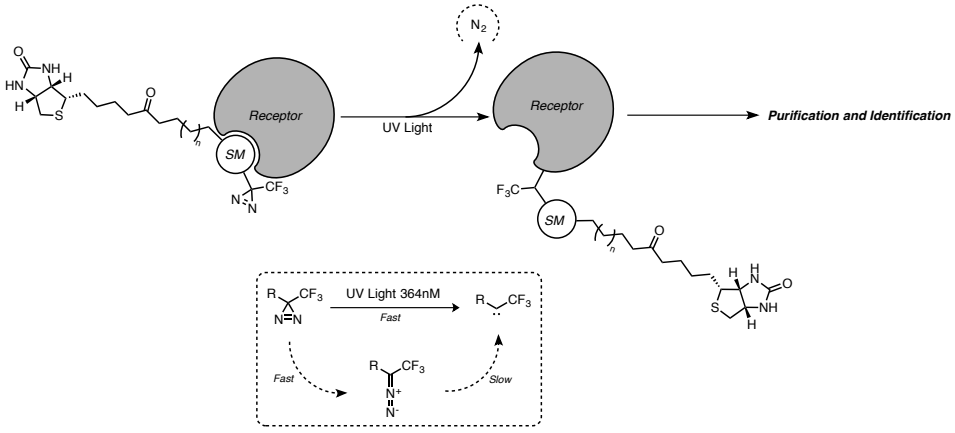

Figure 4.5 A - Schematic representation of the photoaffinity crosslinking process involving covalently attaching a small molecule probe (SM) to its putative target (insertion into amino acids) followed by affinity-based purification. **B** - decomposition pathways in 364nM UV light

Considering the potential time investment of producing a photoaffinity probe it is prudent to first examine the pre-existing SAR of the compound class, so as to ascertain which particular probe molecule has the largest chance of retaining activity as well as labelling the target protein.

For the CCZ scaffold, substitution of the para positions of the phenyl rings is permitted and the molecule retains potency throughout a broad range of analogues, even in the case of introduction of a sterically demanding O^{t}Bu group. This presents an attractive location for the introduction of a diazirine moiety due to the fact that some steric bulk is tolerated, whilst also being localized in the presumed binding pocket. At the top of the molecule as drawn, substitutions of the piperazine ring consisting of long polyethylene glycol chains have been shown to *improve* the potency of the molecule, and so with the distance from the presumed binding site of the bulk of the central scaffold, this represents an ideal place to attach an affinity handle. Indeed biotinylated CCZ has already been demonstrated to potently inhibit HCV replication. The long distance from the central scaffold of the molecule serves to minimize interactions between the biotin moiety and the binding site, retaining potency, and secondly to allow the space required for the streptavidin to bind to the biotin during pull-down without steric interference from the target protein.

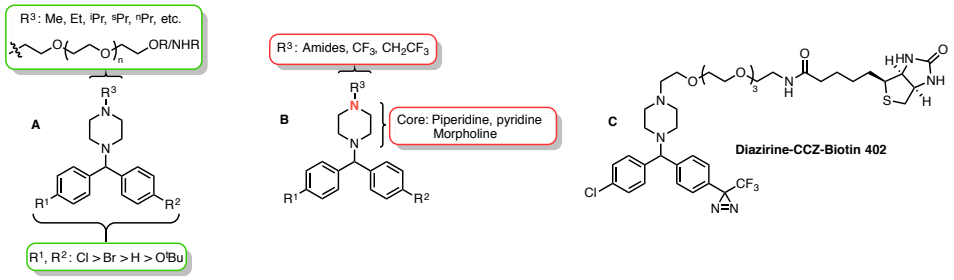

Figure 4.6 Highlighting key structural differences allowed. Substitutions permitted in **A** were broad in nature so long as the amphiphilic nature of the molecule was maintained. Removal of the acidity of the terminal **N** atom by induction with CF_3 or delocalization into a ring or amide bond abolished activity. **C** – Proposed photoaffinity probe, CCZ-Diazirine-Biotin.

4.2 Synthesis of Diazirine-CCZ-Biotin

Several strategies exist for the synthesis of trifluormethyl diazirine containing compounds[158]. In general, these involve the synthesis of a trifluoromethyl phenyl ketone, which is then elaborated to the diazirine in a short sequence and so the synthesis of the probe molecule was commenced along these lines.

The actual diazirine functional group is often developed in the latter stages to avoid chemoselectivity issues. Additionally, late stage addition of the Biotin handle allows other late stage functionalization to be introduced if necessary for example alkyne derivatives for click chemistry.

Nucleophilic displacement of *para*-iodo benzaldehyde with para-chloro magnesium bromide (*fig* **4.7***)* yields secondary alcohol **401** in 91% yield following column chromatography. Transformation to the alkyl chloride **402** with $SOCl_2$ in quantitative yield then permits displacement with Boc-protected piperazine affording the central scaffold of CCZ, **403.**

403 then undergoes lithium halogen exchange with nBuLi: after quenching with ethyl trifluoroacetate, furnishing the trifluoroketone intermediate **404** in approximately 40% overall yield from **401**. Two equivalents of n-BuLi are necessary to prevent poisoning of the lithiated CCZ intermediate, **413,** by the n-butyl iodide side-product as shown in *fig* **4.8A**. Excess butyllithium can intercept the primary alkyl iodide that is formed generating non-reactive by products. In a confirmation experiment, following addition of BuLi, quenching the reaction mixture with deuterated methanol yields deuterium or hydrogen insertion adducts when using 2 or 1 eq. of nBuLi respectively (detection by LC/MS) *figure* **4.8B**. Transformation from ketone **404** to diazirine **407** proceeds via oxime formation from the ketone using hydroxylamine HCl under basic conditions, tosylation of oxime **405** to **406** with tosyl chloride proceeds smoothly in 72% yield after purification. Reaction of the tosylate with $LiNH_2$ in liquid ammonia at -78°C afforded the Boc-protected 4-diazirinyl CCZ **407** in 91% from **406**. Synthesis of the probe molecule is completed by removal of the Boc group in HCl/Dioxane generating CCZ-diazirine **408**, followed by a thermally driven alkylation with tosylated polyethylene glycol derivative **412** to give protected intermediate **409.**

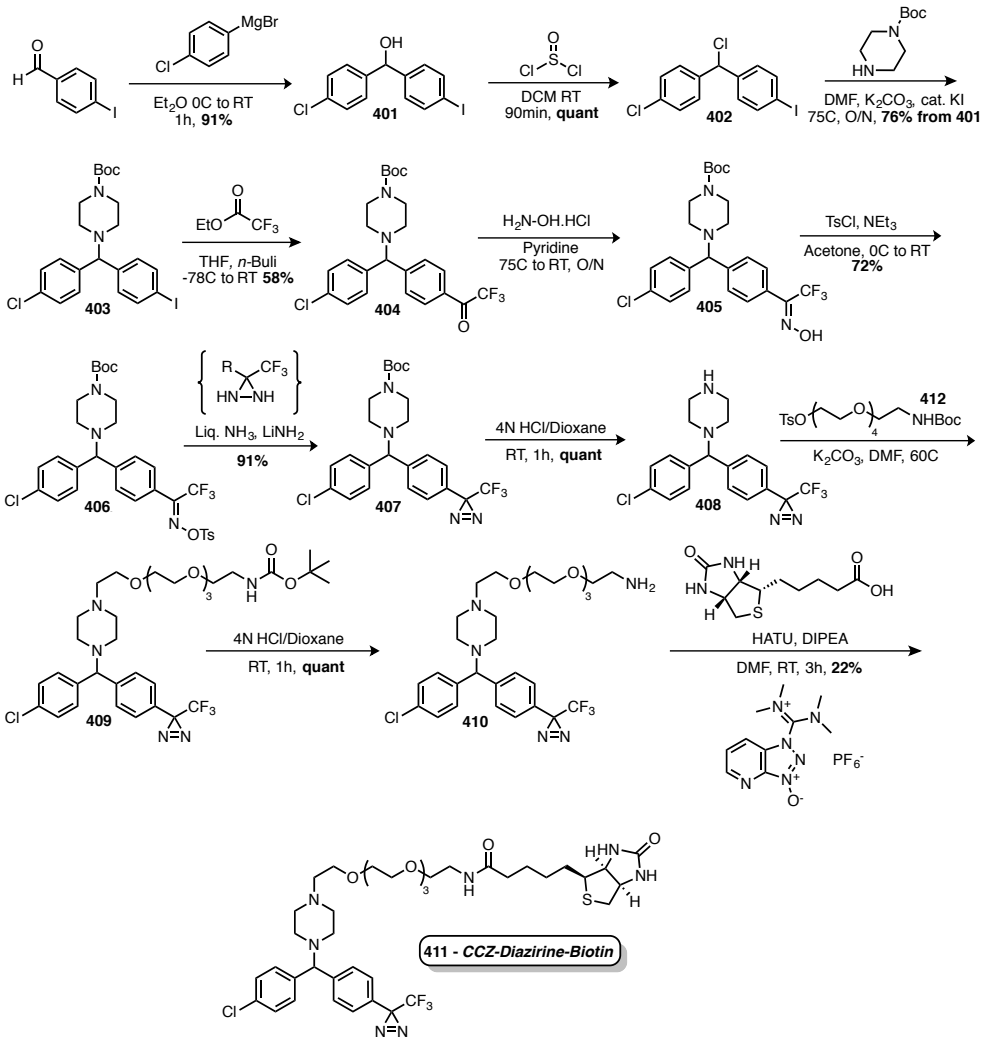

Figure 4.7 An 11 linear step synthesis of Diazirine-CCZ-Biotin

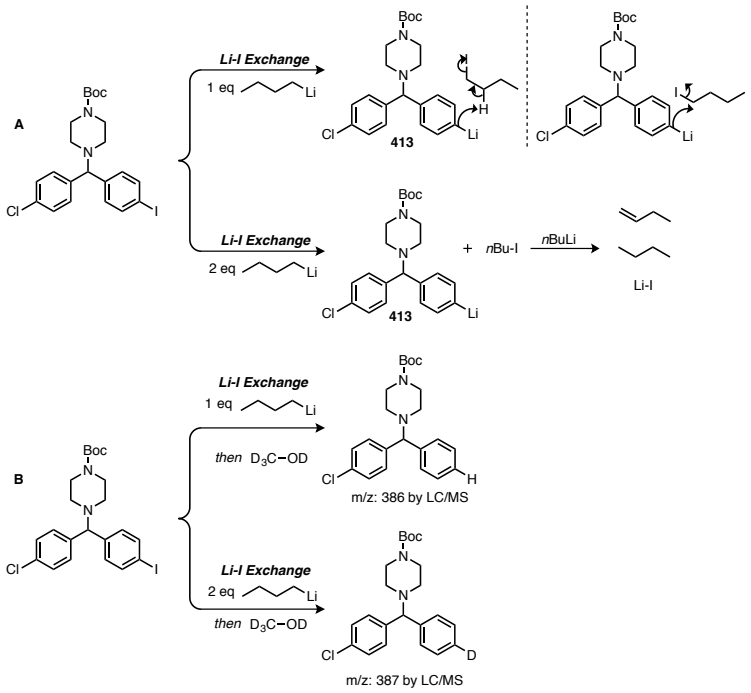

Figure 4.8 **A -** 1 equivalent of *n*-BuLi leads to substrate degradation through quenching of the reactive phenyllithium intermediate, which can be circumvented by employing two equivalents of *n*-BuLi, leading to benign spectator side products. **B** Evidence that reaction failure was due to abstraction from *n*-butyl iodide from lack of deuterium insertion.

Subsequent Boc cleavage gave primary amine **410**, a useful intermediate for a range of probe molecules. Condensation with biotin using HATU finally gives CCZ-diazirine-biotin **411,** which was purified by reverse phase column chromatography, and isolated as a TFA salt in its final form. The diazirine CCZ derivatives appear to be stable to ambient light conditions as are generally found in a laboratory, but they decompose quickly upon exposure to direct sunlight (as determined by LCMS). Once the diazirine functionality had been installed the intermediates/reactions were generally stored/conducted in the dark to prevent trace decomposition.

4.3 Biological and chemical characterization of Diazirine-CCZ-Biotin

Analysis of the anti-HCV activity of these probe molecules shows that potency is retained or increased in the HCVcc assay (increased in the case of **411**) as outlined in figure **4.9**, without increasing cytotoxicity, indicating that they share a mechanism of action with CCZ, *fig* **4.9**. On the basis of these results, it was decided to move ahead with **411** as the probe molecule for the mechanism of action (MoA) studies.

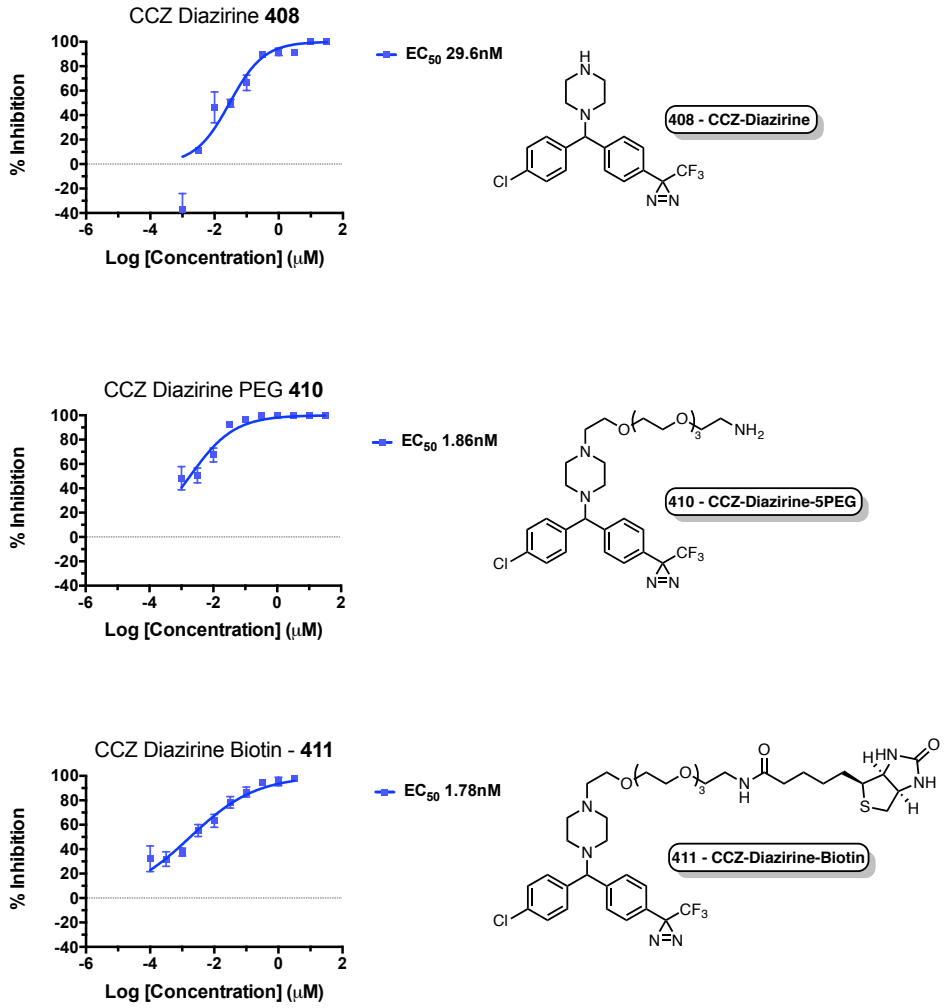

Figure 4.9 *Diazirinyl CCZ derivatives retain their potency in the HCVcc assay*

The degradation of **408** under UV light is studied to determine the optimal length of irradiation time of **411** that can be translated to a live-cell environment. 4.5mg of **408** is dissolved in 3mL of water, which is added to a watch glass and held under either i) a 4 watt TLC UV lamp at a distance of 2cm or ii) a 100 watt mercury bulb with a 365nM wavelength bypass filter. At predetermined time intervals over the course of 2 hours, 100uL is removed and analysed by LC/MS, the decomposition of this material and insertion into the solvent is outlined in *fig* **4.10.** Using the 4W TLC lamp diazirine activations is slow and is completed between 20 and 50 minutes of exposure.

Also observed are significant amounts of the transiently stable diazo rearrangement isomer **408C** *fig* **4.11**, indicating less than quantitative conversion to **415** in the given time frame. After 50 minutes the diazirine is completely depleted as detected by LCMS, however the concentration of **415** continues to increase, presumably due to slow turnover from **413**, *fig* **4.10**. On the other hand, decomposition using the 100-watt lamp results in full conversion to **415** and complete depletion of the diazirine starting material within 5 minutes. The results described were instrumental in the planning of the in-vitro crosslinking experiments, as described in the experimental section.

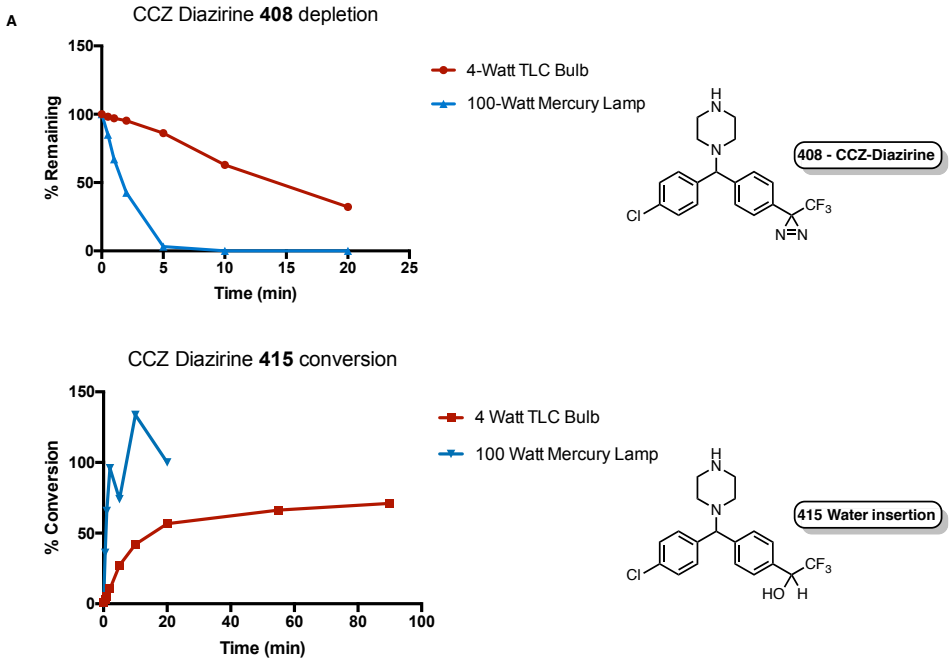

Figure 4.10 Conversion of CCZ-Diazirine to the water insertion product **415** as analysed by LCMS, a comparative analysis of how the wattage of the UV source affects the rate of reaction

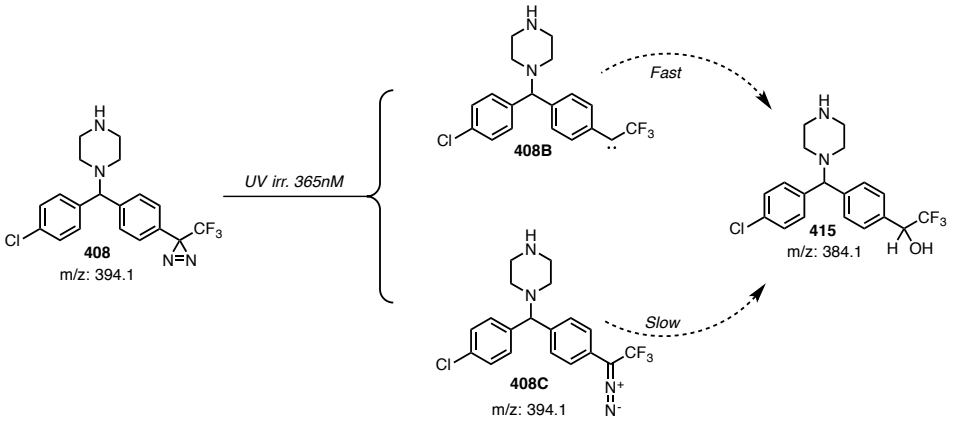

Figure 4.11 Mechanistic pathways involved decomposition of **408** and rationalization of the kinetics of diazirine-CCZ decomposition

4.4 *In-vitro* photoaffinity crosslinking

In a general experimental protocol investigating the binding partners of diazirine-CCZ-biotin, compound **411** is added to a cell culture dish containing Huh7.5.1 cells that was seeded 12 hours previously. The experiment is incubated for a specified amount of time after which, the experiment is irradiated from a few centimetres away, on ice, with the UV light source (4-watt TLC UV lamp or 100-watt mercury lamp with 365 nM filter) converting the CCZ-diazirine to the carbene. The cells are lysed, the lysate is harvested, and incubated with streptavidin bound to agarose beads (Pierce™ NeutrAvidin™ Agarose, *cat no. 29200*) to extract biotinylated molecules, then the beads are washed with detergents to remove non-specific binding proteins. The specifically bound, now purified biotinylated proteins can then be eluted using a denaturant buffer of 30mM biotin, 6M urea and 2M thiourea in PBS[160]. The protein samples are resolved via SDS-PAGE and transferred to a PVDF membrane, which is probed for biotinylated proteins using streptavidin-HRP. The bands are subsequently visualized using a high sensitivity chemiluminescent HRP substrate, the blot is analysed to look for specific bands in the experimental lanes, in comparison to controls.

4.4.1 Results

Initially experiments were performed using 1-hour incubation times at 1μM concentration of **411** and 25 minutes of irradiation using a 4-watt TLC lamp, with the time course based on experimental evidence – *fig* **4.10** the PVDF membranes are shown in *fig* **4.12.** 1 μM was chosen as the initial concentration, being >3-fold greater than the EC_{90} of 0.3 μM, which should ensure receptor saturation, while being significantly below the CC_{50} for the

molecule. Despite the increased intensity of the bands in the experimental lane (fig **4.12,** lane **4**), no *specific* bands were observed and this result could not be replicated. It was hoped that greater crosslinking efficiency could be achieved by using a high-powered lamp. A 100-watt mercury lamp utilizing a 365nM wavelength bypass filter was shown to completely activate the diazirine within 5 minutes (*fig* **4.10**). However again in the experimental lane no specific crosslinking bands were observed. Incubation of the CCZ diazirine probe with the cell lysate followed by irradiation yielded no specific crosslinking. Increasing the concentration of the probe from 1 μM to 10 μM (>30 x the EC_{90}) in an attempt to further saturate the presumed receptor again resulted in no specific crosslinking. Repeating these experiments re-affirmed the lack of ability to pull down a putative target (*fig* **4.12 B** Lanes **3** and **4**). Analysis of the cell culture medium from the cell lysate cross linking experiment reveals isolation of a protein with the same molecular weight as albumin, with similar decomposition products in western blot (*fig* **4.12,** lane **5**)

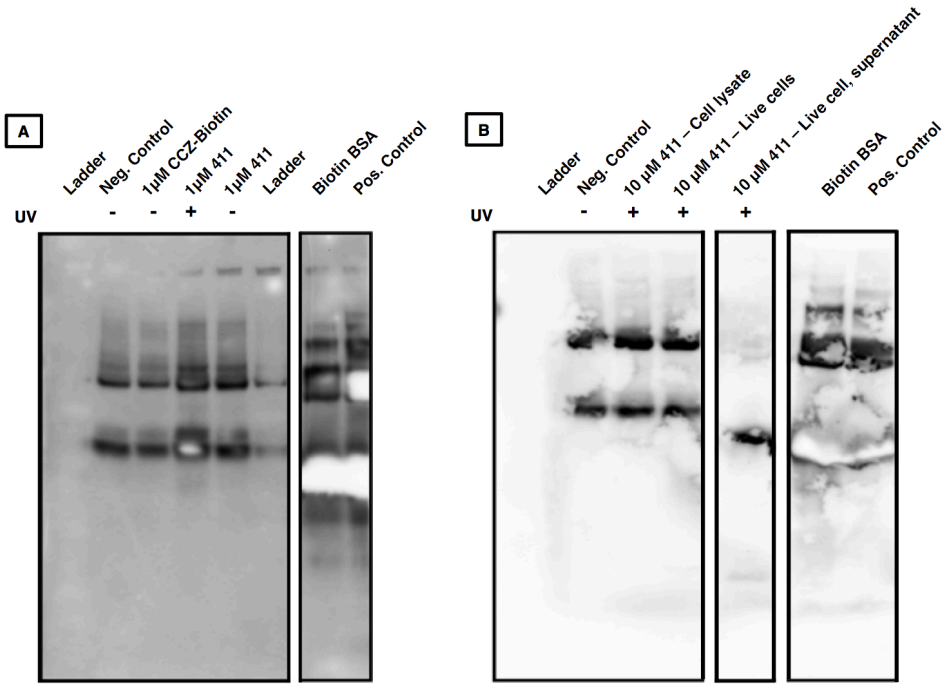

Figure 4.12 **A** Isolated biotinylated proteins from attempted crosslinking of **411** at 1μM in a live cell environment. **B** Isolated biotinylated proteins from attempted crosslinking of **411** at 10μM in a cell lysate, and live cell environment.

4.5 Analysis and discussion - mechanism of action of CCZ

The probe that was designed and synthesized was highly potent towards HCV, demonstrating that the molecule penetrates the cells, reaches its site of action and that it very likely interacts with the same target as CCZ. The compound decomposes quickly under 100W UV light and yields only the water insertion product in the pilot experiment and so seems a suitable candidate for the pulldown assay. Biotinylated BSA is used as a positive control for pulldown at a concentration of 2ug/mL, in addition to this, analysis of the cell medium from the assay reveals the isolation of a protein with the same molecular weight as albumin, demonstrating that the molecule has the ability to bind to proteins covalently and be extracted from the experiment.

It could be the case that CCZ does not bind to its receptor in a manner that would permit covalent binding. If the diazirine is not located towards the pocket being occupied then it could be quenched in the solvent resulting in inefficient binding that may not be detected. Secondly, if the pocket for CCZ is deep, binding between biotin and streptavidin may be disrupted by steric clashes from the protein. This could be remedied by making the linker longer, however this would adversely affect the penetration of the compound into the cell, and the 5-mer PEG chain is as long or longer than literature examples[159]. However albumin was successfully extracted non-specifically from the culture medium.

Alternatively, it could be the case that CCZ does not exert its effect through binding to a protein target, but that it binds to lipids or DNA, several potential mechanisms are discussed below

4.5.1 CCZ as a lysosomotropic agent

CCZ possesses a weakly basic amine as a part of its piperazine moiety, which can become protonated at physiological pH. The non-protonated derivative is lipophilic and can presumably diffuse passively thorough lipid bilayers, however upon protonation the molecule cannot move through the bilayer. This property renders the molecule susceptible to being trapped in acidic sub-cellular compartments such as lysosomes and mitochondria. Lysosomes utilize a proton-pumping V-type ATPase that expends ATP to pump protons into the lysosome lumen against a concentration gradient, resulting in an acidic interior (approx. pH 4.5-5).[123] This effectively traps and concentrates some weakly basic drugs in lysosomes and acidic endosomes, molecules that localize in lysosomes are known as lysosomotropic.[24]

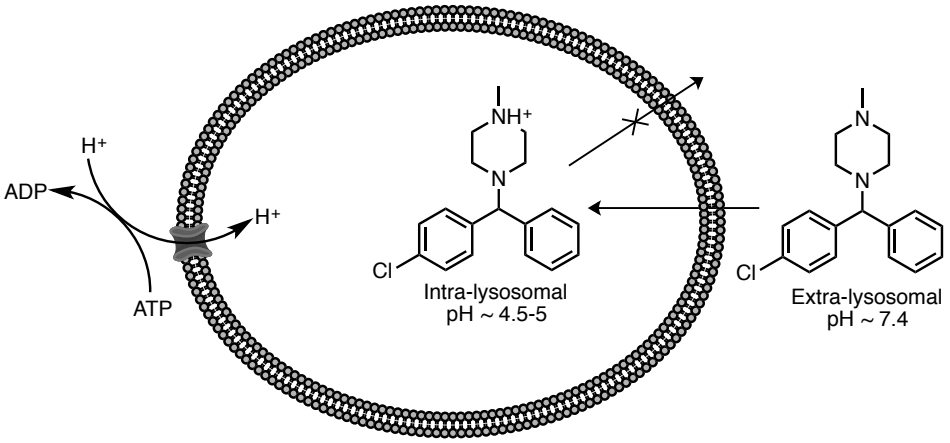

Figure 4.13. Acidification of the lysosome traps weakly basic drugs in the lumen

CCZ has been demonstrated to localise extensively in lysosomes (not shown). A fluorescent, cell permeable derivative, BODIPY-CCZ localizes in lysosomes as determined by comparison with the lysosome detection reagent LysoTracker. Lysosomotropic reagents have been shown to be efficacious against HCV[24], there are a number of plausible molecular mechanisms involving the localization and interactions of small molecules with lipid membranes that CCZ could be acting through which are worthy of investigation. In this manner, the action of CCZ would have to be specific towards HCV, as CCZ does not block the entry of other viruses that share similar endocytic pathways for entry

Lysosomotropic drugs raise the internal pH of the lysosomes and acidic compartments, the endocytic compartments involved in HCV entry gradually become more acidic as the entry pathway progresses from pH 6.0–6.5 in early endosomes to pH4.5–5.5 in late endosomes and lysosomes.[161] The fusion of the HCV with the host membrane post entry has been shown to be pH dependant and it is therefore hypothesized that compounds increasing lysosomal pH have the opportunity to inhibit host/virus fusion.[24]

4.5.2 Functional inhibition of acid sphingomyelinase

As well as being pH dependant, the fusion of HCV (and other enveloped flaviviridae family viruses - West Nile, Dengue) is also dependant on the lipid compositions of both the viral envelope and the target membrane, particularly on the presence of lipids cholesterol and sphingomyelin. Cholesterol and cholesterol/sphingomyelin-rich microdomains or ‘lipid rafts’ have been shown to be important for efficient host-virus fusion[162]. Notably CD81 mediated

entry has been shown to be dependant on the presence of ceramide in membranes. CD81 has also been implicated in virus fusion.[163]
Ceramide is synthesized from sphingomyelin, by the activity of the enzyme acid sphingomyelinase. Functional inhibitors of acid sphingomyelinase (FIASMAs) are a class of compounds that inhibit the function of ASM.[164,165] FIASMA is a functional classification, however the compounds all seem to have particular structural features in common, they are cationic amphiphiles with a lipophilic section and a basic amine that is cationic at the pH of the lysosomal lumen. These compounds insert themselves into the inner (cytosolic) leaflet of the lipid bilayer with the cationic ammonium species protruding into the lumen, and interfere with the electrostatic interactions anchoring ASM to the membrane.[166] ASM detaches and is hydrolysed in the lysosome by lysosomal peptidases, greatly altering the ability of cells to regulate lipid homeostasis and the constitution of membranes with respect to ceramide and sphingomyelin specifically.

Several antihistamines have been classified as FIASMAs, (ex. hydroxyzine, astemizole, chlorpromazine) and several of the ones that are not officially designated as antihistamines, display striking similarities to the class in terms of chemical structures. In a high-throughput screen of approved drugs against Ebola virus, several of the compounds identified as inhibitors of entry were designated as FIASMAs.[167] Critically, SAR for the CCZ series displays a dependence on the maintenance of the aforementioned FIASMA structural features – cationic amphilicity, fig **4.2.**

4.5.3 Alteration of membrane fluid dynamics

Phenothiazines have been shown to inhibit hepatitis C virus entry by intercalating into cholesterol rich domains of lipid bilayers and increasing membrane fluidity.[168] Some phenothiazines possess antihistamine activity and were included in the small focus library screen of anti-histamines carried out by our group to further identify inhibitors of HCV, table in *fig.* **4.1 - 10.** The molecules are purported to inhibit HCV by increasing the fluidity of cholesterol rich domains, interfering with cholesterol clustering, and essentially effecting HCV fusion by changing the physical and structural dynamics of the membrane.[169] It was also noted that with the removal of the piperazine group from the molecule, potency was reduced, indicating that these molecules may possess a similar SAR profile to CCZ.

Rigid amphiphilic fusion inhibitors (RAFIs) are another compound class that are known to interact with biological membranes and effect membrane and lipid dynamics.[170] RAFIs are groups of compounds, again classified by function, that have the ability to insert themselves into biological membranes, changing the curvature and structural dynamics, in doing so altering the ability of membranes to reorganize on demand, since membrane curvature is not simply a passive consequence of cellular activity and lipid structure, but a tightly controlled dynamic system. During the fusion process between the HCV envelopes and host membranes a local negative membrane curvature develops which can be caused by alterations in lipid or membrane protein composition, scaffolding, or folding by actin cytoskeletons.[169] RAFIs simply promote positive curvature of membranes by possessing a hydrophilic head portion larger than a hydrophobic, lipophilic tail section, mimicking phospholipids, which forces positive membrane curvature, increasing the energy barrier for viral fusion.[170]

4.6 Summary, conclusions, and future work

The H_1 anti-histamine **401** and structural analogues have been identified as potent inhibitors of the late stages of HCV entry. The compound was discovered through a phenotypic high-throughput cell based screen and as such the molecular mechanism of action of the drug is not known. In an attempt to elucidate the binding partner of CCZ I designed and successfully implemented the synthesis of a diazirine based photoaffinity probe. The probe retains its anti-HCV properties and conversion occurs smoothly to the carbene intermediate occurs smoothly upon exposure to UV light. Despite these encouraging properties, I was not able to isolate any specific proteins from either live cells or cell lysates on increasing concentrations of the probe molecule. While it was the case that the CCZ probe was not shown to isolate any specific proteins this does not necessarily imply that CCZ does not exert its effect through protein binding – it may be the case that no proteins were isolated or detected from the pulldown assay for specific experimental reasons. Having said that, there are numerous non-experimental reasons protein targets may not be isolated. It is hypothesized therefore, that CCZ exerts its effects based on a non-protein target, which is founded principally on the atypical patterns observed in the SAR – a wide range of substitutions are tolerated so long as the principal structural cationic amphiphilicity of the molecule is not compromised. The fact that the only active molecules synthesized so far are cationic amphiphiles with no exceptions suggests that this is intrinsic to the mechanism. These types of molecules have specific intrinsic physiological parameters and biological properties; the modulation of these particular biological properties should be investigated for their effect on HCV. Future work will focus on pursuing these avenues, for which the biotin-CCZ-diazirine may still be of use.

This work serves to highlight the advantages and disadvantages of phenotypic screening – attractive drug candidates may be discovered but the mechanisms by which these drugs act may be convoluted, esoteric and difficult to rationalise, considering the breadth of all possible targets and mechanisms that could result in inhibition of the orchestra that is HCV replication.

5

Conclusion

To address therapeutic need in a continuously developing landscape of niche patient cohorts in HCV, we specifically chose to develop candidates that target the entry and assembly stages, and host factors of the HCV life cycle, as combination of these therapeutics with the current replication stage inhibitors will reduce the probability of viral resistant mutations as an intrinsic pharmacodynamic property of the therapies, as well as reducing treatment duration, and Importantly treatment cost. We leveraged the inherent advantages of target and phenotype based drug discovery in a complimentary manner.

I developed mechanistic parameters of asymmetric transfer hydrogenation of ketones, allowing a short, modular and enantioselective synthesis of MeBmt, uncovering important factors and subtleties in how intramolecular hydrogen bonding effects and possibly even dictates the reactivity of the material. I optimised a novel assembly inhibitor of HCV, CT3, resulting in a lead compound **372** which boasts approximately 15 fold increase in efficacy against HCV, more than 10 fold increase in metabolic half life and an increase in other molecular efficiency metrics as compared to the original hit, which culminated in an *in-vivo* PK study in mice, this investigation is on-going.

Lastly, I designed and successfully implemented a synthesis of a potent photoaffinity probe, designed around the framework of a novel inhibitor of HCV entry – chlorcyclizine. The probe was utilized in chemical biology experiments in an attempt to understand molecular mechanism of action of chlorcyclizine against HCV and while no targets have been identified so far, work is on-going, and such probe molecule will undoubtedly be of use in several ways depending on which direction this line of enquiry is taken.

6

References

(1) Santolini, E.; Migliaccio, G.; La Monica, N. *Journal of Virology* **1994**, *68*, 3631.

(2) Peel, M.; Scribner, A. *Bioorganic & medicinal chemistry letters* **2013**, *23*, 4485.

(3) Moradpour, D.; Penin, F. *Current topics in microbiology and immunology* **2013**, *369*, 113.

(4) Madan, V.; Bartenschlager, R. *Viruses* **2015**, *7*.

(5) Bentham, M. J.; Foster, T. L.; McCormick, C.; Griffin, S. *The Journal of general virology* **2013**, *94*, 2236.

(6) Bartenschlager, R.; Lohmann, V.; Wilkinson, T.; Koch, J. O. *Journal of Virology* **1995**, *69*, 7519.

(7) Li, X.-D.; Sun, L.; Seth, R. B.; Pineda, G.; Chen, Z. J. *Proc. Natl. Acad. Sci. U. S. A.* **2005**, *102*, 17717.

(8) EH, S. In *Hepatitis C Viruses: Genomes and Molecular Biology* 2006.

(9) Belda, O.; Targett-Adams, P. *Virus Research* **2012**, *170*, 1.

(10) Simmonds, P.; Holmes, E. C.; Cha, T. A.; Chan, S. W.; McOmish, F.; Irvine, B.; Beall, E.; Yap, P. L.; Kolberg, J.; Urdea, M. S. *The Journal of general virology* **1993**, *74 (Pt 11)*, 2391.

(11) Magiorkinis, G.; Magiorkinis, E.; Paraskevis, D.; Ho, S. Y. W.; Shapiro, B.; Pybus, O. G.; Allain, J.-P.; Hatzakis, A. *PLoS Med* **2009**, *6*, e1000198.

(12) Simmonds, P. *Curr. Top. Microbiol. Immunol.* **2013**, *369*, 1.

(13) Nakano, Y.; Matsuda, K.; Yoshikawa, R.; Yamada, E.; Misawa, N.; Hirsch, V. M.; Koyanagi, Y.; Sato, K. *J. Gen. Virol.* **2015**, *96*, 2867.

(14) Kapoor, A.; Simmonds, P.; Gerold, G.; Qaisar, N.; Jain, K.; Henriquez, J. A.; Firth, C.; Hirschberg, D. L.; Rice, C. M.; Shields, S.; Lipkin, W. I. *Proceedings of the National Academy of Sciences* **2011**, *108*, 11608.

(15) Bennett, H.; McEwan, P.; Sugrue, D.; Kalsekar, A.; Yuan, Y. *PLoS ONE* **2015**, *10*, e0125846.

(16) Choo, Q. L.; Kuo, G.; Weiner, A. J.; Overby, L. R.; Bradley, D. W.; Houghton, M. *Science* **1989**, *244*, 359.

(17) Gao, M.; Nettles, R. E.; Belema, M.; Snyder, L. B.; Nguyen, V. N.; Fridell, R. A.; Serrano-Wu, M. H.; Langley, D. R.; Sun, J.-H.; O'Boyle, D. R., II; Lemm, J. A.; Wang, C.; Knipe, J. O.; Chien, C.; Colonno, R. J.; Grasela, D. M.; Meanwell, N. A.; Hamann, L. G. *Nature (London, U. K.)* **2010**, *465*, 96.

(18) Lindenbach, B. D.; Rice, C. M. *Nat. Rev. Microbiol.* **2013**, *11*, 688.

(19) Dubuisson, J.; Cosset, F.-L. *Journal of Hepatology* **2014**, *61*, S3.

(20) Wieland, S.; Makowska, Z.; Campana, B.; Calabrese, D.; Dill, M. T.; Chung, J.; Chisari, F. V.; Heim, M. H. *Hepatology (Baltimore, Md.)* **2014**, *59*, 2121.

(21) Mothes, W.; Sherer, N. M.; Jin, J.; Zhong, P. *Journal of Virology* **2010**, *84*, 8360.

(22) Blanchard, E.; Belouzard, S.; Goueslain, L.; Wakita, T.; Dubuisson, J.; Wychowski, C.; Rouillé, Y. *Journal of Virology* **2006**, *80*, 6964.

(23) Meertens, L.; Bertaux, C.; Dragic, T. *Journal of Virology* **2006**, *80*, 11571.

(24) Ashfaq, U. A.; Javed, T.; Rehman, S.; Nawaz, Z.; Riazuddin, S. *Virology Journal* **2011**, *8*, 1.

(25) Niepmann, M. In *Hepatitis C Virus: From Molecular Virology to Antiviral Therapy*; Bartenschlager, R., Ed.; Springer Berlin Heidelberg: Berlin, Heidelberg, 2013, p 143.

(26) Gosert, R.; Egger, D.; Lohmann, V.; Bartenschlager, R.; Blum, H. E.; Bienz, K.; Moradpour, D. *Journal of Virology* **2003**, *77*, 5487.

(27) Khromykh, A. A.; Varnavski, A. N.; Sedlak, P. L.; Westaway, E. G. *Journal of Virology* **2001**, *75*, 4633.

(28) Lindenbach, B. D. *Current topics in microbiology and immunology* **2013**, *369*, 199.

(29) Simmonds, P. *Hepatology (Baltimore, Md.)* **1995**, *21*, 570.

(30) De Andrea, M.; Ravera, R.; Gioia, D.; Gariglio, M.; Landolfo, S. *European journal of paediatric neurology : EJPN : official journal of the European Paediatric Neurology Society* **2002**, *6 Suppl A*, A41.

(31) Feld, J. J.; Hoofnagle, J. H. *Nature* **2005**, *436*, 967.

(32) Hoofnagle, J. H.; Mullen, K. D.; Jones, D. B.; Rustgi, V.; Di Bisceglie, A.; Peters, M.; Waggoner, J. G.; Park, Y.; Jones, E. A. *New England Journal of Medicine* **1986**, *315*, 1575.

(33) de Veer, M. J.; Holko, M.; Frevel, M.; Walker, E.; Der, S.; Paranjape, J. M.; Silverman, R. H.; Williams, B. R. *Journal of leukocyte biology* **2001**, *69*, 912.

(34) McHutchison, J. G.; Poynard, T. *Seminars in liver disease* **1999**, *19 Suppl 1*, 57.

(35) Maag, D.; Castro, C.; Hong, Z.; Cameron, C. E. *Journal of Biological Chemistry* **2001**, *276*, 46094.

(36) Crotty, S.; Maag, D.; Arnold, J. J.; Zhong, W.; Lau, J. Y. N.; Hong, Z.; Andino, R.; Cameron, C. E. *Nat Med* **2000**, *6*, 1375.

(37) Thomas, E.; Feld, J. J.; Li, Q.; Hu, Z.; Fried, M. W.; Liang, T. J. *Hepatology (Baltimore, Md.)* **2011**, *53*, 32.

(38) Bacon , B. R.; Gordon , S. C.; Lawitz , E.; Marcellin , P.; Vierling , J. M.; Zeuzem , S.; Poordad , F.; Goodman , Z. D.; Sings , H. L.; Boparai , N.; Burroughs , M.; Brass , C. A.; Albrecht , J. K.; Esteban , R. *New England Journal of Medicine* **2011**, *364*, 1207.

(39) Kwo, P. Y.; Lawitz, E. J.; McCone, J.; Schiff, E. R.; Vierling, J. M.; Pound, D.; Davis, M. N.; Galati, J. S.; Gordon, S. C.; Ravendhran, N.; Rossaro, L.; Anderson, F. H.; Jacobson, I. M.; Rubin, R.; Koury, K.; Pedicone, L. D.; Brass, C. A.; Chaudhri, E.; Albrecht, J. K. *The Lancet*, *376*, 705.

(40) Jacobson , I. M.; McHutchison , J. G.; Dusheiko , G.; Di Bisceglie , A. M.; Reddy , K. R.; Bzowej , N. H.; Marcellin , P.; Muir , A. J.; Ferenci , P.; Flisiak , R.; George , J.; Rizzetto , M.; Shouval , D.; Sola , R.; Terg , R. A.; Yoshida , E. M.; Adda , N.; Bengtsson , L.; Sankoh , A. J.; Kieffer , T. L.; George , S.; Kauffman , R. S.; Zeuzem , S. *New England Journal of Medicine* **2011**, *364*, 2405.

(41) Sherman, K. E.; Flamm, S. L.; Afdhal, N. H.; Nelson, D. R.; Sulkowski, M. S.; Everson, G. T.; Fried, M. W.; Adler, M.; Reesink, H. W.; Martin, M.; Sankoh, A. J.; Adda, N.; Kauffman, R. S.; George, S.; Wright, C. I.; Poordad, F. *New England Journal of Medicine* **2011**, *365*, 1014.

(42) Delang, L.; Neyts, J.; Vliegen, I.; Abrignani, S.; Neddermann, P.; De Francesco, R. *Current topics in microbiology and immunology* **2013**, *369*, 289.

(43) Lawitz, E.; Gane, E.; Pearlman, B.; Tam, E.; Ghesquiere, W.; Guyader, D.; Alric, L.; Bronowicki, J. P.; Lester, L.; Sievert, W.; Ghalib, R.; Balart, L.; Sund, F.; Lagging, M.; Dutko, F.; Shaughnessy, M.; Hwang, P.; Howe, A. Y.; Wahl, J.; Robertson, M.; Barr, E.; Haber, B. *Lancet (London, England)* **2015**, *385*, 1075.

(44) Lawitz, E.; Lalezari, J. P.; Hassanein, T.; Kowdley, K. V.; Poordad, F. F.; Sheikh, A. M.; Afdhal, N. H.; Bernstein, D. E.; Dejesus, E.; Freilich, B.; Nelson, D. R.; Dieterich, D. T.; Jacobson, I. M.; Jensen, D.; Abrams, G. A.; Darling, J. M.; Rodriguez-Torres, M.; Reddy, K. R.; Sulkowski, M. S.; Bzowej, N. H.; Hyland, R. H.; Mo, H.; Lin, M.; Mader, M.; Hindes, R.; Albanis, E.; Symonds, W. T.; Berrey, M. M.; Muir, A. *Lancet Infect Dis* **2013**, *13*, 401.

(45) Mangia, A.; Piazzolla, V. *Digestive and Liver Disease* **2014**, *46, Supplement 5*, S179.

(46) Vernaz, N.; Girardin, F.; Goossens, N.; Brugger, U.; Riguzzi, M.; Perrier, A.; Negro, F. *PLoS One* **2016**, *11*, e0157098/1.

(47) Kowdley, K. V.; Gordon, S. C.; Reddy, K. R.; Rossaro, L.; Bernstein, D. E.; Lawitz, E.; Shiffman, M. L.; Schiff, E.; Ghalib, R.; Ryan, M.; Rustgi, V.; Chojkier, M.; Herring, R.; Di Bisceglie, A. M.; Pockros, P. J.; Subramanian, G. M.; An, D.; Svarovskaia, E.; Hyland, R. H.; Pang, P. S.; Symonds, W. T.; McHutchison, J. G.; Muir, A. J.; Pound, D.; Fried, M. W. *The New England journal of medicine* **2014**, *370*, 1879.

(48) Naggie, S.; Muir, A. J. *Annu. Rev. Med.* **2016**, Ahead of Print.

(49) Zeisel, M. B.; Lupberger, J.; Fofana, I.; Baumert, T. F. *Journal of Hepatology* **2013**, *58*, 375.

(50) Qian, X.-J.; Zhu, Y.-Z.; Zhao, P.; Qi, Z.-T. *Emerging Microbes & Infections* **2016**, *5*, e3.

(51) Bandiera, S.; Pfeffer, S.; Baumert, T. F.; Zeisel, M. B. *Journal of Hepatology* **2015**, *62*, 448.

(52) Janssen, H. L.; Reesink, H. W.; Lawitz, E. J.; Zeuzem, S.; Rodriguez-Torres, M.; Patel, K.; van der Meer, A. J.; Patick, A. K.; Chen, A.; Zhou, Y.; Persson, R.; King, B. D.; Kauppinen, S.; Levin, A. A.; Hodges, M. R. *The New England journal of medicine* **2013**, *368*, 1685.

(53) Luna, J. M.; Scheel, T. K.; Danino, T.; Shaw, K. S.; Mele, A.; Fak, J. J.; Nishiuchi, E.; Takacs, C. N.; Catanese, M. T.; de Jong, Y. P.; Jacobson, I. M.; Rice, C. M.; Darnell, R. B. *Cell* **2015**, *160*, 1099.

(54) van der Ree, M. H.; van der Meer, A. J.; de Bruijne, J.; Maan, R.; van Vliet, A.; Welzel, T. M.; Zeuzem, S.; Lawitz, E. J.; Rodriguez-Torres, M.; Kupcova, V.; Wiercinska-Drapalo, A.; Hodges, M. R.; Janssen, H. L. A.; Reesink, H. W. *Antiviral Research* **2014**, *111*, 53.

(55) Arias, A.; Aguilera, A.; Soriano, V.; Benitez-Gutierrez, L.; Lledo, G.; Navarro, D.; Trevino, A.; Otero, E.; Pena, J. M.; Cuervas-Mons, V.; de Mendoza, C. *Antiviral therapy* **2016**.

(56) Benitez-Gutierrez, L.; Barreiro, P.; Labarga, P.; de Mendoza, C.; Fernandez-Montero, J. V.; Arias, A.; Pena, J. M.; Soriano, V. *Expert opinion on pharmacotherapy* **2016**, *17*, 1215.

(57) Paeshuyse, J.; Kaul, A.; De Clercq, E.; Rosenwirth, B.; Dumont, J. M.; Scalfaro, P.; Bartenschlager, R.; Neyts, J. *Hepatology (Baltimore, Md.)* **2006**, *43*, 761.

(58) Kamal-Yanni, M. *The Lancet Global Health*, *3*, e73.

(59) Baugh, J. M.; Garcia-Rivera, J. A.; Gallay, P. A. *Antiviral research* **2013**, *100*, 555.

(60) Manzano, M.; Padia, J.; Padmanabhan, R. *Methods in molecular biology (Clifton, N.J.)* **2014**, *1138*, 331.

(61) Swinney, D. C.; Anthony, J. *Nat. Rev. Drug Discovery* **2011**, *10*, 507.
(62) Silverman, R. B.; Holladay, M. W. *The Organic Chemistry of Drug Design and Drug Action*; Third ed., 2014.
(63) Hu, Z.; Lan, K.-H.; He, S.; Swaroop, M.; Hu, X.; Southall, N.; Zheng, W.; Liang, T. J. *Antimicrob. Agents Chemother.* **2014**, *58*, 995.
(64) Svarstad, H.; Bugge, H. C.; Dhillion, S. S. *Biodiversity & Conservation* **2000**, *9*, 1521.
(65) Wu, X.; Stockdill, J. L.; Wang, P.; Danishefsky, S. J. *Journal of the American Chemical Society* **2010**, *132*, 4098.
(66) Tanasescu, C.; Serbanescu, A.; Spadaro, A.; Jen, L. H.; Oliani, C. *Curr. Toxicol. Ther.* **1998**, *6*, 13.
(67) Ismailos, G.; Reppas, C.; Dressman, J. B.; Macheras, P. *The Journal of pharmacy and pharmacology* **1991**, *43*, 287.
(68) Stamnes, M. A.; Rutherford, S. L.; Zuker, C. S. *Trends Cell Biol.* **1992**, *2*, 272.
(69) Walsh, C. T.; Zydowsky, L. D.; McKeon, F. D. *J. Biol. Chem.* **1992**, *267*, 13115.
(70) Ivery, M. T. G. *Bioorg. Med. Chem.* **1999**, *7*, 1389.
(71) Schreiber, S. L.; Crabtree, G. R. *Immunol. Today* **1992**, *13*, 136.
(72) Faulds, D.; Goa, K. L.; Benfield, P. *Drugs* **1993**, *45*, 953.
(73) Scribner, A.; Houck, D.; Huang, Z.; Mosier, S.; Peel, M.; Scorneaux, B. *Bioorg. Med. Chem. Lett.* **2010**, *20*, 6542.
(74) Peel, M.; Scribner, A. *Bioorg. Med. Chem. Lett.* **2013**, *23*, 4485.
(75) Kaul, A.; Stauffer, S.; Berger, C.; Pertel, T.; Schmitt, J.; Kallis, S.; Lopez, M. Z.; Lohmann, V.; Luban, J.; Bartenschlager, R. *PLoS Pathog.* **2009**, *5*, No pp. given.
(76) Garcia-Rivera, J. A.; Bobardt, M.; Chatterji, U.; Hopkins, S.; Gregory, M. A.; Wilkinson, B.; Lin, K.; Gallay, P. A. *Antimicrob Agents Chemother* **2012**, *56*, 5113.
(77) Rosnoblet, C.; Fritzinger, B.; Legrand, D.; Launay, H.; Wieruszeski, J.-M.; Lippens, G.; Hanoulle, X. *J. Biol. Chem.* **2012**, *287*, 44249.
(78) Chatterji, U.; Lim, P.; Bobardt, M. D.; Wieland, S.; Cordek, D. G.; Vuagniaux, G.; Chisari, F.; Cameron, C. E.; Targett-Adams, P.; Parkinson, T.; Gallay, P. A. *J Hepatol* **2010**, *53*, 50.
(79) Yang, F.; Robotham, J. M.; Nelson, H. B.; Irsigler, A.; Kenworthy, R.; Tang, H. *J Virol* **2008**, *82*, 5269.
(80) Arai, M.; Tsukiyama-Kohara, K.; Takagi, A.; Tobita, Y.; Inoue, K.; Kohara, M. *Biochem Biophys Res Commun* **2014**, *448*, 56.
(81) Puyang, X.; Poulin, D. L.; Mathy, J. E.; Anderson, L. J.; Ma, S.; Fang, Z.; Zhu, S.; Lin, K.; Fujimoto, R.; Compton, T.; Wiedmann, B. *Antimicrob Agents Chemother* **2010**, *54*, 1981.
(82) Wenger, R. M.; France, J.; Bovermann, G.; Walliser, L.; Widmer, A.; Widmer, H. *FEBS Lett.* **1994**, *340*, 255.
(83) Ke, H.; Mayrose, D.; Belshaw, P. J.; Alberg, D. G.; Schreiber, S. L.; Chang, Z. Y.; Etzkorn, F. A.; Ho, S.; Walsh, C. T. *Structure (London)* **1994**, *2*, 33.
(84) Mikol, V.; Kallen, J.; Walkinshaw, M. D. *Protein Eng.* **1994**, *7*, 597.
(85) Gallay, P. A.; Lin, K. *Drug Des Devel Ther* **2013**, *7*, 105.
(86) Hopkins, S.; Scorneaux, B.; Huang, Z.; Murray, M. G.; Wring, S.; Smitley, C.; Harris, R.; Erdmann, F.; Fischer, G.; Ribeill, Y. *Antimicrobial Agents and Chemotherapy* **2010**, *54*, 660.
(87) Scribner, A.; Houck, D.; Huang, Z.; Mosier, S.; Peel, M.; Scorneaux, B. *Bioorganic and Medicinal Chemistry Letters* **2010**, *20*, 6542.
(88) Ma, S.; Boerner, J. E.; TiongYip, C.; Weidmann, B.; Ryder, N. S.; Cooreman, M. P.; Lin, K. *Antimicrob Agents Chemother* **2006**, *50*, 2976.
(89) Hopkins, S.; Gallay, P. *Viruses* **2012**, *4*, 2558.
(90) Blaser, D.; Ko, S. Y.; Seebach, D. *J. Org. Chem.* **1991**, *56*, 6230.
(91) Tuch, A.; Saniere, M.; Merrer, Y. L.; Depezay, J.-C. *Tetrahedron: Asymmetry* **1997**, *8*, 1649.

(92) Aurelio, L.; Brownlee, R. T. C.; Hughes, A. B. *Chem. Rev. (Washington, DC, U. S.)* **2004**, *104*, 5823.
(93) Cook, G. R.; Shanker, P. S. *J Org Chem* **2001**, *66*, 6818.
(94) Cook, G. R.; Shanker, P. S. *J. Org. Chem.* **2001**, *66*, 6818.
(95) Deyo, D. T.; Aebi, J. D.; Rich, D. H. *Synthesis* **1988**, 608.
(96) Durand, J.-O.; Genet, J.-P. *Bull. Soc. Chim. Fr.* **1994**, *131*, 612.
(97) Evans, D. A.; Weber, A. E. *J. Am. Chem. Soc.* **1986**, *108*, 6757.
(98) Genet, J.-P. *Pure Appl. Chem.* **1996**, *68*, 593.
(99) Kim, Y.; Yoon, D.-H.; Ha, H.-J.; Kang, K. Y.; Lee, W. K. *Tetrahedron Lett.* **2011**, *52*, 5918.
(100) Lubell, W. D., 1989.
(101) Lubell, W. D.; Jamison, T. F.; Rapoport, H. *J. Org. Chem.* **1990**, *55*, 3511.
(102) McCombie, S. W.; Shankar, B. B.; Ganguly, A. K. *Tetrahedron Lett.* **1989**, *30*, 7029.
(103) Raghavan, S.; Rasheed, M. A. *Tetrahedron* **2004**, *60*, 3059.
(104) Rao, A. V. R.; Dhar, T. G. M.; Bose, D. S.; Chakraborty, T. K.; Gurjar, M. K. *Tetrahedron* **1989**, *45*, 7361.
(105) Rao, A. V. R.; Dhar, T. G. M.; Chakraborty, T. K.; Gurjar, M. K. *Tetrahedron Lett.* **1988**, *29*, 2069.
(106) Rao, A. V. R.; Yadav, J. S.; Chandrasekhar, S.; Rao, C. S. *Tetrahedron Lett.* **1989**, *30*, 6769.
(107) Rich, D. H.; Sun, C. Q.; Guillaume, D.; Dunlap, B.; Evans, D. A.; Weber, A. E. *J. Med. Chem.* **1989**, *32*, 1982.
(108) Savignac, M.; Durand, J. O.; Genet, J. P. *Tetrahedron: Asymmetry* **1994**, *5*, 717.
(109) Tung, R. D.; Rich, D. H. *Tetrahedron Lett.* **1987**, *28*, 1139.
(110) Yoda, H.; Shirai, T.; Katagiri, T.; Takabe, K.; Hosoya, K. *Chem. Express* **1992**, *7*, 477.
(111) Wenger, R. M. *Helvetica Chimica Acta* **1983**, *66*, 2308.
(112) Schmidt, U.; Siegel, W. *Tetrahedron Letters* **1987**, *28*, 2849.
(113) Togni, A.; Pastor, S. D.; Rihs, G. *Helvetica Chimica Acta* **1989**, *72*, 1471.
(114) Seebach, D.; Juaristi, E.; Miller, D. D.; Schickli, C.; Weber, T. *Helvetica Chimica Acta* **1987**, *70*, 237.
(115) Rao, A. V. R.; Dhar, T. G. M.; Chakraborty, T. K.; Gurjar, M. K. *Tetrahedron Letters* **1988**, *29*, 2069.
(116) Dewick, P. M. *Medicinal Natural Products*; 2 ed., 2009.
(117) Misaki, T.; Nagase, R.; Matsumoto, K.; Tanabe, Y. *Journal of the American Chemical Society* **2005**, *127*, 2854.
(118) Noyori, R.; Ikeda, T.; Ohkuma, T.; Widhalm, M.; Kitamura, M.; Takaya, H.; Akutagawa, S.; Sayo, N.; Saito, T.; et, a. *J. Am. Chem. Soc.* **1989**, *111*, 9134.
(119) Genet, J. P.; Pinel, C.; Mallart, S.; Juge, S.; Thorimbert, S.; Laffitte, J. A. *Tetrahedron: Asymmetry* **1991**, *2*, 555.
(120) Kumaraswamy, G.; Narayana Murthy, A.; Narayanarao, V.; Vemulapalli, S. P. B.; Bharatam, J. *Org. Biomol. Chem.* **2013**, *11*, 6751.
(121) Limanto, J.; Krska, S. W.; Dorner, B. T.; Vazquez, E.; Yoshikawa, N.; Tan, L. *Org. Lett.* **2010**, *12*, 512.
(122) Seashore-Ludlow, B.; Villo, P.; Somfai, P. *Chem. - Eur. J.* **2012**, *18*, 7219.
(123) Wang, D.; Astruc, D. *Chemical Reviews* **2015**, *115*, 6621.
(124) Mohar, B.; Valleix, A.; Desmurs, J.-R.; Felemez, M.; Wagner, A.; Mioskowski, C. *Chemical Communications* **2001**, 2572.
(125) Cartigny, D.; Püntener, K.; Ayad, T.; Scalone, M.; Ratovelomanana-Vidal, V. *Organic Letters* **2010**, *12*, 3788.
(126) Wu, X.; Liu, J.; Di Tommaso, D.; Iggo, J. A.; Catlow, C. R.; Bacsa, J.; Xiao, J. *Chemistry (Weinheim an der Bergstrasse, Germany)* **2008**, *14*, 7699.
(127) Ireland, R. E.; Mueller, R. H.; Willard, A. K. *Journal of the American Chemical Society* **1976**, *98*, 2868.

(128) Masako Nagatsuma, F. S., Noboru Sayo, Takeshi Nakai *Chemistry Letters* **1984**, *13*, 1393.
(129) Zhou, G.; Lim, D.; Coltart, D. M. *Organic Letters* **2008**, *10*, 3809.
(130) ; National Institutes of Health.
(131) Hu, Z.; Hu, X.; He, S.; Yim, H. J.; Xiao, J.; Swaroop, M.; Tanega, C.; Zhang, Y.-q.; Yi, G.; Kao, C. C.; Marugan, J.; Ferrer, M.; Zheng, W.; Southall, N.; Liang, T. J. *Antiviral Research* **2015**, *124*, 20.
(132) Meertens, L.; Bertaux, C.; Dragic, T. *J. Virol.* **2006**, *80*, 11571.
(133) Steinmann, E.; Pietschmann, T. *Current topics in microbiology and immunology* **2013**, *369*, 17.
(134) Lipinski, C. A. *Drug Discovery Today: Technologies* **2004**, *1*, 337.
(135) Moore, R. D.; Chaisson, R. E. *Aids* **1999**, *13*, 1933.
(136) Duvignaud, J.-B.; Majeau, N.; Delisle, P.; Voyer, N.; Gagne, S. M.; Leclerc, D. *Can. J. Microbiol.* **2012**, *58*, 475.
(137) Goldwasser, J.; Cohen, P. Y.; Lin, W.; Kitsberg, D.; Balaguer, P.; Polyak, S. J.; Chung, R. T.; Yarmush, M. L.; Nahmias, Y. *J. Hepatol.* **2011**, *55*, 963.
(138) Qu, X.; Pan, X.; Weidner, J.; Yu, W.; Alonzi, D.; Xu, X.; Butters, T.; Block, T.; Guo, J.-T.; Chang, J. *Antimicrob. Agents Chemother.* **2011**, *55*, 1036.
(139) Cheng, Y.-L.; Lan, K.-H.; Lee, W.-P.; Tseng, S.-H.; Hung, L.-R.; Lin, H.-C.; Lee, F.-Y.; Lee, S.-D.; Lan, K.-H. *Clin. Sci.* **2013**, *125*, 439.
(140) Bush, C. O.; Pokrovskii, M. V.; Saito, R.; Morganelli, P.; Canales, E.; Clarke, M. O.; Lazerwith, S. E.; Golde, J.; Reid, B. G.; Babaoglu, K.; Pagratis, N.; Zhong, W.; Delaney, W. E.; Paulson, M. S.; Beran, R. K. F. *Antimicrobial Agents and Chemotherapy* **2014**, *58*, 386.
(141) Kota, S.; Takahashi, V.; Ni, F.; Snyder, J. K.; Strosberg, A. D. *PLoS ONE* **2012**, *7*, e32207.
(142) Herker, E.; Harris, C.; Hernandez, C.; Carpentier, A.; Kaehlcke, K.; Rosenberg, A. R.; Farese, R. V.; Ott, M. *Nat Med* **2010**, *16*, 1295.
(143) DeVita, R. J.; Pinto, S. *J. Med. Chem.* **2013**, *56*, 9820.
(144) Database., N. C. T. R. http://www.novctrd.com/ctrdWebApp/clinicaltrialrepository/displayFile.do?trialResult=8064.
(145) Nahmias, Y.; Goldwasser, J.; Casali, M.; van Poll, D.; Wakita, T.; Chung, R. T.; Yarmush, M. L. *Hepatology (Baltimore, Md.)* **2008**, *47*, 1437.
(146) Shultz, M. D. *Bioorganic & medicinal chemistry letters* **2013**, *23*, 5980.
(147) Hughes, J. D.; Blagg, J.; Price, D. A.; Bailey, S.; DeCrescenzo, G. A.; Devraj, R. V.; Ellsworth, E.; Fobian, Y. M.; Gibbs, M. E.; Gilles, R. W.; Greene, N.; Huang, E.; Krieger-Burke, T.; Loesel, J.; Wager, T.; Whiteley, L.; Zhang, Y. *Bioorganic & medicinal chemistry letters* **2008**, *18*, 4872.
(148) Veber, D. F.; Johnson, S. R.; Cheng, H.-Y.; Smith, B. R.; Ward, K. W.; Kopple, K. D. *Journal of medicinal chemistry* **2002**, *45*, 2615.
(149) Leurs, R.; Smit, M. J.; Timmerman, H. *Pharmacol. Ther.* **1995**, *66*, 413.
(150) Simons , F. E. R. *New England Journal of Medicine* **2004**, *351*, 2203.
(151) He, S.; Lin, B.; Chu, V.; Hu, Z.; Hu, X.; Xiao, J.; Wang, A. Q.; Schweitzer, C. J.; Li, Q.; Imamura, M.; Hiraga, N.; Southall, N.; Ferrer, M.; Zheng, W.; Chayama, K.; Marugan, J. J.; Liang, T. J. *Science Translational Medicine* **2015**, *7*, 282ra49.
(152) Chamoun-Emanuelli, A. M.; Pécheur, E.-I.; Chen, Z. *Antiviral Research* **2014**, *109*, 141.
(153) Center, N. C. G.
(154) Lin, B.; He, S.; Yim, H. J.; Liang, T. J.; Hu, Z. *Antiviral therapy* **2016**.
(155) He, S.; Xiao, J.; Dulcey, A. E.; Lin, B.; Rolt, A.; Hu, Z.; Hu, X.; Wang, A. Q.; Xu, X.; Southall, N.; Ferrer, M.; Zheng, W.; Liang, T. J.; Marugan, J. J. *Journal of medicinal chemistry* **2016**, *59*, 841.
(156) Robinette, D.; Neamati, N.; Tomer, K. B.; Borchers, C. H. *Expert review of proteomics* **2006**, *3*, 399.

(157) Brunner, J.; Senn, H.; Richards, F. M. *The Journal of biological chemistry* **1980**, *255*, 3313.
(158) Dubinsky, L.; Krom, B. P.; Meijler, M. M. *Bioorganic & Medicinal Chemistry* **2012**, *20*, 554.
(159) MacKinnon, A. L.; Taunton, J. *Current protocols in chemical biology* **2009**, *1*, 55.
(160) Rybak, J. N.; Scheurer, S. B.; Neri, D.; Elia, G. *Proteomics* **2004**, *4*, 2296.
(161) Sorkin, A.; von Zastrow, M. *Nat Rev Mol Cell Biol* **2002**, *3*, 600.
(162) Haid, S.; Pietschmann, T.; Pecheur, E. I. *The Journal of biological chemistry* **2009**, *284*, 17657.
(163) Sharma, N. R.; Mateu, G.; Dreux, M.; Grakoui, A.; Cosset, F. L.; Melikyan, G. B. *The Journal of biological chemistry* **2011**, *286*, 30361.
(164) Kornhuber, J.; Muehlbacher, M.; Trapp, S.; Pechmann, S.; Friedl, A.; Reichel, M.; Mühle, C.; Terfloth, L.; Groemer, T. W.; Spitzer, G. M.; Liedl, K. R.; Gulbins, E.; Tripal, P. *PLoS ONE* **2011**, *6*, e23852.
(165) Beckmann, N.; Sharma, D.; Gulbins, E.; Becker, K. A.; Edelmann, B. *Frontiers in Physiology* **2014**, *5*, 331.
(166) Kolzer, M.; Werth, N.; Sandhoff, K. *FEBS Lett* **2004**, *559*, 96.
(167) Johansen, L. M.; DeWald, L. E.; Shoemaker, C. J.; Hoffstrom, B. G.; Lear-Rooney, C. M.; Stossel, A.; Nelson, E.; Delos, S. E.; Simmons, J. A.; Grenier, J. M.; Pierce, L. T.; Pajouhesh, H.; Lehar, J.; Hensley, L. E.; Glass, P. J.; White, J. M.; Olinger, G. G. *Sci Transl Med* **2015**, *7*, 290ra89.
(168) Chamoun-Emanuelli, A. M.; Pecheur, E. I.; Simeon, R. L.; Huang, D.; Cremer, P. S.; Chen, Z. *Antimicrob Agents Chemother* **2013**, *57*, 2571.
(169) McMahon, H. T.; Gallop, J. L. *Nature* **2005**, *438*, 590.
(170) St.Vincent, M. R.; Colpitts, C. C.; Ustinov, A. V.; Muqadas, M.; Joyce, M. A.; Barsby, N. L.; Epand, R. F.; Epand, R. M.; Khramyshev, S. A.; Valueva, O. A.; Korshun, V. A.; Tyrrell, D. L. J.; Schang, L. M. *Proceedings of the National Academy of Sciences* **2010**, *107*, 17339.

7

Experimental Section

All air or moisture sensitive reactions were performed under positive pressure of nitrogen with oven-or flame dried glassware where stated. Anhydrous solvents were purchased from Sigma-Aldrich (St. Louis, MO). 'Normal phase chromatography', column chromatography, or gradient column chromatography refers to automatic purification using a 'Tyledyne ISCO CombiFlash® Rf+' system with pre-loaded silica gel 'Redisep RF flash columns' of an appropriate size. Preparative purification was performed on a Waters semi-preparative HPLC system (Waters Corp., Milford, MA). The column used was a Phenomenex Luna C_{18} (5 micron, 30 x 75 mm; Phenomenex, Inc., Torrance, CA) at a flow rate of 45.0 mL/min. The mobile phase consisted of acetonitrile and water (each containing 0.1% trifluoroacetic acid). A gradient of 10% to 50% acetonitrile over 8 min was used during the purification. Fraction collection was triggered by UV detection at 220 nM. Analytical analysis was performed on an Agilent LC/MS (Agilent Technologies, Santa Clara, CA).

-Method 1: A 7-min gradient of 4% to 100% acetonitrile (containing 0.025% trifluoroacetic acid) in water (containing 0.05% trifluoroacetic acid) was used with an 8-min run time at a flow rate of 1.0 mL/min.

-Method 2: A 3-min gradient of 4% to 100% acetonitrile (containing 0.025% trifluoroacetic acid) in water (containing 0.05% trifluoroacetic acid) was used with a 4.5-min run time at a flow rate of 1.0 mL/min.

Retention time (RT) and m/z for M+1 is reported, occasionally M+Na is observed exclusively.

A Phenomenex Luna C_{18} column (3 micron, 3 x 75 mm) was used at a temperature of 50 °C. Purity determination was performed using an Agilent diode array detector for both Method 1 and Method 2. Mass determination was performed using an Agilent 6130 mass spectrometer with electrospray ionization in the positive mode. ^{1}H and ^{13}C NMR spectra were recorded on Varian 400 MHz spectrometers (Agilent Technologies, Santa Clara, CA). Signals are described as singlets (*s*), doublets (*d*), triplets (*t*), quadruplets (*q*), septuplets (*sept*), doublet of doublets (*dd*) and doublet of triplets (*dt*).

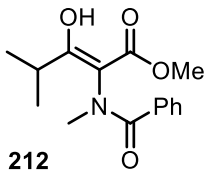

212

Methyl-3-hydroxy-4-methyl-2-(N-methylbenzamido)pent-2-enoate (209A)[115]

Isobutyryl chloride (0.506 mL, 4.83 mmol) was added to a stirred solution of methyl N-benzoyl-N-methylglycinate (1.0 g, 4.83 mmol) and 1-methyl-1H-imidazole (0.462 mL, 5.79 mmol) in DCM (10mL) at -45 ˚C under an Ar atmosphere, followed by stirring at the same temp. for 10 min. $TiCl_4$ (1.862 mL, 16.89 mmol)and Hunig's base (3.37 mL, 19.30 mmol) were successively added to the mixture, which was stirred at the same temp. for 30 min. The mixture was quenched with water (20 ml), which was extracted twice with EtOAc. The combined organic phase was washed with water, brine, dried over $MgSO_4$ and concentrated. The crude oil was purified by column chromatography to yield methyl 4-methyl-2-(N-methylbenzamido)-3-oxopentanoate, **209** as a white solid (0.575 g, 2.075 mmol, 43 % yield) LCMS RT (Method 2) 3.24-3.4 min (m/z 278.1) ^{1}H NMR (400 MHz, $CDCl_3$) δ 12.16 (d, *J* = 1.5 Hz, 1H), 7.51 – 7.23 (m, 6H), 3.83 – 3.80 (m, 3H), 3.16 (s, 3H), 2.81 – 2.70 (m, 1H), 1.11 (d, *J* = 6.8, 3H), 0.77 (d, *J* = 6.7, 3H ^{13}C NMR (101 MHz, $CDCl_3$) δ 180.97, 172.64, 170.86, 136.07, 129.72, 127.92, 126.74, 108.16, 52.16, 37.32, 29.15, 20.38, 17.72. HRMS (ESI) *m/z* calcd for [M + H] 278.1392, found 278.1384.

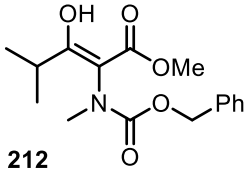

212

Methyl-2-(((benzyloxy)carbonyl)(methyl)amino)-3-hydroxy-4-methylpent-2-enoate (209B)

Following the procedure for preparation of **209A**, the condensation of isobutyryl chloride (0.442 mL, 4.21 mmol) and methyl N-((benzyloxy)carbonyl)-N-methylglycinate (1.0 g, 4.21 mmol) catalysed by 1-methyl-1H-imidazole (0.403 mL, 5.06 mmol), $TiCl_4$ (1.627 mL, 14.75 mmol) and diisopropylethylamine (2.94 mL, 16.86 mmol) gives methyl 2-

(((benzyloxy)carbonyl) (methyl)amino)-4-methyl-3-oxopentanoate (0.492 g, 1.602 mmol, 38% yield) **(209B)** as a colourless oil. LCMS RT (Method 2) 3.64 min (m/z 308.1) ^{1}H NMR (400 MHz, $CDCl_3$) enol (major) reported δ 12.19 (s, 1H), 7.49 – 7.11 (m, 5H), 5.17 – 5.01 (m, 2H), 3.77 – 3.62 (m, 3H), 3.03 – 2.95 (m, 3H), 2.84 – 2.75 (m, 1H), 1.13 – 0.97 (m, 6H). ^{13}C NMR (101 MHz, $CDCl_3$) δ 206.64, 180.66, 171.11, 156.63, 136.69, 128.33, 127.87, 127.74, 105.57, 67.21, 51.81, 37.72, 29.11, 18.88.

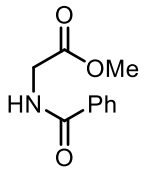

Methyl N-benzamidoacetate

To 2-benzamidoacetic acid (5g, 27.9 mmol) in methanol (140 ml) under cooling with an ice bath (0-5˚C) was added thionyl chloride (2.85 ml, 39.1 mmol) over a period of 2 mins. The mixture was stirred overnight, after which time TLC indicated consumption of the starting 2-benzamidoacetic acid. The reaction mixture was concentrated under reduced pressure to give the crude product, which was taken up in ethyl acetate (100mL), washed extracted with sat. $NaHCO^3$ (2x30mL) organics were dried over $MgSO_4$ and dried to give a crude white solid which was purified by silica gel column chromatography (100% ethyl acetate) affording methyl 2-benzamidoacetate (4.37 g, 22.60 mmol, 81% yield) as a white solid. LCMS RT (Method 2) 2.40 min (m/z 194.0) ^{1}H NMR (400 MHz, $CDCl_3$) δ 7.83 – 7.75 (m, 2H), 7.52 – 7.43 (m, 1H), 7.44 – 7.34 (m, 2H), 6.87 (s, 1H), 4.20 (d, *J* = 5.1 Hz, 2H), 3.75 (s, 3H ^{13}C NMR (101 MHz, $CDCl_3$) δ 170.50, 167.51, 133.62, 131.75, 131.48, 128.54, 127.06, 77.36, 77.04, 76.72, 52.40, 41.68. HRMS (ESI) *m/z* calcd for [M + H] 194.0812, found 194.0815.

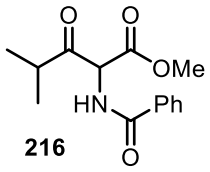

216

Procedure ref: J. Am. Chem. Soc., 2005, 127 (9), pp 2854-2855

Isobutyryl chloride (2.66 mL, 25.4 mmol) was added to a stirred solution of methyl 2-benzamidoacetate (4.9g, 25.4 mmol) and 1-methyl-1H-imidazole (2.426 mL, 30.4 mmol) in DCM (50mL) at -45 ˚C under an N_2 atmosphere, followed by being stirred at the same temperature for 10 min. TiCl4 (9.79 mL, 89 mmol) and diisopropylethylamine (17.72 mL, 101 mmol) were successively added to the mixture, which was stirred at same temp. for 1hr. The mixture was quenched with water (100 ml), which was extracted twice with EtOAc. The combined organic phase was washed with water, brine, dried over with MgSO4 and concentrated. Purification by gradient normal phase chromatography yields methyl 2-benzamido-4-methyl-3-oxopentanoate, **216** (3.61 g, 13.70 mmol, 54 % yield) as a colourless oil. LCMS RT (Method 2) 3.14 min (m/z 264.1) ^{1}H NMR (400 MHz, $CDCl_3$) δ 7.86 – 7.79 (m, 2H), 7.52 – 7.46 (m, 1H), 7.45 – 7.38 (m, 2H), 7.37 – 7.34 (m, 1H), 5.59 (d, J = 6.7 Hz, 1H), 3.78 (s, 3H), 3.19 – 3.02 (sept, 1H), 1.24 – 1.08 (dd, 6H). ^{13}C NMR (101 MHz, $CDCl_3$) δ 205.02, 166.94, 132.98, 132.05, 128.59, 127.23, 61.03, 53.26, 38.76, 18.81, 17.66. HRMS (ESI) *m/z* calcd for [M + H] 264.1230, found 264.1226.

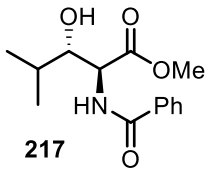

217

Methyl (2S,3S)-2-benzamido-3-hydroxy-4-methylpentanoate

Under N_2, to a solution of methyl 2-benzamido-4-methyl-3-oxopentanoate (2g, 7.60 mmol) in DCM (25mL) was added 50mL sodium formate solution (5N) followed by TBAI (5.61 g, 15.19 mmol) and pre-activated Ru(p-cymene)[(S,S)-Ts-DPEN] (**226**) (0.140 g, 0.228 mmol, 3% loading). After 48 hours the reaction was added to a seperatory funnel and diluted with EtOAc and sat. $NaHCO_3$, organics are removed and aqueous is extracted with twice with EtOAc, the crude oil was purified by gradient column chromatography yielding (2S,3S)-methyl 2-benzamido-3-hydroxy-4-methylpentanoate, **217**

(1.794 g, 6.76 mmol, 89% yield), a colourless oil, as an inseperable mixture of *syn* and *anti* diasteromers (12:87 by NMR). Major isomer (anti) reported: LCMS RT (Method 2) 2.89 min (m/z 266.1) ^{1}H NMR (400 MHz, $CDCl_3$) δ 7.82 – 7.75 (m, 2H), 7.52 – 7.43 (m, 1H), 7.43 – 7.34 (m, 2H), 7.29 – 7.20 (m, 1H), 4.93 (dd, *J* = 7.6, 3.4 Hz, 1H), 3.76 (s, 3H), 3.63 – 3.51 (m, 1H), 3.27 (d, *J* = 7.7 Hz, 1H), 1.77 (dsept, *J* = 8.5, 6.7 Hz, 1H), 0.99 (t, *J* = 6.5 Hz, 6H). ^{13}C NMR (101 MHz, $CDCl_3$) δ 171.37, 167.41, 133.41, 131.91, 128.57, 127.16, 78.71, 55.80, 52.51, 31.38, 19.08. HRMS (ESI) *m/z* calcd for [M + H^+] 266.1392, found 266.1327. For copies of HPLC chromatograms – see appendix.

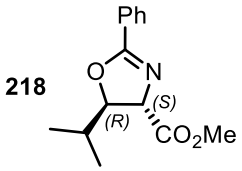

Methyl (4S,5R)-5-isopropyl-2-phenyl-4,5-dihydrooxazole-4-carboxylate

(2S,3S)-methyl 2-benzamido-3-hydroxy-4-methylpentanoate, **217** (1.3g, 4.90 mmol) dissolved in DCM is added portionwise to thionyl chloride (5mL, 68.5 mmol) under an atmosphere of N_2 with cooling in an ice bath, the reaction is stirred overnight. Excess thionyl chloride is removed under vaccuum. Residue is dissolved in EtOAc (50mL), washed with 10% Na_2CO_3 (3x20mL), washed with brine, dried over $MgSO_4$, volatiles are again removed under rotary evaporation and the crude is purified by gradient column chromatography to yield) Methyl 5-isopropyl-2-phenyl-4,5-dihydrooxazole-4-carboxylate **218** (1.054 g, 4.26 mmol, 87 % yield), a colourless oil, as a seperable mixture of *syn* and *anti* diastereomers. Major diastereomer, (4R,5S) reported. LCMS RT (Method 2) 3.85 min (m/z 248.1) ^{1}H NMR (400 MHz, $CDCl_3$) δ 8.01 – 7.95 (m, 2H), 7.53 – 7.44 (m, 1H), 7.44 – 7.35 (m, 2H), 4.66 (dd, *J* = 6.9, 6.3, Hz, 1H), 4.55 (d, *J* = 7.1 Hz, 1H), 3.79 (s, 3H), 2.01 – 1.88 (m, *J* = 6.7 Hz, 1H), 1.00 (dd, *J* = 13.7, 6.7, Hz, 6H).. ^{13}C NMR (101 MHz, $CDCl_3$) δ 172.00, 165.75, 131.79, 128.52, 128.31, 127.08, 87.20, 71.19, 52.68, 32.40, 17.38, 17.26. HRMS (ESI) *m/z* calcd for [M + H] 248.1286, found 248.1284.

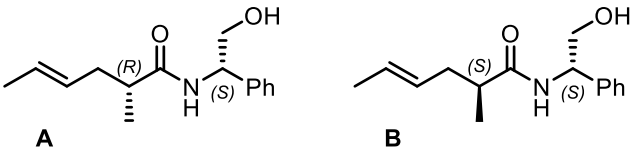

Literature ref. Deyo, D. T.; Aebi, J. D.; Rich, D. H. *Synthesis* **1988**, 608

To a solution of (E)-2-methylhex-4-enoic acid (rac-**206)** (2.5 g, 19.51 mmol) in DCM was added HATU (8.90 g, 23.41 mmol) and DIPEA (4.09 ml, 23.41 mmol). After allowing 5 minutes for preactivation, (S)-2-amino-2-phenylethanol (3.48 g, 25.4 mmol) was added and the reaction was stirred overnight. The solvent was removed by rotary evaporation, then the crude was dissolved in EtOAc, which was washed with 1N HCl, 1N NaOH and brine. Organics were dried over MgSO4, filtered, evaporated and purified by column chromatography (30% EtOAc in Hexanes) to yield (E)-N-((S)-2-hydroxy-1-phenylethyl)-2-methylhex-4-enamide (4.36 g, 17.63 mmol, 90 % yield) as a seperable mixture of diastereomers.

(R,E)-N-((S)-2-hydroxy-1-phenylethyl)-2-methylhex-4-enamide - **A**

LCMS RT (Method 1) 2.89 min (m/z 248.1) ^{1}H NMR (400 MHz, $CDCl_3$) δ 7.39 – 7.22 (m, 5H), 6.23 (d, *J* = 7.1 Hz, 1H), 5.51 – 5.38 (m, 1H), 5.32 (dddd, *J* = 15.1, 6.8, 5.2, 1.5 Hz, 1H), 5.03 (dt, *J* = 7.1, 4.9 Hz, 1H), 3.84 (td, *J* = 5.0, 4.4, 1.4 Hz, 2H), 2.96 – 2.88 (m, 1H), 2.35 – 2.20 (m, 2H), 2.15 – 2.01 (m, 1H), 1.59 (dq, *J* = 6.3, 1.2 Hz, 3H), 1.15 (d, *J* = 6.4 Hz, 3H). ^{13}C NMR (101 MHz, $CDCl_3$) δ 176.67, 139.03, 128.82, 128.12, 127.79, 127.73, 126.66, 66.69, 55.72, 41.73, 37.34, 17.90, 17.43. HRMS (ESI) *m/z* calcd for [M + H] 248.1645, found 248.1647.

(S,E)-N-((S)-2-hydroxy-1-phenylethyl)-2-methylhex-4-enamide - **B**

LCMS RT (Method 1) 2.89 min (m/z 248.1) ^{1}H NMR (400 MHz, $CDCl_3$) δ 7.39 – 7.13 (m, 5H), 6.73 (d, *J* = 7.1 Hz, 1H), 5.51 – 5.27 (m, 2H), 5.01 – 4.86 (m, 1H), 3.71 (d, *J* = 5.2 Hz, 2H), 3.49 (s, 1H), 2.24 (h, *J* = 7.1 Hz, 2H), 2.03 (q, *J* = 10.5, 9.4 Hz, 1H), 1.69 – 1.56 (m, 3H), 1.04 (d, *J* = 6.6 Hz, 3H) ^{13}C NMR (101 MHz, $CDCl_3$) δ 176.85, 139.31, 128.64, 128.17, 127.55, 126.62, 66.11, 55.66, 41.33, 37.18, 17.96, 17.28.

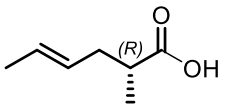

(R,E)-2-methylhex-4-enoic acid

A solution of (R,E)-N-((S)-2-hydroxy-1-phenylethyl)-2-methylhex-4-enamide (1g, 4.04 mmol)
in 6N H_2SO_4 in 60mL (H_2O/Dioxane) is heated to 80˚C for 3 hours, following this the reaction is cooled to room temperature. The reaction is diluted with water (50mL) and is extracted with DCM and dried with $MgSO_4$. The volatiles are removed under reduced pressure to yield (R,E)-2-methylhex-4-enoic acid (0.503 g, 3.92 mmol, 97 % yield) as a transllucent, yellow oil.

LCMS RT (Method 1) 2.95 min (no m/z in +ve mode) ^{1}H NMR (400 MHz, $CDCl_3$) δ 5.59 – 5.43 (m, 1H), 5.43 – 5.31 (m, 1H), 2.48 (h, *J* = 6.9 Hz, 1H), 2.43 – 2.30 (m, 1H), 2.19 – 2.05 (m, 1H), 1.69 – 1.60 (m, 3H), 1.15 (dd, *J* = 7.0, 0.4 Hz, 3H). ^{13}C NMR (101 MHz, $CDCl_3$) δ 182.54, 127.76, 127.49, 39.52, 36.32, 17.88, 16.22.

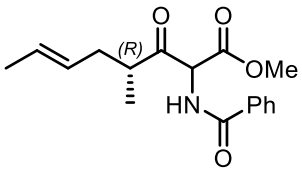

Methyl (4R,E)-2-benzamido-4-methyl-3-oxooct-6-enoate

(R,E)-2-methylhex-4-enoic acid (116mg, 0.905 mmol), methyl phenylglycinate (150 mg, 0.905 mmol) and 2,2,2-trichloroacetyl chloride (0.122 mL, 1.086 mmol) were dissolved in DCM (1mL). This solution was added to anhydrous NaH (26.1 mg, 1.086 mmol) in DCM (1mL) with cooling inan ice bath. This reaction was stirred for 15 minutes to allow for activation. The reaction was then cooled to -45˚C followed by the addition of 1-methyl-1H-imidazole (0.087 mL, 1.086 mmol), the reaction was stirred for 10 minutes. TiCl4 (0.349 mL, 3.17 mmol) and N-ethyl-N-isopropylpropan-2-amine (0.631 mL, 3.62 mmol) are added sequentially and the subsequent black solution is stirred for 30 minutes at -45˚C. The reaction is quenched by the addition of 5mL of water, the solution is extracted twice with EtOAc, dried over $MgSO_4$ and purified by gradient column chromatography yielding methyl (4R,E)-4-methyl-3-oxo-2-(phenylamino)oct-6-enoate (57mg, 0.207 mmol, 22.87 % yield) LCMS RT (Method 2) 3.38 min (m/z 304.1) ^{1}H NMR (400 MHz, $CDCl_3$) δ 7.85 – 7.81 (m, 2H), 7.53 (ddd, *J* = 7.8, 6.2, 1.9 Hz, 1H), 7.49 – 7.34 (m, 3H), 6.21 (s, 1H), 5.56 (dd, *J* = 11.0, 6.7 Hz, 1H), 5.45 (dddd, *J* =

13.6, 12.2, 8.4, 6.4, Hz, 1H), 5.38 – 5.19 (m, 1H), 3.81 (dd, *J* = 6.1, 0.7 Hz, 3H), 3.18 – 3.05 (m, 1H), 2.45 – 2.31 (m, 1H), 2.21 – 1.99 (m, 1H), 1.60 (dq, *J* = 6.4, 1.9, Hz, 3H), 1.23 – 1.03 (m, 3H) ^{13}C NMR (101 MHz, $CDCl_3$) δ 204.37, 203.98, 167.35, 166.68, 166.28, 132.29, 128.69, 128.02, 127.28, 126.65, 62.12, 53.25, 44.16, 36.59, 35.32, 17.85, 16.90, 15.56.

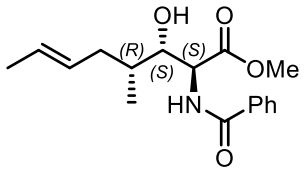

Methyl (2S,3S,4R,E)-2-benzamido-3-hydroxy-4-methyloct-6-enoate

To a methyl (4R,E)-4-methyl-3-oxo-2-(phenylamino)oct-6-enoate (50mg, 0.165 mmol) under N_2 was added degassed DCM (1.7mL), (R,R)-RuTethTsDPEN (9.62 mg, 0.016 mmol) followed by TBAI (122 mg, 0.330 mmol) and 1.7mL of a 5N solution of HCO_2Na in H_2O. The reaction is stirred at 1400RPM for 48 hours. Following complete consumption of the starting material, the reaction is diluted with 3mL of sat.$NaHCO_3$, which is extracted with 2x3mL of EtOAc. The organics are combined, dried over $MgSO_4$ and purified by gradient column chromatography to yield methyl (2S,3S,4R,E)-2-benzamido-3-hydroxy-4-methyloct-6-enoate (36.7 mg, 0.120 mmol, 73 % yield) as a colourless oil. ^{1}H NMR (400 MHz, $CDCl_3$) δ 7.84 – 7.76 (m, 2H), 7.56 – 7.48 (m, 1H), 7.44 (ddt, *J* = 8.2, 6.6, 1.3 Hz, 2H), 7.00 (d, *J* = 7.9 Hz, 1H), 5.54 – 5.30 (m, 2H), 4.96 (dd, *J* = 7.8, 4.8 Hz, 1H), 3.79 (s, 3H), 3.79 – 3.73 (m, 1H), 2.81 (s, 1H), 2.19 (dddd, *J* = 13.3, 5.4, 3.9, 2.6 Hz, 1H), 2.00 – 1.88 (m, 1H), 1.65 (dq, *J* = 6.3, 1.2 Hz, 3H), 0.98 (d, *J* = 6.7 Hz, 3H). ^{13}C NMR (101 MHz, $CDCl_3$) δ 171.77, 167.31, 133.42, 131.97, 128.63, 128.33, 127.42, 127.13, 76.04, 55.67, 52.60, 36.55, 35.99, 17.96, 14.50.HRMS (ESI) *m/z* calcd for [M + H] 306.1705, found 306.1706. IR (neat)3357, 2957, 1735, 1640, 1526.

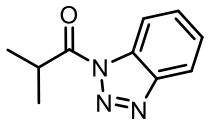

1-(1H-benzo[d][1,2,3]triazol-1-yl)-2-methylpropan-1-one

Prcedure ref. Katritzky, A. R.; Kirichenko, B. V. *Synthesis,* **2003**, 2777-2780

$SOCl_2$ (1.823 ml, 24.97 mmol) was added to a stirred solution of 1H-benzo[d][1,2,3]triazole (10.82 g, 91 mmol) in DCM (114 ml). Stirring was continued for 30 min. isobutyric acid (2.062 ml, 22.70 mmol)was added to the reaction mixture and stirring was continued for another 16 h. The white precipitate was filtered off and washed with CH2Cl2. The combined DCM filtrate was washed with 1N NaOH aqueous solution, extracted with sat. $NaCl_{(aq)}$, dried over $MgSO_4$, and concentrated to give a yellow oil. The product was purified by gradient column chromatography 5-10% etoac/hex to yield 1-(1H-benzo[d][1,2,3]triazol-1-yl)-2-methylpropan-1-one (3.741 g, 19.77 mmol, 87 % yield) as a pale, straw coloured, free flowing oil. LCMS RT (Method 2) 3.50 min (no m/z in +ve mode) ^{1}H NMR (400 MHz, $CDCl_3$) δ 8.28 (d, *J* = 8.3 Hz, 1H), 8.10 (d, *J* = 8.3 Hz, 1H), 7.63 (t, *J* = 7.7 Hz, 1H), 7.48 (t, *J* = 7.7 Hz, 1H), 4.14 (hept, *J* = 6.9 Hz, 1H), 1.41 (s, 3H) ^{13}C NMR (101 MHz, $CDCl_3$) δ 176.59, 146.12, 131.27, 130.28, 126.01, 120.04, 114.54, 77.32, 77.20, 77.00, 76.68, 33.96, 19.07.

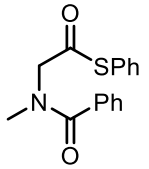

S-phenyl 2-(N-methylbenzamido)ethanethioate

Procedure ref. Synthesis 2002, No. 8, 1121–1123

An oven-dried round-bottomed flask was equipped with a magnetic stirring bar. The flask was charged with N-benzoyl-N-methylglycine (3g, 15.53 mmol) and anhydrous DCM (31.1 ml, 0.5M) with cooling in an icewater bath. To the flask were added successively isobutyl chloroformate (2.333 g, 17.08 mmol) and triethylamine (1.571 g, 15.53 mmol), which was allowed 10mins for activation. Following this, benzenethiol (3.76 g, 34.2 mmol) and a second equivalent of triethylamine (1.571 g, 15.53 mmol) were added and the reaction was allowed to warm to room temperature and stirred for 4 hours. The reaction is diluted with Et2O (30mL) to facilitate precipitation of triethylamine HCl, the salt is filtered off and the filter cake is washed with Et2O, (50mL). The combined organics are reduced on a rotary evaporator. The residue is taken up in EtOAc, and washed with 1N HCl, 1N NaOH, and brine. Organics are then

dried over MgSO4, and concentrated by rotary evaporation. The crude material is purified by gradient column chromatography to yield. S-phenyl 2-(N-methylbenzamido)ethanethioate (3.54 g, 12.42 mmol, 80 % yield) as a colourless oil, which eventually solidified on standing. LCMS RT (Method 1) ^{1}H NMR (400 MHz, $CDCl_3$) (Rotamers) δ 7.73 – 7.31 (m, 10H), 4.55 (s, 1.4H), 4.24 (s, 0.6 H), 3.13 (s, 3H). ^{13}C NMR (101 MHz, $CDCl_3$) δ 194.86, 171.97, 135.18, 134.76, 130.02, 129.67, 129.34, 128.48, 127.07, 57.02, 39.14. HRMS (ESI) *m/z* calcd for [M + Na] 308.0716 , found 308.0720.

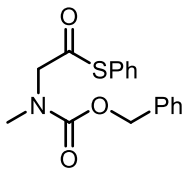

S-phenyl 2-(((benzyloxy)carbonyl)(methyl)amino)ethanethioate

Following the procedure above, 2-(((benzyloxy)carbonyl)(methyl)amino) acetic acid (5g, 22.40 mmol) was transformed into its derived phenyl thioester with isobutyl chloroformate (3.22 ml, 24.64 mmol) benzenethiol (5.03 ml, 49.3 mmol) and triethylamine (6.24 ml, 44.8 mmol). Following aqueous work-up the material was purified by gradient column chromatography (10-30% EtOAc in hexanes) to yield S-phenyl 2-(((benzyloxy)carbonyl)(methyl)amino)ethanethioate (6.27g, 19.88 mmol, 89 % yield) as a colourless oil. LCMS RT (Method 2) 3.57 min (m/z 316.1) ^{1}H NMR (400 MHz, $CDCl_3$) δ 7.46 – 7.26 (m, 9H), 5.19 (d, J = 6.9 Hz, 2H), 4.29 (s, 1H), 4.20 (s, 1H), 3.09 (d, J = 13.5 Hz, 3H). ^{13}C NMR (101 MHz, $CDCl_3$) δ 196.04, 195.74, 156.59, 155.76, 136.36, 136.25, 134.70, 134.61, 129.58, 129.55, 129.27, 128.50, 128.11, 128.01, 127.86, 126.52, 77.33, 77.01, 76.70, 67.77, 67.73, 58.65, 58.47, 36.58, 35.81. HRMS (ESI) *m/z* calcd for [M + H] 316.1002, found 316.1013.

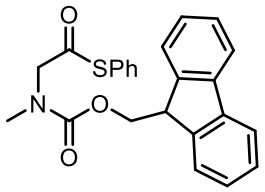

S-phenyl2-((((9H-fluoren-9 yl)methoxy)carbonyl)(methyl)amino)ethane thioate

Following the procedure for above, 2-((((9H-fluoren-9-yl)methoxy)carbonyl)(methyl)amino)acetic acid (5g, 16.06 mmol) was transformed into its derived phenyl thioester with isobutyl carbonochloridate (2.309 ml, 17.67 mmol) benzenethiol (3.60 ml, 35.3 mmol) and triethylamine (4.48 ml, 32.1 mmol). Following aqueous work-up the material was purified by gradient column chromatography (0-30% EtOAc in hexanes) to yield S-phenyl 2-(((benzyloxy)carbonyl)(methyl)amino)ethanethioate (6.27g, 19.88 mmol, 89 % yield) as a colourless oil. S-phenyl 2-((((9H-fluoren-9yl)methoxy)carbonyl)(methyl)amino) ethanethioate (1.07 g, 2.65 mmol, 17 % yield) LCMS RT (Method 1) 3.83 min (m/z 404.1 (M+H), 426.1 (M+Na) ^{1}H NMR (400 MHz, $CDCl_3$) δ 7.76 (dd, *J* = 7.7, 3.0 Hz, 2H), 7.60 (dd, *J* = 18.7, 7.5 Hz, 2H), 7.44 – 7.24 (m, 8H), 4.53 – 4.44 (m, 2H), 4.29 (s, 1H), 4.34 – 4.21 (m, 1H), 4.16 (s, 1H), 3.08 (d, *J* = 1.9 Hz, 3H), 1.55 (s, 1H). ^{13}C NMR (101 MHz, $CDCl_3$) δ 143.81, 141.31, 134.70, 134.60, 129.57, 129.27, 127.71, 127.08, 125.01, 124.93, 119.99, 77.31, 76.99, 76.67, 68.05, 58.61, 58.35, 47.23, 36.50, 35.81. HRMS (ESI) *m/z* calcd for [M + H] 404.1315, found 404.1298. IR (neat) 3059, 2925, 1694, 1633, 1383

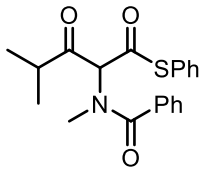

S-phenyl 4-methyl-2-(N-methylbenzamido)-3-oxopentanethioate

Under N_2 with cooling in an ice-bath, magnesium bromide diethyl etherate (1.27 g, 4.91 mmol) was added to a stirred solution of1-(1H-benzo[d][1,2,3]triazol-1-yl)-2-methylpropan-1-one (265 mg, 1.402 mmol) in DCM (6ml), which is followed by the addition of S-phenyl 2-(N-methylbenzamido)ethanethioate (400mg, 1.402 mmol) and hunig's base (0.979 ml, 5.61 mmol). The ice-bath was removed and the reaction is allowd to warm to ambient temperature, the reaction was left to stir overnight (18h). upon completion, the reaction is cooled back down to 0-5˚C, then 10% aqueous HCl (8 mL) was added dropwise. Stirring was continued for 5 min

and the mixture was partitioned between EtOAc (30 mL) and H2O (20 mL). The aqueous phase was extracted with EtOAc (2 x 20 mL) and the combined organic extracts were washed with brine, dried over MgSO4, and evaporated to give a cloudy oil. This was purified by gradient column chromatography to give S-phenyl 4-methyl-2-(N-methylbenzamido)-3-oxopentanethioate (379 mg, 1.065 mmol, 76 % yield) as a colourless oil which solidifies upon standing.

LCMS RT (Method 1) 3.64 min (m/z 356.0) ^{1}H NMR (400 MHz, $CDCl_3$) (Mixture of rotamers and tautomers, major product reported) δ 12.79 (d, *J* = 1.5 Hz, 1H), 7.69 – 7.57 (m, 2H), 7.46 (s, 5H), 7.43 – 7.30 (m, 3H), 3.37 (s, 3H), 2.54 (heptd, *J* = 6.5, 1.8 Hz, 1H), 1.14 (d, *J* = 6.8 Hz, 3H), 0.69 (d, *J* = 6.7 Hz, 3H). ^{13}C NMR (101 MHz, $CDCl_3$) δ 195.17, 180.01, 172.73, 135.36, 135.19, 135.06, 130.23, 129.89, 129.35, 129.20, 128.53, 127.93, 127.52, 126.87, 126.43, 116.65, 41.35, 38.66, 36.61, 30.26, 29.90, 29.68, 24.66, 20.54, 19.36, 19.23, 17.60. HRMS (ESI) *m/z* calcd for [M + H] 356.1320, found 356.1437

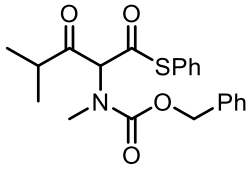

S-phenyl 2-(((benzyloxy)carbonyl)(methyl)amino)-4-methyl-3-oxopentanethioate

According the the procedure of above-(1H-benzo[d][1,2,3]triazol-1-yl)-2-methylpropan-1-one (1.143 g, 6.04 mmol was coupled to S-phenyl 2-(((benzyloxy)carbonyl)(methyl)amino)ethanethioate (2g, 6.34 mmol) using magnesium bromide diethyl etherate (5.46 g, 21.14 mmol)) and hunig's base (4.22 ml, 24.16 mmol) in DCM (24.16 ml), which, following purification by gradient column chromatography (15-30%), affords S-phenyl 2-(((benzyloxy)carbonyl)(methyl)amino)-4-methyl-3-oxopentanethioate (2.165 g, 5.62 mmol, 93 % yield) as a colourless, mobile oil. *Rotameric, keto enol.* ^{1}H NMR (400 MHz, $CDCl_3$) δ 12.89 – 12.74 (m, 1H), 7.53 – 7.21 (m, 10H), 5.29 – 5.13 (m, 2H), 3.25 – 3.20 (m, 3H), 2.62 (ttd, *J* = 8.3, 6.5, 1.5 Hz, 1H), 1.08 (dd, *J* =6.8, 0.7 Hz, 6H). ^{13}C NMR (101 MHz, $CDCl_3$) δ 195.00, 194.65, 180.38, 179.41, 156.27, 136.34, 135.24, 135.12, 129.63, 129.58, 129.17, 129.13, 128.49, 128.40, 128.12, 128.07, 128.05, 127.90, 126.84, 126.76, 114.04, 67.89, 67.78, 38.36, 38.09, 30.07, 29.85, 19.31, 18.98, 18.69. [M + H^+]; HRMS (ESI) *m/z* calcd for [M + H] 386.1421, found 386.1427. IR (neat) 2967, 1706, 1607, 1454, 1327.

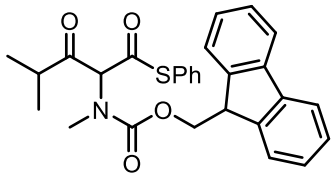

S-phenyl 2-((((9H-fluoren-9-yl)methoxy)carbonyl)(methyl)amino)-4-methyl-3-oxopentanethioate

According the the procedure above 1-(1H-benzo[d][1,2,3]triazol-1-yl)-2-methylpropan-1-one (1.117 g, 5.90 mmol) S-phenyl 2-((((9H-fluoren-9-yl)methoxy)carbonyl)(methyl)amino)ethanethioate (2.5 g, 6.20 mmol) using magnesium bromide diethyl etherate (4.57 g, 17.70 mmol) and hunig's (4.12 ml, 23.60 mmol) in DCM (23 ml), which, following purification by gradient column chromatography (0-30%), S-phenyl 2-((((9H-fluoren-9-yl)methoxy)carbonyl)(methyl)amino)-4-methyl-3-oxopentanethioate (570mg, 1.204 mmol, 20 % yield) as a colourless, mobile oil. *Rotameric, keto enol.* LCMS RT (Method 2) 4.0 min (m/z 474.7) ^{1}H NMR (400 MHz, $CDCl_3$) δ 12.85 (d, *J* = 1.5 Hz, 1H), 7.81 – 7.71 (m, 2H), 7.65 – 7.49 (m, 2H), 7.46 – 7.30 (m, 7H), 7.28 – 7.21 (m, 2H), 4.51 (dd, *J* = 10.3, 7.4 Hz, 1H), 4.31 (dd, *J* = 10.4, 7.2 Hz, 1H), 4.19 (t, *J* = 7.3 Hz, 1H), 3.16 (s, 3H), 2.67 (sep, *J* = 6.8, 1.5 Hz, 1H), 1.10 (dd, *J* = 6.8 Hz, 6H). ^{13}C NMR (101 MHz, $CDCl_3$) δ 195.09, 179.62, 156.34, 143.69, 143.64, 141.26, 141.23, 135.23, 135.16, 129.67, 129.14, 129.13.

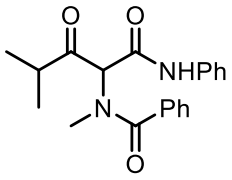

N-methyl-N-(4-methyl-1,3-dioxo-1-(phenylamino)pentan-2-yl)benzamide

(2,2,2-trifluoroacetyl)silver (63.4 mg, 0.309 mmol) was added to a stirring solution of S-phenyl 4-methyl-2-(N-methylbenzamido)-3-oxopentanethioate (100mg, 0.281 mmol) and aniline (31.4 mg, 0.338 mmol) in THF (2.010 mL). EtOAc (20 mL) was added and the mixture was passed through a pad of celite with was washed with EtOAc. The filtrate was concentrated followed by purification by flash chromatography over silica gel affording (15-35% EtOAc/Hexanes affords. N-methyl-N-(4-methyl-1,3-dioxo-1-(phenylamino)pentan-2-yl)benzamide (89 mg, 0.264 mmol, 94 % yield) as a pale yellow oil. *Rotameric, keto/enol.* LCMS RT (Method 1) 3.49 min (m/z 339.1) ^{1}H NMR (400 MHz, $CDCl_3$) δ 14.07 (s, 1H), 9.72 (keto, s, 0.3H) 8.41 (s, 1H), 7.63 (d, *J* = 8.6 Hz, 2H), 7.48 – 7.30 (m, 6H), 7.21 (dd, *J* = 12.9, 7.3

Hz, 2H), 5.55 (keto, s, 0.3H) 3.20 (s, 3H), 3.11 (s, 1H), 2.47 – 2.33 (m, 1H), 1.09 (d, *J* = 6.8 Hz, 3H), 0.50 (d, *J* = 6.7 Hz, 3H). ^{13}C NMR (101 MHz, $CDCl_3$) δ 180.04, 173.32, 168.77, 136.91, 134.49, 130.56, 130.52, 129.07, 129.01, 128.48, 128.04, 127.46, 125.10, 121.31, 119.99, 109.05, 38.07, 29.36, 20.51, 17.64. [M + H^+]; HRMS (ESI) *m/z* calcd for [M + H] 339.1703, found 339.1712.

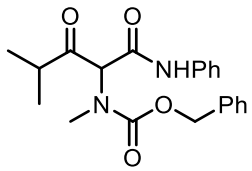

Benzyl methyl(4-methyl-1,3-dioxo-1-(phenylamino)pentan-2-yl)carbamate

Following the procedure above amide formation with S-phenyl 2-(((benzyloxy)carbonyl) (methyl)amino)-4-methyl-3-oxopentanethioate (370mg, 0.960 mmol) in THF (6.4 ml) with aniline (134 mg, 1.440 mmol) and silver trifluoroacetate (276 mg, 1.248 mmol) afford benzyl methyl(4-methyl-1,3-dioxo-1-(phenylamino)pentan-2-yl)carbamate (325 mg, 0.883 mmol, 92 % yield). *Rotameric, keto/enol* LCMS RT (Method 2) 3.61, 3.78 min (m/z 369.2) ^{1}H NMR (400 MHz, $CDCl_3$) δ 14.01 (d, *J* = 1.4 Hz, 1H), 7.70 – 6.96 (m, 11H), 5.31 – 4.98 (m, 2H), 3.13 (s, 3H), 2.55 (sept, *J* = 7.0, 6.4 Hz, 1H), 1.06 (dd, *J* = 66.1, 6.8 Hz, 6H). ^{13}C NMR (101 MHz, $CDCl_3$) δ 169.10, 158.45, 137.21, 129.00, 128.60, 128.24, 127.77, 124.71, 120.06, 75.21, 68.15, 60.71, 33.12, 30.22, 19.49, 17.87. HRMS (ESI) *m/z* calcd for [M + H] 369.1814, found 369.1810. IR (neat) 3331, 2974, 1686, 16223, 1596, 1532 1310.

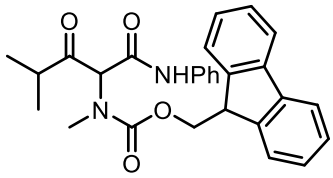

(9H-fluoren-9-yl)methylmethyl(4-methyl-1,3-dioxo-1-(phenylamino)pentan-2-yl)carbamate

Following the procedure above, amide formation with S-phenyl 2-((((9H-fluoren-9-yl)methoxy)carbonyl)(methyl)amino)-4-methyl-3-oxopentanethioate (370mg, 0.781 mmol) in THF (5.2mL) with aniline (109 mg, 1.172 mmol) and silver trifluoroacetate (224 mg, 1.016 mmol) affords (9H-fluoren-9-yl)methyl methyl(4-methyl-1,3-dioxo-1-(phenylamino)pentan-2-yl)carbamate (193 mg, 0.422 mmol, 54 % yield). *Rotameric, keto/enol*. LCMS RT (Method 1) 3.85, 4.01 min (m/z 457.2) ^{1}H NMR (400 MHz, $CDCl_3$) δ 14.23 (s, 1H), 7.80 – 7.70 (m, 1H), 7.69 – 7.60 (m, 2H), 7.56 – 7.45 (m, 2H), 7.45 – 7.40 (m, 1H), 7.39 – 7.32 (m, 3H), 7.31 – 7.22 (m, 2H), 7.22 – 7.10 (m, 2H), 7.06 (t, *J* = 7.5 Hz, 1H), 4.55 – 4.34 (m, 1H), 4.28 (d, *J* = 7.3 Hz, 2H), 3.12 (d, *J* = 29.3 Hz, 3H), 2.68 – 2.53 (m, 1H), 1.17 (d, *J* = 6.7 Hz, 3H), 1.02 (d, *J* = 6.8 Hz, 3H). ^{13}C NMR (101 MHz, $CDCl_3$) δ 180.16, 168.61, 156.94, 143.55, 142.87, 141.11, 136.76, 129.01, 128.96, 127.76, 127.71, 127.12, 127.08, 125.03, 124.88, 124.82, 121.16, 120.18, 119.94, 119.90, 47.14, 46.78, 38.00, 36.63, 29.64, 24.68, 23.37, 19.67, 18.87. [M + H^+]; HRMS (ESI) *m/z* calcd for [M + H] 457.2122, found 456.2122.

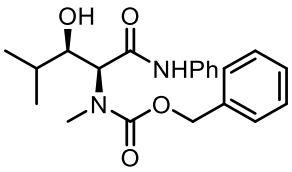

Benzyl ((2S,3R)-3-hydroxy-4-methyl-1-oxo-1-(phenylamino)pentan-2-yl)(methyl)carbamate – 221.

To benzyl methyl(4-methyl-1,3-dioxo-1-(phenylamino)pentan-2-yl)carbamate (50mg, 0.136 mmol)) under N_2 was added degassed DCM (1.75mL), [(R,R)-Teth-TsDpen Ru] (7.92 mg, 0.014 mmol followed by TBAI (122 mg, 0.330 mmol) and 1.7mL of a 5N solution of HCO_2Na in H_2O. The reaction is sealed and stirred at 1400RPM for 48 hours. Following complete consumption of the starting material, the reaction is diluted with 3mL of sat.$NaHCO_3$, which is extracted with 2x3mL of EtOAc. The organics are combined, dried over $MgSO_4$ and purified by gradient column chromatography to yield methyl benzyl ((2S,3R)-3-hydroxy-4-methyl-1-oxo-1-(phenylamino)pentan-2-yl)(methyl)carbamate (32.2 mg, 0.087 mmol, 64 % yield) as a white solid. LCMS RT (Method 1) 3.38 min (m/z 371.1) ^{1}H NMR (400 MHz, $CDCl_3$) δ 8.20 (s, 1H), 7.43 (d, *J* = 7.6 Hz, 2H), 7.40 – 7.26 (m, 7H), 7.14 – 7.09 (m, 1H), 5.27 – 5.14 (m, 2H), 4.79 – 4.70 (m, 1H), 3.99 – 3.91 (m, 1H), 3.56 (d, *J* = 4.4 Hz, 1H), 3.13 (s, 3H), 1.81 (h, *J* = 6.7 Hz, 1H), 0.99 (dd, *J* = 35.7, 6.7 Hz, 6H). ^{13}C NMR (101 MHz, $CDCl_3$) δ 169.10, 158.45, 129.00, 128.60, 128.24, 127.77, 124.71, 120.06, 77.00, 75.21, 68.15, 30.22, 19.49, 17.87.) HRMS (ESI) *m/z* calcd for [M + H] 371.1965, found 371.1963. IR (neat) 3313, 2934, 1666, 1599, 1532, 1441. See appendix **(A5)** for crystal structure analysis. Chiral HPLC CHIRALPAK AD (4.6 x 250 mm, 5 uM) Mobile Phase: Methanol/ Diethylamine 100:0.01 Flow rate: 1.0 mL/min. peak area: (**2R,3S**) : (**2S,3R**) : (**2S,3S**) : (**2R,3R**) 1.8 : 97.9 : 0.3 : 0.

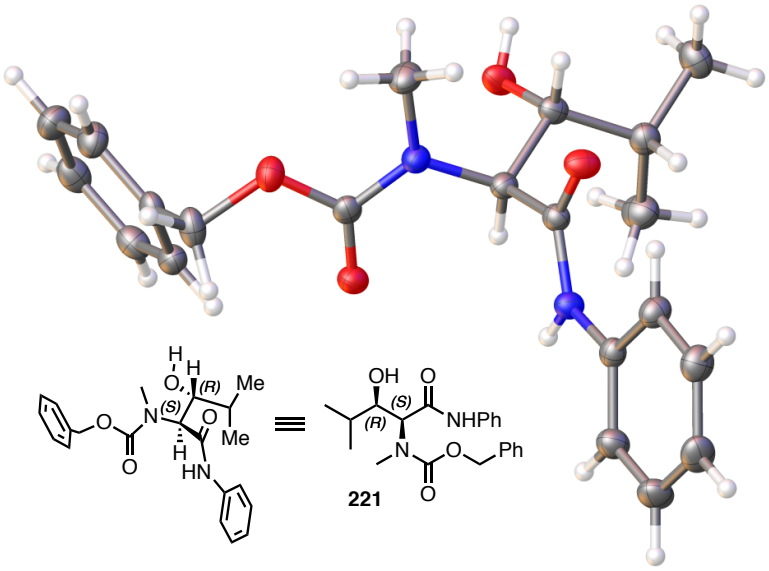

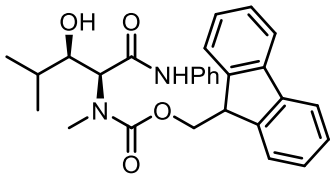

(9H-fluoren-9-yl)methyl((2S,3R)-3-hydroxy-4-methyl-1-oxo-1-(phenylamino)pentan-2-yl)(methyl) carbamate.

Following an analagous procedure for **221** above, (9H-fluoren-9-yl)methylmethyl(4-methyl-1,3-dioxo-1-(phenylamino)pentan-2-yl)carbamate undergoes transferhydrogenation to yield (9H-fluoren-9-yl)methyl((2S,3R)-3-hydroxy-4-methyl-1-oxo-1-(phenylamino)pentan-2-yl)(methyl) carbamate as a white solid. LCMS RT (Method 2) 3.77 min (m/z 459.2) ^{1}H NMR (400 MHz, $CDCl_3$) δ 8.19 (s, 1H), 7.75 (dd, *J* = 7.5, 4.9 Hz, 2H), 7.57 (dd, *J* = 7.6, 4.0 Hz, 2H), 7.47 (d, *J* = 8.0 Hz, 2H), 7.39 – 7.24 (m, 6H), 7.13 (t, *J* = 7.4 Hz, 1H), 4.68 (d, *J* = 5.5 Hz, 1H), 4.52 (qd, *J* = 10.8, 6.8 Hz, 2H), 4.26 (t, *J* = 6.7 Hz, 1H), 3.95 (d, *J* = 5.3 Hz, 1H), 3.06 (s, 3H), 1.77 (q, *J* = 6.8 Hz, 1H), 1.03 (d, *J* = 6.7 Hz, 3H), 0.94 (d, *J* = 6.7 Hz, 3H).^{13}C NMR (101 MHz, $CDCl_3$) δ 168.94, 158.30, 143.69, 143.44, 141.36, 137.22, 128.99, 127.83, 127.08, 124.82, 120.25, 120.03, 75.17, 68.11, 47.25, 36.61, 30.21, 24.66, 23.33, 19.56, 17.77. HRMS (ESI) *m/z* calcd for [M + H] 459.2278, found 459.2288. Chiral HPLC *dr* > 95:5, er > 99:1

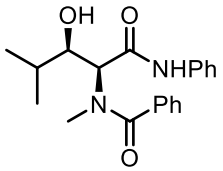

N-((2S,3R)-3-hydroxy-4-methyl-1-oxo-1-(phenylamino)pentan-2-yl)-N-methylbenzamide

Following an analagous procedure for **221** above, N-methyl-N-(4-methyl-1,3-dioxo-1-(phenylamino)pentan-2-yl)benzamide undergoes transfer hydrogenation to N-((2S,3R)-3-hydroxy-4-methyl-1-oxo-1-(phenylamino)pentan-2-yl)-N-methylbenzamide as a white solidLCMS RT (Method 2) 3.18 min (m/z 341.1). ^{1}H NMR (400 MHz, $CDCl_3$) δ 8.87 (s, 1H), 7.53 (dd, *J* = 15.0, 8.0 Hz, 4H), 7.45 (p, *J* = 6.6 Hz, 3H), 7.34 (t, *J* = 7.8 Hz, 2H), 7.13 (t, *J* = 7.4 Hz, 1H), 5.17 (d, *J* = 4.8 Hz, 1H), 4.06 – 3.99 (m, 1H), 3.16 (s, 3H), 1.96 (dq, *J* = 13.3, 6.6 Hz, 1H), 1.12 (d, *J* = 6.6 Hz, 3H), 0.99 (d, *J* = 6.8 Hz, 3H). ^{13}C NMR (101 MHz, $CDCl_3$) δ 178.65, 174.00, 137.42, 130.87, 129.06, 128.57, 127.88, 124.66, 120.07, 75.61, 74.03, 30.56, 19.34, 18.26.

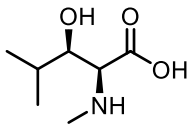

^{1}H NMR (400 MHz, Deuterium Oxide) δ 3.73 (dd, *J* = 7.1, 5.0 Hz, 1H), 3.60 (d, *J* = 7.1 Hz, 1H), 2.79 – 2.74 (m, 4H), 1.85 (tdd, *J* = 13.1, 6.7, 1.6 Hz, 1H), 1.00 (dd, *J* = 6.8, 4.9 Hz, 6H). ^{13}C NMR (101 MHz, cd_3od) δ 169.88, 73.44, 65.79, 31.18, 30.98, 17.46, 14.10.

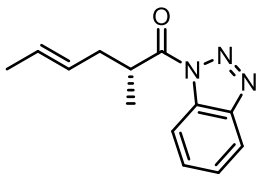

$SOCl_2$ (157 µl, 2.146 mmol) was added to a stirring solution of 1H-benzo[d][1,2,3]triazole (929 mg, 7.80 mmol) in DCM (9mL), in one portion at room temperature. Stirring was continued for 30 min. (R,E)-2-methylhex-4-enoic acid (250mg, 1.951 mmol) in DCM (1mL) was added to the reaction mixture, followed by almost immediate precipitation of 1H-benzo[d][1,2,3]triazole HCl. Reaction mixture is agitated to continue stirring. Stirring is continued overnight. The white precipitate was filtered off and washed with DCM. The combined DCM filtrate was evaporated and the crude slurry was purified by column chromatography (100% DCM) to yield (R,E)-1-(1H-benzo[d][1,2,3]triazol-1-yl)-2-methylhex-4-en-1-one (422mg, 1.841 mmol, 94 %). α_D^{20} – 64.5 (*c* 1.00, $CHCl_3$) LCMS RT (Method 1) 3.68 min (m/z 230.1) ^{1}H NMR (400 MHz, $CDCl_3$) δ 8.29 (dt, *J* = 8.3, 1.0 Hz, 1H), 8.11 (dt, *J* = 8.3, 1.0 Hz, 1H), 7.64 (ddd, *J* = 8.3, 7.1, 1.0 Hz, 1H), 7.49 (ddd, *J* = 8.2, 7.1, 1.1 Hz, 1H), 5.57 – 5.37 (m, 2H), 4.13 (h, *J* = 6.9 Hz, 1H), 2.68 – 2.55 (m, 1H), 2.41 – 2.29 (m, 1H), 1.61 – 1.54 (m, 3H), 1.38 (d, *J* = 6.9 Hz, 3H). ^{13}C NMR (101 MHz, $CDCl_3$) δ 175.80, 146.17, 131.21, 130.27, 128.34, 127.00, 126.03, 120.05, 114.57, 39.35, 36.54, 17.85, 16.78.

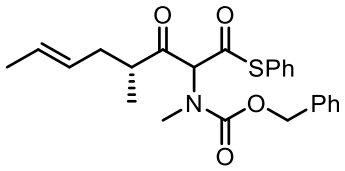

S-phenyl (4R,E)-2-(((benzyloxy)carbonyl)(methyl)amino)-4-methyl-3-oxooct-6-enethioate

To a stirring solution of (R,E)-1-(1H-benzo[d][1,2,3]triazol-1-yl)-2-methylhex-4-en-1-one (385 mg, 1.679 mmol) in anhydrous DCM (6.72 mL) under cooling with an ice bath was added S-phenyl 2-(((benzyloxy)carbonyl)(methyl)amino)ethanethioate (556 mg, 1.763 mmol) followed by magnesium bromide diethyl etherate (1518 mg, 5.88 mmol) and N, N-diisopropylethylamine (1.231 mL, 7.05 mmol). The ice bath was removed and the reaciton is allowed to warm to rrom temperature. The reaction is monitroed by TLC and stirred for 24h. At this point the reaction is cooled back to 0C and is slowly quenched by the initially dropwise addition of 1N HCl (10mL) stirring is continued with cooling for 5 minutes, the ice bath is removed. The reaction is diluted with brine and EtOAc, organics are separated, aqueous is reextracted with EtOAc, dried over $MgSO_4$ and evaporated to yield an oil which is purified by gradient column chromatography (0-30% EtOAc in Hexanes over 10 CV) to yield S-phenyl

(4R,E)-2-(((benzyloxy)carbonyl)(methyl)amino)-4-methyl-3-oxooct-6-enethioate as a colourless oil (426mg, 1.001 mmol, 60 % yield). LCMS RT (Method 2) 4.03 min (m/z 426.1) TLC R_f 0.5 (15%EtOAc in Hexanes) ^{1}H NMR (400 MHz, $CDCl_3$) δ 7.70 – 6.94 (m, 10H), 5.46 (dd, *J* = 13.6, 6.9 Hz, 1H), 5.37 – 5.20 (m, 2H), 5.07 (dd, *J* = 25.8, 12.4 Hz, 1H), 3.18 (d, *J* = 16.7 Hz, 3H), 2.57 – 2.37 (m, 1H), 2.23 (ddt, *J* = 26.6, 12.6, 7.1 Hz, 1H), 2.11 – 1.96 (m, 1H), 1.65 – 1.52 (m, 3H), 1.04 (dd, *J* = 59.9, 7.2 Hz, 3H). ^{13}C NMR (101 MHz, $CDCl_3$) δ 195.03, 194.88, 178.79, 178.64, 156.29, 136.34, 136.29, 135.24, 135.14, 135.12, 129.64, 129.59, 129.17, 129.13, 128.51, 128.48, 128.41, 128.40, 128.34, 128.14, 128.09, 128.07, 128.00, 127.98, 127.95, 127.94, 127.86, 127.81, 127.57, 127.55, 126.75, 126.70, 115.03, 114.66, 67.86, 67.78, 67.75, 38.34, 38.12, 36.66, 36.40, 36.27, 35.59, 17.86, 17.82, 17.01, 17.00. HRMS (ESI) *m/z* calcd for [M + H] 426.1734, found 426.1744.

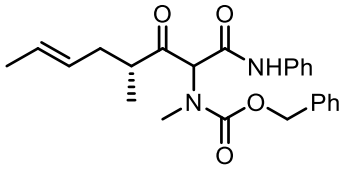

Benzyl methyl((4R,E)-4-methyl-1,3-dioxo-1-(phenylamino)oct-6-en-2-yl)carbamate

To a solution of S-phenyl (4R,E)-2-(((benzyloxy)carbonyl)(methyl)amino)-4-methyl-3-oxooct-6-enethioate (300mg, 0.705 mmol) and aniline (77 µl, 0.846 mmol) in THF (5mL) at room temerature was added silver trifluoroacetate (187 mg, 0.846 mmol) with stirring. Precipitation of Ag salts requires efficient stirring. Upon completion the reaction is diluted with EtOAc and filtered through celite. ^{1}H NMR (400 MHz, $CDCl_3$) δ 14.01 (s, 1H) 7.54 – 7.19 (m, 9H), 7.18 – 7.07 (m, 1H), 5.58 – 5.29 (m, 2H), 5.23 – 4.95 (m, 2H), 3.19 – 3.02 (m, 3H), 2.40 (d, *J* = 6.9 Hz, 1H), 2.35 – 2.22 (m, 1H), 2.12 – 1.98 (m, 1H), 1.63 – 1.56 (m, 3H), 1.04 (dd, *J* = 65.2, 6.8 Hz, 3H).). ^{13}C NMR (101 MHz, $CDCl_3$) δ 208.77, 179.14, 168.45, 156.12, 128.98, 128.60, 128.56, 128.24, 128.10, 128.01, 127.56, 124.83, 120.83, 68.25, 67.87, 38.32, 36.78, 36.36, 17.92, 17.82. HRMS (ESI) *m/z* calcd for [M + H] 409.2122, found 409.2131.

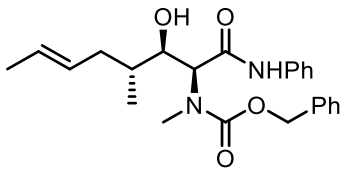

Benzyl ((2S,3R,4R,E)-3-hydroxy-4-methyl-1-oxo-1-(phenylamino)oct-6-en-2-yl)(methyl)carbamate

To benzyl methyl((4R,E)-4-methyl-1,3-dioxo-1-(phenylamino)oct-6-en-2-yl)carbamate (26mg, 0.064 mmol) under N_2 was added degassed DCM (0.5mL), [(R,R)-Teth-TsDpenRu] (3.72 mg, 6.36μmol) followed by TBAI (47 mg, 0.127 mmol) and 0.5mL of a 5N solution of HCO_2Na in H_2O. The reaction is sealed and stirred at 1400RPM for 48 hours. Following complete consumption of the starting material, the reaction is diluted with 3mL of sat.$NaHCO_3$, which is extracted with 2x3mL of EtOAc. The organics are combined, dried over $MgSO_4$ and purified by gradient column chromatography to yield benzyl ((2S,3R,4R,E)-3-hydroxy-4-methyl-1-oxo-1-(phenylamino)oct-6-en-2-yl)(methyl)carbamate (10.3mg, 0.025 mmol, 39.4 % yield). ^{1}H NMR (400 MHz, $CDCl_3$) δ 8.19 (s, 1H), 7.59 – 7.26 (m, 9H), 7.12 (t, *J* = 7.7 Hz, 1H), 5.45 (dt, *J* = 12.4, 6.0 Hz, 2H), 5.20 (q, *J* = 12.2 Hz, 2H), 4.77 (d, *J* = 4.1 Hz, 1H), 4.01 (dt, *J* = 7.9, 3.9 Hz, 1H), 3.86 (s, 1H), 3.14 (s, 3H), 2.39 (d, *J* = 13.4 Hz, 1H), 1.96 (dt, *J* = 13.7, 7.8 Hz, 1H), 1.65 (d, *J* = 5.8 Hz, 4H), 0.88 (d, *J* = 6.6 Hz, 3H). ^{13}C NMR (101 MHz, $CDCl_3$) δ 169.40, 158.45, 137.18, 136.11, 128.99, 128.89, 128.60, 128.23, 127.74, 127.13, 124.72, 120.11, 74.33, 68.16, 60.34, 35.35, 35.06, 33.32, 18.01, 15.82.

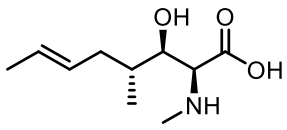

(2S,3R,4R,E)-3-hydroxy-4-methyl-2-(methylamino)oct-6-enoic acid, MeBmt – 202.

Lit. ref. Evans D. A., *J. Am. Chem. Soc.* **1986**, *108,* 6757

benzyl(E)-(3-hydroxy-4-methyl-1-oxo-1-(phenylamino)oct-6-en-2-yl)(methyl)carbamate (20mg, 0.049 mmol) was added to 0.5mL of 2N KOH, in a sealed reaction vessel and heated to 80C by means of an oil bath. The reaction is stirred as such overnight. The following day the reaction is cooled to room temperature and diluted with 2mL of water, which is extracted with 2x2mL Et_2O. The resultant aqueous layer is acidified with DOWEX ion exchange resin, which is washed with water and the amino acid is eluted with 1N NH_3 in H_2O, to yield (E)-3-hydroxy-4-methyl-2-(methylamino)oct-6-enoic acid as a white solid. LCMS RT (Method 2) 2.24 min (m/z) 202.1. ^{1}H NMR (400 MHz, D_2O) δ 5.56 – 5.31 (m, 2H), 3.68 (t, *J* = 6.0 Hz, 1H), 3.54 (d, *J* = 6.0 Hz, 1H), 2.65 (s, 3H), 2.19 (d, *J* = 13.9 Hz, 1H), 1.87 – 1.74 (m, 1H), 1.61 (dtd, *J* = 9.6, 6.5, 3.3 Hz, 1H), 1.56 (dd, *J* = 5.9, 1.3 Hz, 3H), 0.85 (d, *J* = 6.8 Hz, 3H).

Lit. Spectra	**202**
5.52-5.29 (m. 2 H)	δ 5.56 – 5.31 (m, 2H)
3.65 (t, 1 N-CH3)	3.68 (t, *J* = 6.0 Hz, 1H)
3.50 (d, 1 H, J = 5.8 Hz)	3.54 (d, *J* = 6.0 Hz, 1H)
2.61 (s, 3 H)	2.65 (s, 3H)
2.15 (br d, 1 H, 13.0 Hz)	2.19 (d, *J* = 13.9 Hz, 1H)
1.82-1.70 (m, 1 H)	1.87 – 1.74 (m, 1H)
1.62-1.53 (m, 1 H)	1.61 (dtd, *J* = 9.6, 6.5, 3.3 Hz, 1H)
1.52 (d, 3 H, J = 5.4)	1.56 (dd, *J* = 5.9, 1.3 Hz, 3H)
0.81 (d, 3 H, J = 6.7)	0.85 (d, *J* = 6.8 Hz, 3H)

Chapter 3

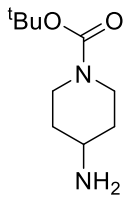

1-Boc-4-amino piperidine ***(commercially available)***
^{1}H NMR (400 MHz, $CDCl_3$) δ 4.00 (s, 2H), 2.74 (m, 3H), 1.74 (d, *J* = 10.6 Hz, 2H), 1.42 (s, 9H), 1.33 – 1.10 (m, 4H).

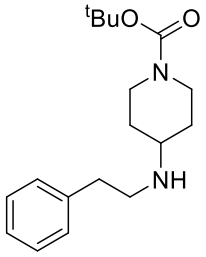

tert-butyl 4-(phenethylamino)piperidine-1-carboxylate – 306

To the solution of tert-butyl 4-aminopiperidine-1-carboxylate (5 g, 24.97 mmol) and 2-phenylacetaldehyde (3.15 g, 26.2 mmol) in MeOH (Volume: 45 ml) was added acetic acid (0.143 ml, 2.497 mmol). After 15 minutes, sodium cyanoborohydride (2.353 g, 37.4 mmol) was added in three portions. The resulting solution was stirred at room temperature for 30 minutes and then partitioned between ethyl acetate and water. The separated organic layer was washed with brine, dried over magnesium sulfate and concentrated in vacuo. Purified by normal phase chromatography (100%) EtOAc to yield tert-butyl 4-(phenethylamino)piperidine-1-carboxylate (6.23 g, 20.47 mmol, 82 % yield) as a thick yellow oil. LCMS RT (Method 2) 2.78 min (m/z 305.1) ^{1}H NMR (400 MHz, $CDCl_3$) δ 7.37 – 7.25 (m, 2H), 7.23 – 7.08 (m, 3H), 4.01 (s, 2H), 2.91 (dd, *J* = 8.1, 6.8 Hz, 2H), 2.86 – 2.67 (m, 4H), 2.62 (tt, *J* = 10.5, 3.9 Hz, 1H), 1.98 (s, 1H), 1.86 – 1.76 (m, 2H), 1.43 (s, 9H), 1.30 – 1.16 (m, 2H). ^{13}C NMR (101 MHz, $CDCl_3$) δ 154.67, 139.22, 128.84, 128.61, 128.53, 128.29, 126.36, 79.48, 55.02, 47.59, 42.30, 35.76, 31.69, 28.39. HRMS (ESI) *m/z* calcd for $[M + Na]^+$ 327.2043, found 327.2028 .

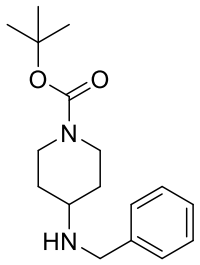

Tert-butyl 4-(benzylamino)piperidine-1-carboxylate

To a solution of tert-butyl 4-aminopiperidine-1-carboxylate (5 g, 24.97 mmol) and benzaldehyde (2.67 ml, 26.2 mmol) in MeOH (45 ml) was added acetic acid (0.143 ml, 2.497 mmol)and after 1 hour, sodium cyanoborohydride (2.353 g, 37.4 mmol)was added in three portions. The resulting solution was stirred at room temperature overnight and then partitioned between ethyl acetate and water. The separated organic layer was washed with brine, dried over magnesium sulfate and concentrated in vacuo. Crude was purified by column chromatography gradient 55-80% Hexane:EtOAc. Tert-butyl 4-(benzylamino)piperidine-1-carboxylate (5.67 g, 19.52 mmol, 78 % yield) LCMS RT (Method 2) 2.62 min (m/z 291.1) ^{1}H NMR (400 MHz, $CDCl_3$) δ 7.38 – 7.17 (m, 5H), 4.01 (s, 2H), 3.81 (s, 2H), 2.78 (t, *J* = 12.4 Hz, 2H), 2.65 (tt, *J* = 10.2, 3.8 Hz, 1H), 1.85 (d, *J*= 12.3 Hz, 2H), 1.44 (s, 9H), 1.38 – 1.20 (m, 2H). ^{13}C NMR (101 MHz, $CDCl_3$) δ 154.62, 128.67, 128.58, 127.58, 128.58, 79.51, 54.17, 49.94, 42.35 (broad), 31.25, 28.40. HRMS (ESI) *m/z* calcd for $[M + Na]^+$ 313.1886, found 313.1882.

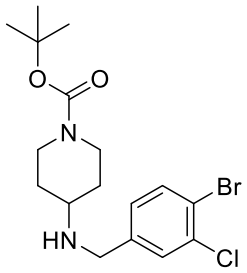

Tert-butyl 4-((4-bromo-3-chlorobenzyl)amino)piperidine-1-carboxylate – 363

To a solution of tert-butyl 4-aminopiperidine-1-carboxylate (5 g, 24.97 mmol) and 4-bromo-3-chlorobenzaldehyde (7.12 g, 32.5 mmol) in MeOH (45 ml) was added acetic acid (0.143 ml, 2.497 mmol)and after 1 hour, sodium cyanoborohydride (2.353 g, 37.4 mmol)was added in three portions. The resulting solution was stirred at room temperature overnight and then

partitioned between ethyl acetate and water. The separated organic layer was washed with brine, dried over magnesium sulfate and concentrated in vacuo. Crude was purified by column chromatography gradient 55-80% Hexane:EtOAc. tert-butyl 4-((4-bromo-3-chlorobenzyl)amino)piperidine-1-carboxylate RT (Method 1) 2.85 min (m/z 403.0) ^{1}H NMR (400 MHz, $CDCl_3$) δ 7.51 (d, *J* = 8.2 Hz, 1H), 7.44 (d, *J* = 2.0 Hz, 1H), 7.09 (dd, *J* = 8.2, 2.0 Hz, 1H), 3.99 (d, *J* = 15.3 Hz, 2H), 3.74 (s, 2H), 3.23 (s, 1H), 2.73 (t, *J* = 12.5 Hz, 2H), 2.64 (tt, *J* = 10.3, 3.9 Hz, 1H), 1.89 – 1.76 (m, 2H), 1.41 (s, 9H), 1.36 – 1.23 (m, 2H).^{13}C NMR (101 MHz, $CDCl_3$) δ 154.64, 140.12, 134.44, 133.65, 130.10, 127.83, 120.96, 79.51, 54.26, 49.11, 42.21, 31.76, 28.39. HRMS (ESI-TOF) *m/z* calcd for [M + H] 403.0782, found 403.0767.

General procedure A – Synthesis of CT3 derivatives by reductive amination

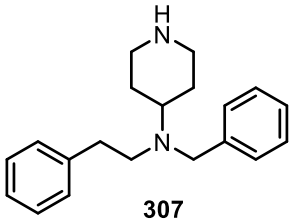

307

Representative example – synthesis of N-benzyl-N-phenethylpiperidin-4-amine, ***307***

To a solution of tert-butyl 4-(phenethylamino)piperidine-1-carboxylate (50mg, 0.164 mmol) in dichloroethane (DCE) (0.5ml) was added benzaldehyde (33µL, 0.328 mmol) followed by sodium triacetoxyborohydride (55.7 mg, 0.263 mmol). The reaction was stirred at room temperature overnight.

The reaction is quenched with $NaHCO_3$ (3mL), and extracted with EtOAc (2x4mL). The combined organics are removed by blowing down under a stream of nitrogen at 40C, followed by the addition of 2ml of 4N HCl in dioxane to facilitate Boc deprotection - the reaction is stirred for 2 hours. Completion is determined by complete loss of starting material (LCMS) the dioxane is removed by blowing down under a stream of nitrogen at 40C, the crude is dissolved in a solution of MeOH/DMSO and purified by semi-preparative scale reverse phase HPLC. Pure fractions are lyophilised and combined to give N-benzyl-N-phenethylpiperidin-4-amine, **307**. (63mg, 0.120 mmol, 73 % yield) as a di-TFA salt > 95% purity by LCMS. LCMS RT (Method 2) 3.15 min (m/z 295.2). ^{1}H NMR (400 MHz, DMSO-d_6) δ 11.65 (s, 1H), 9.47 (d, *J* = 9.3 Hz, 1H), 9.35 (q, *J* = 9.8 Hz, 1H), 7.82 (dd, *J* = 6.5, 3.0 Hz, 2H), 7.51 – 7.40 (m, 3H), 7.28 (t, *J* = 7.2 Hz, 2H), 7.21 (t, *J* = 7.3 Hz, 1H), 7.11 (d, *J* = 6.9 Hz, 2H), 4.52 (dd, *J* = 13.1, 3.9 Hz, 1H), 4.35 (dd, *J* = 13.1,

7.0 Hz, 1H), 3.77 – 3.65 (m, 1H), 3.40 (d, *J* = 10.4 Hz, 2H), 3.15 (t, *J* = 13.5 Hz, 3H), 3.01 – 2.79 (m, 3H), 2.43 (t, *J* = 14.9 Hz, 2H), 2.25 (dt, *J* = 20.2, 12.6 Hz, 2H). ^{13}C NMR (101 MHz, DMSO-d_6) δ 137.42, 131.89, 130.75, 129.87, 129.20, 129.07, 128.99, 127.28, 58.12, 53.87, 50.60, 42.32, 30.07, 23.06, 22.95. HRMS (ESI) *m/z* calcd for [M + H] 295.2169, found 295.2161.

N-benzyl-N-phenethylpiperidin-4-amine, 307

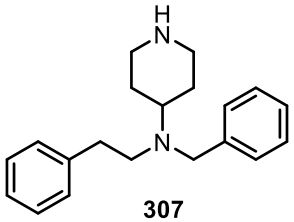

307

Appearance: Cloudy, white/transparent oil as free base, white solid as di-TFA salt.

LCMS RT (Method 2) 3.15 min (m/z 295.2) .

HRMS (ESI) *m/z* calcd for [M + H] 295.2169, found 295.2161.

IR (neat) 2934, 2808, 1602, 1493, 1451.

Free base: ^{1}H NMR (400 MHz,) δ 7.48 – 6.89 (m, 10H), 3.73 – 3.63 (m, 2H), 3.10 – 2.84 (m, 2H), 2.68-2.48 (m, *J* = 8.0 Hz, 5H), 2.36 (t, *J* = 11.7 Hz, 2H), 1.59 (d, *J* = 11.3 Hz, 2H), 1.34 (d, *J* = 10.5 Hz, 2H). **^{13}C NMR** (101 MHz, DMSO-d_6) δ 141.56, 140.98, 129.05, 128.51, 128.48, 128.43, 126.86, 126.09, 57.94, 54.18, 52.36, 45.95, 35.24, 29.01

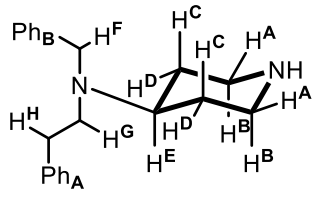

A 3.10 - 2.84 (m, 2H)
B 2.36 (dd, *J* = 2H)
C 1.34 (d, *J* = 2H)
D 1.59 (d, *J* = 11.3 Hz, 2H)
E 2.60 (m, 1H)
F 3.73 - 3.63 (m, 2H)
G 2.60 (m, 2H)
H 2.60 (m, 2H)
Ph 7.48 - 6.89 (m, 10H)

Di- TFA Salt: ^{1}H NMR (400 MHz, DMSO-d_6) δ 11.65 (s, 1H), 9.47 (d, *J* = 9.3 Hz, 1H), 9.35 (q, *J* = 9.8 Hz, 1H), 7.82 (dd, *J* = 6.5, 3.0 Hz, 2H), 7.51 –

7.40 (m, 3H), 7.28 (t, *J* = 7.2 Hz, 2H), 7.21 (t, *J* = 7.3 Hz, 1H), 7.11 (d, *J* = 6.9 Hz, 2H), 4.52 (dd, *J* = 13.1, 3.9 Hz, 1H), 4.35 (dd, *J* = 13.1, 7.0 Hz, 1H), 3.77 – 3.65 (m, 1H), 3.40 (d, *J* = 10.4 Hz, 2H), 3.15 (t, *J* = 13.5 Hz, 3H), 3.01 – 2.79 (m, 3H), 2.43 (t, *J* = 14.9 Hz, 2H), 2.25 (dt, *J* = 20.2, 12.6 Hz, 2H). **^{13}C NMR** (101 MHz, DMSO-d_6) δ 137.42, 131.89, 130.75, 129.87, 129.20, 129.07, 128.99, 127.28, 58.12, 53.87, 50.60, 42.32, 30.07, 23.06, 22.95.

See appendix A8 for hard copies of spectal and chromatographic analyses.

General procedure B – Synthesis of CT3 derivatives by displacement of primary alkyl-bromides

Representative example – synthesis of N-(2-bromobenzyl)-N-phenethylpiperidin-4-amine

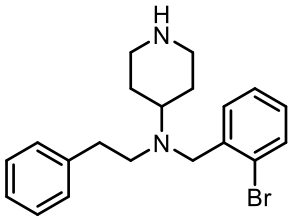

N-(2-bromobenzyl)-N-phenethylpiperidin-4-amine - 321

To a solution of tert-butyl 4-(phenethylamino)piperidine-1-carboxylate (60mg, 0.197 mmol) in MeCN (1 ml) was added 2-bromobenzyl bromide (54.2 mg, 0.217 mmol) followed by K_2CO_3 (43.6 mg, 0.315 mmol). The reaction was stirred at room temperature overnight, completion confirmed by LCMS.

The reaction was diluted with $NaCl_{(aq)}$ (3mL) and EtOAc (4mL), organics are separated and the aqueous was extracted twice with EtOAc (2x4mL). Combined organics were blown down under a stream of nitrogen. To the resultant crude oil was added 2ml of 4N HCl in Dioxane to facilitate Boc deprotection. The reaction was stirred for 2 hours, then blown down under N2. The crude is dissolved in a solution of MeOH/DMSO and purified by semi-preparative scale reverse phase HPLC. Pure fractions are lyophilised and combined to give N-(2-bromobenzyl)-N-phenethylpiperidin-4-amine, **321.** (51 mg, 0.085 mmol, 43 % yield) as a di-TFA salt, >95% purity by LCMS.

LCMS RT (Method 2) 3.43 min (m/z 375.1) ^{1}H NMR (400 MHz, DMSO-d_6) δ 8.95 (d, *J* = 64.5 Hz, 1H), 8.60 (s, 1H), 8.22 (s, 1H), 7.58 (d, *J* = 8.8 Hz, 1H), 7.51 – 7.41 (m, 1H), 7.32 (d, *J* = 7.0 Hz, 1H), 7.28 – 7.20 (m, 3H), 7.17 (d, *J* = 7.1 Hz, 1H), 7.12 (d, *J* = 7.2 Hz, 2H), 3.36 (dd, *J* = 34.8, 13.0 Hz, 4H),

3.01 – 2.79 (m, 4H), 2.68 (s, 3H), 2.32 – 2.14 (m, 1H), 1.88 (s, 2H), 1.70 (s, 2H). ^{13}C NMR (101 MHz, dmso) δ 158.74, 139.18, 132.94, 129.10, 128.68, 126.45, 125.39, 118.76, 54.05, 52.52, 43.47, 32.09, 25.13.^{19}F NMR (376 MHz, DMSO-d_6) δ -73.91. HRMS (ESI-TOF) *m/z* calcd for [M + H] 375.1262, found 375.1255.

General Procedure C – Synthesis of CT3 amide analogues 331, 332, 336, 337, 342 and 343

Representative example – synthesis of N,N-dimethyl-2-((phenethyl(piperidin-4-yl)amino)methyl)benzamide – ***336***

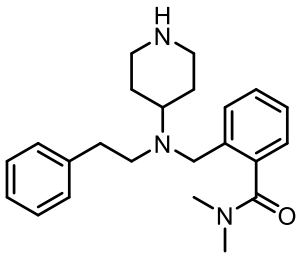

N,N-dimethyl-2-((phenethyl(piperidin-4-yl)amino)methyl)benzamide – 342

To a solution of tert-butyl 4-(phenethylamino)piperidine-1-carboxylate (500mg, 1.642 mmol) in dichloroethane (DCE) (8 ml) was added 2-formylbenzoic acid (370 mg, 2.464 mmol) followed by sodium triacetoxyborohydride (557 mg, 2.63 mmol). The reaction was stirred at room temperature overnight: conversion to carboxyl intermediate is confirmed by LCMS. Volatiles were removed by blowing down under a stream of nitrogen at 40°C. The crude material was dissolved in 6mL of DMF with sonication and a 2mL aliquot was removed and added to a new reaction vessel (approx 0.5mmol of intermediate). To this was added HATU (347 mg, 0.912 mmol) and the resulting homogenous solution was stirred for 10 min at room temperature. Dimethylamine hydrochloride (93 mg, 1.140 mmol) was added followed by DIPEA (0.119 ml, 0.684 mmol). The mixture was stirred for 16 h at room temperature.

The reaction is quenched with $NaHCO_3$ (3mL), and extracted with EtOAc (2x4mL). The combined organics are removed by blowing down under a stream of nitrogen at 40C, followed by the addition of 3ml of 4N HCl in dioxane to facilitate Boc deprotection - the reaction is stirred for 2 hours. Completion is determined by complete loss of starting material (LCMS) the dioxane is removed by blowing down under a stream of nitrogen at 40C, the crude is dissolved in a solution of MeOH/DMSO and purified by reverse

phase column chromatography to yield N,N-dimethyl-2-((phenethyl(piperidin-4-yl)amino)methyl)benzamide, **342.** (5.4 mg, 0.015 mmol, 13 % yield).

LCMS RT (Method 2) 3.00 min (m/z 366.2) ^{1}H NMR (400 MHz, DMSO-d_6) δ 7.37 – 7.26 (m, 3H), 7.26 – 7.18 (m, 3H), 7.18 – 7.07 (m, 3H), 3.70 (s, 2H), 2.98 (s, 4H), 2.86 (s, 3H), 2.73 – 2.55 (m, 5H), 2.47 – 2.35 (m, 2H), 1.80 – 1.66 (m, 1H), 1.63 (d, J = 11.2 Hz, 2H), 1.35 (q, J = 9.6 Hz, 2H). ^{13}C NMR (101 MHz, DMSO-d_6) δ 170.71, 141.83, 140.94, 136.69, 129.40, 129.06, 128.48, 128.43, 126.92, 126.12, 125.53, 58.06, 53.90, 52.38, 46.03, 35.22, 35.13, 29.15.^{19}F NMR (376 MHz, DMSO-d_6) δ -73.47. HRMS (ESI-TOF) *m/z* calcd for [M + H] 366.2540, found 366.2556.

N-(4-chlorobenzyl)-N-phenethylpiperidin-4-amine - 308

LCMS RT (Method 2) 3.50 min (m/z 329.2) ^{1}H NMR (400 MHz, DMSO-d_6) δ 10.36 (s, 1H), 8.85 (s, 1H), 8.55 (s, 1H), 7.62 – 7.39 (m, 4H), 7.27 (t, J = 7.4 Hz, 2H), 7.19 (s, 1H), 7.14 (d, J = 7.4 Hz, 2H), 4.37 (br, 1H), 3.97 (s, 2H), 3.39 (s, 3H), 3.16 (s, 1H), 2.92 (s, 3H), 2.79 (s, 1H), 2.22 (s, 2H), 1.93 (s, 2H). ^{13}C NMR (151 MHz, DMSO-d_6) δ 161.49, 139.71, 136.27, 131.79, 130.02, 117.01, 60.53, 55.80, 53.55, 45.18, 32.73, 26.13. ^{19}F NMR (376 MHz, DMSO-d_6) δ -73.94. HRMS (ESI-TOF) *m/z* calcd for [M + H] 329.1779, found 329.1769.

N-(4-bromobenzyl)-N-phenethylpiperidin-4-amine - 309

LCMS RT (Method 2) 3.54 min (m/z 373.1) ^{1}H NMR (400 MHz, DMSO-d_6) δ 10.33 (s, 1H), 8.86 (s, 1H), 8.56 (s, 1H), 7.71 – 7.49 (m, 4H), 7.29 (t, J = 7.4 Hz, 2H), 7.16 (d, J = 7.4 Hz, 2H), 4.38 (s, 1H), 4.03 (s, 2H), 3.71 (s, 1H), 3.40 (s, 3H), 3.18 (s, 1H), 2.94 (s, 3H), 2.25 (s, 1H), 1.84 (m, Hz, 3H). ^{13}C NMR (151 MHz, DMSO-d_6) δ 161.25, 139.78, 136.50, 134.88, 131.79, 129.77, 126.42, 118.98, 60.49, 55.87, 53.55, 45.22, 32.72, 26.17.^{19}F NMR (376 MHz, DMSO-d_6) δ -73.94. HRMS (ESI-TOF) *m/z* calcd for [M + H] 373.1274, found 373.1278.

N-(4-fluorobenzyl)-N-phenethylpiperidin-4-amine - 310

LCMS RT (Method 2) 3.27 min (m/z 313.4) ^{1}H NMR (400 MHz, DMSO-d_6) δ 10.03 (s, 1H), 8.78 (s, 1H), 8.44 (s, 1H), 8.04 (s, 1H), 7.79 – 6.89 (m, 9H), 4.47 (d, J = 49.3 Hz, 1H), 3.65 (s, 4H), 3.50 – 3.43 (m, 1H), 3.26 (d, J = 19.5 Hz, 2H), 3.00 (s, 1H), 2.82 (s, 1H), 2.66 (s, 1H), 2.30 (s, 1H), 1.98 (s, 1H), 1.81 (s, 1H), 1.63 (s, 1H). ^{19}F NMR (376 MHz, DMSO-d_6) δ -73.82. ^{13}C NMR (151 MHz, DMSO-d_6) δ 161.17, 139.61, 136.78, 132.88, 131.78, 131.25, 130.15, 129.54, 117.96, 60.53, 55.83, 53.36, 45.19, 32.67, 26.10.HRMS (ESI-TOF) *m/z* calcd for [M + H] 313.2075, found 313.2071.

N-phenethyl-N-(4-(trifluoromethyl)benzyl)piperidin-4-amine – 311

LCMS RT (Method 2) 3.77 min (m/z 363.2) ^{1}H NMR (400 MHz, DMSO-d_6) δ 10.49 (s, 1H), 8.65 (s, 1H), 7.82 – 7.58 (m, 5H), 7.25 (t, *J* = 7.3 Hz, 2H), 7.21 – 7.15 (m, 1H), 7.16 – 7.08 (m, 2H), 4.38 (s, 2H), 3.83 (s, 1H), 3.35 (s, 3H), 3.23 – 3.05 (m, 1H), 2.99 – 2.83 (m, 3H), 2.76 (s, 1H), 1.87 (s, 4H). ^{13}C NMR (151 MHz, DMSO-d_6) δ 161.47, 134.93, 133.26, 131.79, 131.50, 129.96, 128.67, 126.36, 122.86, 118.91, 57.61, 55.99, 53.88, 45.82, 32.58, 26.28.^{19}F NMR (376 MHz, DMSO-d_6) δ -60.83 (s, 3F, *CF_3*), -74.00 (s, 6F *2-TFA*). HRMS (ESI) *m/z* calcd for [M + H] 363.2043, found 363.2040.

N-phenethyl-N-(4-(trifluoromethoxy)benzyl)piperidin-4-amine – 312

LCMS RT (Method 2) 3.91 min (m/z 379.2) ^{1}H NMR (400 MHz, DMSO-d_6) δ 10.36 (s, 1H), 8.83 (s, 1H), 8.56 (s, 1H), 7.64 (s, 1H), 7.41 (s, 3H), 7.26 (t, *J* = 7.1 Hz, 2H), 7.20 (q, *J* = 6.1, 5.6 Hz, 1H), 7.12 (d, *J* = 7.0 Hz, 2H), 4.11 (s, 2H), 3.70 (s, 1H), 3.39 (s, 3H), 3.17 (s, 1H), 2.92 (s, 3H), 2.75 (s, 1H), 2.21 (s, 2H), 1.93 (s, 2H). ^{13}C NMR (151 MHz, DMSO-d_6) δ 161.28, 139.60, 136.56, 132.82, 131.76, 129.94, 124.33, 116.97, 60.81, 55.74, 53.62, 45.25, 32.73, 26.07.^{19}F NMR (376 MHz, DMSO-d_6) δ -56.80 (s, 3F, *OCF_3*), -73.98 (s, 6F, *2TFA*). HRMS (ESI) *m/z* calcd for [M + H] 379.1922, found 379.1995.

N-(4-methylbenzyl)-N-phenethylpiperidin-4-amine – 313

LCMS RT (Method 2) 3.43 min (m/z 309.3) ^{1}H NMR (400 MHz, DMSO-d_6) δ 10.40 (s, 1H), 9.07 (d, *J* = 10.7 Hz, 1H), 8.78 (d, *J* = 11.4 Hz, 1H), 7.54 – 7.43 (m, 2H), 7.34 – 7.18 (m, 5H), 7.18 – 7.10 (m, 2H), 4.39 (d, *J* = 37.0 Hz, 2H), 3.77 – 3.63 (m, 1H), 3.44 (d, *J* = 12.5 Hz, 2H), 3.25 – 3.13 (m, 2H), 2.98 (q, *J* = 12.0 Hz, 3H), 2.81 (s, 1H), 2.31 (s, 5H), 2.10 – 1.93 (m, 2H). ^{13}C NMR (101 MHz, DMSO-d_6) δ 158.90, 139.62, 137.16, 131.52, 129.92, 129.07, 127.68, 127.34, 112.29, 57.91, 53.84, 50.74, 42.50, 30.11, 23.45, 21.22. ^{19}F NMR (376 MHz, DMSO-d_6) δ -74.47. HRMS (ESI-TOF) *m/z* calcd for [M + H] 309.2325, found 309.2327.

N-(3-chlorobenzyl)-N-phenethylpiperidin-4-amine – 314

LCMS RT (Method 2) 3.50 min (m/z 329.2) ^{1}H NMR (400 MHz, DMSO-d_6) δ 9.05 (d, *J* = 11.5 Hz, 1H), 8.73 (d, *J* = 11.5 Hz, 1H), 7.70 (s, 1H), 7.56 – 7.43 (m, 3H), 7.28 (dd, *J* = 8.1, 6.6 Hz, 2H), 7.24 – 7.18 (m, 1H), 7.17 – 7.11 (m, 2H), 4.38 (s, 2H), 3.66 (s, 1H), 3.44 (d, *J* = 12.5 Hz, 2H), 3.16 (t, *J* = 8.5 Hz, 2H), 2.98 (q, *J* = 12.1 Hz, 2H), 2.86 (s, 2H), 2.26 (d, *J* = 12.8 Hz, 2H), 1.98 (dd, *J* = 18.9, 8.4 Hz, 2H).^{13}C NMR (101 MHz, DMSO-d_6) δ 159.25, 133.90, 131.11, 129.80, 129.08, 127.29, 115.34, 57.88, 53.28, 51.07, 42.57, 30.41, 23.60. ^{19}F NMR (376 MHz, DMSO-d_6) δ -74.35 HRMS (ESI-TOF) *m/z* calcd for [M + H] 329.1779, found 329.1767.

N-(3-bromobenzyl)-N-phenethylpiperidin-4-amine - 315

LCMS RT (Method 2) 3.64 min (m/z 375.1) ^{1}H NMR (400 MHz, DMSO-d_6) δ 10.41 (s, 1H), 8.86 (s, 1H), 8.59 (s, 1H), 7.59 (d, *J* = 12.5 Hz, 2H), 7.43 – 7.32 (m, 1H), 7.31 – 7.23 (m, 3H), 7.20 (d, *J* = 7.1 Hz, 1H), 7.13 (d, *J* = 7.6 Hz, 2H), 4.21 (s, 2H), 3.72 (s, 1H), 3.39 (s, 3H), 3.16 (s, 1H), 2.93 (s, 3H), 2.73 (s, 1H), 2.26 (s, 1H), 1.94 (s, 3H). NMR (376 MHz, DMSO-d_6) δ -73.93. HRMS (ESI-TOF) *m/z* calcd for [M + H] 375.1255, found 375.1255.

N-(3-fluorobenzyl)-N-phenethylpiperidin-4-amine - 316

LCMS RT (Method 2) 3.32 min (m/z 313.2^{1}H NMR (400 MHz, DMSO-d_6) δ 10.44 (s, 1H), 8.81 (s, 1H), 8.51 (s, 1H), 7.44 (s, 3H), 7.29 – 7.24 (m, 2H), 7.20 (d, *J* = 6.8 Hz, 1H), 7.13 (d, *J* = 7.0 Hz, 3H), 4.19 (s, 2H), 3.38 (s, 3H), 3.08 (s, 1H), 2.92 (s, 3H), 2.77 (s, 1H), 2.34 – 2.05 (m, 2H), 1.88 (s, 2H] ^{19}F NMR (376 MHz, DMSO-d_6) δ -73.97, -112.14. HRMS (ESI-TOF) *m/z* calcd for [M + H] 313.2075, found 313.2070.

N-phenethyl-N-(3-(trifluoromethyl)benzyl)piperidin-4-amine - 317

LCMS RT (Method 2) 3.80 min (m/z 363.20) ^{1}H NMR (400 MHz, DMSO-d_6) δ 10.63 (s, 1H), 8.84 (s, 1H), 8.58 (s, 1H), 7.63 (s, 4H), 7.25 (t, *J* = 7.1 Hz, 2H), 7.19 (d, *J* = 5.9 Hz, 1H), 7.11 (d, *J* = 6.9 Hz, 2H), 4.48 (s, 3H), 3.80 (s, 1H), 3.38 (s, 2H), 2.92 (s, 3H), 2.72 (s, 2H), 2.25 (s, 1H), 1.88 (s, 3H). ^{13}C NMR (151 MHz, DMSO-d_6) δ 161.28, 139.57, 138.48, 134.94, 132.88, 131.73, 129.96, 129.49, 126.30, 116.93, 60.58, 55.88, 53.56, 45.25, 32.56, 27.65, 26.40.^{19}F NMR (376 MHz, DMSO-d_6) δ -61.11 (s, 3H, *CF_3*), -74.02 (s, 3H, *2TFA*) HRMS (ESI-TOF) *m/z* calcd for [M + H] 363.2043, found 363.2036.

N-phenethyl-N-(3-(trifluoromethoxy)benzyl)piperidin-4-amine - 318

LCMS RT (Method 2) 3.93 min (m/z 379.2) ^{1}H NMR (400 MHz, DMSO-d_6) δ 10.64 (s, 1H), 8.65 (d, 2H), 7.55 (s, 4H), 7.28 (t, *J* = 7.2 Hz, 2H), 7.22 (d, *J* = 6.9 Hz, 1H), 7.17 – 7.07 (m, 2H), 4.07 (s, 6H), 3.39 (s, 2H), 2.94 (d, *J* = 10.9 Hz, 2H), 2.75 (s, 1H), 2.18 (s, 2H), 1.89 (s, 2H). ^{13}C NMR (151 MHz, DMSO-d_6) δ 161.30, 151.56, 134.00, 131.72, 131.57, 129.37, 126.80, 125.23, 123.99, 122.29, 115.42, 61.09, 55.86, 53.67, 45.29, 32.71, 26.38. ^{19}F NMR (376 MHz, DMSO-d_6) δ -56.74, -74.03. HRMS (ESI-TOF) *m/z* calcd for [M + H] 379.1992, found 379.1998.

N-(3-methylbenzyl)-N-phenethylpiperidin-4-amine, 319

LCMS RT (Method 2) 3.43 min (m/z 309.3) ^{1}H NMR (400 MHz, DMSO-d_6) δ 10.26 (s, 1H), 8.93 (s, 1H), 8.64 (s, 1H), 7.52 – 7.19 (m, 7H), 7.14 (d, J = 7.0 Hz, 2H), 4.40 (d, J = 69.3 Hz, 2H), 3.61 (s, 5H), 3.44 (s, 2H), 3.19 (s, 1H), 3.03 – 2.94 (m, 2H), 2.76 (s, 1H), 2.35 – 2.30 (m, 3H), 2.01 (s, 2H), 1.74 (s, 1H). ^{13}C NMR (151 MHz, DMSO-d_6) δ 161.67 (q, TFA), 141.40, 139.72, 134.74, 133.41, 131.95, 131.76, 131.34, 130.05,123.09 (q, TFA), 60.73, 56.65, 53.31, 45.22, 32.50, 26.30, 26.08, 24.01. ^{19}F NMR (376 MHz, DMSO-d_6) δ -73.81. HRMS (ESI-TOF) *m/z* calcd for [M + H] 309.2325, found 309.2313.

N-(2-chlorobenzyl)-N-phenethylpiperidin-4-amine - 320

LCMS RT (Method 2) 3.35 min (m/z 329.2) ^{1}H NMR (400 MHz, DMSO-d_6) δ 10.00 (s, 1H), 8.63 (s, 1H), 8.26 (s, 1H), 7.46 (s, 3H), 7.35 – 7.29 (m, 1H), 7.27 – 7.23 (m, 2H), 7.18 (d, J = 6.8 Hz, 1H), 7.13 (d, J = 7.3 Hz, 2H), 4.33 (s, 3H), 3.86 (s, 1H), 3.35 (s, 3H), 2.95 – 2.83 (m, 3H), 2.72 (s, 1H), 1.90 (s, 2H), 1.80 – 1.59 (m, 2H). ^{13}C NMR (151 MHz, DMSO-d_6) δ 161.18, 142.67, 135.14, 131.79, 131.47, 128.61, 116.87, 57.50, 53.97, 46.06, 45.96, 37.30, 27.53.^{19}F NMR (376 MHz, DMSO-d_6) δ -74.06. HRMS (ESI-TOF) *m/z* calcd for [M + H] 329.1779, found 329.1769.

N-(2-bromobenzyl)-N-phenethylpiperidin-4-amine - 321

LCMS RT (Method 2) 3.43 min (m/z 375.1) ^{1}H NMR (400 MHz, DMSO-d_6) δ 8.95 (d, J = 64.5 Hz, 1H), 8.60 (s, 1H), 8.22 (s, 1H), 7.58 (d, J = 8.8 Hz, 1H), 7.51 – 7.41 (m, 1H), 7.32 (d, J = 7.0 Hz, 1H), 7.28 – 7.20 (m, 3H), 7.17 (d, J = 7.1 Hz, 1H), 7.12 (d, J = 7.2 Hz, 2H), 3.36 (dd, J = 34.8, 13.0 Hz, 4H), 3.01 – 2.79 (m, 4H), 2.68 (s, 3H), 2.32 – 2.14 (m, 1H), 1.88 (s, 2H), 1.70 (s, 2H).^{19}F NMR (376 MHz, DMSO-d_6) δ -73.91. HRMS (ESI-TOF) *m/z* calcd for [M + H] 375.1262, found 375.1255.

N-(2-fluorobenzyl)-N-phenethylpiperidin-4-amine - 322

LCMS RT (Method 2) 3.18 min (m/z 313.2^{1}H NMR (400 MHz, DMSO-d_6) δ 10.26 (s, 1H), 8.84 (s, 1H), 8.49 (s, 1H), 7.52 (d, J = 40.9 Hz, 3H), 7.30 – 7.25 (m, 3H), 7.22 (s, 1H), 7.16 (d, J = 6.8 Hz, 2H), 4.20 (s, 2H), 3.78 (s, 1H), 3.38 (s, 3H), 3.14 (s, 1H), 2.93 (s, 3H), 2.83 (s, 1H), 2.15 (s, 1H), 1.90 (s, 3H). ^{13}C NMR (101 MHz, DMSO-d_6) δ 158.50, 147.55, 129.10, 128.91, 125.16, 124.78, 118.70, 59.97, 51.85, 47.40, 42.99, 30.68, 24.12.^{19}F NMR (376 MHz, DMSO-d_6) δ -73.98, -114.12.) HRMS (ESI-TOF) *m/z* calcd for [M + H] 313.2075, found 313.2064.

N-phenethyl-N-(2-(trifluoromethyl)benzyl)piperidin-4-amine - 323

LCMS RT (Method 2) 4.06 min (m/z 363.2 ^{1}H NMR (400 MHz, DMSO-d_6) δ 8.55 (s, 1H), 8.14 (d, J = 19.3 Hz, 1H), 7.67 (dd, J = 12.8, 7.8 Hz, 2H), 7.53 (t, J = 7.6 Hz, 1H), 7.40 (t, J = 7.7 Hz, 1H), 7.27 – 7.19 (m, 2H), 7.19 – 7.12 (m, 1H), 3.83 (s, 2H), 3.28 (d, J = 12.4 Hz, 2H), 2.88 (dq, J = 24.3, 12.8 Hz, 4H), 2.67 (d, J = 7.7 Hz, 3H), 1.83 (d, J = 13.4 Hz, 2H), 1.63 (q, J = 12.8, 12.0 Hz, 2H ^{13}C NMR (101 MHz, DMSO-d_6) δ 158.39, 132.82, 130.16, 129.08, 128.60, 126.33, 125.92, 55.10, 52.70, 50.07, 43.61, 34.73, 25.06.^{19}F NMR (376 MHz, DMSO-d_6) δ -58.35, -73.92. HRMS (ESI-TOF) *m/z* calcd for [M + H] 363.2043, found 363.2036.

N-phenethyl-N-(thiophen-3-ylmethyl)piperidin-4-amine – 324

LCMS RT (Method 2) 3.12 min (m/z 301.1) ^{1}H NMR (400 MHz, DMSO-d_6) δ 10.37 (s, 1H), 8.93 (s, 1H), 8.64 (s, 1H), 7.89 (s, 1H), 7.66 (s, 1H), 7.29 (t, J = 7.2 Hz, 3H), 7.25 – 7.19 (m, 1H), 7.15 (d, J = 7.0 Hz, 2H), 4.44 (s, 2H), 3.66 (s, 3H), 3.40 (s, 2H), 3.17 (s, 1H), 2.94 (s, 2H), 2.76 (s, 1H), 2.30 (s, 2H), 1.96 (s, 2H). ^{13}C NMR (151 MHz, DMSO-d_6) δ 161.33, 139.72, 133.51, 132.49, 132.31, 131.80, 130.91, 130.06, 119.14, 60.62, 53.35, 51.22, 45.17, 32.76, 26.27.^{19}F NMR (376 MHz, DMSO-d_6) δ -73.80. HRMS (ESI) *m/z* calcd for [M + H] 301.1733, found 301.1744.

N-phenethyl-N-(thiophen-2-ylmethyl)piperidin-4-amine - 325

LCMS RT (Method 2) 3.11 min (m/z 301.2) ^{1}H NMR (400 MHz, DMSO-d_6) δ 10.55 (s, 1H), 8.72 (s, 2H), 7.64 (s, 1H), 7.31 (dd, J = 16.0, 8.6 Hz, 3H), 7.23 (d, J = 7.1 Hz, 1H), 7.19 (d, J = 7.0 Hz, 2H), 7.10 (s, 1H), 4.68 (s, 2H), 3.94 (s, 4H), 3.38 (s, 2H), 2.94 (s, 2H), 2.82 (s, 1H), 2.16 (s, 2H), 1.85 (s, 2H). ^{13}C NMR (101 MHz, DMSO-d_6) δ 137.41, 133.14, 129.12, 128.93, 127.27, 115.84, 52.09, 50.91, 48.36, 42.76, 32.07, 24.12. ^{19}F NMR (376 MHz, DMSO-d_6) δ -73.90. HRMS (ESI-TOF) *m/z* calcd for [M + H] 301.1733, found 301.1733.

N-([1,1'-biphenyl]-4-ylmethyl)-N-phenethylpiperidin-4-amine – 326

LCMS RT (Method 2) 3.98 min (m/z 371.2) ^{1}H NMR (400 MHz, DMSO-d_6) δ 10.31 (s, 1H), 8.93 (s, 1H), 8.63 (s, 1H), 7.90 – 7.53 (m, 6H), 7.46 (t, J = 7.5 Hz, 2H), 7.42 – 7.34 (m, 1H), 7.28 (t, J = 7.1 Hz, 2H), 7.21 (d, J = 7.0 Hz, 1H), 7.16 (d, J = 7.1 Hz, 2H), 4.48 (d, J = 52.7 Hz, 2H), 3.82 (d, J = 42.5 Hz, 3H), 3.45 (s, 2H), 3.27 (s, 1H), 2.99 (s, 2H), 2.81 (s, 1H), 2.31 (s, 1H), 2.03 (s, 2H). ^{13}C NMR (151 MHz, DMSO-d_6) δ 161.49, 144.32, 142.15, 139.71, 134.95, 132.14, 131.80, 130.14, 129.83, 117.10, 60.65, 56.34, 53.51, 45.21, 32.71, 26.23.^{19}F NMR (376 MHz, DMSO-d_6) δ -73.85. HRMS (ESI) *m/z* calcd for [M + H] 371.2482, found 371.2490.

N-(4-methoxybenzyl)-N-phenethylpiperidin-4-amine – 327

LCMS RT (Method 2) 3.31 min (m/z 325.2) ^{1}H NMR (400 MHz, DMSO-d_6) δ 10.26 (s, 1H), 9.04 (d, *J* = 10.7 Hz, 1H), 8.75 (d, *J* = 11.4 Hz, 1H), 7.57 – 7.47 (m, 2H), 7.33 – 7.25 (m, 2H), 7.25 – 7.18 (m, 1H), 7.18 – 7.11 (m, 2H), 7.05 – 6.97 (m, 2H), 4.39 (s, 3H), 3.76 (d, *J* = 0.6 Hz, 3H), 3.73 – 3.62 (m, 1H), 3.44 (d, *J* = 12.6 Hz, 2H), 3.23 – 3.13 (m, 2H), 2.99 (dd, *J* = 17.4, 5.9 Hz, 2H), 2.83 (s, 1H), 2.29 (d, *J* = 13.2 Hz, 2H), 2.01 (qd, *J* = 12.9, 4.0 Hz, 2H). ^{13}C NMR (101 MHz, DMSO-d_6) δ 160.55, 158.84, 137.15, 133.13, 129.08, 127.36, 122.35, 114.72, 57.78, 55.66, 53.69, 50.55, 42.51, 30.19, 23.43. ^{19}F NMR (376 MHz, DMSO-d_6) δ -74.38. HRMS (ESI-TOF) *m/z* calcd for [M + H] 325.2274, found 325.2267.

4-((phenethyl(piperidin-4-yl)amino)methyl)benzonitrile - 328

LCMS RT (Method 2) 3.25 min (m/z 320.2) ^{1}H NMR (400 MHz, DMSO-d_6) δ 10.46 (s, 1H), 8.58 (s, 1H), 8.21 (s, 1H), 7.82 (s, 2H), 7.54 (s, 1H), 7.42 – 6.98 (m, 4H), 4.82 – 3.90 (m, 5H), 3.90 – 3.72 (m, 1H), 3.34 (s, 2H), 2.96 – 2.82 (m, 2H), 2.81 – 2.60 (m, 2H), 2.12 – 1.51 (m, 3H). ^{13}C NMR (151 MHz, DMSO-d_6) δ 161.12, 135.31, 131.80, 131.41, 129.03, 121.80, 118.87, 57.55, 56.15, 55.01, 46.07, 37.44, 27.83. ^{19}F NMR (376 MHz, DMSO-d_6) δ -74.03. HRMS (ESI-TOF) *m/z* calcd for [M + H] 320.2121, found 320.2112.

N-phenethyl-N-(pyridin-4-ylmethyl)piperidin-4-amine – 329

LCMS RT (Method 2) 2.88 min (m/z 296.2) ^{1}H NMR (400 MHz, DMSO-d_6) δ 8.80 (d, *J* = 10.3 Hz, 1H), 8.74 (d, *J* = 5.6 Hz, 2H), 8.54 – 8.43 (m, 1H), 7.79 (d, *J* = 5.7 Hz, 2H), 7.24 (dd, *J* = 8.1, 6.5 Hz, 2H), 7.20 – 7.10 (m, 2H), 4.08 (s, 2H), 3.07 (s, 1H), 2.85 (t, *J* = 11.9 Hz, 3H), 2.73 (dd, *J* = 9.6, 5.7 Hz, 2H), 1.94 (d, *J* = 13.1 Hz, 2H), 1.81 – 1.56 (m, 2H). ^{13}C NMR (101 MHz, DMSO-d_6) δ 159.19, 143.12, 139.59, 129.16, 128.70, 126.61, 126.00, 114.29, 56.18, 53.04, 52.52, 43.26, 32.81, 24.79. ^{19}F NMR (376 MHz, DMSO-d_6) δ -74.43. HRMS (ESI-TOF) *m/z* calcd for [M + H] 296.2121, found 296.2133.

N-([1,1'-biphenyl]-3-ylmethyl)-N-phenethylpiperidin-4-amine - 333

LCMS RT (Method 2) 3.88 min (m/z 371.3) ^{1}H NMR (400 MHz, DMSO-d_6) δ 10.45 (s, 1H), 8.95 (s, 1H), 8.65 (s, 1H), 7.96 (s, 1H), 7.79 (s, 1H), 7.69 (s, 2H), 7.61 (s, 2H), 7.49 (t, *J* = 7.5 Hz, 2H), 7.43 – 7.37 (m, 1H), 7.32 – 7.17 (m, 3H), 7.14 (d, *J* = 7.4 Hz, 2H), 4.53 (d, *J* = 68.1 Hz, 2H), 3.78 (s, 4H), 3.46 (s, 2H), 3.27 (s, 1H), 3.00 (s, 2H), 2.77 (s, 1H), 2.35 (d, *J* = 8.8 Hz, 1H), 2.04 (s, 1H). ^{13}C NMR (101 MHz, DMSO-d_6) δ 158.57, 130.43, 129.97, 129.39, 129.07, 128.26, 127.18, 126.99, 118.43, 58.78, 54.12, 49.97, 42.60, 30.00, 23.60. ^{19}F NMR (376 MHz, DMSO-d_6) δ -73.82. HRMS (ESI-TOF) *m/z* calcd for [M + H] 371.2482, found 371.2476.

N-phenethyl-N-(pyridin-3-ylmethyl)piperidin-4-amine – 334

LCMS RT (Method 2) 2.73 min (m/z 296.2) ^{1}H NMR (400 MHz, DMSO-d_6) δ 9.21 – 8.54 (m, 4H), 8.42 (s, 1H), 8.06 – 7.89 (m, 1H), 7.58 – 7.45 (m, 1H), 7.41 – 7.00 (m, 5H), 3.96 (s, 5H), 3.38 (s, 2H), 3.26 – 3.13 (m, 1H), 2.97 – 2.88 (m, 2H), 2.78 (s, 1H), 2.21 – 1.92 (m, 2H), 1.88 – 1.63 (m, 2H). ^{13}C NMR (101 MHz, DMSO-d_6) δ 129.09, 128.80, 127.29, 126.78, 124.68, 124.15, 65.71, 51.25, 43.14, 41.96, 32.01, 25.71. ^{19}F NMR (376 MHz, DMSO-d_6) δ -73.93. HRMS (ESI-TOF-TOF) *m/z* calcd for [M + H] 296.2121, found 296.2125.

N-(3-((phenethyl(piperidin-4-yl)amino)methyl)phenyl)acetamide - 335

LCMS RT (Method 2) 2.92 min (m/z 352.2) ^{1}H NMR (400 MHz, DMSO-d_6) δ 10.17 (d, J = 25.8 Hz, 2H), 8.98 (s, 1H), 8.70 (s, 1H), 7.97 (s, 1H), 7.50 (d, J = 7.4 Hz, 1H), 7.39 (s, 1H), 7.35 – 7.19 (m, 4H), 7.17 (d, J = 7.2 Hz, 2H), 4.44 (d, J = 48.3 Hz, 2H), 3.70 (s, 1H), 3.44 (s, 2H), 3.21 (s, 2H), 2.97 (s, 3H), 2.81 (s, 1H), 2.31 (s, 2H), 2.06 (s, 3H), 1.98 (d, J = 13.8 Hz, 2H). ^{13}C NMR (101 MHz, DMSO-d_6) δ 168.93, 140.17, 129.12, 125.80, 121.71, 120.21, 66.63, 58.04, 54.29, 42.71, 30.28, 24.41, 23.48.^{19}F NMR (376 MHz, DMSO-d_6) δ -73.86. HRMS (ESI-TOF) *m/z* calcd for [M + Na] 374.2203, found 374.2207.

3-((phenethyl(piperidin-4-yl)amino)methyl)benzamide - 337

LCMS RT (Method 2) 2.63 min (m/z 338.2) ^{1}H NMR (400 MHz, DMSO-d_6) δ 7.90 (s, 1H), 7.83 (s, 1H), 7.71 (d, J = 7.6 Hz, 1H), 7.44 (d, J = 7.5 Hz, 1H), 7.39 – 7.26 (m, 2H), 7.22 (t, J = 7.3 Hz, 2H), 7.13 (dd, J = 16.7, 7.2 Hz, 3H), 3.71 (s, 2H), 3.05 – 2.88 (m, 2H), 2.64 (s, 4H), 2.41 (t, J = 12.0 Hz, 2H), 1.75 (t, J = 11.5 Hz, 1H), 1.66 (d, J = 10.5 Hz, 2H), 1.47 – 1.28 (m, 2H). ^{13}C NMR (101 MHz, DMSO-d_6) δ 168.00, 141.34, 140.47, 134.08, 130.92, 128.57, 128.05, 127.83, 127.40, 125.66, 125.58, 57.62, 53.62, 52.03, 45.53, 34.76, 28.66. ^{19}F NMR (376 MHz, DMSO-d_6) δ -73.45. HRMS (ESI-TOF) *m/z* calcd for [M + H] 338.2227, found 338.2239.

N-(3-((phenethyl(piperidin-4-yl)amino)methyl)phenyl)methanesulfonamide – 338

LCMS RT (Method 2) 3.00 min (m/z 388.2) ^{1}H NMR (400 MHz, DMSO-d_6) δ 10.26 (s, 1H), 9.93 (d, J = 17.5 Hz, 1H), 8.89 (s, 1H), 8.59 (s, 1H), 7.39 (s, 3H), 7.26 (d, J = 7.0 Hz, 3H), 7.21 (d, J = 6.3 Hz, 1H), 7.14 (d, J = 7.1 Hz, 2H), 4.44 (d, J = 46.6 Hz, 2H), 3.83 (s, 3H), 3.40 (s, 2H), 3.15 (s, 1H), 2.98 (s, 3H), 2.94 (s, 1H), 2.78 (s, 2H), 2.28 (s, 2H), 1.98 (s, 2H). ^{13}C NMR (101 MHz, DMSO-d_6) δ 158.52, 139.26, 131.65, 130.38, 129.09, 127.34, 115.85, 58.18, 53.94, 50.92, 42.69, 30.34, 23.59.^{19}F NMR (376 MHz, DMSO-d_6) δ -73.89. HRMS (ESI) *m/z* calcd for [M + Na] 410.1873, found 401.1884.

N-(2-methoxybenzyl)-N-phenethylpiperidin-4-amine - 339

LCMS RT (Method 2) 3.32 min (m/z 325.2) ^{1}H NMR (400 MHz, DMSO-d_6) δ 9.49 (s, 1H), 8.97 (s, 1H), 8.67 (s, 1H), 7.49 (s, 2H), 7.35 – 7.26 (m, 2H), 7.24 (d, J = 6.7 Hz, 1H), 7.18 (d, J = 7.2 Hz, 2H), 7.16 – 7.07 (m, 1H), 7.02 (s, 1H), 4.48 (d, J = 11.9 Hz, 1H), 4.27 (s, 1H), 3.83 (s, 3H), 3.72 (s, 2H), 3.47 (s, 2H), 3.25 (s, 2H), 2.99 (s, 2H), 2.91 (s, 1H), 2.28 (d, J = 20.6 Hz, 2H), 2.16 – 1.91 (m, 2H). ^{13}C NMR (151 MHz, DMSO-d_6) δ 161.01, 139.88, 135.92, 134.91, 131.79, 130.07, 123.74, 114.53, 60.74, 58.68, 54.65, 52.14, 45.27, 32.59, 26.56, 25.42.^{19}F NMR (376 MHz, DMSO-d_6) δ -73.77. HRMS (ESI-TOF) *m/z* calcd for [M + H] 325.2274, found 325.2282.

N-phenethyl-N-(pyridin-2-ylmethyl)piperidin-4-amine – 340

LCMS RT (Method 2) 4.63 min (m/z 296.2) ^{1}H NMR (400 MHz, DMSO-d_6) δ 8.85 (s, 1H), 8.64 (ddd, J = 4.9, 1.8, 0.9 Hz, 1H), 7.92 (td, J = 7.7, 1.8 Hz, 1H), 7.56 (d, J = 7.8 Hz, 1H), 7.45 (ddd, J = 7.6, 4.8, 1.1 Hz, 1H), 7.34 – 7.10 (m, 5H), 4.44 (s, 2H), 3.55 (d, J = 13.1 Hz, 1H), 3.39 (d, J = 12.7 Hz, 2H), 3.18 (t, J = 8.3 Hz, 2H), 2.89 (qd, J = 9.7, 8.3, 4.8 Hz, 4H), 2.24 – 2.07 (m, 2H), 1.86 (dt, J = 14.5, 11.0 Hz, 2H).^{13}C NMR (151 MHz, DMSO-d_6) δ 160.91, 156.62, 152.25, 141.14, 139.92, 131.84, 131.73, 129.98, 127.21, 119.08, 82.15, 65.15, 56.22, 44.67, 31.13, 28.86. ^{19}F NMR (376 MHz, DMSO-d_6) δ -73.80. HRMS (ESI-TOF) *m/z* calcd for [M + H] 296.2121, found 325. 296.2136.

N-(2-((phenethyl(piperidin-4-yl)amino)methyl)phenyl)acetamide – 341

LCMS RT (Method 2) 3.05 min (m/z 352.3) ^{1}H NMR (400 MHz, DMSO-d_6) δ 9.97 (s, 1H), 8.89 (s, 1H), 8.57 (s, 1H), 8.23 (s, 1H), 4.53 – 3.90 (m, 5H), 3.75 (s, 1H), 3.37 (s, 2H), 2.90 (s, 2H), 2.70 (s, 2H), 2.21 (s, 2H), 1.95 (s, 2H), 1.73 (s, 2H). ^{13}C NMR (151 MHz, DMSO-d_6) δ 173.32, 161.44, 161.22, 140.65, 135.68, 131.67, 131.42, 129.98, 126.65, 124.50, 116.87, 60.92, 54.09, 46.19, 45.24, 33.06, 27.48, 26.09. ^{19}F NMR (376 MHz, DMSO-d_6) δ -70.19. HRMS (ESI) *m/z* calcd for [M + H] 352.2383, found 352.2386.

N,N-dimethyl-2-((phenethyl(piperidin-4-yl)amino)methyl)benzamide - 342

LCMS RT (Method 2) 3.3 min (m/z 366.2) ^{1}H NMR (400 MHz, DMSO-d_6) δ 7.43 (d, J = 7.3 Hz, 1H), 7.35 – 7.19 (m, 4H), 7.12 (dd, J = 12.2, 6.6 Hz, 4H), 3.57 (s, 4H), 2.97 (s, 4H), 2.73 (s, 3H), 2.58 (d, J = 15.2 Hz, 4H), 2.41 (t, J = 11.3 Hz, 2H), 1.81 – 1.66 (m, 1H), 1.62 (d, J = 8.2 Hz, 2H), 1.33 (q, J = 12.3, 11.1 Hz, 2H). ^{13}C NMR (101 MHz, DMSO-d_6) δ 170.38, 140.96, 137.96, 137.33, 129.95, 128.98, 128.59, 128.57, 127.03, 126.26, 126.15, 57.80, 52.26,

51.54, 45.97, 38.72, 34.80, 34.43. ^{19}F NMR (376 MHz, DMSO-d_6) δ -73.47. HRMS (ESI-TOF) *m/z* calcd for [M + H] 366.2540, found 366.2543.

2-((phenethyl(piperidin-4-yl)amino)methyl)benzamide - 343

LCMS RT (Method 2) 2.90 min (m/z 338.2) ^{1}H NMR (400 MHz, DMSO-d_6) δ 8.39 (d, *J* = 22.4 Hz, 1H), 7.46 (d, *J* = 7.5 Hz, 2H), 7.39 – 7.33 (m, 2H), 7.32 – 7.27 (m, 1H), 7.23 (t, *J* = 7.3 Hz, 2H), 7.17 – 7.12 (m, 1H), 7.07 (d, *J* = 7.0 Hz, 2H), 3.83 (s, 2H), 3.32 (s, 4H), 2.99 (dd, *J* = 26.5, 11.3 Hz, 2H), 2.68 – 2.62 (m, 2H), 2.57 – 2.54 (m, 1H), 1.76 (t, *J* = 10.8 Hz, 1H), 1.67 (d, *J* = 10.9 Hz, 2H), 1.47 – 1.33 (m, 2H) ^{13}C NMR (101 MHz, DMSO-d_6) δ 140.78, 137.58, 130.33, 129.67, 129.01, 128.57, 127.04, 126.19, 58.01, 52.11, 45.77, 35.26, 28.46, 22.83.^{19}F NMR (376 MHz, DMSO-d_6) δ -73.45. HRMS (ESI-TOF) *m/z* calcd for [M + Na] 360.2046, found 360.2063.

N,N-diphenethylpiperidin-4-amine - 344

LCMS RT (Method 2) 3.41 min (m/z 309.4) ^{1}H NMR (400 MHz, DMSO-d_6) δ 10.06 (s, 1H), 8.75 (s, 1H), 8.37 (s, 1H), 7.29 (d, *J* = 23.4 Hz, 10H), 3.78 (s, 1H), 3.40 (s, 6H), 3.12 – 2.90 (m, 5H), 2.22 (s, 2H), 1.91 (d, *J* = 12.8 Hz, 2H). ^{19}F NMR (376 MHz, DMSO-d_6) δ -73.67. HRMS (ESI-TOF) *m/z* calcd for [M + H] 309.2325, found 309.2324.

N-phenethyl-N-(3-phenylpropyl)piperidin-4-amine - 345

LCMS RT (Method 2) 3.59 min (m/z 323.2) ^{1}H NMR (400 MHz, DMSO-d_6) δ 9.65 (s, 1H), 8.63 (s, 1H), 8.28 (s, 1H), 7.47 – 7.01 (m, 10H), 3.69 (s, 1H), 3.23 (s, 3H), 3.07 – 2.87 (m, 4H), 2.66 (s, 2H), 2.18 (d, *J* = 11.9 Hz, 2H), 2.02 (d, *J* = 8.2 Hz, 2H), 1.84 (d, *J* = 13.5 Hz, 2H), 1.59 (d, *J* = 53.5 Hz, 2H), 1.24 (s, 1H). ^{19}F NMR (376 MHz, DMSO-d_6) δ -73.55. HRMS (ESI-TOF) *m/z* calcd for [M + H] 323.2482, found 323.2487.

N-phenethyl-N-(piperidin-4-yl)benzamide – 346

To a solution of tert-butyl 4-(phenethylamino)piperidine-1-carboxylate (60mg, 0.197 mmol) in DCM (0.5 mL) was added benzoyl chloride (0.027 ml, 0.237 mmol) followed by triethylamine (0.060 ml, 0.434 mmol) and DMAP (2.408 mg, 0.020 mmol) at room temperature. The reaction was stirred overnight, solvent was removed under nitrogen. Boc deprotection and purification was carried out in an analogous manner to general procedure **A**, yielding N-phenethyl-N-(piperidin-4-yl)benzamide, as a mono-TFA salt. LCMS RT (Method 2) 3.83 min (m/z 309.2) ^{1}H NMR (400 MHz, DMSO-d_6) δ 8.63 (s, 1H), 8.34 (s, 1H), 7.44 (dd, *J* = 5.0, 1.9 Hz, 3H), 7.37 – 7.31 (m, 2H), 7.21 (d, *J* = 18.0 Hz, 4H), 6.83 (s, 1H), 4.23 (s, 1H), 3.52 (s, 2H), 3.31 (d, *J* = 15.5 Hz, 3H), 2.78 (d, *J* = 48.4 Hz, 3H), 2.25 (s, 1H), 1.81 (d, *J* = 68.1 Hz, 3H). ^{13}C NMR (151 MHz, DMSO-d_6) δ 161.10, 142.33, 141.19, 140.54, 139.80,

132.49, 131.58, 129.52, 129.10, 117.23, 56.71, 54.07, 51.61, 46.33, 45.63, 39.34, 37.68, 29.51, 29.05. ^{19}F NMR (376 MHz, DMSO-d_6) δ -73.71. [M + H^+]; HRMS (ESI) *m/z* calcd for [M + H] 309.1961, found 309.1957.

N-phenethyl-N-(piperidin-4-yl)benzenesulfonamide - 347

To a solution of tert-butyl 4-(phenethylamino)piperidine-1-carboxylate (60mg, 0.197 mmol) in DCM (0.5mL) was added benzenesulfonyl chloride (30.2 µl, 0.237 mmol) followed by triethylamine (35.7 µl, 0.256 mmol) at room temperature, the reaction was stirred overnight. Boc deprotection and purification is carried out in an analogous manner to general procedure **A** to yield N-phenethyl-N-(piperidin-4-yl)benzenesulfonamide. LCMS RT (Method 2) 4.19 min (m/z 345.2 ^{1}H NMR (400 MHz, DMSO-d_6) δ 8.42 (s, 2H), 7.92 – 7.82 (m, 2H), 7.70 – 7.62 (m, 1H), 7.62 – 7.54 (m, 2H), 7.34 – 7.25 (m, 2H), 7.21 (tt, *J* = 7.9, 1.4 Hz, 3H), 3.99 (tt, *J* = 12.0, 3.9 Hz, 1H), 3.24 (tdd, *J* = 8.5, 5.7, 3.5 Hz, 4H), 3.00 – 2.79 (m, 4H), 1.83 (qd, *J* = 13.1, 4.1 Hz, 2H), 1.51 (dd, *J* = 13.7, 3.6 Hz, 2H ^{13}C NMR (101 MHz, DMSO-d_6) δ 141.01, 138.81, 133.37, 129.98, 129.10, 128.94, 127.10, 126.96, 53.21, 45.82, 43.35, 38.01, 27.25. ^{19}F NMR (376 MHz, DMSO-d_6) δ -73.58. [M + H^+]; HRMS (ESI) *m/z* calcd for [M + H] 345.1631, found 345.1641.

N-phenethyl-N-propylpiperidin-4-amine - 348

LCMS RT (Method 2) 2.61 min (m/z 247.1) ^{1}H NMR (400 MHz, DMSO-d_6) δ 10.07 (s, 1H), 8.95 (s, 1H), 8.63 (s, 1H), 7.49 – 7.15 (m, 5H), 3.76 – 3.63 (m, 1H), 3.43 (s, 3H), 3.29 (s, 2H), 3.13 (s, 2H), 3.04 – 2.93 (m, 3H), 2.20 (s, 2H), 1.91 (q, *J* = 10.3, 9.3 Hz, 2H), 1.73 (s, 2H), 0.93 (t, *J* = 7.3 Hz, 3H). ^{13}C NMR (101 MHz, DMSO-d_6) δ 129.26, 129.03, 127.34, 57.53, 52.01, 51.60, 42.55, 30.44, 23.40, 18.17, 11.33.^{19}F NMR (376 MHz, DMSO-d_6) δ -73.71. HRMS (ESI-TOF) *m/z* calcd for [M + H]247.2169, found 247.2165.

N-isobutyl-N-phenethylpiperidin-4-amine – 349

LCMS RT (Method 2) 3.02 min (m/z 261.2) HRMS (ESI) *m/z* calcd for [M + H] 261.2325, found 261.2337.

N-(cyclopentylmethyl)-N-phenethylpiperidin-4-amine - 350

LCMS RT (Method 2) 3.22 min (m/z 287.4) ^{1}H NMR (400 MHz, DMSO-d_6) δ 9.70 (s, 1H), 8.95 (s, 1H), 8.64 (s, 1H), 7.39 – 7.22 (m, 5H), 3.80 – 3.71 (m, 1H), 3.59 (s, 2H), 3.44 (d, *J* = 11.7 Hz, 2H), 3.30 (s, 1H), 3.19 (s, 2H), 3.02 (d, *J* = 22.7 Hz, 3H), 2.34 – 2.13 (m, 3H), 2.03 – 1.78 (m, 4H), 1.59 (d, *J* = 39.7 Hz, 4H), 1.23 (s, 2H). ^{13}C NMR (101 MHz, DMSO-d_6) δ 158.60, 137.27, 129.27, 129.06, 127.36, 57.86, 55.64, 52.39, 42.54, 36.12, 31.07, 30.13, 24.93, 23.41, 22.86.^{19}F NMR (376 MHz, DMSO-d_6) δ -73.76. HRMS (ESI-TOF) *m/z* calcd for [M + H] 287.2482 , found 287.2484.

N-(cyclohexylmethyl)-N-phenethylpiperidin-4-amine – 351

LCMS RT (Method 2) 3.40 min (m/z 301.4) ^{1}H NMR (400 MHz, DMSO-d_6) δ 9.49 (s, 1H), 8.90 (s, 1H), 8.59 (s, 1H), 7.54 – 6.98 (m, 5H), 3.70 (s, 1H), 3.42 (d, J = 12.6 Hz, 2H), 3.27 (s, 2H), 3.01 (d, J = 10.2 Hz, 5H), 2.19 (dd, J = 27.0, 12.4 Hz, 2H), 1.98 – 1.56 (m, 7H), 1.33 – 1.05 (m, 3H), 0.95 (dd, J = 17.1, 7.3 Hz, 2H). ^{13}C NMR (151 MHz, DMSO-d_6) δ 161.30, 139.89, 131.99, 131.74, 130.04, 119.18, 60.74, 59.60, 55.81, 45.14, 36.73, 33.38, 32.70, 28.54, 28.09, 28.01, 26.07, 25.15.^{19}F NMR (376 MHz, DMSO-d_6) δ -73.76. HRMS (ESI-TOF) *m/z* calcd for [M + H] 301.2638, found 301.2638.

N-(3,5-dichlorobenzyl)-N-phenethylpiperidin-4-amine – 352

LCMS RT (Method 2) 3.91 min (m/z 363.1) ^{1}H NMR (600 MHz, DMSO-d_6) δ 8.60 (s, 1H), 8.26 (s, 1H), 7.64 (d, J = 66.3 Hz, 1H), 7.57 – 7.36 (m, 1H), 7.26 (s, 2H), 7.19 (s, 1H), 7.14 (d, J = 6.3 Hz, 2H), 4.86 – 3.83 (m, 3H), 3.68 (s, 1H), 3.43 – 3.18 (m, 2H), 3.01 – 2.77 (m, 3H), 2.77 – 2.59 (m, 2H), 2.31 – 1.46 (m, 4H).^{13}C NMR (101 MHz, DMSO-d_6) δ 158.54, 135.52, 134.50, 133.92, 129.10, 128.78, 128.28, 126.79, 115.65, 52.75, 51.76, 45.44, 43.10, 41.94, 32.07, 24.45. ^{19}F NMR (376 MHz, DMSO-d_6) δ -73.50 HRMS (ESI) *m/z* calcd for [M + H] 363.1389, found 363.1396.

N-(3-bromo-5-chlorobenzyl)-N-phenethylpiperidin-4-amine – 353

^{1}H NMR (600 MHz, DMSO-d_6) δ 10.58 (s, 1H), 8.56 (s, 1H), 8.19 (s, 1H), 7.78 (s, 3H), 7.42 – 6.94 (m, 7H), 3.68 (s, 2H), 3.35 (s, 3H), 2.71 (s, 7H), 1.79 (s, 4H). ^{13}C NMR (151 MHz, DMSO-d_6) δ 161.26, 139.56, 137.31, 131.79, 131.48, 129.96, 125.38, 116.82, 60.83, 55.30, 55.16, 53.85, 45.73, 32.59, 26.76. . ^{19}F NMR (376 MHz, DMSO-d_6) δ -70.13 [M + H^{+}]; HRMS (ESI) *m/z* calcd for [M + Na] 431.0683, found 431.0704.

N-(4-bromo-3-chlorobenzyl)-N-phenethylpiperidin-4-amine – 354

LCMS RT (Method 2) 3.79 min (m/z 407.1**)** ^{1}H NMR (600 MHz, DMSO-d_6) δ 8.29 – 6.79 (m, 8H), 3.88 (d, J = 278.1 Hz, 4H), 3.28 (d, J = 115.5 Hz, 3H), 2.86 (d, J = 47.3 Hz, 4H), 2.30 – 1.45 (m, 4H). ^{13}C NMR (151 MHz, DMSO-d_6) δ 161.24, 137.01, 135.98, 134.70, 133.29, 131.81, 131.57, 129.80, 116.84, 60.63, 55.30, 53.82, 45.43, 32.67, 26.12^{19}F NMR (376 MHz, DMSO-d_6) δ -73.11 HRMS (ESI) *m/z* calcd for [M + H] 407.0884, found 407.0899.

N-(3-chloro-4-fluorobenzyl)-N-phenethylpiperidin-4-amine – 355

LCMS RT (Method 2) 3.68 min (m/z 347.7) ^{1}H NMR (400 MHz, DMSO-d_6) δ 10.52 (s, 1H), 9.05 (s, 1H), 8.87 (s, 1H), 8.16 – 7.01 (m, 8H), 3.36 (d, J = 10.8 Hz, 2H), 3.15 (s, 1H), 3.01 – 2.82 (m, 3H), 2.76 (s, 1H), 2.19 (t, J = 13.1 Hz, 4H). ^{13}C NMR (151 MHz, DMSO-d_6) δ 161.31, 136.58, 133.60, 131.79, 131.58, 129.95, 120.17, 117.01, 60.43, 55.24, 53.49, 45.42, 32.62, 26.14. ^{19}F NMR (376 MHz, DMSO-d_6) δ -73.92, -114.90. HRMS (ESI) *m/z* calcd for [M + Na] 369.1504, found 369.1486.

N-(3,4-dichlorobenzyl)-N-phenethylpiperidin-4-amine – 356

LCMS RT (Method 2) 3.93 min (m/z 363.1) ^{1}H NMR (400 MHz, DMSO-d_6) δ 10.51 (s, 1H), 8.64 (s, 1H), 8.28 (s, 1H), 7.58 (s, 2H), 7.25 (ddd, J = 8.8, 4.4, 2.5 Hz, 2H), 7.23 – 7.17 (m, 1H), 7.14 (d, J = 7.2 Hz, 2H), 4.20 (br, 7H), 2.98 – 2.81 (m, 3H), 2.73 (s, 2H), 2.04 – 1.52 (m, 4H). ^{13}C NMR (151 MHz, dmso) δ 161.23, 134.47, 133.57, 131.80, 131.37, 129.41, 117.04, 60.43, 55.26, 53.56, 46.06, 37.49, 27.78. ^{19}F NMR (376 MHz, DMSO-d_6) δ -73.90. HRMS (ESI) *m/z* calcd for [M + H] 363.1389, found 363.1373.

N-(3-bromo-4-chlorobenzyl)-N-phenethylpiperidin-4-amine – 357

LCMS RT (Method 2) 3.85 min (m/z 407.1) ^{1}H NMR (600 MHz, DMSO-d_6) δ 10.51 (s, 1H), 8.90 (s, 1H), 8.57 (s, 1H), 8.07 (s, 1H), 7.60 (s, 2H), 7.41 – 6.96 (m, 5H), 4.39 (s, 2H), 3.66 (s, 2H), 3.23 (s, 1H), 3.00 – 2.65 (m, 4H), 2.26 (s, 2H), 2.08 – 1.52 (m, 4H).^{13}C NMR (101 MHz, DMSO-d_6) δ 158.53, 135.18, 131.86, 131.46, 130.97, 129.12, 128.86, 127.28, 52.53, 45.44, 42.96, 40.55, 32.07, 25.58. ^{19}F NMR (376 MHz, DMSO-d_6) δ -73.89. HRMS (ESI) *m/z* calcd for [M + H] 407.0884, found 407.0874.

N-(2,3-dichlorobenzyl)-N-phenethylpiperidin-4-amine – 358

LCMS RT (Method 2) 3.90 min (m/z 363.1) ^{1}H NMR (400 MHz, DMSO-d_6) δ 8.57 (s, 1H), 8.19 (s, 1H), 7.49 (s, 1H), 7.47 – 7.36 (m, 1H), 7.37 – 7.19 (m, 3H), 7.14 (dd, J = 17.8, 7.1 Hz, 3H), 3.77 (s, 2H), 3.29 (d, J = 10.6 Hz, 3H), 3.00 – 2.78 (m, 3H), 2.70 (d, J = 40.5 Hz, 3H), 1.87 (s, 2H), 1.67 (s, 2H). ^{13}C NMR (151 MHz, DMSO-d_6) δ 176.30, 143.84, 131.81, 131.77, 131.66, 131.54, 131.24, 130.89, 128.98, 57.89, 55.39, 54.91, 46.30, 37.56, 27.81. ^{19}F NMR (376 MHz, DMSO-d_6) δ -73.77 HRMS (ESI) *m/z* calcd for [M + Na] 385.1209, found 385.1190.

N-(2-chloro-3-(trifluoromethyl)benzyl)-N-phenethylpiperidin-4-amine – 359

LCMS RT (Method 2) 4.23 min (m/z 397.2 ^{1}H NMR (400 MHz, DMSO-d_6) δ 8.85 (s, 1H), 8.54 (s, 1H), 7.81 – 7.61 (m, 2H), 7.51 – 7.37 (m, 1H), 7.34 – 7.19 (m, 2H), 7.19 – 7.09 (m, 2H), 4.41 (s, 1H), 3.86 (s, 2H), 3.33 (d, *J* = 45.2 Hz, 2H), 3.00 – 2.78 (m, 3H), 2.75 (s, 1H), 2.65 (d, *J* = 8.6 Hz, 2H), 1.86 (s, 2H), 1.65 (s, 2H). ^{13}C NMR (151 MHz, DMSO-d_6) δ 161.14, 144.01, 143.13, 137.15, 131.82, 131.28, 130.38, 129.06, 125.25, 58.05, 55.34, 54.10, 46.20, 37.45, 27.68.^{19}F NMR (376 MHz, DMSO-d_6) δ -60.88, -74.03. HRMS (ESI) *m/z* calcd for [M + H] 397.1653, found 397.1655.

N-(2-chloro-3-fluorobenzyl)-N-phenethylpiperidin-4-amine – 360

LCMS RT (Method 2) 3.6 min (m/z 347.1) ^{1}H NMR (600 MHz, DMSO-d_6) δ 8.59 (s, 1H), 8.17 (s, 1H), 7.45 – 7.27 (m, 3H), 7.24 (t, *J* = 7.2 Hz, 2H), 7.17 (d, *J* = 7.3 Hz, 1H), 7.15 – 7.09 (m, 2H), 4.18 (s, 4H), 3.83 (s, 2H), 2.88 (s, 3H), 2.69 (s, 2H), 1.89 (s, 2H), 1.68 (s, 2H).^{13}C NMR (151 MHz, DMSO-d_6) δ 161.19, 136.88, 131.82, 131.28, 130.38, 129.07, 127.04, 125.24, 118.80, 58.01, 55.32, 54.09, 46.18, 37.58, 27.66. ^{19}F NMR (376 MHz, DMSO-d_6) δ -74.00 [M + H^+]; HRMS (ESI) *m/z* calcd for [M + H] 347.1685, found 347.1684

N-(2,4-dichlorobenzyl)-N-phenethylpiperidin-4-amine - 361

LCMS RT (Method 2) 3.85 min (m/z 363.1) ^{1}H NMR (400 MHz, DMSO-d_6) δ 8.59 (s, 1H), 8.21 (s, 1H), 7.60 (s, 1H), 7.47 (d, *J* = 5.1 Hz, 1H), 7.37 (s, 1H), 7.27 (t, *J* = 7.4 Hz, 3H), 7.20 (d, *J* = 7.1 Hz, 1H), 7.16 (d, *J* = 7.3 Hz, 3H), 4.35 (s, 5H), 3.79 (s, 2H), 2.89 (d, *J* = 9.9 Hz, 2H), 2.71 (s, 2H), 1.90 (s, 2H), 1.70 (s, 2H^{13}C NMR (151 MHz, DMSO-d_6) δ 161.17, 140.07, 136.41, 134.57, 131.82, 131.34, 130.32, 129.12, 116.89, 57.86, 55.19, 53.50, 46.12, 37.45, 27.67.^{19}F NMR (376 MHz, DMSO-d_6) δ -74.08. HRMS (ESI-TOF) *m/z* calcd for [M + H] 363.1389, found 363.1392.

N-(2-chloro-4-fluorobenzyl)-N-phenethylpiperidin-4-amine – 362

LCMS RT (Method 2) 3.55 min (m/z 346.1) ^{1}H NMR (400 MHz, DMSO-d_6) δ 8.60 (s, 1H), 8.21 (s, 1H), 7.40 (s, 3H), 7.25 (t, *J* = 7.4 Hz, 2H), 7.16 (dd, *J* = 18.4, 7.1 Hz, 3H), 4.27 (s, 2H), 3.80 (s, 2H), 3.32 (s, 2H), 2.90 (s, 3H), 2.65 (s, 2H), 1.88 (s, 2H), 1.74 (s, 2H). ^{13}C NMR (101 MHz, dmso) δ 158.45, 129.11, 128.71, 126.60, 126.19, 116.77, 114.68, 52.24, 50.75, 43.38, 42.04, 24.87, 24.78. ^{19}F NMR (376 MHz, DMSO-d_6) δ -68.22. HRMS (ESI) *m/z* calcd for [M + H] 347.1685, found 347.1677.

N-(4-bromo-3-chlorobenzyl)-N-(2-methyl-2-phenylpropyl)piperidin-4-amine – 364

LCMS RT (Method 2) 5.08 min (m/z 437.0^{1}H NMR (600 MHz, DMSO-d_6) δ 8.37 – 8.23 (m, 1H), 7.99 – 7.79 (m, 1H), 7.63 (d, J = 8.2 Hz, 1H), 7.39 (d, J = 1.9 Hz, 1H), 7.37 – 7.30 (m, 2H), 7.23 (t, J = 7.7 Hz, 2H), 7.16 – 7.08 (m, 2H), 3.33 (s, 2H), 3.19 (d, J = 12.4 Hz, 2H), 2.59 (d, J = 15.5 Hz, 4H), 2.32 (tt, J = 11.9, 3.7 Hz, 1H), 1.72 – 1.62 (m, 2H), 1.47 (qd, J = 13.3, 4.1 Hz, 2H), 1.23 (s, 6H). ^{13}C NMR (151 MHz, dmso) δ 166.51, 145.90, 136.58, 132.56, 131.22, 130.99, 129.14, 122.13, 65.41, 58.32, 55.58, 46.41, 29.94, 27.31. ^{19}F NMR (376 MHz, dmso) δ -73.90. HRMS (ESI) *m/z* calcd for [M + H] 437.1176, found 437.1158.

N-(4-bromo-3-chlorobenzyl)-N-(2-phenylcyclopentyl)piperidin-4-amine – 365

LCMS RT (Method 2) 3.55 min (m/z 449.0) HRMS (ESI) *m/z* calcd for [M + H] 449.1177, found 449.1168.

N-(4-bromo-3-chlorobenzyl)-N-(3-methyl-2-phenylbutyl)piperidin-4-amine – 366

LCMS RT (Method 2) 4.46 min (m/z 449.0) ^{1}H NMR (600 MHz, DMSO-d_6) δ 8.49 (s, 1H), 8.14 (s, 2H), 7.55 (s, 1H), 7.31 – 7.20 (m, 2H), 7.17 (s, 1H), 7.11 (s, 1H), 7.02 (d, J = 6.1 Hz, 2H), 6.91 (s, 1H), 4.09 (s, 3H), 3.57 (s, 1H), 3.44 (s, 1H), 3.33 – 3.13 (m, 2H), 2.83 (s, 1H), 2.73 (s, 2H), 2.60 (d, J = 34.9 Hz, 2H), 1.81 (s, 2H), 1.56 (s, 2H), 1.38 (s, 1H), 0.85 (s, 2H), 0.58 (s, 2H). ^{13}C NMR (151 MHz, dmso) δ 161.18, 145.96, 136.30, 135.82, 132.89, 131.83, 131.39, 130.71, 128.94, 120.62, 57.27, 55.98, 55.66, 53.71, 46.29, 33.71, 28.16, 26.44, 24.35, 23.07. ^{19}F NMR (376 MHz, dmso) δ -73.60 [M + H^{+}]; HRMS (ESI) *m/z* calcd for [M + H] 451.1333, found 451.1353.

N-(4-bromo-3-chlorobenzyl)-N-(2,3-dihydro-1H-inden-2-yl)piperidin-4-amine – 367

LCMS RT (Method 2) 4.13 min (m/z 421.0) ^{1}H NMR (600 MHz, DMSO-d_6) δ 8.69 – 8.44 (m, 1H), 8.36 – 8.05 (m, 1H), 7.86 – 7.49 (m, 2H), 7.39 – 7.24 (m, 1H), 7.21 – 7.13 (m, 2H), 7.13 – 7.01 (m, 2H), 4.46 (s, br, 1H), 3.75 (s, 2H), 3.37 – 3.24 (m, 2H), 3.11 – 2.95 (m, 2H), 2.91 – 2.83 (m, 2H), 1.90 (s, 2H), 1.70 (s, 2H).^{13}C NMR (151 MHz, dmso) δ 161.21, 144.01, 136.79, 136.08, 129.60, 129.20, 127.65, 127.39, 118.59, 74.30, 64.23, 58.10, 46.14, 40.20, 28.90. ^{19}F NMR (376 MHz, dmso) δ -73.68. HRMS (ESI) *m/z* calcd for [M + H] 421.0863, found 421.0879.

N-(4-bromo-3-chlorobenzyl)-N-(3-phenylcyclobutyl)piperidin-4-amine – 368

LCMS RT (Method 2) 3.76 min (m/z 435.1) ^{1}H NMR (600 MHz, DMSO-d_6) δ 10.63 (s, 1H), 8.90 (s, 1H), 8.64 (s, 1H), 7.84 (d, *J* = 48.1 Hz, 2H), 7.48 (s, 1H), 7.34 – 7.24 (m, 2H), 7.25 – 7.10 (m, 3H), 4.31 (d, *J* = 44.5 Hz, 2H), 4.00 (s, 1H), 3.62 (s, 2H), 3.39 (s, 3H), 3.08 (s, 1H), 2.94 (s, 2H), 2.68 (s, 1H), 2.16 (d, *J* = 52.6 Hz, 3H), 1.95 (s, 2H).^{13}C NMR (151 MHz, dmso) δ 161.31, 145.86, 137.13, 136.04, 134.67, 131.58, 131.40, 129.67, 126.05, 117.01, 59.60, 56.11, 53.57, 46.30, 45.17, 38.96, 35.10, 26.69. ^{19}F NMR (376 MHz, dmso) δ -74.02. HRMS (ESI) *m/z* calcd for [M + H] 435.1020, found 435.1025.

N-(4-bromo-3-chlorobenzyl)-N-(2-phenylbutyl)piperidin-4-amine – 369

LCMS RT (Method 2) 4.27 min (m/z 437.0) ^{1}H NMR (600 MHz, DMSO-d_6) δ 8.51 (s, 1H), 8.14 (s, 1H), 7.70 – 7.54 (m, 1H), 7.31 – 7.24 (m, 2H), 7.20 (q, *J* = 7.6, 7.0 Hz, 1H), 7.09 (s, 2H), 7.04 (s, 1H), 3.57 (d, *J* = 51.1 Hz, 2H), 3.27 (d, *J* = 28.5 Hz, 2H), 2.79 (s, 2H), 2.66 (s, 1H), 2.57 (s, 2H), 1.79 (d, *J* = 44.2 Hz, 3H), 1.61 (s, 1H), 1.53 (s, 2H), 1.41 (s, 1H), 0.66 (s, 3H).^{13}C NMR (151 MHz, dmso) δ 161.39, 136.45, 135.86, 132.85, 131.46, 131.14, 130.93, 129.06, 118.60, 59.27, 57.26, 55.98, 49.08, 46.29, 29.29, 26.94, 15.06. ^{19}F NMR (376 MHz, dmso) δ -73.77. HRMS (ESI) *m/z* calcd for [M + H] 437.1176, found 437.1168.

N-(4-bromo-3-chlorobenzyl)-N-(3-(3-bromophenyl)cyclobutyl)piperidin-4-amine – 371

LCMS RT (Method 2) 4.17 min (m/z 513.1) ^{1}H NMR (400 MHz, DMSO-d_6) δ 9.00 (s, 1H), 8.76 (s, 1H), 7.91 – 7.74 (m, 2H), 7.51 – 7.33 (m, 3H), 7.33 – 7.17 (m, 2H), 4.51 (s, 2H), 4.22 (s, 2H), 3.94 (s, 1H), 3.54 (s, 1H), 3.39 (d, *J* = 12.3 Hz, 3H), 2.93 (t, *J* = 11.7 Hz, 2H), 2.61 (s, 1H), 2.11 (s, 2H), 2.03 – 1.88 (m, 2H). ^{13}C NMR (101 MHz, dmso) δ 158.91, 146.14, 134.51, 133.79, 130.88, 129.83, 126.35, 126.31, 122.20, 56.71, 53.14, 50.72, 42.72, 32.05, 23.88. ^{19}F NMR (376 MHz, dmso) δ -74.13. HRMS (ESI) *m/z* calcd for [M + H] 513.0125, found 513.0119.

N-(4-bromo-3-chlorobenzyl)-N-(3-(4-bromophenyl)cyclobutyl)piperidin-4-amine, 372, mixture of syn and anti cylclobutane isomers.

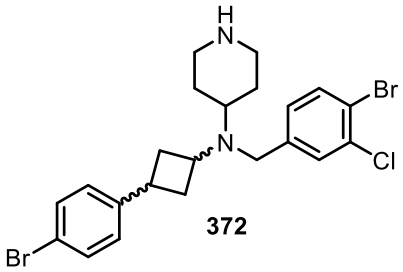

372

Appearance: Transparent, colourless oil as free base, off-white solid as di-TFA or 1:1 oxalate salt.

LCMS RT (Method 2) 4.16 min (m/z 512.9)

HRMS (ESI-TOF) *m/z* calcd for [M + H] 513.0125, found 513.0137.

Free base:

^{1}H NMR (400 MHz, $CDCl_3$) δ 7.54 – 7.44 (m, 2H), 7.39 (ddd, *J* = 14.5, 8.5, 2.1 Hz, 2H), 7.16 – 6.95 (m, 3H), 3.59 (dd, *J* = 9.1, 1.8 Hz, 2H), 3.46 – 3.25 (m, 1H), 3.12 (d, *J* = 11.8 Hz, 2H), 2.99 (td, *J* = 9.8, 7.3 Hz, 1H), 2.60 (td, *J* = 11.9, 2.8 Hz, 1H), 2.53 (t, *J* = 12.2 Hz, 2H), 2.46 – 2.31 (m, 2H), 2.23 (s, 2H), 2.20 – 2.09 (m, 1H), 1.86 (tdd, *J* = 10.9, 6.9, 2.5 Hz, 2H), 1.53 – 1.38 (m, 2H). **^{13}C NMR** (101 MHz, $CDCl_3$) δ 143.89, 143.63, 134.05, 133.24, 133.22, 131.35, 131.23, 129.61, 129.51, 128.48, 128.23, 127.32, 127.17, 119.85, 119.53, 77.30, 57.45, 57.38, 53.46, 52.19, 49.89, 49.53, 46.43, 36.86, 34.86, 32.63, 32.57, 29.75.

1:1 Oxalate salt – Salt form for PK studies:

^{1}H NMR (400 MHz, DMSO-d_6) δ 7.67 (dd, *J* = 8.2, 7.5 Hz, 1H), 7.56 (dd, *J* = 9.5, 2.0 Hz, 1H), 7.52 – 7.38 (m, 2H), 7.29 – 7.09 (m, 3H), 3.70 – 3.50 (m, 3H), 3.44 – 3.30 (m, 1H), 3.22 (d, *J* = 12.0 Hz, 2H), 3.02 (p, *J* = 9.1 Hz, 1H), 2.75 (t, *J* = 12.0 Hz, 2H), 2.37 (ddd, *J* = 11.2, 9.0, 5.2 Hz, 2H), 2.20 – 2.01 (m, 1H), 1.84 – 1.65 (m, 4H), 1.58 (q, *J* = 14.1, 12.9 Hz, 2H). **^{13}C NMR**

Di- TFA Salt:

^{1}H NMR ^{13}C NMR (151 MHz, dmso) δ 161.27, 145.29, 137.14, 136.10, 134.64, 134.22, 132.02, 126.07, 122.58, 59.57, 55.99, 53.59, 45.30, 38.81, 37.57, 34.53, 26.60, 25.86.

See appendix A9 for hard copies of spectal and chromatographic analyses.

Chapter 4.

General:

It was noted that the piperazine compounds have a tendency to decompose under normal phase silica gel chromatography, the addition of 0.2% of triethylamine v/v into the hexanes mobile phase was sufficient to stop the (presumably) acid catalysed decomposition of the products. In such circumstances where the products undergo normal phase chromatographic purification, this additive was used as a precaution in every case, as stated.

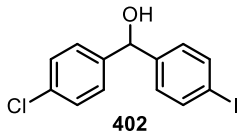

402

(4-chlorophenyl)(4-iodophenyl)methanol, 402.

A flame-dried 500 mL round-bottom flask was charged with 4-iodobenzaldehyde (5 g, 21.55 mmol) and Et_2O (170 ml) under nitrogen. The mixture was cooled to 0 °C and (4-chlorophenyl)magnesium bromide (22.63 ml, 22.63 mmol) was added dropwise. The reaction was stirred at 0 °C for 1h. H_2O (25 mL) was added to quench the reaction, the mixture was poured into a seperatory funnel, diluted with brine (100mL) and EtOAc. Organics are seperated and the aqueous layer was extracted twice with EtOAc (2x150mL). The combined organic phases were dried over magnesium sulfate, and concentrated under reduced pressure to give the crude product, which is purified by gradient column chromatography 15-30% EtOAc in hexanes to yield 1-(4-chlorophenyl)(4-iodophenyl)methanol, **402**, as a white solid. (6.78 g, 19.68 mmol, 91 % yield) LCMS RT (Method 2) 3.61 min, (no m/z in +ve mode) ^{1}H NMR (400 MHz, $CDCl_3$) δ 7.74 – 7.60 (m, 2H), 7.36 – 7.23 (m, 4H), 7.13 – 7.07 (m, 2H), 5.75 (s, 1H), 2.25 (s, 1H). ^{13}C NMR (400 MHz, , $CDCl_3$) δ 142.98, 141.68, 137.64, 133.60, 128.74, 128.37, 127.83, 93.35, 77.32, 77.00, 76.68, 75.06. IR (neat) 3332, 1903, 1586, 1481.

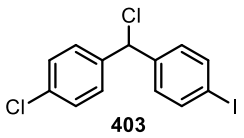

403

1-chloro-4-(chloro(4-iodophenyl)methyl)benzene - 403.

1-(4-chlorophenyl)(4-iodophenyl)methanol (**1**) (4g, 11.61 mmol) was dissolved in DCM (20 ml) in an oven-dried 50mL round-bottom flask at room temperature, to this was added N,N-dimethylformamide (0.1mL, 1.291 mmol) followed by dropwise addition of thionyl chloride (2.54 mL, 34.8 mmol), evoluion of gas is noted. The reaction was stirred for 90 minutes and was found to be complete by TLC. The majority of volatiles were then removed under rotary evaporation, followed by further evaporation under high vaccum to give the title compound -chloro-4-(chloro(4-iodophenyl)methyl)benzene **403**, as a sand-coloured solid (crude product 4.57 g, 12.59 mmol). Crude product was taken through to the next step. LCMS RT (Method 2) 4.02min, (no m/z in +ve mode), ^{1}H NMR (400 MHz, $CDCl_3$) δ 7.71 – 7.66 (m, 2H), 7.35 – 7.29 (m, 4H), 7.14 – 7.11 (m, 2H), 6.02 (s, 1H). ^{13}C NMR (101 MHz, , $CDCl_3$) δ 140.29, 139.00, 137.75, 134.21, 129.53, 129.04, 128.82, 94.05, 77.32, 77.00, 76.68, 62.66. IR (neat) 1901, 1582, 1483, 1398.

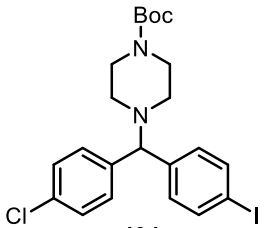

404

Tert-butyl4-((4-chlorophenyl)(4-iodophenyl)methyl)piperazine-1-carboxylate - 404

To a stirring solution of 1-chloro-4-(chloro(4-iodophenyl)methyl)benzene, **403** (4.5 g, 12.40 mmol) in N,N-dimethylformamide (35 ml) in a 100mL round-bottom flask was added potassium carbonate (3.43 g, 24.79 mmol), potassium iodide (2.264 g, 13.64 mmol) and tert-butyl piperazine-1-carboxylate (6.93 g, 37.2 mmol). The reaction vessel is fitted with a reflux condenser and stirred at 75°C for 16 hours.The reaction is poured into a seperatory funnel, diluted with brine EtOAc (150mL) which is extracted with brine (3x100mL). The organic phase was dried over magnesium sulfate, and concentrated under reduced pressure to give the crude product, which is purified by gradient column

chormatography 0-35% gradient EtOAc in hexanes (containing 0.2% triethylamine v/v) to yield tert-butyl 4-((4-chlorophenyl)(4-iodophenyl)methyl)piperazine-1-carboxylate, **404**, as a white solid. (4.86g, 9.48 mmol, 76 % yield for 2 steps) LCMS RT (Method 2) 3.65min (m/z 513.1) ^{1}H NMR (400 MHz, $CDCl_3$) δ 7.61 (d, *J* = 8.4 Hz, 2H), 7.30 (d, *J* = 8.6 Hz, 2H), 7.25 (d, *J* = 8.8 Hz, 2H), 7.12 (d, *J* = 8.3 Hz, 2H), 4.16 (s, 1H), 3.41 (s-br, 4H), 2.30 (s-br, 4H), 1.43 (s, 9H). ^{13}C NMR (101 MHz, $CDCl_3$) δ 154.71, 141.65, 140.29, 137.77, 132.99, 129.69, 129.03, 128.86, 92.63, 79.61, 74.75, 51.56, 43.94 (weak, broad), 28.38. IR(neat) 2975, 2812, 1680, 1482, 1402.

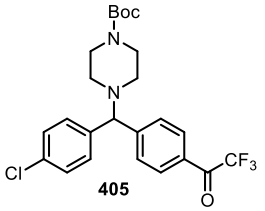

405

Tert-butyl4-((4-chlorophenyl)(4-(2,2,2-trifluoroacetyl)phenyl)methyl)piperazine-1-carboxylate, 405

To a solution of tert-butyl 4-((4-chlorophenyl)(4-iodophenyl)methyl) piperazine-1-carboxylate, **404** (2g, 3.90 mmol) in THF (Volume: 40 mL) in a flame-dried 250mL round bottom flask at -78 °C was added n-butyllithium (5.00 mL of 1.6M solution in hexanes, 8.00 mmol) dropwise and the reaction was stirred for 20 minutes at -78 °C. To this was added ethyl 2,2,2-trifluoroacetate (0.928 mL, 7.80 mmol) and the reaction is stirred for 20 minutes at -78 °C then allowed to warm to room temperature, and stirring is continued for 30 mins. Reaction is quenched with sat.$NH_4Cl_{(aq)}$ (20mL), poured into a seperatory funnel and diluted with EtOAc, which is washed with sat. $NaCl_{(aq)}$ organics dried over magnisium sulfate, evaporated under reduced pressure and purified by gradient column chromatography 10-25% gradient EtOAc in hexanes (containing 0.2% triethylamine v/v). Yields tert-butyl 4-((4-chlorophenyl)(4-(2,2,2-trifluoroacetyl)phenyl)methyl)piperazine-1-carboxylate **405** as an off-white/yellow solid (1.122 g, 2.116 mmol, 58% yield) LCMS RT (Method 2) 3.133 (m/z 501.2 (hydrate)) ^{1}H NMR (400 MHz, $CDCl_3$) δ 8.03 – 7.97 (m, 2H), 7.59 (dd, *J* = 8.6, 2.1 Hz, 2H), 7.35 – 7.26 (m, 4H), 4.31 (s, 1H), 3.43 (m, 4H), 2.34 (d, *J* = 6.9 Hz, 4H), 1.43 (s, 9H) ^{13}C NMR (101 MHz, $CDCl_3$) δ 154.68, 150.42, 139.24, 133.50, 130.73, 129.19, 129.11, 129.04, 128.94, 128.88, 128.29, 79.72, 75.06, 51.62, 44.47, 28.38. ^{19}F NMR (376 MHz, $CDCl_3$) δ -71.44. HRMS (ESI) *m/z* calcd for [M (hydrate) + H] 501.1767, found 501.1731. IR (neat) 2975, 1668, 1420, 1246.

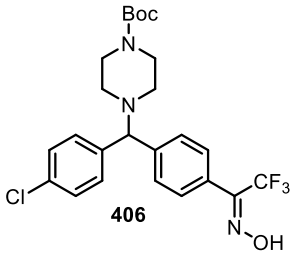

406

Tert-butyl4-((4-chlorophenyl)(4-(2,2,2-trifluoro-1-(hydroxyimino)ethyl)phenyl)methyl)piperazine-1-carboxylate, 406.

tert-butyl4-((4-chlorophenyl)(4-(2,2,2-trifluoroacetyl)phenyl)methyl) piperazine-1-carboxylate, **405** (976 mg, 2.021 mmol) was dissolved in pyridine 20mL, hydroxylamine hydrochloride (211 mg, 3.03 mmol) is added, the reaction was stirred at 70C for 3 hours, then stirred at room temperature over night. The reaction was subjected to rotary evaporation to remove the pyridine, resultant crude oil was then purified directly by gradient column chromatography 0-30% gradient EtOAc in hexanes (containing 0.2% triethylamine v/v) to yield tert-butyl 4-((4-chlorophenyl)(4-(2,2,2-trifluoro-1-(hydroxyimino)ethyl)phenyl)methyl)piperazine-1-carboxylate, **406** as a white solid. NMRs display approx 1:0.8 mixture of conformational isomers (viz. *syn/anti* oximes). LCMS RT (Method 2) 3.36 min (498.1 m/z) ^{1}H NMR (400 MHz, $CDCl_3$) δ 7.49 – 7.22 (m, 8H), 4.23 (d, J = 4.1 Hz, 1H), 3.42 (d, J = 5.3 Hz, 4H), 2.33 (t, J = 5.0 Hz, 4H), 2.22 (d, J = 4.6 Hz, 1H), 1.43 (s, 9H). ^{13}C NMR (101 MHz, $CDCl_3$) δ 154.91, 154.89, 148.98, 144.09, 143.75, 140.00, 139.97, 136.93, 133.11, 129.57, 129.24, 129.17, 129.13, 129.02, 128.89, 128.70, 127.79, 127.75, 127.65, 125.41, 124.08, 117.03, 79.94, 75.18, 51.67, 51.64, 44.62, 28.37. ^{19}F NMR (376 MHz, $CDCl_3$) -62.30, -66.19. HRMS (ESI) *m/z* calcd for [M + H] 498.1766, found 498.1790. IR (neat) 2977, 1662, 1431, 1247, 1164.

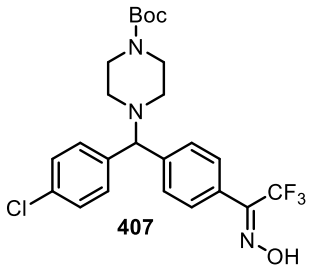

407

Tert-butyl(Z)-4-((4-chlorophenyl)(4-(2,2,2-trifluoro-1 ((tosyloxy)imino)ethyl)phenyl)methyl) piperazine-1-carboxylate, 407.

To a solution of (Z)-tert-butyl 4-((4-chlorophenyl)(4-(2,2,2-trifluoro-1 (hydroxyimino)ethyl)phenyl) methyl)piperazine-1-carboxylate (1.2g, 2.410 mmol) in acetone (15 mL) at 0°C was added triethylamine (1.008 mL, 7.23 mmol). Following this, 4-methylbenzene-1-sulfonyl chloride (0.551 g, 2.89 mmol) was added and the reaction mixture was stirred at room temperature for 1 or until determined complete as monitored by TLC. Upon completion the volatiles were removed by rotaty evaporation and the crude transparent red oil was purified directly by gradient column chromatography 0-40% gradient EtOAc in hexanes over 10 CV (containing 0.2% triethylamine v/v) which gave (Z)-tert-butyl4-((4-chlorophenyl)(4-(2,2,2-trifluoro-1((tosyloxy)imino)ethyl) phenyl)methyl)piperazine-1-carboxylate (**6)** (1.132 g, 1.735 mmol, 72 % yield) as a transparent colourless oil. LCMS RT (Method 2) 3.83min (652.2m/z) ^{1}H NMR (400 MHz, $CDCl_3$) δ 7.87 (d, *J* = 8.4 Hz, 2H), 7.50 (d, *J* = 8.4 Hz, 2H), 7.40 – 7.27 (m, 6H), 4.26 (s, 1H), 3.43 (d, *J* = 5.2 Hz, 4H), 2.47 (s, 3H), 2.37 – 2.27 (m, 4H), 1.44 (d, *J* = 1.0 Hz, 9H). ^{13}C NMR (101 MHz, $CDCl_3$) δ 154.69, 153.14, 146.12, 146.06, 139.59, 133.29, 131.09, 129.82, 129.27, 129.25, 129.00, 128.02, 123.34, 120.94, 79.62, 51.61, 28.37, 21.76. ^{19}F NMR (376 MHz, $CDCl_3$) δ -61.50, -66.46.

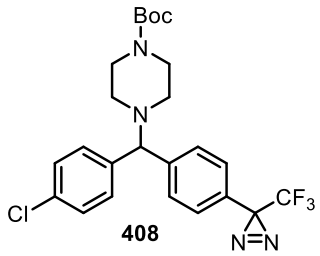

408

Procedure reference: [163]

tert-butyl 4-((4-chlorophenyl)(4-(3-(trifluoromethyl)-3H-diazirin-3-yl)phenyl)methyl)piperazine-1-carboxylate - 408

To condensed neat liquid ammonia (5mL) at -78°C was added tert-butyl (Z)-4-((4-chlorophenyl)(4-(2,2,2-trifluoro-1 ((tosyloxy)imino)ethyl)phenyl)methyl) piperazine-1-carboxylate (400 mg, 0.613 mmol) dissolved in 3mL of Et_2O. To this was added lithium amide (70.4 mg, 3.07 mmol). The sealed tube was closed and the reaction was allowed to warm to room temperature and stirred overnight, The following day, the reaction was cooled to -78°C, opened, and allowed to warm to room temperature under a stream of nitrogen. White solid resulted after ether and ammonia had evaporated which was taken up in solvent DCM and purified directly by gradient column chromatography 0-80% gradient EtOAc in hexanes over 15 CV (containing 0.2% triethylamine v/v) yielding tert-butyl 4-((4-chlorophenyl)(4-(3-(trifluoromethyl)-3H-diazirin-3-yl)phenyl)methyl)piperazine-1-carboxylate (0.760 g, 1.535 mmol, 91 % yield). LCMS RT (Method 2) 3.82 min (m/z 495.1) ^{1}H NMR (400 MHz, $CDCl_3$) δ 7.43 – 7.37 (m, 2H), 7.31 – 7.21 (m, 4H), 7.12 – 7.06 (m, 2H), 4.21 (s, 1H), 3.44 – 3.32 (m, 4H), 2.28 (s, 4H), 1.42 (s, 9H). ^{13}C NMR (101 MHz, $CDCl_3$) δ 154.69, 143.75, 140.04, 133.12, 129.07, 128.91, 128.13, 128.12, 126.81, 126.80, 123.39, 120.66, 79.62, 74.80, 51.57, 36.61, 28.36, 24.65. ^{19}F NMR (376 MHz, $CDCl_3$) δ -65.23. HRMS (ESI) *m/z* calcd for [M + H] 495.1769, found 495.1784.

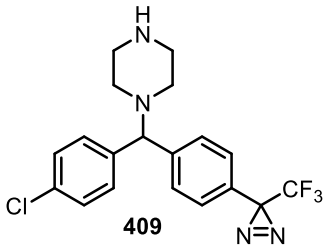

409

1-((4-chlorophenyl)(4-(3-(trifluoromethyl)-3H-diazirin-3yl)phenyl)methyl) piperazine - 409

To tert-butyl 4-((4-chlorophenyl)(4-(3-(trifluoromethyl)-3H-diazirin-3yl)phenyl)methyl) piperazine-1-carboxylate (550mg, 1.111 mmol) at 0C in the dark was added a commercially available solution of HCl in Dioxane (4M, 9 mL, 36.0 mmol) followed by 1mL of methanol. The reaction was allowed to warm to room temperature was stirred for 3 hours. On completion as determined by LCMS, the solvent was removed by rotary evaporation under reduced pressure. Diazirinyl CCZ · HCl is isolated as a yellow solid in quantitative yield and is used as such for the next step. LCMS RT (Method 2) 3.09 min (m/z 395.0) ^{1}H NMR (400 MHz, $CDCl_3$) δ 9.67 (s, 2H), 7.97 (s, 2H), 7.83 (s, 2H), 7.39 (s, 2H), 7.25 (d, *J* = 9.2 Hz, 4H), 5.69 (s, 1H), 3.84 (s, 4H), 3.52 (s, 4H). ^{13}C NMR (101 MHz, $CDCl_3$) δ 135.61, 131.36, 130.48, 129.97, 128.87, 127.74, 123.18, 120.45, 74.28, 48.46, 41.20, 28.35, 27.94.^{19}F NMR (376 MHz, $CDCl_3$) δ -65.04. [M + H^+]; HRMS (ESI) *m/z* calcd for [M + H] 395.1245, found 395.1226. IR (neat) 3378, 2933, 2490, 1641, 1438.

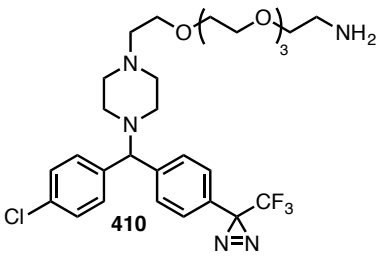

410

14-(4-((4-chlorophenyl)(4-(3-(trifluoromethyl)-3H-diazirin-3-yl)phenyl)methyl)piperazin-1-yl)-3,6,9,12-tetraoxatetradecan-1-amine – 410

To a solution of 1-((4-chlorophenyl)(4-(3-(trifluoromethyl)-3H-diazirin-3-yl)phenyl)methyl)piperazine (200mg, 0.507 mmol) in DMF (Volume: 2.533 mL) with K_2CO_3 (280mg, 2.086 mmol) was added 2,2-dimethyl-4-oxo-3,8,11,14,17-pentaoxa-5-azanonadecan-19-yl 4-methylbenzenesulfonate (398 mg, 0.810 mmol) and the reaction was stirred at 60˚C and monitored by LCMS. After 6 hours, almost full consumption of starting material was noted, with the concomitant production of Boc-(**410**) (LCMS RT (Method 2) 3.46 min (m/z 714.2)). At this point, the solvent was removed by rotary evaporation under reduced pressure. The crude is solubilised in approx 1mL of anhydrous dioxane and 0.5mL of MeOH, followed by the addition of 4mL of 4N HCl in dioxane at room temperature, disappearance of the peak for Boc-(**410**) was noted after 30 mins by LCMS. Excess HCl was removed from the reaction mixture by bubbling with nitrogen for 20 minutes, followed by evaporation of volatiles under reducted pressure and purification by gradient reverse phase chromtography and lyophilisation of pure fractions to yield 14-(4-((4-chlorophenyl)(4-(3-(trifluoromethyl)-3H-diazirin-3-yl)phenyl)methyl)piperazin-1-yl)-3,6,9,12-tetraoxatetradecan-1-amine – **410**, an oil, as a TFA salt. (83mg, 0.135 mmol, 26.7 % yield) LCMS RT (Method 2) 2.95 min (m/z 614.2) ^{1}H NMR (400 MHz, $CDCl_3$) δ 8.30 (s, 3H), 7.95 (d, *J* = 7.9 Hz, 2H), 7.82 (d, *J* = 7.3 Hz, 2H), 7.35 (d, *J* = 8.1 Hz, 2H), 7.20 (d, *J* = 7.9 Hz, 2H), 5.73 (s, 1H), 3.98 (s, 4H), 3.82 (t, *J* = 4.6 Hz, 2H), 3.74 – 3.52 (m, 18H), 3.36 (s, 2H), 3.19 (s, 2H). ^{13}C NMR (101 MHz, $CDCl_3$) δ 135.63, 130.31, 130.07, 129.94, 129.04, 127.70, 123.19, 120.47, 70.03, 69.88, 69.49, 66.47, 64.68, 61.61, 56.76, 48.38, 39.73. HRMS (ESI) *m/z* calcd for [M + H] 614.2720, found 614.2729.

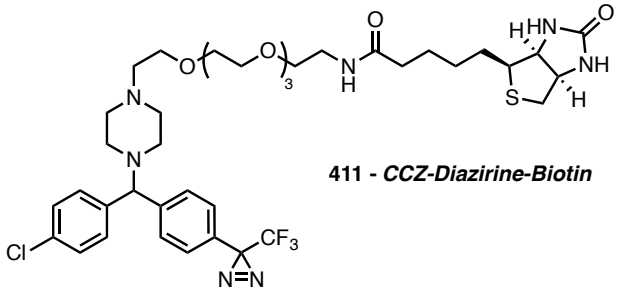

411 - *CCZ-Diazirine-Biotin*

N-(14-(4-((4-chlorophenyl)(4-(3-(trifluoromethyl)-3H-diazirin-3-yl)phenyl)methyl)piperazin-1-yl)-3,6,9,12-tetraoxatetradecyl)-5-((3aS,4S,6aR)-2-oxohexahydro-1H-thieno[3,4-d]imidazol-4-yl)pentanamide – CCZ-Diazirine-Biotin – 411.

To a solution of Biotin (9.01 mg, 0.037 mmol) in DMF (Volume: 307 µl) at room temperature under an atmosphere of nitrogen was added HATU (14.03 mg, 0.037 mmol) and Hunig'sBase (6.44 µl, 0.037 mmol) . The reaction was allowed 15 minutes stirring for pre-activation then to this was added 14-(4-((4-chlorophenyl)(4-(3-(trifluoromethyl)-3H-diazirin-3-yl)phenyl)methyl)piperazin-1-yl)-3,6,9,12-tetraoxa tetradecan-1-amine hydrochloride (20mg, 0.031 mmol). followed by 3 further equivalents of Hunigs base. The reaction was stirred for 2 hours and monitored by LCMS. Following completion the reaction mixture was purified directly by gradient reverse phase preparative HPLC and lyophilized to yield N-(14-(4-((4-chlorophenyl)(4-(3-(trifluoromethyl)-3H-diazirin-3-yl)phenyl)methyl)piperazin-1-yl)-3,6,9,12-tetraoxatetradecyl)-5-((3aR,4R,6aS)-2-oxohexahydro-1H-thieno[3,4-d]imidazol-4-yl)pentanamide (15.8mg, 0.019 mmol, 40.8 % yield) diazirine-CCZ-Biotin a white solid as its TFA salt.

LCMS RT (Method 2) 3.14min (m/z 840.2) ^{1}H NMR (400 MHz, $CDCl_3$) δ 7.56 (d, *J* = 8.4 Hz, 2H), 7.44 (d, *J* = 8.5 Hz, 2H), 7.33 (d, *J* = 8.5 Hz, 2H), 7.18 (d, *J* = 8.2 Hz, 2H), 6.94 (s, 1H), 6.75 (s, 1H), 4.72 (s, 1H), 4.60 (dd, *J* = 7.9, 4.7 Hz, 1H), 4.40 (dd, *J* = 7.9, 4.5 Hz, 1H), 3.88 – 3.80 (m, 2H), 3.69 – 3.49 (m, 19H), 3.43 (d, *J* = 4.6 Hz, 2H), 3.37 – 3.31 (m, 2H), 3.25 – 3.16 (m, 1H), 3.08 (s, 4H), 2.95 (dd, *J* = 13.1, 4.9 Hz, 1H), 2.77 (d, *J* = 13.1 Hz, 1H), 2.28 (td, *J* = 7.2, 3.4 Hz, 2H), 1.68 (tt, *J* = 13.5, 7.5 Hz, 4H), 1.45 (p, *J* = 7.1 Hz, 2H). ^{19}F NMR (376 MHz, $CDCl_3$) δ -65.20, -75.96. ^{13}C NMR (101 MHz, $CDCl_3$) δ 174.84, 164.79, 160.78, 139.18, 135.62, 132.97, 129.70, 129.16, 128.17, 127.51, 116.88, 114.00, 74.48, 70.22, 70.19, 70.08, 69.84, 69.41, 64.93, 62.34, 60.80, 56.51, 55.17, 51.34, 48.49, 40.26, 39.44, 35.24, 27.67, 25.35. HRMS (ESI) *m/z* calcd for [M + H] 840.3496, found 840.3521

Biology

Materials and Methods

Growth and Maintenance of cells

Human hepatoma cell line Huh7.5.1 were maintained as a 2D monolayer in Dulbecco's modification of Eagle's medium (DMEM) (Life Technologies, Grand Island, NY, USA) with 10% fetal bovine serum (FBS) and 1% Penicillin/Streptomycin within a breathable culture flask (Falcon) in 5% CO_2 at 37°C.

Passaging protocol

Once the cells reached 80 % confluence, the medium was removed and the flask rinsed with sterile PBS. The cells were then incubated in trypsin/0.05 %EDTA (Invitrogen) for 4 min at 37 °C to detach from the flask and neighboring cells. The reaction is terminated by adding DMEM to the flask (4x volume of trypsin used), the cells may then be pelleted by centrifugation (2000RPM, 5min) and suspended in DMEM. 50 µl of the cell suspension was pipetted into a new flask along with 15 ml of fresh growth medium. Cells were incubated in a 37C/ 5 % CO_2 incubator. After cells reached passage 30 they were discarded.

HCVcc Assay and ATP Lite Assay

Huh 7.5.1 cells were cultured as described, and plated in white bottomed 96-well plates at a density of 10^4 cells/well and incubated for 24 hours. The cells were then infected with HCV-Luc in the presence of increasing concentrations of the compound of interest to develop a 10-point dose response curve. The viral load was measured 48 hours following treatment using a Renilla luciferase assay system (Promega, Madison, WI, USA), efficacy is expressed as a percentage in terms of a measured minimal response (DMSO control wells) and theoretical maximal response (0 Luminescence). ATP-based cell viability assay was carried out in parallel using an ATPlite assay kit (PerkinElmer, Waltham, MA, USA) cytotoxicity is expressed as a percentage in terms of a measured minimal response (DMSO control wells) and theoretical maximal cytotoxicity (0 Luminescence). The concentration of the compound of interest that led to 50% viral inhibition or 50% cytotoxicity (EC_{50} and CC_{50} respectively) was calculated and graphs are produced using the nonlinear regression equation in GraphPad Prism 5.0 (GraphPad Software Inc, La Jolla, CA, USA). Cyclosporin A was utilized as a positive control in the HCVcc assay.

Photoaffinity cross-linking protocol

- $3x10^6$ Huh7.5.1 cells in 10mL of DMEM (10%FBS, 1% penicillin/streptomycin) are plated in a 10cm dish and left to adhere overnight, for 24 hours.
- Medium is removed and 2mL of DMEM containing HCVLuc followed by an aliquot of CCZ-Diazirine-Biotin from a 10mM stock solution in DMSO, to an appropriate concentration depending on the experimentla protocol underway (1mM/10mM)
- Samples are incubated for stated times (0.5-3hours), samples are timed so that the irradiation occurs in a direct successive series. Irradtion is carried out with a 4-watt TLC lamp at 365nm for 20 minutes or a UVP Blak-Ray™ 100watt, 115V mercury lamp with a 365nm filter. (Fisher Scientific catalogue no. UVP95004403) for 5 minutes, from a distance of approx 5cm from light source, on ice.
- Supernatant is removed and kept if necessary, cells are washed well with 2 x 5mL cold phosphate buffered saline
- 1mL of lysis buffer (30mM Tris pH 7.5, 1mM EDTA, 150mM NaCl, 0.3%NP40, 0.05% SDS) is added to each experiment plate and 110uL of protease inhibitor cocktail, which is washed around the plate for 1 minute.
- The cells are scraped off and left to lyse minutes on ice in an eppendorf vial for a 15 mins, vortex for 20 seconds, then 15 mins more lyse time.
- Cells are spun at 4C at 20k RCF on centrifuge, 5 mins.
- Supernatant is removed, labeled and stored on ice.

- 50uL of Neutravidin resin slurry (Pierce NeutrAvidin Agarose, ThermoFisher product no. 29200) is spun down and the supernatant is discarded, the beads are washed with 1mL of PBS x2.
- To each of the Neutravidin resin beds is added the appropriate cell lysate sample for affinity purification, samples are mixed and placed on rocker for 60 minutes.
- Samples are spun down and supernatant is discarded.
- Wash with 2x1000uL PBS, 2x1mL lysis buffer described above, and 1000uL PBS, spin down, discard supernatant.
-

Preparing samples for gel.

Procedure ref. for quantitative elution: Proteomics 2004, 4, 2296–2299 Buffer for elution of biotinylated proteins comprised of 2% SDS, 3mM biotin, 6M urea and 2M thiourea in PBS.

- Add 20uL of elution buffer and 8uL of 1:4 laemmli sample buffer to experiments A-G incubate at RT for 10 mins.
- BiotinBSA standard: 2uL of 2ug/mL+28uL of 1 x SDS buffer.
- Ladder – 8uL + 40uL of 1x SDS buffer – working solution
- In all plus 2uL of reducing agent
  Boil all 95C 10 min, briefly pellet, use supernatant for gel

SDS PAGE is performed on NuPage 4-12% BT gels and eluted eith MOPS buffer, the gel is developed at 150V for approx 90 minutes. Membrane is blocked with 20mL of 3% BSA in PBS for 1.5 hours, followed by incubation with 2.5uL of high-sensitivity Strep-HRP conjugate in 20mL of 3% BSA/PBS (1:8000) for 1.5 hours. Membrane is washed with PBS (2x2min) then TBS-T (5x5min) solutions. Membrane is drained, 2mL of 1:1 mixture of super signal west femto maximum sensitivity substrate is added and incubated for 5 minutes.

Appendix

Chapter 2.

A2: Racemic methyl-2-benzamido-3-hydroxy-4-methylpentanoate **- 217**

A3: Methyl (2S,3S)-2-benzamido-3-hydroxy-4-methylpentanoate **– 217**

A4: Racemic benzyl-3-hydroxy-4-methyl-1-oxo-1-(phenylamino)pentan-2-yl)(methyl)carbamate – **221**

A5: Enantiopure Benzyl ((2S,3R)-3-hydroxy-4-methyl-1-oxo-1-(phenylamino)pentan-2 yl)(methyl)carbamate – **221**

A6-A16: 221 Crystal structure analysis and assignment of absolute stereochemistry

A17:Benzyl(2S,3R,4R,E)-3-hydroxy-4-methyl-1-oxo-1-(phenylamino)oct-6-en-2yl)(methyl) carbamate Chiral HPLC chromatograms.

A18 MeBmt – **202**. ^{1}H and ^{13}C NMR

Chapter 3.

A19-21 N-benzyl-N-phenethylpiperidin-4-amine, 307. ^{1}H, ^{13}C and COSY NMR, LCMS.

A22 N-(4-bromo-3-chlorobenzyl)-N-(3-(4-bromophenyl)cyclobutyl)piperidin-4-amine**, 372.** ^{1}H NMR – oxalate.

Chapter 4.

A23-24. CCZ-diazirine biotin, **411**. ^{1}H, ^{13}C, ^{19}F NMR and LCMS.

Method Info : Chiralpac AD 4.6x250
60% isoprpoanol/hex 1 mL/min

Sample Info : AD, Hex/EtOH/DEA 80:20:0.05

Additional Info : Peak(s) manually integrated

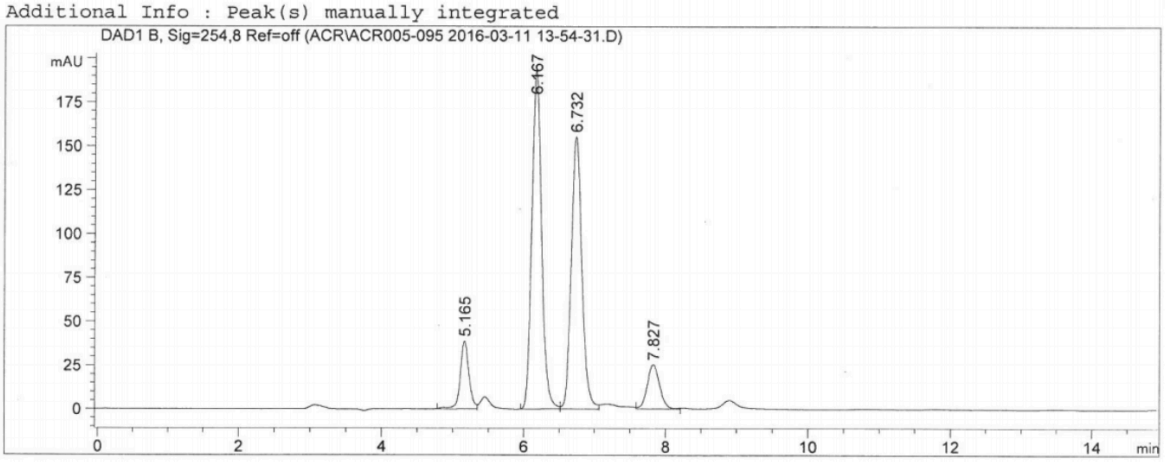

==========

Area Percent Report

==========

Sorted By : Signal
Multiplier : 1.0000
Dilution : 1.0000
Sample Amount: : 10.00000 [ng/ul] (not used in calc.)
Do not use Multiplier & Dilution Factor with ISTDs

Signal 1: DAD1 B, Sig=254,8 Ref=off

Peak #	RetTime [min]	Type	Width [min]	Area [mAU*s]	Height [mAU]	Area %
1	5.165	BV	0.1294	330.65033	38.82796	8.0586
2	6.167	BV	0.1477	1851.14319	193.40125	45.1162
3	6.732	VV	0.1594	1617.41663	155.40376	39.4198
4	7.827	VB	0.1842	303.84552	25.28092	7.4053

Method Info : Chiralpac IB 4.6x250
100% ethanol 1 mL/min

Sample Info : AD, Hex/EtOH/DEA 80:20:0.08

Additional Info : Peak(s) manually integrated

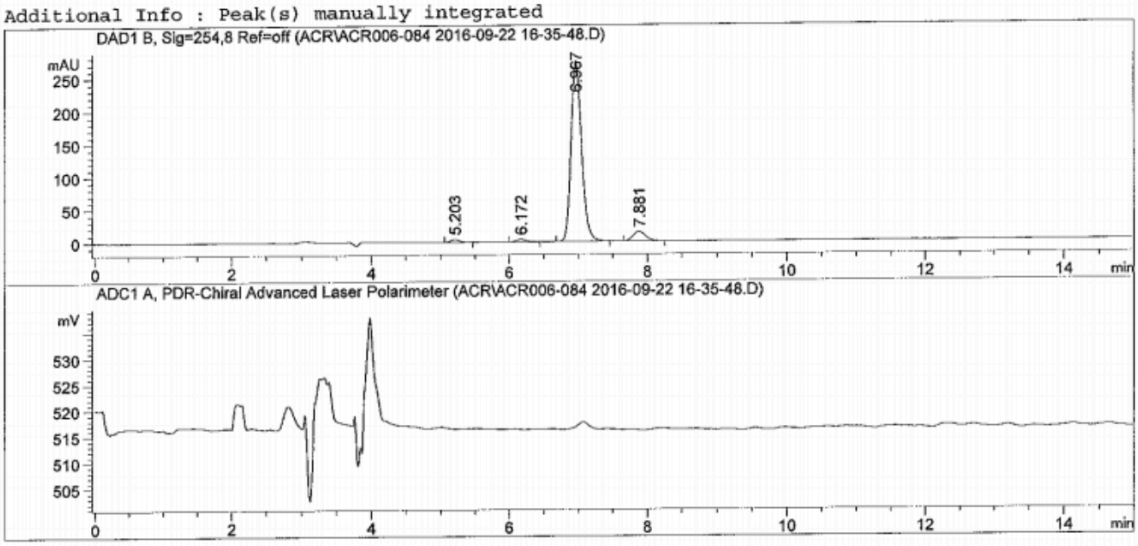

==========

Area Percent Report

==========

Sorted By : Signal
Multiplier : 1.0000
Dilution : 1.0000
Sample Amount: : 10.00000 [ng/ul] (not used in calc.)
Do not use Multiplier & Dilution Factor with ISTDs

Signal 1: DAD1 B, Sig=254,8 Ref=off

Peak #	RetTime [min]	Type	Width [min]	Area [mAU*s]	Height [mAU]	Area %
1	5.203	BB	0.1354	38.57858	4.35255	1.2173
2	6.172	BB	0.1456	37.19813	3.81936	1.1738
3	6.967	BB	0.1618	2918.01953	274.89832	92.0765

```
File ..\ACR006-040E 2016-06-02 14-14-46\031-0101.D Tgt Mass (CHM):
Injection Date    : 02-Jun-16, 14:16:12              Seq. Line : 1
Sample Name       : ACR006-040                  Location  : Vial 31
Acq. Operator     : SYSTEM                         Inj : 1
Spec. Reported    : <None>                     Inj Volume : 5 ul
Acq. Method       : C:\Chem32\1\DATA\ACR\ACR006-040E 2016-06-02 14-14-46\AD100MEOH.M
Analysis Method   : C:\Chem32\1\DATA\ACR\ACR006-040E 2016-06-02 14-14-46\AD100MEOH.M
Sample Info :
Method Info : Chiralpac AD  4.6x250
              100%  methanol 1 mL/min
```

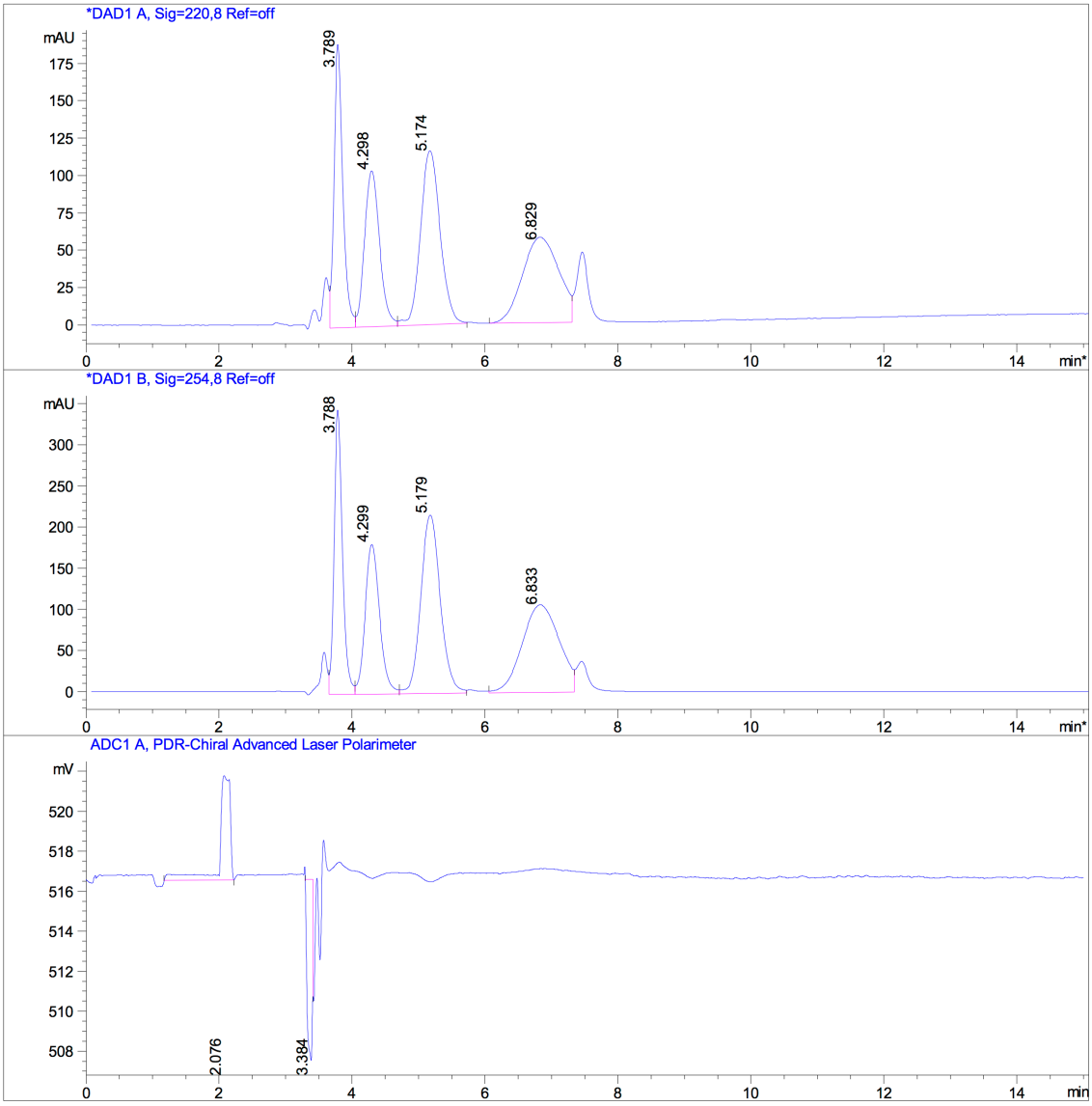

Method Info : Chiralpac ~~IB~~ 4.6x250 AD, MeOH/DEA 100:0.1
100% ethanol 1 mL/min

Additional Info : Peak(s) manually integrated

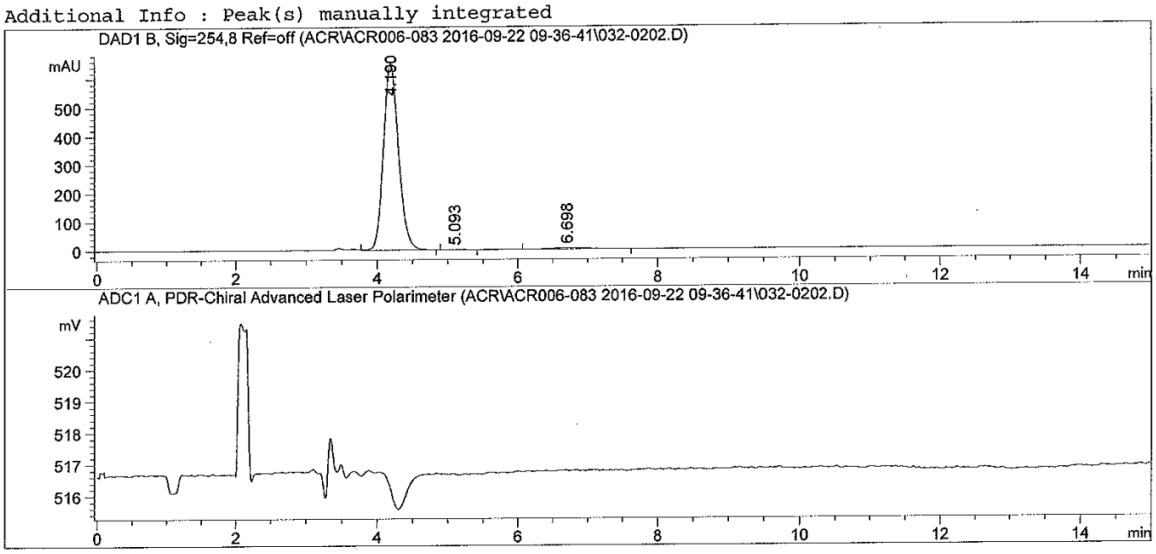

==========

Area Percent Report

==========

Sorted By : Signal
Multiplier : 1.0000
Dilution : 1.0000
Do not use Multiplier & Dilution Factor with ISTDs

Signal 1: DAD1 B, Sig=254,8 Ref=off

Peak #	RetTime [min]	Type	Width [min]	Area [mAU*s]	Height [mAU]	Area %
1	4.190	VB	0.2334	9783.07324	650.60669	98.0307
2	5.093	BB	0.2230	24.75652	1.34312	0.2481
3	6.698	BB	0.4745	171.77136	4.37093	1.7212

Experimental Summary

The single crystal X-ray diffraction studies were carried out on a Bruker D8 Platinum[135] CCD diffractometer equipped with Cu K_α radiation (λ = 1.5478). A 0.217 x 0.053 x 0.051 mm piece of a colorless rod was mounted on a Cryoloop with Paratone oil. Data were collected in a nitrogen gas stream at 125(2) K using ϕ and ϖ scans. Crystal-to-detector distance was 45 mm using variable exposure time (2s-5s) depending on θ with a scan width of 2.0°. Data collection was 98.4% complete to 68.00° in θ. A total of 33864 reflections were collected covering the indices, -11<=h<=10, -12<=k<=14, -19<=l<=19. 3547 reflections were found to be symmetry independent, with a R_{int} of 0.0549. Indexing and unit cell refinement indicated a primitive, orthorhombic lattice. The space group was found to be $P2_12_12_1$. The data were integrated using the Bruker SAINT software program and scaled using the SADABS software program. Solution by direct methods (SHELXT) produced a complete phasing model consistent with the proposed structure.

All nonhydrogen atoms were refined anisotropically by full-matrix least-squares (SHELXL-2014). All carbon bonded hydrogen atoms were placed using a riding model. Their positions were constrained relative to their parent atom using the appropriate HFIX command in SHELXL-2014. All other hydrogen atoms (H-bonding) were located in the difference map. Their relative positions were restrained using DFIX commands and their thermals freely refined. The absolute stereochemistry of the molecule was established by anomalous dispersion using the Parson's method with a Flack parameter of 0.050(34). Crystallographic data are summarized in Table 1.

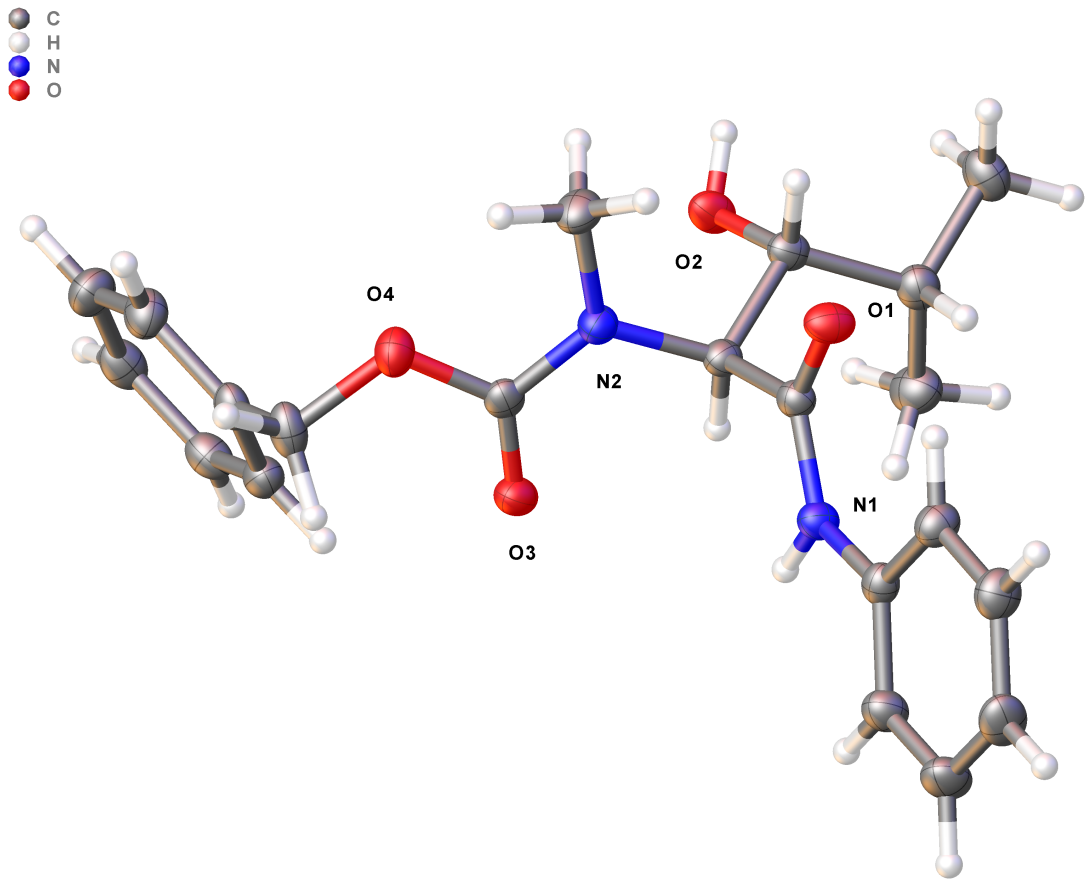
C
H
N
O
O4
O2
O1
N2
O3
N1

Table 1. Crystal data and structure refinement for NIH18.

Report date	2016-08-15	
Identification code	NIH18	
Empirical formula	C21 H26 N2 O4	
Molecular formula	C21 H26 N2 O4	
Formula weight	370.44	
Temperature	125 K	
Wavelength	1.54178 Å	
Crystal system	Orthorhombic	
Space group	$P2_12_12_1$	
Unit cell dimensions	a = 10.2972(4) Å	α= 90°.
	b = 11.7362(4) Å	β= 90°.
	c = 16.2355(6) Å	γ = 90°.
Volume	1962.06(12) $Å^3$	
Z	4	
Density (calculated)	1.254 Mg/m^3	
Absorption coefficient	0.707 mm^{-1}	
F(000)	792	
Crystal size	0.217 x 0.053 x 0.051 mm^3	
Crystal color, habit	Colorless Rod	
Theta range for data collection	4.649 to 68.273°.	
Index ranges	-11<=h<=10, -12<=k<=14, -19<=l<=19	
Reflections collected	33864	
Independent reflections	3547 [R(int) = 0.0549, R(sigma) = 0.0205]	
Completeness to theta = 68.000°	98.4 %	
Absorption correction	Semi-empirical from equivalents	
Max. and min. transmission	0.3201 and 0.2018	
Refinement method	Full-matrix least-squares on F^2	
Data / restraints / parameters	3547 / 2 / 255	
Goodness-of-fit on F^2	1.086	
Final R indices [I>2sigma(I)]	R1 = 0.0252, wR2 = 0.0636	
R indices (all data)	R1 = 0.0256, wR2 = 0.0639	
Absolute structure parameter	0.05(3)	
Extinction coefficient	n/a	
Largest diff. peak and hole	0.113 and -0.179 e.$Å^{-3}$	

Table 2. Atomic coordinates (x 10^4) and equivalent isotropic displacement parameters ($Å^2$x 10^3) for NIH18. U(eq) is defined as one third of the trace of the orthogonalized U^{ij} tensor.

	x	y	z	U(eq)
O(1)	5258(1)	4409(1)	4552(1)	27(1)
O(2)	3340(1)	7221(1)	5607(1)	27(1)
O(3)	5869(1)	8264(1)	3925(1)	27(1)
O(4)	4199(1)	8020(1)	3038(1)	27(1)
N(1)	7149(1)	5422(1)	4660(1)	21(1)
N(2)	4456(1)	6774(1)	4066(1)	22(1)
C(1)	5841(2)	5306(1)	4671(1)	20(1)
C(2)	5073(2)	6405(1)	4837(1)	20(1)
C(3)	4073(2)	6193(1)	5520(1)	22(1)
C(4)	4726(2)	5832(2)	6332(1)	26(1)
C(5)	3694(2)	5499(2)	6967(1)	32(1)
C(6)	5636(2)	6748(2)	6674(1)	35(1)
C(7)	3349(2)	6134(2)	3740(1)	29(1)
C(8)	4918(2)	7723(1)	3696(1)	21(1)
C(9)	8088(2)	4562(1)	4501(1)	21(1)
C(10)	7768(2)	3418(2)	4387(1)	26(1)
C(11)	8756(2)	2631(2)	4245(1)	30(1)
C(12)	10040(2)	2962(2)	4217(1)	32(1)
C(13)	10350(2)	4102(2)	4330(1)	33(1)
C(14)	9380(2)	4902(2)	4472(1)	27(1)
C(15)	4685(2)	8978(2)	2553(1)	30(1)
C(16)	4124(2)	10092(1)	2842(1)	24(1)
C(17)	2932(2)	10458(2)	2541(1)	30(1)
C(18)	2419(2)	11493(2)	2790(1)	33(1)
C(19)	3097(2)	12171(2)	3340(1)	31(1)
C(20)	4278(2)	11812(2)	3647(1)	28(1)
C(21)	4791(2)	10775(2)	3398(1)	26(1)

O(1)-C(1)	1.227(2)	C(12)-C(13)	1.387(3)
O(2)-H(2)	0.890(19)	C(13)-H(13)	0.9500
O(2)-C(3)	1.4299(18)	C(13)-C(14)	1.391(2)
O(3)-C(8)	1.225(2)	C(14)-H(14)	0.9500
O(4)-C(8)	1.345(2)	C(15)-H(15A)	0.9900
O(4)-C(15)	1.462(2)	C(15)-H(15B)	0.9900
N(1)-H(1)	0.906(17)	C(15)-C(16)	1.504(2)
N(1)-C(1)	1.354(2)	C(16)-C(17)	1.389(3)
N(1)-C(9)	1.421(2)	C(16)-C(21)	1.390(2)
N(2)-C(2)	1.469(2)	C(17)-H(17)	0.9500
N(2)-C(7)	1.464(2)	C(17)-C(18)	1.385(3)
N(2)-C(8)	1.352(2)	C(18)-H(18)	0.9500
C(1)-C(2)	1.536(2)	C(18)-C(19)	1.385(3)
C(2)-H(2A)	1.0000	C(19)-H(19)	0.9500
C(2)-C(3)	1.535(2)	C(19)-C(20)	1.380(3)
C(3)-H(3)	1.0000	C(20)-H(20)	0.9500
C(3)-C(4)	1.540(2)	C(20)-C(21)	1.387(3)
C(4)-H(4)	1.0000	C(21)-H(21)	0.9500
C(4)-C(5)	1.531(2)		
C(4)-C(6)	1.530(3)	C(3)-O(2)-H(2)	110.1(15)
C(5)-H(5A)	0.9800	C(8)-O(4)-C(15)	115.95(13)
C(5)-H(5B)	0.9800	C(1)-N(1)-H(1)	117.6(14)
C(5)-H(5C)	0.9800	C(1)-N(1)-C(9)	127.42(14)
C(6)-H(6A)	0.9800	C(9)-N(1)-H(1)	114.8(14)
C(6)-H(6B)	0.9800	C(7)-N(2)-C(2)	119.49(13)
C(6)-H(6C)	0.9800	C(8)-N(2)-C(2)	118.01(13)
C(7)-H(7A)	0.9800	C(8)-N(2)-C(7)	122.46(14)
C(7)-H(7B)	0.9800	O(1)-C(1)-N(1)	124.81(15)
C(7)-H(7C)	0.9800	O(1)-C(1)-C(2)	119.73(14)
C(9)-C(10)	1.395(2)	N(1)-C(1)-C(2)	115.46(14)
C(9)-C(14)	1.390(2)	N(2)-C(2)-C(1)	108.72(12)
C(10)-H(10)	0.9500	N(2)-C(2)-H(2A)	108.8
C(10)-C(11)	1.393(2)	N(2)-C(2)-C(3)	111.94(13)
C(11)-H(11)	0.9500	C(1)-C(2)-H(2A)	108.8
C(11)-C(12)	1.379(3)	C(3)-C(2)-C(1)	109.66(12)
C(12)-H(12)	0.9500	C(3)-C(2)-H(2A)	108.8

O(2)-C(3)-C(2)	106.79(12)	C(9)-C(10)-H(10)	120.4
O(2)-C(3)-H(3)	108.7	C(11)-C(10)-C(9)	119.20(16)
O(2)-C(3)-C(4)	112.23(13)	C(11)-C(10)-H(10)	120.4
C(2)-C(3)-H(3)	108.7	C(10)-C(11)-H(11)	119.4
C(2)-C(3)-C(4)	111.75(13)	C(12)-C(11)-C(10)	121.25(17)
C(4)-C(3)-H(3)	108.7	C(12)-C(11)-H(11)	119.4
C(3)-C(4)-H(4)	107.6	C(11)-C(12)-H(12)	120.4
C(5)-C(4)-C(3)	110.08(14)	C(11)-C(12)-C(13)	119.21(16)
C(5)-C(4)-H(4)	107.6	C(13)-C(12)-H(12)	120.4
C(6)-C(4)-C(3)	112.64(14)	C(12)-C(13)-H(13)	119.7
C(6)-C(4)-H(4)	107.6	C(12)-C(13)-C(14)	120.53(17)
C(6)-C(4)-C(5)	111.11(15)	C(14)-C(13)-H(13)	119.7
C(4)-C(5)-H(5A)	109.5	C(9)-C(14)-C(13)	119.96(17)
C(4)-C(5)-H(5B)	109.5	C(9)-C(14)-H(14)	120.0
C(4)-C(5)-H(5C)	109.5	C(13)-C(14)-H(14)	120.0
H(5A)-C(5)-H(5B)	109.5	O(4)-C(15)-H(15A)	109.3
H(5A)-C(5)-H(5C)	109.5	O(4)-C(15)-H(15B)	109.3
H(5B)-C(5)-H(5C)	109.5	O(4)-C(15)-C(16)	111.68(13)
C(4)-C(6)-H(6A)	109.5	H(15A)-C(15)-H(15B)	107.9
C(4)-C(6)-H(6B)	109.5	C(16)-C(15)-H(15A)	109.3
C(4)-C(6)-H(6C)	109.5	C(16)-C(15)-H(15B)	109.3
H(6A)-C(6)-H(6B)	109.5	C(17)-C(16)-C(15)	119.95(16)
H(6A)-C(6)-H(6C)	109.5	C(17)-C(16)-C(21)	119.15(16)
H(6B)-C(6)-H(6C)	109.5	C(21)-C(16)-C(15)	120.89(17)
N(2)-C(7)-H(7A)	109.5	C(16)-C(17)-H(17)	119.8
N(2)-C(7)-H(7B)	109.5	C(18)-C(17)-C(16)	120.39(17)
N(2)-C(7)-H(7C)	109.5	C(18)-C(17)-H(17)	119.8
H(7A)-C(7)-H(7B)	109.5	C(17)-C(18)-H(18)	120.0
H(7A)-C(7)-H(7C)	109.5	C(17)-C(18)-C(19)	119.98(17)
H(7B)-C(7)-H(7C)	109.5	C(19)-C(18)-H(18)	120.0
O(3)-C(8)-O(4)	123.18(15)	C(18)-C(19)-H(19)	119.9
O(3)-C(8)-N(2)	124.98(15)	C(20)-C(19)-C(18)	120.14(17)
O(4)-C(8)-N(2)	111.83(14)	C(20)-C(19)-H(19)	119.9
C(10)-C(9)-N(1)	123.19(15)	C(19)-C(20)-H(20)	120.1
C(14)-C(9)-N(1)	116.96(15)	C(19)-C(20)-C(21)	119.88(17)
C(14)-C(9)-C(10)	119.84(16)	C(21)-C(20)-H(20)	120.1

C(9)-C(10)-H(10)	120.4	C(9)-C(10)-H(10)	120.4
C(11)-C(10)-C(9)	119.20(16)	C(11)-C(10)-C(9)	119.20(16)
C(11)-C(10)-H(10)	120.4	C(11)-C(10)-H(10)	120.4
C(10)-C(11)-H(11)	119.4	C(10)-C(11)-H(11)	119.4
C(12)-C(11)-C(10)	121.25(17)	C(12)-C(11)-C(10)	121.25(17)
C(12)-C(11)-H(11)	119.4	C(12)-C(11)-H(11)	119.4
C(11)-C(12)-H(12)	120.4	C(11)-C(12)-H(12)	120.4
C(11)-C(12)-C(13)	119.21(16)	C(11)-C(12)-C(13)	119.21(16)
C(13)-C(12)-H(12)	120.4	C(13)-C(12)-H(12)	120.4
C(12)-C(13)-H(13)	119.7	C(12)-C(13)-H(13)	119.7
C(12)-C(13)-C(14)	120.53(17)	C(12)-C(13)-C(14)	120.53(17)
C(14)-C(13)-H(13)	119.7	C(14)-C(13)-H(13)	119.7
C(9)-C(14)-C(13)	119.96(17)	C(9)-C(14)-C(13)	119.96(17)
C(9)-C(14)-H(14)	120.0	C(9)-C(14)-H(14)	120.0
C(13)-C(14)-H(14)	120.0	C(13)-C(14)-H(14)	120.0
O(4)-C(15)-H(15A)	109.3	O(4)-C(15)-H(15A)	109.3
O(4)-C(15)-H(15B)	109.3	O(4)-C(15)-H(15B)	109.3
O(4)-C(15)-C(16)	111.68(13)	O(4)-C(15)-C(16)	111.68(13)
H(15A)-C(15)-H(15B)	107.9	H(15A)-C(15)-H(15B)	107.9
C(16)-C(15)-H(15A)	109.3	C(16)-C(15)-H(15A)	109.3
C(16)-C(15)-H(15B)	109.3	C(16)-C(15)-H(15B)	109.3
C(17)-C(16)-C(15)	119.95(16)	C(17)-C(16)-C(15)	119.95(16)
C(17)-C(16)-C(21)	119.15(16)	C(17)-C(16)-C(21)	119.15(16)
C(21)-C(16)-C(15)	120.89(17)	C(21)-C(16)-C(15)	120.89(17)
C(16)-C(17)-H(17)	119.8	C(16)-C(17)-H(17)	119.8
C(18)-C(17)-C(16)	120.39(17)	C(18)-C(17)-C(16)	120.39(17)
C(18)-C(17)-H(17)	119.8	C(18)-C(17)-H(17)	119.8
C(17)-C(18)-H(18)	120.0	C(17)-C(18)-H(18)	120.0
C(17)-C(18)-C(19)	119.98(17)	C(17)-C(18)-C(19)	119.98(17)
C(19)-C(18)-H(18)	120.0	C(19)-C(18)-H(18)	120.0
C(18)-C(19)-H(19)	119.9	C(18)-C(19)-H(19)	119.9
C(20)-C(19)-C(18)	120.14(17)	C(20)-C(19)-C(18)	120.14(17)
C(20)-C(19)-H(19)	119.9	C(20)-C(19)-H(19)	119.9
C(19)-C(20)-H(20)	120.1	C(19)-C(20)-H(20)	120.1
C(19)-C(20)-C(21)	119.88(17)	C(19)-C(20)-C(21)	119.88(17)
C(21)-C(20)-H(20)	120.1	C(21)-C(20)-H(20)	120.1

C(16)-C(21)-H(21)	119.8
C(20)-C(21)-C(16)	120.46(17)
C(20)-C(21)-H(21)	119.8

Table 4. Anisotropic displacement parameters ($Å^2 x\ 10^3$) for NIH18. The anisotropic displacement factor exponent takes the form: $-2\pi^2[\ h^2\ a^{*2}U^{11} + ...\ + 2\ h\ k\ a^*\ b^*\ U^{12}\ ]$

	U^{11}	U^{22}	U^{33}	U^{23}	U^{13}	U^{12}
O(1)	23(1)	20(1)	38(1)	-3(1)	2(1)	-1(1)
O(2)	23(1)	20(1)	37(1)	2(1)	8(1)	5(1)
O(3)	21(1)	24(1)	35(1)	6(1)	0(1)	-2(1)
O(4)	32(1)	23(1)	26(1)	3(1)	-4(1)	2(1)
N(1)	20(1)	18(1)	26(1)	0(1)	1(1)	0(1)
N(2)	21(1)	20(1)	25(1)	1(1)	-2(1)	-1(1)
C(1)	20(1)	20(1)	20(1)	1(1)	1(1)	0(1)
C(2)	19(1)	18(1)	24(1)	1(1)	-1(1)	-1(1)
C(3)	20(1)	18(1)	28(1)	0(1)	3(1)	1(1)
C(4)	26(1)	26(1)	26(1)	1(1)	3(1)	3(1)
C(5)	38(1)	30(1)	27(1)	2(1)	7(1)	0(1)
C(6)	32(1)	42(1)	30(1)	-1(1)	-2(1)	-3(1)
C(7)	27(1)	27(1)	34(1)	0(1)	-8(1)	-4(1)
C(8)	19(1)	21(1)	23(1)	0(1)	4(1)	5(1)
C(9)	23(1)	22(1)	19(1)	1(1)	1(1)	3(1)
C(10)	25(1)	23(1)	31(1)	-1(1)	-3(1)	2(1)
C(11)	34(1)	24(1)	33(1)	-1(1)	-1(1)	5(1)
C(12)	31(1)	31(1)	35(1)	3(1)	8(1)	13(1)
C(13)	23(1)	35(1)	40(1)	5(1)	9(1)	3(1)
C(14)	24(1)	26(1)	32(1)	2(1)	4(1)	1(1)
C(15)	42(1)	25(1)	22(1)	5(1)	5(1)	6(1)
C(16)	30(1)	23(1)	19(1)	4(1)	4(1)	2(1)
C(17)	34(1)	28(1)	27(1)	2(1)	-5(1)	0(1)
C(18)	27(1)	32(1)	40(1)	6(1)	-1(1)	7(1)
C(19)	35(1)	22(1)	35(1)	2(1)	11(1)	4(1)
C(20)	33(1)	25(1)	27(1)	0(1)	5(1)	-5(1)
C(21)	24(1)	29(1)	26(1)	5(1)	1(1)	0(1)

Table 5. Hydrogen coordinates (x 10^4) and isotropic displacement parameters ($Å^2$x 10^3) for NIH18.

	x	y	z	U(eq)
H(2)	2545(19)	7060(20)	5790(14)	44(6)
H(1)	7480(20)	6132(15)	4723(12)	30(5)
H(2A)	5690	7010	5023	24
H(3)	3474	5571	5340	26
H(4)	5261	5140	6216	31
H(5A)	3160	6165	7099	48
H(5B)	4120	5223	7469	48
H(5C)	3143	4896	6740	48
H(6A)	6424	6783	6337	52
H(6B)	5869	6559	7243	52
H(6C)	5197	7489	6662	52
H(7A)	2558	6358	4035	44
H(7B)	3501	5316	3817	44
H(7C)	3247	6299	3152	44
H(10)	6888	3178	4406	31
H(11)	8541	1851	4167	36
H(12)	10704	2417	4120	39
H(13)	11232	4337	4310	39
H(14)	9600	5681	4548	33
H(15A)	4460	8861	1967	36
H(15B)	5644	9008	2597	36
H(17)	2466	9996	2162	36
H(18)	1601	11737	2584	40
H(19)	2748	12884	3506	37
H(20)	4739	12275	4028	34
H(21)	5604	10530	3610	31

Table 6. Hydrogen bonds for NIH18 [Å and °].

D-H...A	d(D-H)	d(H...A)	d(D...A)	<(DHA)
O(2)-H(2)...O(3)#1	0.890(19)	1.828(19)	2.7157(17)	175(2)
N(1)-H(1)...O(2)#2	0.906(17)	2.193(18)	3.0566(18)	159.2(18)

Symmetry transformations used to generate equivalent atoms:

#1 x-1/2,-y+3/2,-z+1 #2 x+1/2,-y+3/2,-z+1

Method Info : Chiralpac IB 4.6x250 ID, Hex/IPA/DEA 40:60:0.04
100% ethanol 1 mL/min

Additional Info : Peak(s) manually integrated

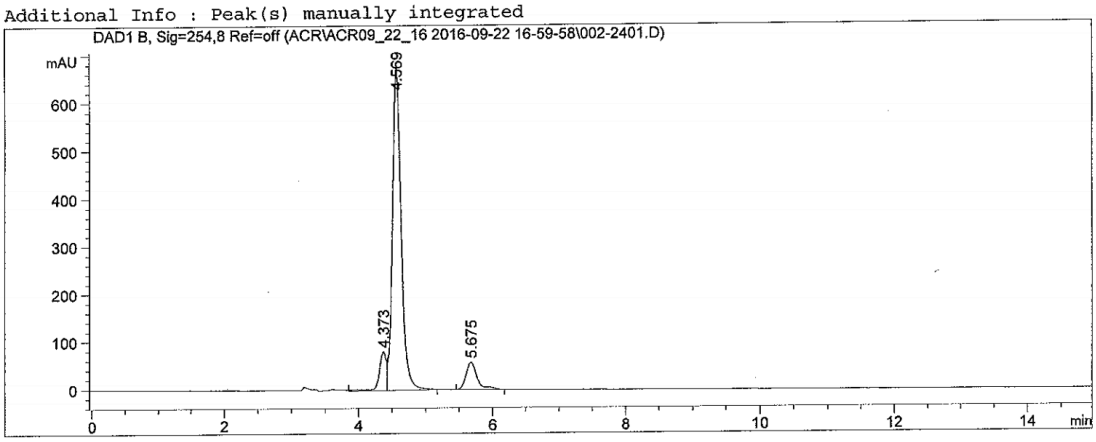

==========

Area Percent Report

==========

Sorted By : Signal
Multiplier : 1.0000
Dilution : 1.0000
Do not use Multiplier & Dilution Factor with ISTDs

Signal 1: DAD1 B, Sig=254,8 Ref=off

Peak #	RetTime [min]	Type	Width [min]	Area [mAU*s]	Height [mAU]	Area %
1	4.373	VV	0.1109	599.91284	80.55659	8.1919
2	4.569	VB	0.1350	6081.17676	675.74957	83.0396
3	5.675	BB	0.1699	642.13733	56.78867	8.7685
Totals :				7323.22693	813.09483	

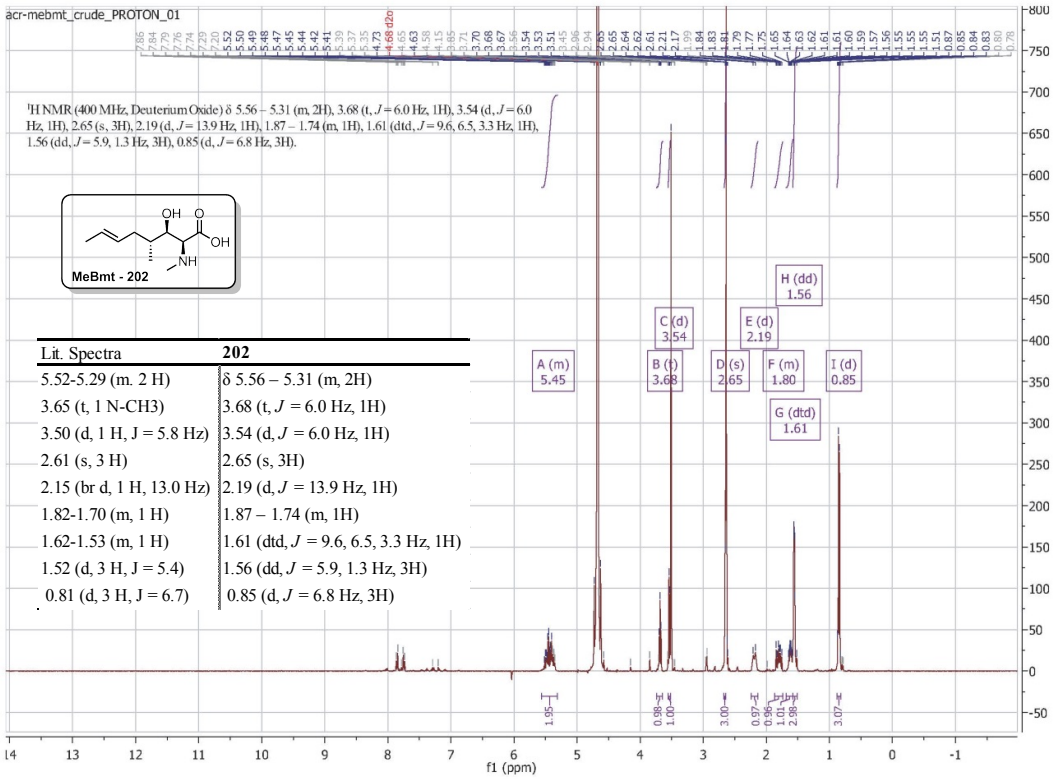

Lit. Spectra	**202**
5.52-5.29 (m. 2 H)	δ 5.56 – 5.31 (m, 2H)
3.65 (t, 1 N-CH3)	3.68 (t, *J* = 6.0 Hz, 1H)
3.50 (d, 1 H, J = 5.8 Hz)	3.54 (d, *J* = 6.0 Hz, 1H)
2.61 (s, 3 H)	2.65 (s, 3H)
2.15 (br d, 1 H, 13.0 Hz)	2.19 (d, *J* = 13.9 Hz, 1H)
1.82-1.70 (m, 1 H)	1.87 – 1.74 (m, 1H)
1.62-1.53 (m, 1 H)	1.61 (dtd, *J* = 9.6, 6.5, 3.3 Hz, 1H)
1.52 (d, 3 H, J = 5.4)	1.56 (dd, *J* = 5.9, 1.3 Hz, 3H)
0.81 (d, 3 H, J = 6.7)	0.85 (d, *J* = 6.8 Hz, 3H)

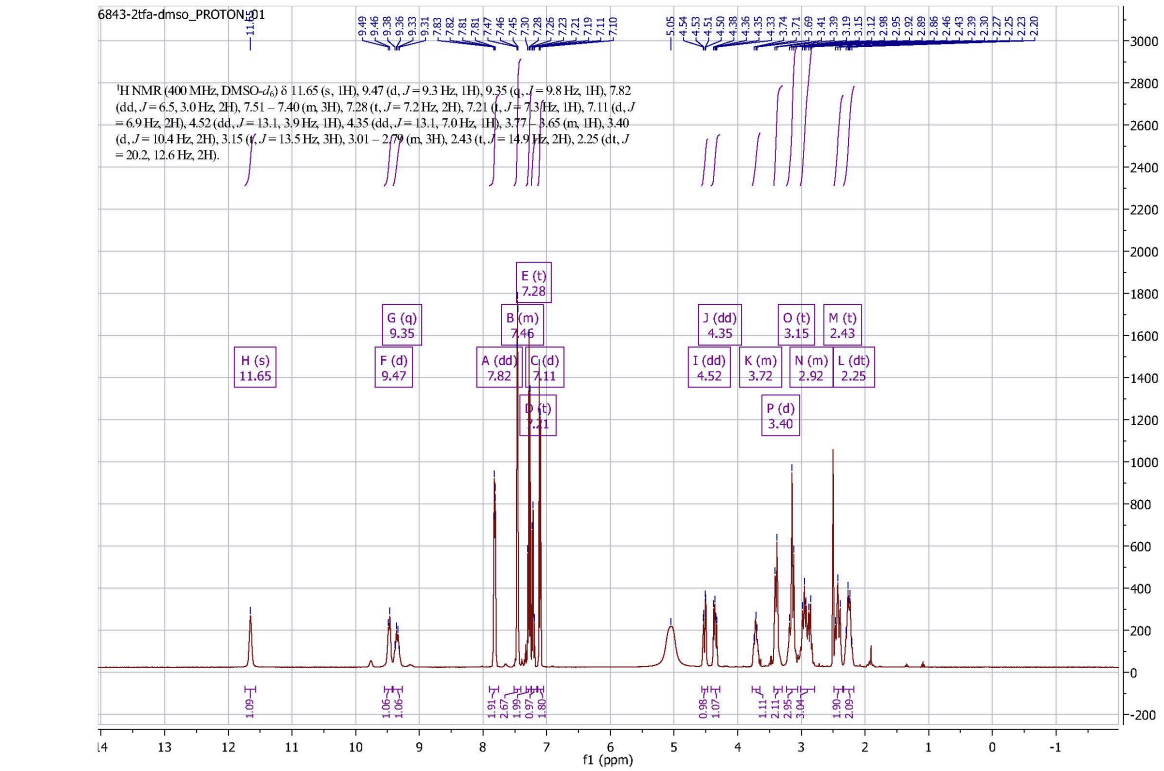
6843-2tfa-dmso_PROTON_01
¹H NMR (400 MHz, DMSO-d_6) δ 11.65 (s, 1H), 9.47 (d, J = 9.3 Hz, 1H), 9.35 (q, J = 9.8 Hz, 1H), 7.82 (dd, J = 6.5, 3.0 Hz, 2H), 7.51 – 7.40 (m, 3H), 7.28 (t, J = 7.2 Hz, 2H), 7.21 (t, J = 7.3 Hz, 1H), 7.11 (d, J = 6.9 Hz, 2H), 4.52 (dd, J = 13.1, 3.9 Hz, 1H), 4.35 (dd, J = 13.1, 7.0 Hz, 1H), 3.77 – 3.65 (m, 1H), 3.40 (d, J = 10.4 Hz, 2H), 3.15 (t, J = 13.5 Hz, 3H), 3.01 – 2.79 (m, 3H), 2.43 (t, J = 14.9 Hz, 2H), 2.25 (dt, J = 20.2, 12.6 Hz, 2H).
H (s) 11.65
G (q) 9.35
F (d) 9.47
A (dd) 7.82
E (t) 7.28
B (m) 7.46
C (d) 7.11
D (t) 7.21
J (dd) 4.35
I (dd) 4.52
K (m) 3.72
P (d) 3.40
O (t) 3.15
N (m) 2.92
M (t) 2.43
L (dt) 2.25
f1 (ppm)

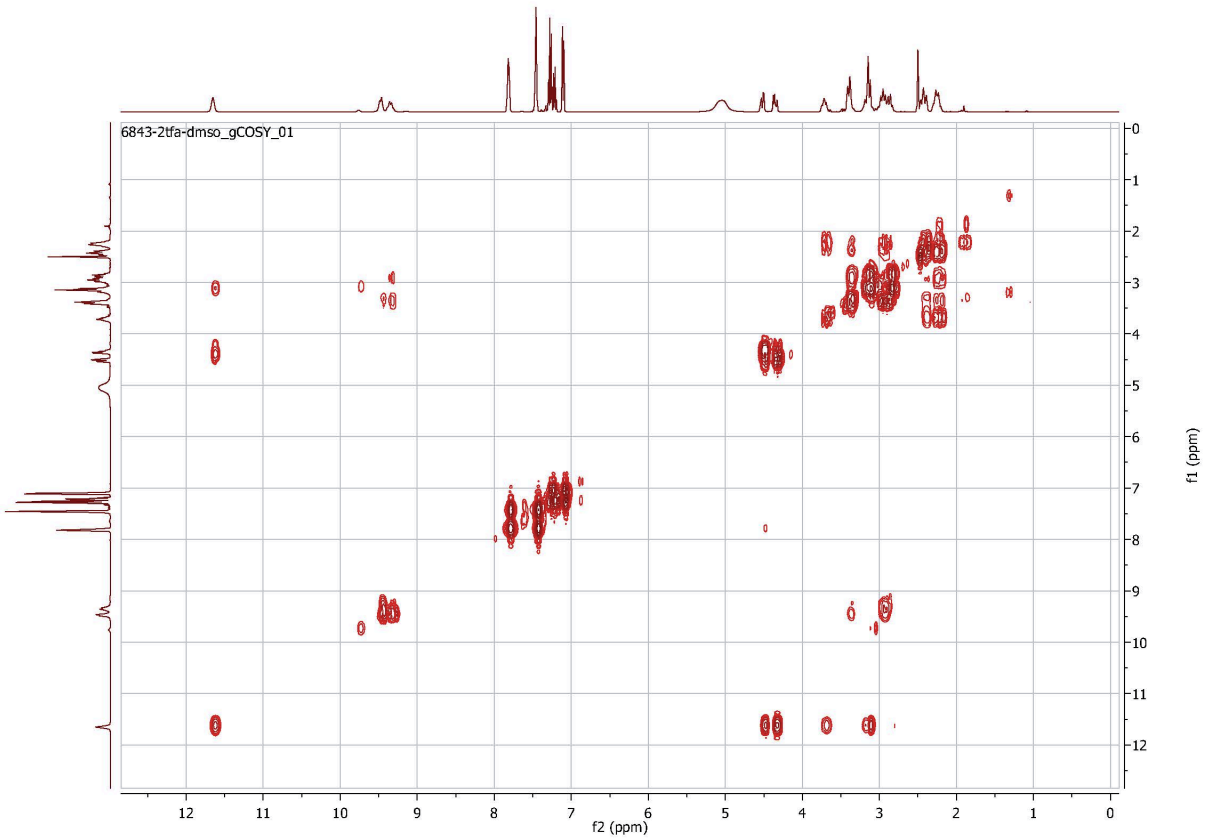
6843-2tfa-dmso_gCOSY_01
f2 (ppm)
f1 (ppm)

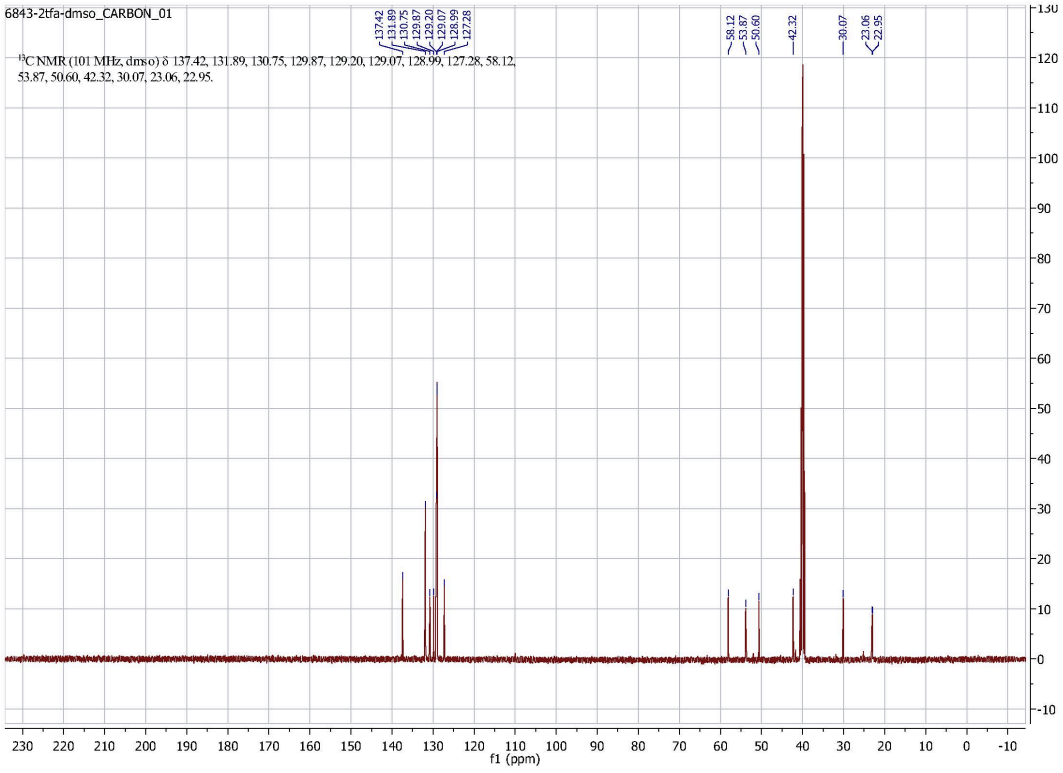
6843-2tfa-dmso_CARBON_01
13C NMR (101 MHz, dmso) δ 137.42, 131.89, 130.75, 129.87, 129.20, 129.07, 128.99, 127.28, 58.12, 53.87, 50.60, 42.32, 30.07, 23.06, 22.95.
137.42
131.89
130.75
129.87
129.20
129.07
128.99
127.28
58.12
53.87
50.60
42.32
30.07
23.06
22.95
f1 (ppm)

Instrument: AGILENT06 Datafile: Z:\PurGroup\Instr\AG06Raw\chemist\09-16\190916-68431-27320.D

```
File ..\AG06RAW\CHEMIST\09-16\190916-68431-27320.D Tgt Mass (EZX): 295.00
Injection Date    : 19-Sep-16, 20:39:13                Seq. Line : 0
Sample Name       : 6843                          Location  : P1-B-02
Acq. Operator     : adam rolt                            Inj : 0
Spec. Reported    : UV Integration                 Inj Volume : 3 ul
Acq. Method       : C:\Chem32\1\METHODS\A_STD_GRAD.M
Analysis Method   : C:\Chem32\1\METHODS\A_STD_GRAD.M
Sample Info : Easy-Access Method: 'A_STD_GRAD'  295.00
Method Info : Standard Gradient 4% to 100% Acetonitrile (0.05% TFA) over 3 minutes
              Luna C18 3 micron 3 x 75mm
```

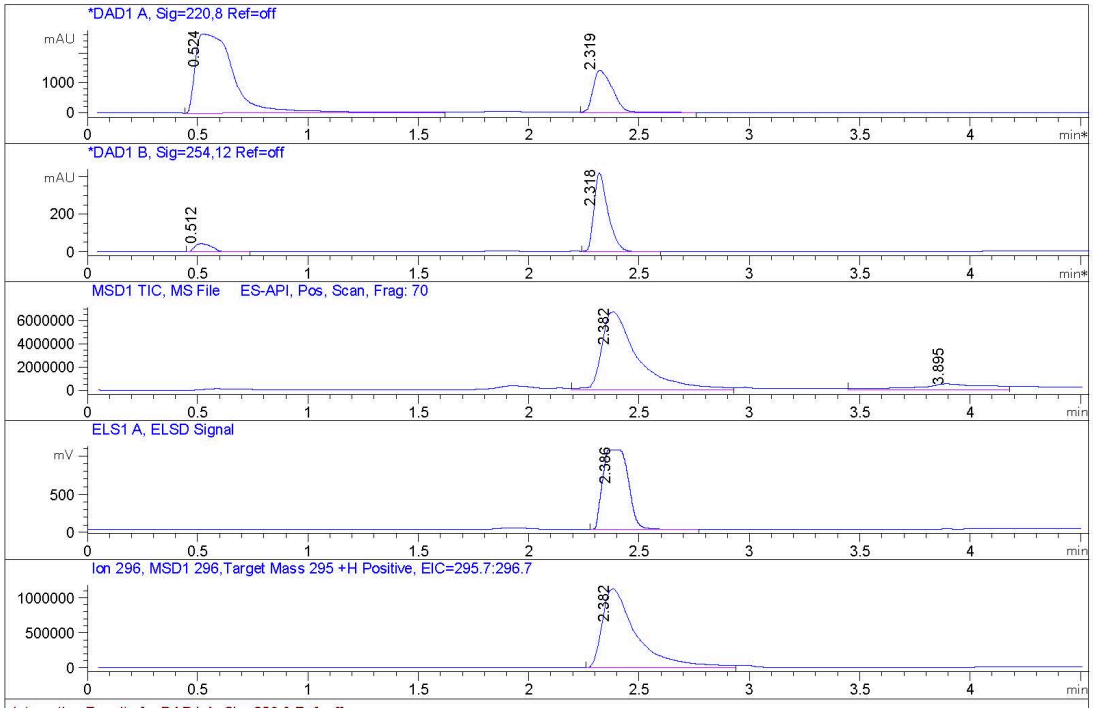

Integration Results for DAD1 A, Sig=220,8 Ref=off

RetTim	Width	Area	Height	Area%	MS(+)
0.52	0.19	32276.64	2635.46	79.08	179
2.32	0.10	8540.38	1417.05	20.92	295

Integration Results for DAD1 B, Sig=254,12 Ref=off

RetTim	Width	Area	Height	Area%	MS(+)
0.51	0.07	225.92	44.19	10.99	179
2.32	0.06	1829.52	419.07	89.01	295

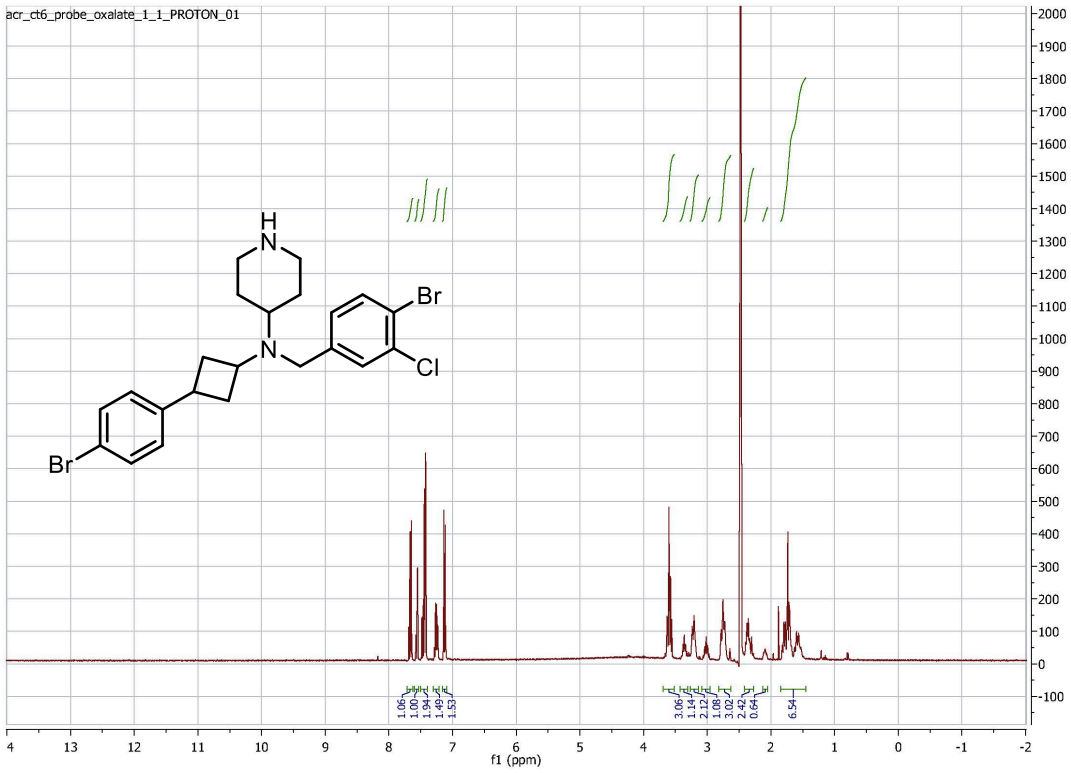
acr_ct6_probe_oxalate_1_1_PROTON_01
H
N
N
Br
Cl
Br
f1 (ppm)

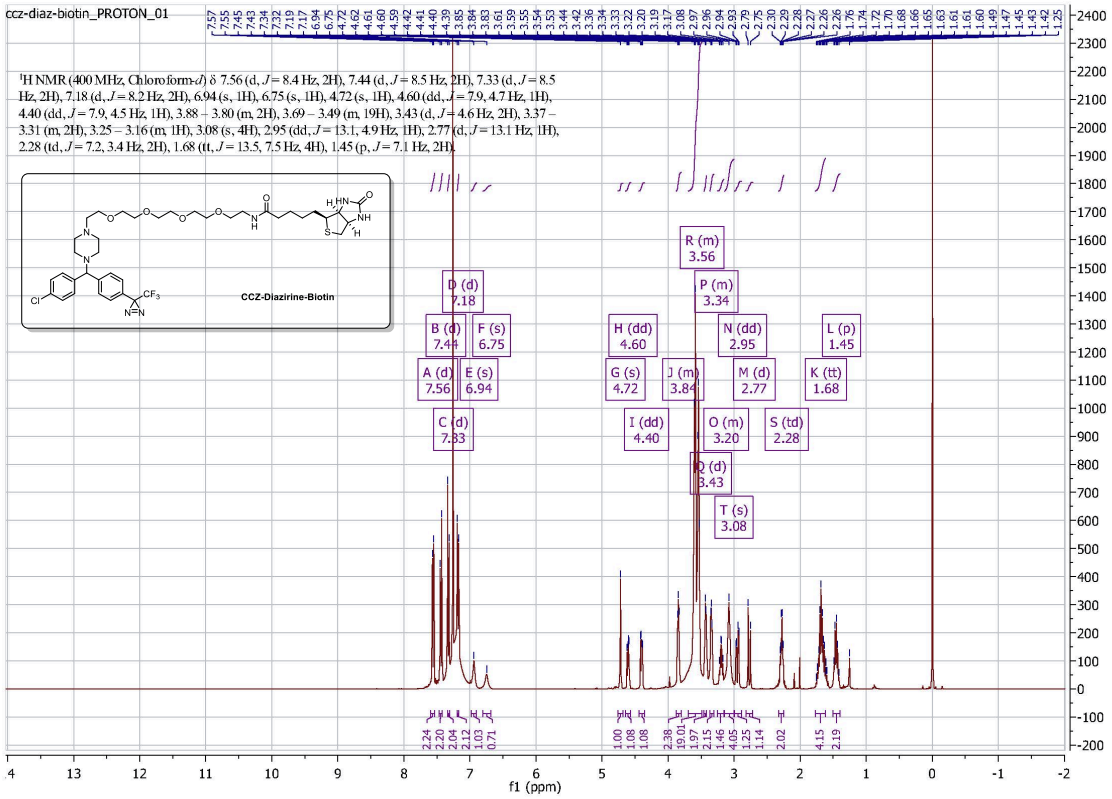
ccz-diaz-biotin_PROTON_01
¹H NMR (400 MHz, Chloroform-d) δ 7.56 (d, J = 8.4 Hz, 2H), 7.44 (d, J = 8.5 Hz, 2H), 7.33 (d, J = 8.5 Hz, 2H), 7.18 (d, J = 8.2 Hz, 2H), 6.94 (s, 1H), 6.75 (s, 1H), 4.72 (s, 1H), 4.60 (dd, J = 7.9, 4.7 Hz, 1H), 4.40 (dd, J = 7.9, 4.5 Hz, 1H), 3.88 – 3.80 (m, 2H), 3.69 – 3.49 (m, 19H), 3.43 (d, J = 4.6 Hz, 2H), 3.37 – 3.31 (m, 2H), 3.25 – 3.16 (m, 1H), 3.08 (s, 4H), 2.95 (dd, J = 13.1, 4.9 Hz, 1H), 2.77 (d, J = 13.1 Hz, 1H), 2.28 (td, J = 7.2, 3.4 Hz, 2H), 1.68 (tt, J = 13.5, 7.5 Hz, 4H), 1.45 (p, J = 7.1 Hz, 2H).
CCZ-Diazirine-Biotin
D (d) 7.18
B (d) 7.44
F (s) 6.75
A (d) 7.56
E (s) 6.94
C (d) 7.33
R (m) 3.56
P (m) 3.34
H (dd) 4.60
N (dd) 2.95
L (p) 1.45
G (s) 4.72
J (m) 3.84
M (d) 2.77
K (tt) 1.68
I (dd) 4.40
O (m) 3.20
S (td) 2.28
Q (d) 3.43
T (s) 3.08
f1 (ppm)

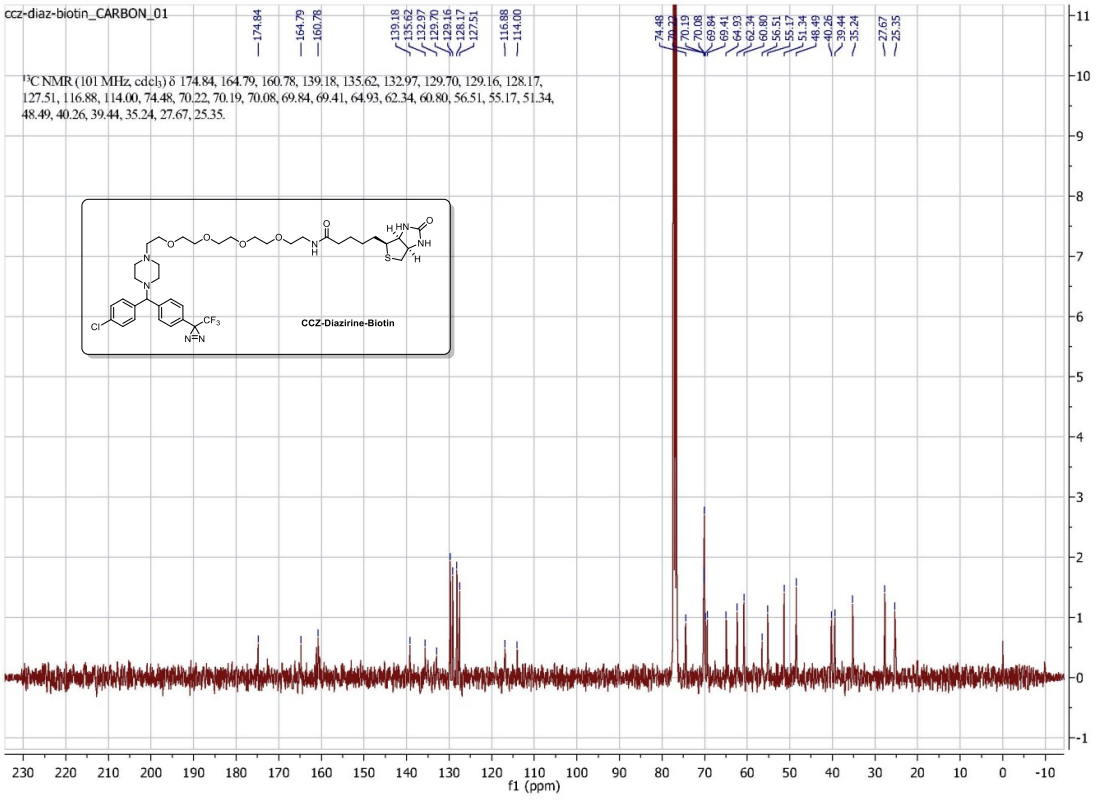
ccz-diaz-biotin_CARBON_01
¹³C NMR (101 MHz, cdcl₃) δ 174.84, 164.79, 160.78, 139.18, 135.62, 132.97, 129.70, 129.16, 128.17, 127.51, 116.88, 114.00, 74.48, 70.22, 70.19, 70.08, 69.84, 69.41, 64.93, 62.34, 60.80, 56.51, 55.17, 51.34, 48.49, 40.26, 39.44, 35.24, 27.67, 25.35.
CCZ-Diazirine-Biotin
f1 (ppm)

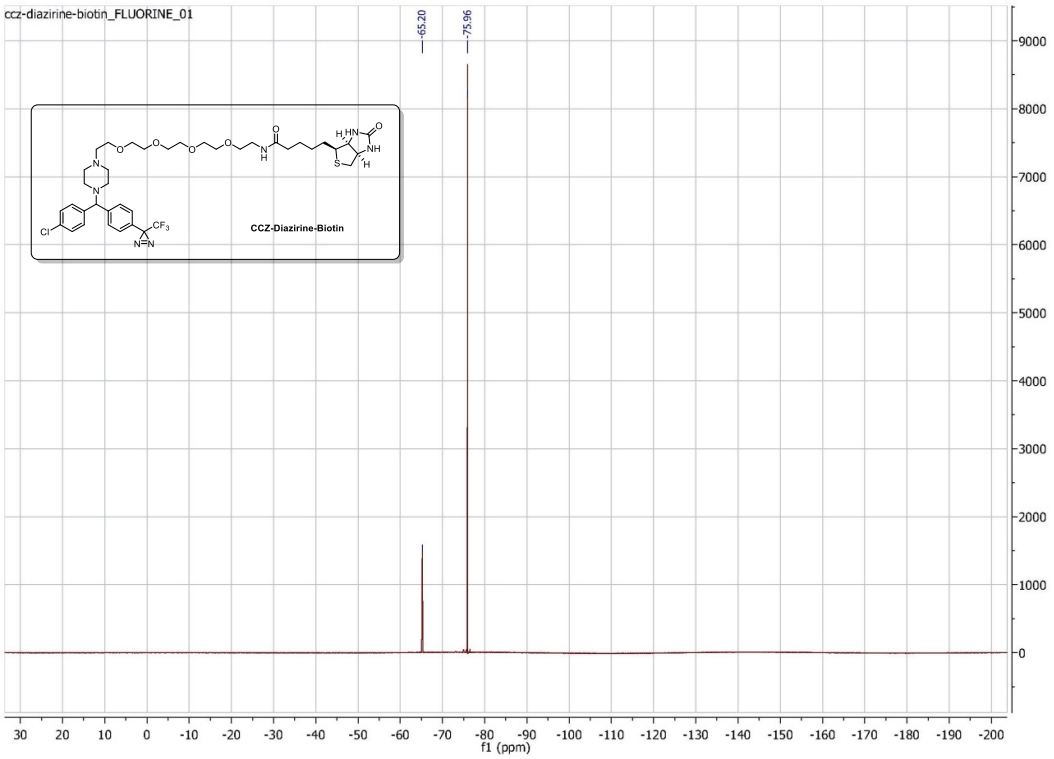
ccz-diazirine-biotin_FLUORINE_01
-65.20
-75.96
CCZ-Diazirine-Biotin
9000
8000
7000
6000
5000
4000
3000
2000
1000
0
30 20 10 0 -10 -20 -30 -40 -50 -60 -70 -80 -90 -100 -110 -120 -130 -140 -150 -160 -170 -180 -190 -200
f1 (ppm)